NASA Contractor Report 189202

Development of an Integrated BEM Approach for Hot Fluid Structure Interaction

BEST-FSI: Boundary Element Solution Technique for Fluid Structure Interaction

G.F. Dargush, P.K. Banerjee, and Y. Shi
State University of New York at Buffalo
Buffalo, New York

March 1992

Prepared for
Lewis Research Center
Under Grant NAG3–712

National Aeronautics and
Space Administration

TABLE OF CONTENTS

SECTION	PAGE
1.0 - Introduction	1.1
2.0 - Theoretical Background	2.1
2.1 - Literature Review	2.2
2.2 - Thermoelastic Deformation	2.3
2.2.1 - Introduction	2.3
2.2.2 - Governing Equations	2.3
2.2.3 - Integral Representations	2.4
2.2.4 - Numerical Implementation	2.5
2.2.4.1 - Introduction	2.5
2.2.4.2 - Temporal Discretization	2.5
2.2.4.3 - Spatial Discretization	2.6
2.2.4.4 - Numerical Integration	2.8
2.2.4.5 - Assembly	2.9
2.2.4.6 - Solution	2.10
2.2.4.7 - Interior Quantities	2.11
2.2.4.8 - Advanced Features	2.13
Appendix 2.2 - Kernel Functions	2.15
2.3 - Incompressible Thermoviscous Flow	2.17
2.3.1 - Introduction	2.17
2.3.2 - Governing Equations	2.17
2.3.3 - Integral Representations	2.18
2.3.3.1 - Steady	2.18
2.3.3.2 - Time-Dependent	2.19
2.3.4 - Numerical Implementation	2.20
2.3.4.1 - Introduction	2.20

2.3.4.2 - Temporal and Spatial Discretization 2.20
2.3.4.3 - Integration 2.22
2.3.4.4 - Assembly 2.23
2.3.4.5 - Solution 2.26
2.3.4.6 - Calculation of Additional Boundary Quantities 2.26
2.3.5 - Concluding Remarks 2.27
Appendix 2.3.1 - Steady Kernel Functions 2.28
Appendix 2.3.2 - Time-Dependent Kernel Functions 2.29
2.4 - Convective Incompressible Thermoviscous Flow 2.33
2.4.1 - Introduction 2.33
2.4.2 - Governing Equations 2.33
2.4.3 - Fundamental Solutions 2.34
2.4.4 - Integral Representations 2.35
2.4.5 - Numerical Implementation 2.36
Appendix 2.4 - Kernel Functions 2.38
2.5 - Convective Potential Flow 2.44
2.5.1 - Introduction 2.44
2.5.2 - Governing Equations 2.44
2.5.3 - Fundamental Solutions 2.45
2.5.3.1 - Compressible Potential Flow 2.45
2.5.3.2 - Convective Compressible Potential Flow 2.46
2.5.3.3 - Incompressible Potential Flow 2.50
2.5.4 - Boundary Integral Representations 2.50
2.5.4.1 - Compressible Potential Flow 2.50
2.5.4.2 - Incompressible Potential Flow 2.52
2.5.5 - Numerical Implementation 2.52
2.5.5.1 - Introduction 2.52
2.5.5.2 - Spatial Discretization 2.52
2.5.5.3 - Integration 2.53

2.5.5.4 - Assembly 2.57
2.5.5.5 - Solution 2.58
2.5.5.6 - Interior Values 2.59
2.6 - Compressible Thermoviscous Flow 2.62
2.6.1 - Introduction 2.62
2.6.2 - Governing Equations 2.62
2.6.3 - Fundamental Solutions 2.64
2.6.3.1 - Unconvective Compressible Flow 2.67
2.6.3.2 - Convective Compressible Flow 2.71
2.6.4 - Boundary Integral Representations 2.79
2.6.5 - Concluding Remarks 2.83
2.7 - Fluid-Structure Interaction 2.91
2.7.1 - Introduction 2.91
2.7.2 - Formulation 2.91
2.7.3 - Numerical Implementation 2.92
3.0 - Applications 3.1
3.1 - Introduction 3.1
3.2 - Thermoelastic Deformation 3.2
3.2.1 - Sudden Heating of Aluminum Block 3.2
3.2.2 - Circular Disk 3.5
3.3 - Incompressible Thermoviscous Flow 3.8
3.3.1 - Converging Channel 3.8
3.3.2 - Transient Couette Flow 3.11
3.3.3 - Flow Between Rotating Cylinders 3.16
3.3.4 - Driven Cavity Flow 3.20
3.3.5 - Transient Driven Cavity Flow 3.25
3.4 - Convective Incompressible Thermoviscous Flow 3.28
3.4.1 - Burgers Flow 3.28
3.4.2 - Flow Over a Cylinder 3.31

3.4.3 - Flow Past Airfoils 3.40
3.5 - Convective Potential Flow 3.55
3.5.1 - One-Dimensional Wave Propagation 3.55
3.5.2 - Flow Over a Wedge 3.57
3.6 - Compressible Thermoviscous Flow 3.72
3.7 - Fluid-Structure Interaction 3.73
3.7.1 - Steady Response of a Thick Cylinder 3.73
3.7.2 - Airfoil Exposed to Hot Gas Flowpath 3.78
4.0 - Guide to Using BEST-FSI 4.1
4.1 - Getting Started 4.2
4.2 - Graphics Interface 4.3
4.3 - Availability of BEST-FSI 4.4
4.4 - File System in BEST-FSI 4.5
4.5 - Special Features of BEST-FSI 4.6
4.5.1 - Definitions 4.6
4.5.2 - Mesh Size 4.8
5.0 - BEST-FSI Input 5.1
5.1 - Case Control 5.9
5.1.1 - Case Control Input Card 5.11
5.1.2 - Title 5.12
5.1.3 - Times for Output 5.13
5.1.4 - Dimensionality of the Problem 5.15
5.1.5 - Type of Analysis 5.16
5.1.6 - Analysis Type Modifiers 5.18
5.1.7 - Algorithm Control 5.21
5.1.8 - Geometric and Loading Symmetry Control 5.27
5.1.9 - Restart Facility 5.29
5.1.10 - Output Options 5.31
5.1.11 - Miscellaneous Control Options 5.37

5.2 - Material Property Definition 5.40
5.2.1 - Material Property Input Card 5.43
5.2.2 - Material Identification 5.44
5.2.3 - Mass Parameters 5.45
5.2.4 - Isotropic Elastic Parameters 5.46
5.2.5 - Isotropic Thermal Parameters 5.48
5.2.6 - Isotropic Viscous Parameters 5.51
5.3 - Definition of Geometry 5.52
5.3.1 - Geometry Input Card 5.54
5.3.2 - Region Identification 5.55
5.3.3 - Nodal Point Definition 5.63
5.3.4 - Surface Element Definition 5.65
5.3.5 - Enclosing Element Definition 5.73
5.3.6 - Volume Cell Definition 5.75
5.3.7 - Sampling Point Definition 5.81
5.4 - Definition of GMR Compatibility 5.83
5.4.1 - Interface Definition Input Card 5.85
5.4.2 - Definition of Interface Surface 1 . . . . . 5.87
5.4.3 - Definition of Interface Surface 2 . . . . . 5.90
5.4.4 - Type of Interface Condition 5.93
5.4.5 - Cyclic Symmetry Parameter Definition 5.96
5.4.6 - Additional Interface Control Options 5.100
5.5 - Definition of Boundary Conditions 5.102
5.5.1 - Boundary Condition Set Card 5.104
5.5.2 - Boundary Condition Identification 5.105
5.5.3 - Identification of Boundary Condition Type 5.106
5.5.4 - Definition of Surface for Application of Boundary Conditions . 5.110
5.5.5 - Value Boundary Conditions for Surface Elements 5.118
5.5.6 - Definition Space/Time Variation 5.124

5.5.7 - Relation Boundary Conditions 5.127
5.6 - Body Force Definition 5.129
5.6.1 - Body Force Input Card 5.130
5.6.2 - Inertial Body Force 5.132
5.6.3 - Convective Body Force 5.136
6.0 - Example Problems 6.1
7.0 - PATBEST Interface 7.1
7.1 - Program Description 7.2
7.2 - Getting Started 7.3
7.3 - PATRAN Input Requirements 7.4
7.3.1 - Geometry Input 7.5
7.3.2 - Boundary Condition Input 7.8
7.4 - PATBEST 7.10
8.0 - References 8.1

1.0 INTRODUCTION

As part of the continuing effort at NASA/Lewis to improve both the durability and reliability of hot section Earth-to-Orbit engine components, significant enhancements must be made in existing finite element and finite difference methods, and advanced techniques, such as the boundary element method, must be explored. Despite this considerable effort, the accurate determination of transient thermal stresses in these hot section components remains one of the most difficult problems facing engine design/analysts. For these problems, the temperature distribution is strongly influenced by the external hot gas flow, the internal cooling system, and the structural deformation. Currently, experimentally-determined film coefficients and ambient temperatures are required for use as boundary conditions for the thermal stress analysis of the structural component. The determination of these coefficients is obviously an expensive and time-consuming task. Recently an attempt was made by Gladden (1989) to use a finite difference-based Navier-Stokes code to approximate the thermal boundary conditions, and to then input these into a finite element structural analysis package. However, the most effective way to deal with this problem is to develop a completely integrated solid mechanics, fluid mechanics, and heat transfer approach.

In the present work, the boundary element method (BEM) is chosen as the basic analysis tool principally because the critical surface variables (i.e., temperature, flux, displacement, traction) can be very precisely determined with a boundary-based discretization scheme. Additionally, model preparation is considerably simplified compared to the more familiar domain-based methods. Furthermore, the hyperbolic character of high speed flow is captured through the use of an analytical fundamental solution, eliminating the dependence of the solution on the discretization pattern. The price that must be paid in order to realize these advantages is that any BEM formulation requires a considerable amount of analytical work, which is typically absent in the other numerical methods.

This report details all of the research accomplishments of a multi-year program, commencing in March 1986, aimed toward the development of a boundary element formulation for the study of hot fluid-structure interaction in Earth-to-Orbit engine hot section components. It should be noted that this work represents approximately four man-years of funding from NASA/Lewis. Most of that effort expended under this program has been directed toward the examination of fluid flow, since boundary element methods for fluids are at a much less developed state. However, significant strides have been made, not only in the analysis of thermoviscous fluids, but also in the solution of the fluid-structure interaction problem.

Early in the research program, a two-dimensional boundary element formulation was developed for the time-dependent response of a thermoelastic solid. This effort resulted in the first time domain, boundary-only implementation for this class of problems. Since volume discretization is completely eliminated and surface transient thermal stresses can

be captured very accurately, the new approach provides distinct advantages over standard finite element methods.

Meanwhile, the initial fluid formulations that were developed, based upon Stokes fundamental solutions, provided solutions in the low-to-moderate Reynolds number range. For creeping flow, these reduce to boundary-only techniques. As the fluid velocities are increased, volume discretization is required, however the solutions are typically very precise, particularly in the determination of surface quantities. At very high speed, these formulations are less effective, because the Stokes fundamental solutions no longer embody the character of the flow field which becomes dominated by convection.

This led to the development of convective viscous integral formulations based upon Oseen fundamental solutions. Since the new convective kernel functions, that were developed as a part of this effort, contain more of the physics of the problem, boundary element solutions can now be obtained at very high Reynolds number. Flow around obstacles can be solved approximately with an efficient linearized boundary-only analysis or more exactly by including all of the nonlinearities present in the neighborhood of the obstacle. This perhaps represents the major accomplishment of the present program.

The other significant development has been the creation of a comprehensive fluid-structure interaction capability within a boundary element computer code. This new facility is implemented in a completely general manner, so that quite arbitrary geometry, material properties and boundary conditions may be specified. Thus, a single analysis code can be used to run structures-only problems, fluids-only problems, or the combined fluid-structure problem. In all three cases, steady or transient conditions can be selected, with or without thermal effects. Nonlinear analyses can be solved via direct iteration or by employing a modified Newton-Raphson approach.

Most of the boundary element formulations developed under this grant have been incorporated in the computer code BEST-FSI (Boundary Element Solution Technique for Fluid Structure Interaction). A few of the general features of this code are enumerated in Table 1.1, while Table 1.2 lists some of the major capabilities relating to the analysis of fluid-structure interaction. An effort has been made to develop a reliable, user-friendly code. However, it should be emphasized that the current version of BEST-FSI is primarily a research code. Additional work is needed to produce a practical engineering analysis tool. In particular, significant improvements could be made regarding computational efficiency, since the primary emphasis during the grant was on development of new boundary element capability.

This document is intended to serve multiple purposes. First, it serves as a report summarizing the work developed under this grant. Section 2 provides all of the relevant theoretical background, while numerous applications are discussed in Section 3. It should be noted that all of those examples were run on Sun SPARC workstations. The remainder of the report focuses on the documentation of the computer code BEST-FSI. Section 4 presents a brief introduction for a first-time boundary element user. Complete details of the input data required to execute BEST-FSI are contained in Section 5. Each data item is described individually and examples of use are provided. Then, in Section 6, several sample problems are examined. After each problem is defined, the entire input dataset is

presented, along with selected BEST-FSI output. The interface between BEST-FSI and the graphics package PATRAN^{TM} is discussed in Section 7. Finally, all references are collected in Section 8.

In addition to this User Manual, source code for BEST-FSI has been delivered to NASA. The code is written in FORTRAN 77 and contains considerable documentation in the form of comment lines. This version of BEST-FSI is suitable for use on Sun SPARC-stations. A series of test problems have also been delivered to aid in the verification process and to provide additional assistance to a user during the preparation of BEST-FSI datasets. Included are complete input datasets and BEST-FSI output files.

TABLE 1.1
GENERAL FEATURES OF BEST-FSI

- Two-dimensional problems
- Conforming element approach to provide inter-element continuity of the field variables, along with efficient solutions
- Substructured regions (super-elements) to permit multiple materials and more efficient solutions
- Automatic adaptive numerical integration schemes
- Cyclic and planar symmetry
- Local or global boundary condition specification
- Sliding, frictional spring and resistance-type interfaces
- Exterior domains
- Block banded solver routines based upon LINPACK
- Restart capability for low cost re-analysis
- Free-format, keyword-driven input
- Automatic error checks of input data
- Automatic check of equilibrium and heat balance
- PATRAN^{TM} interfaces for pre- and post-processing

TABLE 1.2

ANALYSIS CAPABILITIES OF BEST-FSI

- Steady thermoelasticity
- Transient (quasistatic) thermoelasticity
- Steady incompressible thermoviscous flow
    - Stokes-based formulations
    - Oseen-based formulations
    - Full Navier-Stokes formulations
- Unsteady incompressible thermoviscous flow
    - Stokes-based formulations
    - Full Navier-Stokes formulations
- Convective heat transfer
- Buoyancy effects
- Fluid-structure Interaction (involving any of the above formulations)

2.0 THEORETICAL BACKGROUND

This section contains a detailed presentation of all of the boundary element formulations developed under this grant. First, in Section 2.1 a brief review of the applicable literature is provided. The remaining sections described the methodology employed for the analysis of thermoelastic deformation, incompressible thermoviscous flow, convective incompressible thermoviscous flow, convective potential flow, compressible thermoviscous flow, and fluid-structure interaction.

2.1 LITERATURE REVIEW

Very little has appeared in the literature on the analysis of coupled thermoviscous fluid-structure problems via the boundary element method. However, a number of publications have addressed the fluid and structure separately.

In general, the solid portion of the problem has been addressed to a much greater degree. For example, a boundary-only steady-state thermoelastic formulation was initially presented by Cruse et al (1977) and Rizzo and Shippy (1977). Recently, the present authors developed and implemented the quasistatic counterpart (Dargush, 1987; Dargush and Banerjee, 1989b, 1990a, 1990b), which is presented in detail in Section 2.2. Others, notably Sharp and Crouch (1986) and Chaudouet (1987), introduce volume integrals, to represent the equivalent thermal body forces. A similar domain based approach was taken earlier by Banerjee and Butterfield (1981) in the context of the analogous geomechanical problem.

An extensive review of the applications of integral formulations to viscous flow problems was included in a previous annual report (Dargush et al, 1987), and will not be repeated here. Interestingly, only a few groups of researchers are actively pursuing the further development of boundary elements for the analysis of viscous fluids. The work reported in Piva and Morino (1987) and Piva et al (1987) focuses heavily on the development of fundamental solutions and integral formulations with little emphasis on implementation. On the other hand, Tosaka and Kakuda (1986, 1987), Tosaka and Onishi (1986) have implemented single region boundary element formulations using approximate incompressible fundamental solutions. This latter group has developed sophisticated non-linear solution algorithms, and consequently, are able to demonstrate moderately high Reynolds number solutions. Meanwhile, Dargush and Banerjee (1991a, 1991b) present general purpose steady and time-dependent boundary element methods for moderate Reynolds number flows.

The most recent work from the above researchers has been collected into a volume entitled Developments in BEM - Volume 6: Nonlinear Problems of Fluid Dynamics, edited by Banerjee and Morino. Contributions from Wu and Wang, and Bush and Tanner are also included, along with two chapters from the present co-authors. The volume, published by Elsevier Applied Science Publishers became available in mid-1990, and provides a state-of-the-art review of boundary element fluid dynamics. However, it should be noted that the convective thermoviscous formulations of Section 2.4 are not included. These represent a significant further advancement which permit solutions for high Reynolds number flows. Interestingly, the basis for much of this latter development is actually work done early in this century by Oseen (1911, 1927).

For analysis of the interaction problem, a boundary element thermoelastic solid representation must be coupled with a suitable thermoviscous fluid formulation. Only Dargush and Banerjee (1988,1989a) have tackled this problem. These two papers provide a summary of the early work performed under this grant.

2.2 THERMOELASTIC DEFORMATION

2.2.1 INTRODUCTION

In the current section, a surface-only time-domain boundary element method (BEM) will be described for a thermoelastic body under quasistatic loading. Thus, transient heat conduction is included, but inertial effects are ignored. This BEM was first developed as part of the work performed during the second year (1987) of this grant. Since that time a number of improvements and extensions have been incorporated. During 1989, the algorithms for numerical integration have been made more efficient as well as more accurate, and a comprehensive PATRAN interface has been added to aid in the post-processing of the boundary element results. Additionally, a streamlined approach for uncoupled thermoelasticity was introduced (Dargush and Banerjee, 1989b). In 1990, boundary elements with a quartic variation of the field variables were implemented. These elements are particularly well suited for problems involving the bending of components (Deb and Banerjee, 1989).

Details of the integral formulation for 2D plane strain is presented below. (Problems of plane stress can be handled via a simple change in material parameters.) Separate subsections present the governing differential equations, the integral equations, and an overview of the numerical implementation. Similar formulations have also been developed for three-dimensional (Dargush and Banerjee, 1990a) and axisymmetric problems (Dargush and Banerjee, 1992).

2.2.2 GOVERNING EQUATIONS

With the solid assumed to be a linear thermoelastic medium, the governing differential equations for transient thermoelasticity can be written

$$(\lambda+\mu)\frac{\partial^2 u_j}{\partial x_i \partial x_j} + \mu\frac{\partial^2 u_i}{\partial x_j \partial x_j} - (3\lambda+2\mu)\alpha\frac{\partial \theta}{\partial x_i} = 0 \qquad (2.2.1a)$$

$$\rho c_\epsilon \frac{\partial \theta}{\partial t} = k\frac{\partial^2 \theta}{\partial x_j \partial x_j} \qquad (2.2.1b)$$

where

- u_i displacement vector
- θ temperature
- t time
- x_i Lagrangian coordinate

k thermal conductivity
ρ mass density
c_ϵ specific heat at constant deformation
λ, μ Lamé constants
α coefficient of thermal expansion

Standard indicial notation has been employed with summations indicated by repeated indices. For two-dimensional problems considered herein, the Latin indices i and j vary from one to two.

Note that (2.2.1b) is the energy equation and that (2.2.1a) represents the momentum balance in terms of displacements and temperature. The theory portrayed by the above set of equations, formally labeled uncoupled quasistatic thermoelasticity, can be derived from thermodynamic principles. (See Boley and Weiner (1960) for details.) In developing (2.2.1), the dynamic effects of interia have been ignored.

2.2.3 INTEGRAL REPRESENTATIONS

Utilizing equation (2.2.1) for the solid along with a generalized form of the reciprocal theorem, permits one to develop the following boundary integral equation:

$$c_{\beta\alpha}(\xi)u_\beta(\xi,t) = \int_S \Big[g_{\beta\alpha} * t_\beta(X,t) - f_{\beta\alpha} * u_\beta(X,t)\Big] dS(X). \tag{2.2.2}$$

where

α, β indices varying from 1 to 3
S surface of solid
u_α, t_α generalized displacement and traction
$u_\alpha = [u_1 \quad u_2 \quad \theta]^T$
$t_\alpha = [t_1 \quad t_2 \quad q]^T$
θ, q temperature, heat flux
$g_{\alpha\beta}, f_{\alpha\beta}$ generalized displacement and traction kernels
$c_{\alpha\beta}$ constants determined by the relative smoothness of S at ξ

and, for example

$$g_{\alpha\beta} * t_\alpha = \int_0^t g_{\alpha\beta}(x,t;\xi,\tau)t_\alpha(x,\tau)d\tau$$

denotes a Riemann convolution integral. The kernel functions $g_{\alpha\beta}$ and $f_{\alpha\beta}$ are derived from the fundamental infinite space solutions of (2.2.1).

In principle, at each instant of time progressing from time zero, this equation can be written at every point on the boundary. The collection of the resulting equations could then be solved simultaneously, producing exact values for all the unknown boundary quantities. In reality, of course, discretization is needed to limit this process to a finite number of

equations and unknowns. Techniques useful for the discretization of (2.2.2) are the subject of the following section.

2.2.4 NUMERICAL IMPLEMENTATION

2.2.4.1 INTRODUCTION

The boundary integral equation (2.2.2), developed in the last section, is an exact statement. No approximations have been introduced other than those used to formulate the boundary value problem. However, in order to apply (2.2.2) for the solution of practical engineering problems, approximations are required in both time and space. In this section, an overview of a general-purpose, state-of-the-art numerical implementation is presented. Many of the features and techniques to be discussed, in this section, were developed previously for elastostatics (e.g., Banerjee et al, 1985, 1988), and elastodynamics (e.g., Banerjee et al, 1986; Ahmad and Banerjee, 1988), but are here adapted for thermoelastic analysis.

2.2.4.2 TEMPORAL DISCRETIZATION

Consider, first, the time integrals represented in (2.2.2) as convolutions. Clearly, without any loss of precision, the time interval from zero to t can be divided into N equal increments of duration Δt.

By assuming that the primary field variables, t_β and u_β, are constant within each Δt time increment, these quantities can be brought outside of the time integral. That is,

$$g_{\beta\alpha} * t_\beta(X,t) = \sum_{n=1}^{N} t_\beta^n(X) \int_{(n-1)\Delta t}^{n\Delta t} g_{\beta\alpha}(X-\xi, t-\tau)d\tau \qquad (2.2.3a)$$

$$f_{\beta\alpha} * u_\beta(X,t) = \sum_{n=1}^{N} u_\beta^n(X) \int_{(n-1)\Delta t}^{n\Delta t} f_{\beta\alpha}(X-\xi, t-\tau)d\tau \qquad (2.2.3b)$$

where the superscript on the generalized tractions and displacements, obviously, represents the time increment number. Notice, also, that, within an increment, these primary field variables are now functions of position only. Next, since the integrands remaining in (2.2.3) are known in explicit form from the fundamental solutions, the required temporal integration can be performed analytically, and written as

$$G_{\beta\alpha}^{N+1-n}(X-\xi) = \int_{(n-1)\Delta t}^{n\Delta t} g_{\beta\alpha}(X-\xi, t-\tau)d\tau \qquad (2.2.4a)$$

$$F^{N+1-n}_{\beta\alpha}(X-\xi) = \int_{(n-1)\Delta t}^{n\Delta t} f_{\beta\alpha}(X-\xi, t-\tau)d\tau. \qquad (2.2.4b)$$

These kernel functions, $G^n_{\beta\alpha}(X-\xi)$ and $F^n_{\beta\alpha}(X-\xi)$, are detailed in Appendix 2.2. Combining (2.2.3) and (2.2.4) with (2.2.2) produces

$$c_{\beta\alpha}(\xi)u^N_\beta(\xi) = \sum_{n=1}^{N}\int_S \left[G^{N+1-n}_{\beta\alpha}(X-\xi)t^n_\beta(X) - F^{N+1-n}_{\beta\alpha}(X-\xi)u^n_\beta(X)\right]dS(X), \qquad (2.2.5)$$

which is the boundary integral statement after the application of the temporal discretization.

2.2.4.3 SPATIAL DISCRETIZATION

With the use of generalized primary variables and the incorporation of a piecewise constant time stepping algorithm, the boundary integral equation (2.2.5) begins to show a strong resemblance to that of elastostatics, particularly for the initial time step (i.e., $N = 1$). In this subsection, those similarities will be exploited to develop the spatial discretization for the uncoupled quasistatic problem with two-dimensional geometry. This approximate spatial representation will, subsequently, permit numerical evaluation of the surface integrals appearing in (2.2.5). The techniques described here, actually, originated in the finite element literature, but were later applied to boundary elements by Lachat and Watson (1976).

The process begins by subdividing the entire surface of the body into individual elements of relatively simple shape. The geometry of each element is, then, completely defined by the coordinates of the nodal points and associated interpolation functions. That is,

$$X(\zeta) = x_i(\zeta) = N_w(\zeta)x_{iw} \qquad (2.2.6)$$

with

- ζ intrinsic coordinates
- N_w shape functions
- x_{iw} nodal coordinates

and where w is an integer varying from one to W, the number of geometric nodes in the element. Next, the same type of representation is used, within the element, to describe the primary variables. Thus,

$$u^n_\alpha(\zeta) = N_\omega(\zeta)u^n_{\alpha\omega} \qquad (2.2.7a)$$

$$t^n_\alpha(\zeta) = N_\omega(\zeta)t^n_{\alpha\omega} \qquad (2.2.7b)$$

in which $u^n_{\alpha\omega}$ and $t^n_{\alpha\omega}$ are the nodal values of the generalized displacement and tractions, respectively, for time step n. Also, in (2.2.7), the integer ω varies from one to Ω, the total

number of functional nodes in the element. From the above, note that the same number of nodes, and consequently shape functions, are not necessarily used to describe both the geometric and functional variations. Specifically, in the present work, the geometry is exclusively defined by quadratic shape functions. In two-dimensions, this requires the use of three-noded line elements. On the other hand, the variation of the primary quantities can be described, within an element, by linear, quadratic or quartic shape functions. For each quartic element, two additional quarter-point nodes are automatically generated by the program. It should be noted that the introduction of quartic elements provides the foundation for the development of a p-adaptive boundary element capability.

Once the spatial discretization has been accomplished and the body has been subdivided into M elements, the boundary integral equation can be rewritten as

$$c_{\beta\alpha}(\xi)u^N_\beta(\xi) = \sum_{n=1}^{N}\left\{\sum_{m=1}^{M}\int_{S_m}\left[G^{N+1-n}_{\beta\alpha}(X(\zeta)-\xi)N_\omega(\zeta)t^n_{\beta\omega} - F^{N+1-n}_{\beta\alpha}(X(\zeta)-\xi)N_\omega(\xi)u^n_{\beta\omega}\right]dS(X(\zeta))\right\} \tag{2.2.8}$$

where

$$S = \bigcup_{m=1}^{M} S_m.$$

In the above equation, $t^n_{\beta\omega}$ and $u^n_{\beta\omega}$ are nodal quantities which can be brought outside the surface integrals. Thus,

$$c_{\beta\alpha}(\xi)u^N_\beta(\xi) = \sum_{n=1}^{N}\left\{\sum_{m=1}^{M} t^n_{\beta\omega}\int_{S_m} G^{N+1-n}_{\beta\alpha}(X(\zeta)-\xi)N_\omega(\zeta)dS(X(\zeta)) - u^n_{\beta\omega}\int_{S_m} F^{N+1-n}_{\beta\alpha}(X(\zeta)-\xi)N_\omega(\zeta)dS(X(\zeta))\right\} \tag{2.2.9}$$

The positioning of the nodal primary variables outside the integrals is, of course, a key step since now the integrands contain only known functions. However, before discussing the techniques used to numerically evaluate these integrals, a brief discussion of the singularities present in the kernels $G^n_{\beta\alpha}$ and $F^n_{\beta\alpha}$ is in order.

The fundamental solutions to the uncoupled quasistatic problem contain singularities when the load point and field point coincide, that is, is when $r = 0$. The same is true of $G^n_{\beta\alpha}$ and $F^n_{\beta\alpha}$, since these kernels are derived directly from the fundamental solutions. Series expansions of terms present in the evolution functions can be used to deduce the level of singularities existing in the kernels.

A number of observations concerning the results of these expansions should be mentioned. First, as would be expected $F^1_{\alpha\beta}$ has a stronger level of singularity than does the corresponding $G^1_{\alpha\beta}$, since an additional derivative is involved in obtaining $F^1_{\alpha\beta}$ from $G^1_{\alpha\beta}$. Second, the coupling terms do not have as a high degree of singularity as do the corresponding non-coupling terms. Third, all of the kernel functions for the first time step could actually be rewritten as a sum of steady-state and transient components. That is,

$$G^1_{\alpha\beta} = {}^{ss}G_{\alpha\beta} + {}^{tr}G^1_{\alpha\beta}$$

$$F^1_{\alpha\beta} = {}^{ss}F_{\alpha\beta} + {}^{tr}F^1_{\alpha\beta}.$$

Then, the singularity is completely contained in the steady-state portion. Furthermore, the singularity in G^1_{ij} and F^1_{ij} is precisely equal to that for elastostatics, while $G^1_{\theta\theta}$ and $F^1_{\theta\theta}$ singularities are identical to those for potential flow. (For two-dimensions, the subscript θ equals three.) This observation is critical in the numerical integration of the $F_{\alpha\beta}$ kernel to be discussed in the next subsection. However, from a physical standpoint, this means that, at any time t, the nearer one moves toward the load point, the closer the quasistatic response field corresponds with a steady-state field. Eventually, when the sampling and load points coincide, the quasistatic and steady-state responses are indistinguishable. As a final item, after careful examination of Appendix 2.2, it is evident that the steady-state components in the kernels $G^n_{\alpha\beta}$ and $F^n_{\alpha\beta}$, with $n > 1$, vanish. In that case, all that remains is a transient portion that contains no singularities. Thus, all singularities reside in the ${}^{ss}G_{\alpha\beta}$ and ${}^{ss}F_{\alpha\beta}$ components of $G^1_{\alpha\beta}$ and $F^1_{\alpha\beta}$, respectively.

2.2.4.4 NUMERICAL INTEGRATION

Having clarified the potential singularities present in the coupled kernels, it is now possible to consider the evaluation of the integrals in equation (2.2.9). That is, for any element m, the integrals

$$\int_{S_m} G^{N+1-n}(X(\zeta) - \xi) N_\omega(\zeta) dS(X(\zeta)) \tag{2.2.10a}$$

$$\int_{S_m} F^{N+1-n}(X(\zeta) - \xi) N_\omega(\zeta) dS(X(\zeta)) \tag{2.2.10b}$$

will be examined. To assist in this endeavor, the following three distinct categories can be identified.

(1) The point ξ does not lie on the element m.
(2) The point ξ lies on the element m, but only non-singular or weakly singular integrals are involved.
(3) The point ξ lies on the element m, and the integral is strongly singular.

In practical problems involving many elements, it is evident that most of the integration occurring in equation (2.2.9) will be of the category (1) variety. In this case, the integrand is always non-singular, and standard Gaussian quadrature formulas can be employed. Sophisticated error control routines are needed, however, to minimize the computational effort for a certain level of accuracy. This non-singular integration is the most expensive part of a boundary element analysis, and, consequently, must be optimized to achieve an efficient solution. In the present implementation, error estimates, based upon the work of Stroud and Secrest (1966), are employed to automatically select the proper order of the quadrature rule. Additionally, to improve accuracy in a cost-effective manner, a graded subdivision of the element is incorporated, especially when ξ is nearby. For two-dimensional problems, the integration order varies from two to twelve, within each of up to four element subdivisions.

Turning next to category (2), one finds that again Gaussian quadrature is applicable, however, a somewhat modified scheme must be utilized to evaluate the weakly singular integrals. This is accomplished in two-dimensional elements via suitable subsegmentation along the length of the element so that the product of shape function, Jacobian and kernel remains well behaved.

Unfortunately, the remaining strongly singular integrals of category (3) exist only in the Cauchy principal value sense and cannot, in general, be evaluated numerically, with sufficient precision. It should be noted that this apparent stumbling block is limited to the strongly singular portions, ${}^{ss}F_{ij}$ and ${}^{ss}F_{\theta\theta}$, of the $F^1_{\alpha\beta}$ kernel. The remainder of $F^1_{\alpha\beta}$, including ${}^{tr}F^1_{ij}$ and ${}^{tr}F^1_{\theta\theta}$, can be computed using the procedures outlined for category (2). However, as will be discussed in the next subsection, even category (3) ${}^{ss}F_{ij}$ and ${}^{ss}F_{\theta\theta}$ kernels can be accurately determined by employing an indirect 'rigid body' method originally developed by Cruse (1974).

2.2.4.5 ASSEMBLY

The complete discretization of the boundary integral equation, in both time and space, has been described, along with the techniques required for numerical integration of the kernels. Now, a system of algebraic equations can be developed to permit the approximate solution of the original quasistatic problem. This is accomplished by systematically writing (2.2.9) at each global boundary node. The ensuing nodal collocation process, then, produces a global set of equations of the form

$$\sum_{n=1}^{N}\left(\left[G^{N+1-n}\right]\{t^n\}-\left[F^{N+1-n}\right]\{u^n\}\right)=\{0\}, \tag{2.2.11}$$

where

$[G^{N+1-n}]$ unassembled matrix of size $(d+1)P\times(d+1)Q$, with coefficients determined from (2.2.10a)

$[F^{N+1-n}]$ assembled matrix of size $(d+1)P\times(d+1)P$, with coefficients determined from (2.2.10b) and $c_{\beta\alpha}$ included in the diagonal blocks

$\{t^n\}$ global generalized nodal traction vector with $(d+1)Q$ components

$\{u^n\}$ global generalized nodal displacement vector with $(d+1)P$ components

$\{0\}$ null vector with $(d+1)P$ components

P total number of global functional nodes

$Q=\sum_{m=1}^{M}A_m$

A_m number of functional nodes in element m

d dimensionality of the problem.

In the above, recall that the terms generalized displacement and traction refer to the inclusion of the temperature and flux, respectively, as the $(d+1)$ component at any point.

Consider, now, the first step. Thus, for $N = 1$, equation (2.2.11) becomes

$$[G^1]\{t^1\} - [F^1]\{u^1\} = \{0\}. \tag{2.2.12}$$

However, at this point the diagonal block of $[F^1]$ has not been completely determined due to the strongly singular nature of ${}^{ss}F_{ij}$ and ${}^{ss}F_{\theta\theta}$. Following Cruse (1974) and, later, Banerjee et al (1986) in elastodynamics, these diagonal contributions can be calculated indirectly by imposing a uniform 'rigid body' generalized displacement field on the same body, but under steady-state conditions. Then, obviously, the generalized tractions must be zero, and

$$[{}^{ss}F]\{1\} = \{0\}, \tag{2.2.13}$$

where $\{1\}$ is a vector symbolizing a unit uniform motion. Using (2.2.13), the desired diagonal blocks, ${}^{ss}F_{ij}$ and ${}^{ss}F_{\theta\theta}$, can be obtained from the summation of the off-diagonal terms of $[{}^{ss}F]$. The remaining transient portion of the diagonal block is non-singular, and hence can be evaluated to any desired precision. After summing the steady-state and transient contributions, (2.2.12) is once again written as

$$[G^1]\{t^1\} - [F^1]\{u^1\} = \{0\}, \tag{2.2.14}$$

but now the evaluation of $[F^1]$ is complete.

In a well-posed problem, at time Δt, the set of global generalized nodal displacements and tractions will contain exactly $(d+1)P$ unknown components. Then, as the final stage in the assembly process, equation (2.2.14) can be rearranged to form

$$[A^1]\{x^1\} = [B^1]\{y^1\}, \tag{2.2.15}$$

in which

$\{x^1\}$ unknown components of $\{u^1\}$ and $\{t^1\}$

$\{y^1\}$ known components of $\{u^1\}$ and $\{t^1\}$

$[A^1], [B^1]$ associated matrices

2.2.4.6 SOLUTION

To obtain a solution of (2.2.15) for the unknown nodal quantities, a decomposition of matrix $[A^1]$ is required. In general, $[A^1]$ is a densely populated, unsymmetric matrix. The out-of-core solver, utilized here, was developed originally for elastostatics from the LINPACK software package (Dongarra et al, 1979) and operates on a submatrix level. Within each submatrix, Gaussian elimination with single pivoting reduces the block to upper triangular form. The final decomposed form of $[A^1]$ is stored in a direct-access file

for reuse in subsequent time steps. Backsubstitution then completes the determination of $\{x^1\}$. Additional information on this solver is available in Banerjee et al (1985).

After turning from the solver routines, the entire nodal response vectors, $\{u^1\}$ and $\{t^1\}$, at time Δt are known. For solutions at later times, a simple marching algorithm is employed. Thus, from (2.2.11) with $N = 2$,

$$[G^1]\{t^1\} - [F^1]\{u^1\} + [G^1]\{t^2\} - [F^1]\{u^2\} = \{0\}. \tag{2.2.16}$$

Assuming that the same set of nodal components are unknown as in (2.2.14) for the first time step, equation (2.2.16) is reformulated as

$$[A^1]\{x^2\} = [B^1]\{y^2\} - [G^2]\{t^1\} + [F^2]\{u^1\}. \tag{2.2.17}$$

Since, at this point, the right-hand side contains only known quantities, (2.2.17) can be solved for $\{x^2\}$. However, the decomposed form of $[A^1]$ already exists on a direct-access file, so only the relatively inexpensive backsubstitution phase is required for the solution.

The generalization of (2.2.17) to any time step N is simply

$$[A^1]\{x^N\} = [B^1]\{y^N\} - \sum_{n=1}^{N-1} \left([G^{N+1-n}]\{t^n\} - [F^{N+1-n}]\{u^n\} \right) \tag{2.2.18}$$

in which the summation represents the effect of past events. By systematically storing all of the matrices and nodal response vectors computed during the marching process, surprisingly little computing time is required at each new time step. In fact, for any time step beyond the first, the only major computational task is the integration needed to form $[G^N]$ and $[F^N]$. Even this process is somewhat simplified, since now the kernels are non-singular. As a result, reduced subsegmentation and gaussian integration order is appropriate. Also, as time marches on, the effect of events that occurred during the first time step diminishes. Consequently, the terms containing $[G^N]$ and $[F^N]$ will eventually become insignificant compared to those associated with recent events. Once that point is reached, further integration is unnecessary, and a significant reduction in the computing effort per time step can be achieved.

It should be emphasized that the entire boundary element method developed, in this section, has involved surface quantities exclusively. A complete solution to the well-posed linear uncoupled quasistatic problem, with homogeneous properties, can be obtained in terms of the nodal response vectors, without the need for any volume discretization. In many practical situations, however, additional information, such as, the temperature at interior locations or the stress at points on the boundary, is required. The next subsection discusses the calculations of these quantities.

2.2.4.7 INTERIOR QUANTITIES

Once equation (2.2.18) is solved, at any time step, the complete set of primary nodal quantities, $\{u^n\}$ and $\{t^N\}$, is known. Subsequently, the response at points within the body

can be calculated in a straightforward manner. For any point ξ in the interior, the generalized displacement can be determined from (2.2.9) with $c_{\beta\alpha} = \delta_{\beta\alpha}$. That is,

$$u^n_\alpha(\xi) = \sum_{n=1}^{N} \Big\{ \sum_{m=1}^{M} \Big[t^n_{\beta\omega} \int_{S_m} G^{N+1-n}_{\beta\alpha}(X(\zeta) - \xi) N_\omega(\zeta) dS(X(\zeta)) - u^n_{\beta\omega} \int_{S_m} F^{N+1-n}_{\beta\alpha}(X(\zeta) - \xi) N_\omega(\zeta) dS(X(\zeta)) \Big] \Big\}. \tag{2.2.19}$$

Now, all the nodal variables on the right-hand side are known, and, as long as, ξ is not on the boundary, the kernel functions in (2.2.19) remain non-singular. However, when ξ is on the boundary, the strong singularity in ${}^{ss}F_{\beta\alpha}$ prohibits accurate evaluation of the generalized displacement via (2.2.19), and an alternate approach is required. The apparent dilemma is easily resolved by recalling that the variation of surface quantities is completely defined by the elemental shape functions. Thus, for boundary points, the desired relationship is simply

$$u^N_\alpha(\xi) = N_\omega(\zeta) u^N_{\alpha\omega} \tag{2.2.20}$$

where $N_\omega(\zeta)$ are the shape functions for the appropriate element and ζ are the intrinsic coordinates corresponding to ξ within that element. Obviously, from (2.2.20), neither integration nor the explicit contribution of past events are needed to evaluate generalized boundary displacements.

In many problems, additional quantities, such a heat flux and stress, are also important. The boundary integral equation for heat flux, can be written

$$q^N_i(\xi) = \sum_{n=1}^{N} \Big\{ \sum_{m=1}^{M} \Big[t^n_{\beta\omega} \int_{S_m} E^{N+1-n}_{\beta\theta i}(X(\zeta) - \xi) N_\omega(\zeta) dS(X(\zeta)) - u^n_{\beta\omega} \int_{S_m} D^{N+1-n}_{\beta\theta i}(X(\zeta) - \xi) N_\omega(\zeta) dS(X(\zeta)) \Big] \Big\}. \tag{2.2.21}$$

where

$$E^n_{\beta\theta i}(X(\zeta) - \xi) = -k \frac{\partial G^n_{\beta\theta}(X(\zeta) - \xi)}{\partial \xi_i} \tag{2.2.21a}$$

$$D^n_{\beta\theta i}(X(\zeta) - \xi) = -k \frac{\partial F^n_{\beta\theta}(X(\zeta) - \xi)}{\partial \xi_i} \tag{2.2.21b}$$

This is valid for interior points, whereas, when ξ is on the boundary, the shape functions can again be used. In this latter case,

$$N_\omega(\zeta) q^N_\omega = n_i(\xi) q^N_i(\xi) \tag{2.2.22a}$$

$$\frac{\partial N_\omega(\zeta)}{\partial \zeta} \theta^N_\omega = -\frac{1}{k} \frac{\partial x_i}{\partial \zeta} q^N_i(\xi), \tag{2.2.22b}$$

which can be solved for boundary flux. Meanwhile, interior stresses can be evaluated from

$$\sigma^N_{ij}(\xi) = \sum_{n=1}^{N} \Big\{ \sum_{m=1}^{M} \Big[t^n_{\beta\omega} \int_{S_m} E^{N+1-n}_{\beta ij}(X(\zeta) - \xi) N_\omega(\zeta) dS(X(\zeta)) - u^n_{\beta\omega} \int_{S_m} D^{N+1-n}_{\beta ij}(X(\zeta) - \xi) N_\omega(\zeta) dS(X(\zeta)) \Big] \Big\} \tag{2.2.23}$$

in which

$$E^n_{\beta ij}(X(\zeta)-\xi) = \frac{2\mu\nu}{1-2\nu}\delta_{ij}\frac{\partial G^n_{\beta\ell}}{\partial \xi_\ell} + \mu\left(\frac{\partial G^N_{\beta i}}{\partial \xi_j} + \frac{\partial G^N_{\beta j}}{\partial \xi_i}\right) - \beta\delta_{ij}G^n_{\beta\theta} \tag{2.2.23a}$$

$$D^n_{\beta ij}(X(\zeta)-\xi) = \frac{2\mu\nu}{1-2\nu}\delta_{ij}\frac{\partial F^n_{\beta\ell}}{\partial \xi_\ell} + \mu\left(\frac{\partial F^N_{\beta i}}{\partial \xi_j} + \frac{\partial F^N_{\beta j}}{\partial \xi_i}\right) - \beta\delta_{ij}F^n_{\beta\theta}, \tag{2.2.23b}$$

with ν representing the Poisson ratio and $\beta = (3\lambda+2\mu)\alpha$. Equation (2.2.23) is, of course, developed from (2.2.19). Since strong kernel singularities appear when (2.2.23) is written for boundary points, once again an alternate procedure is needed to determine surface stress. This alternate scheme exploits the interrelationships between generalized displacement, traction, and stress and is the straightforward extension of the technique typically used in elastostatic implementation (Cruse and Van Buren, 1971). Specifically, the following can be obtained

$$n_j(\xi)\sigma^N_{ij}(\xi) = N_\omega(\zeta)t^N_{i\omega} \tag{2.2.24a}$$

$$\sigma^N_{ij}(\xi) - \frac{D^e_{ijkl}}{2}\left(u^N_{k,l}(\xi) + u^N_{l,k}(\xi)\right) = -\beta\delta_{ij}N_\omega(\zeta)u^N_{\theta\omega} \tag{2.2.24b}$$

$$\frac{\partial x_j}{\partial \zeta}u^N_{i,j}(\xi) = \frac{\partial N_\omega}{\partial \zeta}u^N_{i\omega} \tag{2.2.24c}$$

in which $u^N_{\theta\omega}$ is obviously the nodal temperatures, and,

$$D^e_{ijkl} = \lambda\delta_{ij}\delta_{kl} + 2\mu\delta_{ik}\delta_{jl}.$$

Equations (2.2.24) form an independent set that can be solved numerically for $\sigma^N_{ij}(\xi)$ and $u^N_{i,j}(\xi)$ completely in terms of known nodal quantities $u^N_{\alpha\omega}$ and $t^N_{\alpha\omega}$, without the need for kernel integration nor convolution. Notice, however, that shape function derivatives appear in (2.2.24c), thus constraining the representation of stress on the surface element to something less than full quadratic variation. The interior stress kernel functions, defined by (2.2.23), are also detailed in Appendix 2.2.

2.2.4.8 ADVANCED FEATURES

The thermoelastic formulation has been implemented as a segment of the general purpose boundary element computer program, BEST-FSI. Consequently, many additional features, beyond those detailed above, are available for the analysis of complex engineering problems. Perhaps, the most significant of these items, is the capability to analyze substructured problems. This, not only extends the analysis to bodies composed of several different materials, but also often provides computational efficiencies. An individual substructure or geometric modeling region (GMR) must contain a single material. During the integration process, each GMR remains a separate entity. The GMR's are then brought together at the assembly stage, where compatibility relationships are enforced on common boundaries between regions. Typically, compatibility ensures continuous displacement and temperature fields across an interface, however, recent enhancements to the code permit

sliding between regions, spring contacts and interfacial thermal resistance to model air gaps or coating resistances. In the latter instances, discontinuities appear at the interface. In any case, the multi-GMR assembly process produces block-banded system matrices that are solved in an efficient manner.

As another feature, a high degree of flexibility is provided for the specification of boundary conditions. In general, time-dependent values can be defined in either global or local coordinates. Not only can generalized displacements and tractions be specified, but also spring and convection boundary conditions are available. Another recent addition permits time-dependent ambient temperatures. A final item, worthy of note, is the availability of a comprehensive symmetry capability which includes provisions for both planar and cyclic symmetry.

During the past three years, an interface to the well-known PATRAN graphics package was developed and enhanced. This interface allows the user an option to view deformed shapes, temperatures and stress boundary profiles or contours. A number of PATRAN-produced illustrations are included throughout this manual. Several examples are presented in Section 3 to demonstrate the validity and applicability of this boundary-only formulation.

APPENDIX 2.2
KERNEL FUNCTIONS

This appendix contains the detailed presentations of all the kernel functions utilized in the formulations contained in Section 2.2. Two-dimensional (plane strain) kernels are provided, based upon continuous source and force fundamental solutions. For time-dependent uncoupled quasistatic thermoelasticity the following relationships must be used to determine the proper form of the functions required in the boundary element discretization. That is,

$$G^n_{\alpha\beta}(X-\xi) = G_{\alpha\beta}(X-\xi, n\Delta t) \qquad \text{for } n = 1$$
$$G^n_{\alpha\beta}(x-\xi) = G_{\alpha\beta}(X-\xi, n\Delta t) - G_{\alpha\beta}X-\xi, (n-1)\Delta t) \qquad \text{for } n > 1,$$

with similar expressions holding for all the remaining kernels. In the specification of these kernels below, the arguments $(X-\xi, t)$ are assumed. The indices

i, j, k, l	vary from 1 to d
α, β	vary from 1 to $(d+1)$
θ	equals $d+1$

where d is the dimensionality of the problem. Additionally,

x_i	coordinates of integration point
ξ_i	coordinates of field point
$y_i = x_i - \xi_i$	$r^2 = y_i y_i$.

For the displacement kernel,

$$G_{ij} = \frac{1}{8\pi}\frac{1}{\mu(1-\nu)}\left[\left(\frac{y_i y_j}{r^2}\right) - (\delta_{ij})(3-4\nu)lnr\right]$$
$$G_{i\theta} = 0$$
$$G_{\theta j} = \frac{r}{2\pi}\left(\frac{\beta}{k(\lambda+2\mu)}\right)\left[\left(\frac{y_j}{r}\right)\bar{g}_4(\eta)\right]$$
$$G_{\theta\theta} = \frac{1}{2\pi}\left(\frac{1}{k}\right)[\bar{g}_5(\eta)]$$

whereas, for the traction kernel,

$$F_{ij} = \frac{1}{4\pi r}\frac{1}{(1-\nu)}\left[-\left(\frac{2y_i y_j y_k n_k}{r^3}\right) - \left(\frac{\delta_{ij}y_k n_k + y_i n_j}{r}\right)(1-2\nu) + \left(\frac{y_j n_i}{r}\right)(1-2\nu)\right]$$
$$F_{i\theta} = 0$$
$$F_{\theta j} = \frac{1}{4\pi}\left(\frac{\beta}{\lambda+2\mu}\right)\left[\left(\frac{y_j y_k n_k}{r^2}\right)\bar{f}_6(\eta) - (n_j)\bar{f}_7(\eta)\right]$$
$$F_{\theta\theta} = \frac{1}{2\pi r}\left[\left(\frac{y_k n_k}{r}\right)\bar{f}_8(\eta)\right].$$

In the above,

$$\eta = \frac{r}{(ct)^{1/2}}$$

$$c = \frac{k}{\rho c_e}$$

$$E_1(z) = \int_z^\infty \frac{e^{-x}}{x} dx$$

$$\bar{h}_1(\eta) = \frac{4}{\eta^2}\left(1 - e^{-\eta^2/4}\right)$$

$$\bar{g}_4(\eta) = \frac{\bar{h}_1(\eta)}{2} + \frac{E_1\left(\frac{\eta^2}{4}\right)}{2}$$

$$\bar{g}_5(\eta) = \frac{E_1\left(\frac{\eta^2}{4}\right)}{2}$$

$$\bar{f}_6(\eta) = \bar{h}_1(\eta)$$

$$\bar{f}_7(\eta) = \frac{\bar{h}_1(\eta)}{2} + \frac{E_1\left(\frac{\eta^2}{4}\right)}{2}$$

$$\bar{f}_i(\eta) = e^{-\eta^2/4}.$$

For the interior stress kernels,

$$E_{\beta ij} = \frac{2\mu\nu}{1-2\nu}\delta_{ij}\frac{\partial G_{\beta l}}{\partial \xi_l} + \mu\left(\frac{\partial G_{\beta i}}{\partial \xi_j} + \frac{\partial G_{\beta j}}{\partial \xi_i}\right) - \beta\delta_{ij}G_{\beta\theta}$$

$$D_{\beta ij} = \frac{2\mu\nu}{1-2\nu}\delta_{ij}\frac{\partial F_{\beta l}}{\partial \xi_l} + \mu\left(\frac{\partial F_{\beta i}}{\partial \xi_j} + \frac{\partial F_{\beta j}}{\partial \xi_i}\right) - \beta\delta_{ij}F_{\beta\theta}$$

where

$$\frac{\partial G_{ij}}{\partial \xi_k} = \frac{1}{8\pi r}\frac{1}{\mu(1-\nu)}\left[\left(\frac{2y_iy_ky_k}{r^3} - \frac{\delta_{jk}y_i}{r} - \frac{\delta_{ik}y_j}{r}\right) + \left(\frac{\delta_{ij}y_k}{r}\right)(3-4\nu)\right]$$

$$\frac{\partial G_{\theta j}}{\partial \xi_k} = \frac{1}{4\pi}\left(\frac{\beta}{k(\lambda+2\mu)}\right)\left[\left(\frac{y_jy_k}{r^2}\right)\{\bar{h}_1\} - (\delta_{jk})\left\{\frac{\bar{h}_1}{2} + \frac{E_1}{2}\right\}\right]$$

$$\frac{\partial F_{ij}}{\partial \xi_k} = \frac{1}{4\pi r^2}\frac{1}{(1-\nu)}\left[-\left(\frac{4y_iy_jy_ky_ln_l}{r^4} - \frac{y_iy_jn_k}{r^2} - \frac{\delta_{jk}y_iy_ln_l}{r^2}\right.\right.$$

$$\left. - \frac{\delta_{ik}y_jy_ln_l}{r^2}\right)\bar{f}_1(\eta) - \left(\frac{2\delta_{ij}y_ky_ln_l}{r^2} - \delta_{ij}n_k + \frac{2y_iy_kn_j}{r^2} - \delta_{ik}n_j\right)\bar{f}_2(\eta)$$

$$\left. + \left(\frac{2y_jy_kn_i}{r^2} - \delta_{jk}n_i\right)\bar{f}_3(\eta)\right]$$

$$\frac{\partial F_{\theta j}}{\partial \xi_k} = \frac{1}{4\pi r}\left(\frac{\beta}{\lambda+2\mu}\right)\left[\left(\frac{2y_jy_ky_ln_l}{r^3}\right)\{2\bar{h}_1 - e^{-\eta^2/4}\} - \left(\frac{y_kn_j}{r} + \frac{y_jn_k}{r} + \frac{\delta_{jk}y_ln_l}{r}\right)\{\bar{h}_1\}\right].$$

$$\bar{f}_1(\eta) = 2$$

$$\bar{f}_2(\eta) = 1 - 2\nu$$

$$\bar{f}_3(\eta) = 1 - 2\nu$$

2.3 INCOMPRESSIBLE THERMOVISCOUS FLOW

2.3.1 INTRODUCTION

In the following, steady and time-dependent formulations are presented for relatively slow incompressible flow. The primary variables in each case are velocity, temperature, traction and heat flux. This is the set of variables for which boundary conditions are most readily defined, and for which the extension to three-dimensions is most easily accomplished. As will be seen, the individual formulations have much in common. The major differences involve the fundamental solutions that are employed, and the treatment of the contributions of past events. Both formulations have been implemented within the computer code BEST-FSI.

2.3.2 GOVERNING EQUATIONS

Application of the Principles of the Conservation of Mass, Momentum and Energy for an incompressible thermoviscous fluid lead to the development of the following differential equations:

$$\frac{\partial v_i}{\partial x_i} = 0 \tag{2.3.1a}$$

$$\mu \frac{\partial^2 v_i}{\partial x_j \partial x_j} - \frac{\partial p}{\partial x_i} - \rho \frac{Dv_i}{Dt} + f_i = 0 \tag{2.3.1b}$$

$$k \frac{\partial^2 \theta}{\partial x_j \partial x_j} - \rho c_\epsilon \frac{D\theta}{Dt} + \psi = 0 \tag{2.3.1c}$$

where

- x_i Eulerian coordinate
- t time
- v_i velocity vector
- p pressure
- θ temperature
- ρ mass density
- μ viscosity
- k thermal conductivity
- c_ϵ specific heat
- f_i body force
- ψ body source,

and the operator

$$\frac{D}{Dt} = \frac{\partial}{\partial t} + v_j \frac{\partial}{\partial x_j} \tag{2.3.2}$$

represents a material time derivative. By introducing a constant free stream velocity U_i and a velocity perturbation u_i, such that

$$v_i = U_i + u_i, \tag{2.3.3}$$

the governing equations can be rewritten as

$$\frac{\partial u_i}{\partial x_i} = 0 \tag{2.3.4a}$$

$$\mu \frac{\partial^2 u_i}{\partial x_j \partial x_j} - \frac{\partial p}{\partial x_i} - \rho \frac{\partial u_i}{\partial t} - \rho U_j \frac{\partial u_i}{\partial x_j} - \rho u_j \frac{\partial u_i}{\partial x_j} + f_i = 0 \tag{2.3.4b}$$

$$k \frac{\partial^2 \theta}{\partial x_j \partial x_j} - \rho c_\epsilon \frac{\partial \theta}{\partial t} - \rho c_\epsilon U_j \frac{\partial \theta}{\partial x_j} - \rho c_\epsilon u_j \frac{\partial \theta}{\partial x_j} + \psi = 0. \tag{2.3.4c}$$

Note that in equations (2.3.4) only the terms $\rho u_j \frac{\partial u_i}{\partial x_j}$ and $\rho c_\epsilon u_j \frac{\partial \theta}{\partial x_j}$ are actually nonlinear, although in some instances the body forces and sources may also contain nonlinearities. A number of distinct integral formulations are possible, depending upon which of the linear terms are included in the differential operator. All terms excluded from the differential operator, must then be grouped together as effective body forces and sources, f_i' and ψ', respectively. Integral formulations based upon Stokes kernels are detailed in the next subsection.

2.3.3 INTEGRAL REPRESENTATIONS

2.3.3.1 STEADY

In this first formulation the time-dependent terms vanish, and the entire contribution of the convective terms are considered as effective body forces and sources. Thus,

$$f_i' = -\rho U_j \frac{\partial u_i}{\partial x_j} - \rho u_j \frac{\partial u_i}{\partial x_j} + f_i \tag{2.3.5a}$$

$$\psi' = -\rho c_\epsilon U_j \frac{\partial \theta}{\partial x_j} - \rho c_\epsilon u_j \frac{\partial \theta}{\partial x_j} + \psi. \tag{2.3.5b}$$

As a result, the well-known fundamental solutions for incompressible Stokes flow and steady-state heat conduction are applicable. The integral formulation, which can be derived directly from the governing differential equation (Dargush and Banerjee, 1990b), can be written

$$c_{\alpha\beta} u_\alpha = \int_S [G_{\alpha\beta} t_\alpha - F_{\alpha\beta} u_\alpha - G_{\alpha\beta} t_\alpha^\circ] \, dS + \int_V [D_{\alpha\beta k} \sigma_{k\alpha}^\circ + G_{\alpha\beta} f_\alpha] \, dV \tag{2.3.6}$$

where

$$u_\alpha = \{u_1 \quad u_2 \quad \theta\} \tag{2.3.7a}$$

$$t_\alpha = \{t_1 \quad t_2 \quad q\} \tag{2.3.7b}$$

$$f_\alpha = \{f_1 \quad f_2 \quad \psi\} \tag{2.3.7c}$$

are generalized velocities, tractions, and body forces. In (2.3.7b), t_i are the surface tractions defined by

$$t_i = \tau_{ij} n_j - p n_i \tag{2.3.8a}$$

with n_i representing the local unit outward normal to the surface S, and τ_{ij} the fluid stresses, while the heat flux is defined via

$$q = -k \frac{\partial \theta}{\partial x_i} n_i. \tag{2.3.8b}$$

Furthermore,

$$c_{\alpha\beta} = \begin{bmatrix} c_{ij} & 0 \\ 0 & c_{\theta\theta} \end{bmatrix} \quad , \quad G_{\alpha\beta} = \begin{bmatrix} G_{ij} & 0 \\ 0 & G_{\theta\theta} \end{bmatrix} \quad , \quad F_{\alpha\beta} = \begin{bmatrix} F_{ij} & 0 \\ 0 & F_{\theta\theta} \end{bmatrix} \tag{2.3.9a,b,c}$$

$$D_{\alpha\beta k} = \frac{\partial G_{\alpha\beta}}{\partial x_k} \tag{2.3.9d}$$

$$\sigma^{\circ}_{k\alpha} = [\rho(U_k + u_k)u_i \qquad \rho c_\epsilon (U_k + u_k)\theta] \tag{2.3.10a}$$

$$t^{\circ}_{\alpha} = \sigma^{\circ}_{k\alpha} n_k. \tag{2.3.10b}$$

In the terminology of Lighthill (1952), σ°_{ki} is the momentum flux tensor or fluctuating Reynolds stress. Here, $\sigma^{\circ}_{k\alpha}$ is labeled the generalized convective stress tensor, while t°_{α} is the generalized convective traction. Both $\sigma^{\circ}_{k\alpha}$ and t°_{α} contain terms which are nonlinear in the generalized velocities.

In (2.3.9a), $c_{ij}(\xi)$ and $c_{\theta\theta}(\xi)$ are constants. When ξ is inside $S, c_{ij} = \delta_{ij}$ and $c_{\theta\theta} = 1$. If ξ is on the boundary then the values are determined by the relative smoothness of S at ξ. For ξ outside the region V, both c_{ij} and $c_{\theta\theta}$ are zero. Meanwhile, the kernel functions $G_{ij}, G_{\theta\theta}, F_{ij}$ and $F_{\theta\theta}$ are provided in Appendix 2.3.1.

2.3.3.2 TIME-DEPENDENT

For this next formulation, the effective body forces and sources are identical to those provided in (2.3.5), however, the time-dependent terms are now included in the linear operator. The required fundamental solution for the viscous portion was first given by Oseen (1927), while the transient heat conduction fundamental solution is well-known (Carslaw and Jaeger, 1959). By applying standard methodology (Banerjee and Butterfield, 1981; Dargush and Banerjee, 1990c), the following governing integral equations can be derived

$$c_{\alpha\beta} u_\alpha = \int_S [g_{\alpha\beta} * t_\alpha - f_{\alpha\beta} * u_\alpha - g_{\alpha\beta} * t^{\circ}_{\alpha}] \, dS + \int_V [d_{\alpha\beta k} * \sigma^{\circ}_{k\alpha} + g_{\alpha\beta} * f_\alpha - g_{\alpha\beta} \rho u^{\circ}_{\alpha}] \, dV \tag{2.3.11}$$

Note that (2.3.11) is similar to (2.3.6) for the steady case, except that Riemann convolution integrals over time have been introduced, along with an initial condition volume integral involving u°_{α}. Once again $\sigma^{\circ}_{k\alpha}$ and t°_{α} contain terms which are nonlinear in the generalized velocities. Kernel functions, $G_{\alpha\beta}$ and $F_{\alpha\beta}$, developed from the instantaneous point force and

source adjoint fundamental solutions $g_{\alpha\beta}$ and $f_{\alpha\beta}$, are provided in Appendix 2.3.2. It should be noted that these functions are considerably more complicated than the corresponding steady kernels.

2.3.4 NUMERICAL IMPLEMENTATION

2.3.4.1 INTRODUCTION

Analytical solutions are possible for only the simplest geometries and boundary conditions. More generally, approximations must be introduced in both time and space to expose the practical utility of these integral equations. Consequently, in this section, state-of-the-art boundary element technology is applied to steady and unsteady incompressible thermoviscous flows. Recent boundary element developments in the fields of elastodynamics (Banerjee et al, 1986; Ahmad and Banerjee, 1988) and thermoelasticity (Dargush and Banerjee, 1989b, 1990a) are directly applicable for these problems. The presentation below will concentrate on those aspects of the numerical implementation which differ from that detailed in Section 2.2. The current implementation is limited to the two-dimensional case, although certainly both of the integral formulations presented in the previous subsection are equally valid in three dimensions.

2.3.4.2 TEMPORAL AND SPATIAL DISCRETIZATION

For time-dependent problems, the total time interval from zero to τ is subdivided into N equal increments of duration $\Delta\tau$. Then, the field variables $t_\alpha, u_\alpha, t^o_\alpha$, and $\sigma^o_{k\alpha}$ are assumed constant within each $\Delta\tau$ time increment. As a result,

$$g_{\alpha\beta} * t_\alpha \cong \sum_{n=1}^{N} t^n_\alpha \int_{(n-1)\Delta\tau}^{n\Delta\tau} g_{\alpha\beta} dt = \sum_{n=1}^{N} t^n_\alpha G^{N-n+1}_{\alpha\beta} \tag{2.3.12}$$

with similar expressions holding for the remaining convolution integrals. This is identical to the treatment discussed in Section 2.2 for thermoelasticity.

The methodology employed for spatial discretization of the bounding surface also follows that described in Section 2.2. Thus, linear, quadratic or quartic shape functions are utilized to portray the functional behavior of the field variables over surface elements with three geometric nodes, as shown in Figure 2.3.1.

However, in addition to the surface description, the domain must be discretized into cells in the regions where the nonlinear convective effects are important, or where nonzero initial conditions are present. Shape functions are once again introduced to approximate the geometric and functional variation with each volume cell. Thus, for any point X within an individual cell

$$x_i(\zeta) = M_w(\zeta) x_{iw} \tag{2.3.13}$$

and

$$\sigma^{\circ}_{i\alpha}(\zeta) = M_{\omega}(\zeta)\sigma^{\circ}_{i\alpha\omega} \tag{2.3.14}$$

where

M_w, M_ω shape functions

x_{iw} nodal coordinates

$\sigma^{\circ}_{i\alpha\omega}$ nodal generalized convective stress .

The current implementation utilizes six and eight-noded cells for the geometric representation, along with linear, quadratic, or quartic functional variation. Typical cells are depicted in Figure 2.3.2. For the quadratic cell, both serendipity (8-noded) and lagrangian (9-noded) variations are included. Serendipity quartic cells were found to have unsatisfactory performance and consequently are not available.

As a result of the spatial discretization, the boundary integral equation for time-dependent thermoviscous flow can now be written

$$c_{\alpha\beta}u^N_{\alpha} = \sum_{n=1}^{N}\left\{\sum_{m=1}^{M}\left[t^n_{\alpha\omega}\int_{S_m} G^{N-n+1}_{\alpha\beta}N_{\omega}dS - u^n_{\alpha\omega}\int_{S_m} F^{N-n+1}_{\alpha\beta}N_{\omega}dS - t^{on}_{\alpha\omega}\int_{S_m} G^{N-n+1}_{\alpha\beta}N_{\omega}dS\right]\right.$$
$$\left. + \sum_{l=1}^{L}\left[\sigma^{on}_{k\alpha\omega}\int_{V_l} D^{N-n+1}_{\alpha\beta k}M_{\omega}dV\right]\right\} + \sum_{l=1}^{L}\left[\rho u^{\circ}_{\alpha\omega}\int_{V_l} g^N_{\alpha\beta}M_{\omega}dV\right] \tag{2.3.15a}$$

while for steady conditions this reduces to

$$c_{\alpha\beta}u_{\alpha} = \sum_{m=1}^{M}\left[t_{\alpha\omega}\int_{S_m} G_{\alpha\beta}N_{\omega}dS - u_{\alpha\omega}\int_{S_m} F_{\alpha\beta}N_{\omega}dS - t^{\circ}_{\alpha\omega}\int_{S_m} G_{\alpha\beta}N_{\omega}dS\right]$$
$$+ \sum_{l=1}^{L}\left[\sigma^{\circ}_{k\alpha\omega}\int_{V_l} D_{\alpha\beta k}M_{\omega}dV\right], \tag{2.3.15b}$$

where M and L are the total number of surface elements and volume cells, respectively, and

$$S = \bigcup_{m=1}^{M} S_m \tag{2.3.16a}$$

$$V = \bigcup_{l=1}^{L} V_l. \tag{2.3.16b}$$

The positioning of the nodal variables outside of the integrals is a key step, since now the integrands of (2.3.15) contain only known functions, which can be evaluated numerically.

Up to this juncture, the region of interest has been assumed to be composed of a single volume V with surface S. However, this need not be the case. In general, space may be subdivided into a number of individual non-overlapping geometric modeling regions (GMRs). Each GMR occupies a certain volume of space, say V_g, bounded by the surface S_g. For a point ξ within V_g, the integration required by (2.3.15) need only be conducted over S_g and V_g, since the contribution to $u_\alpha(\xi)$ from the other GMRs outside S_g will be zero. As a result, integration costs can be dramatically reduced by introducing multiple GMRs for thermoviscous flow problems. Additionally, there is no inherent requirement that all

GMRs utilize the same physical model. For example, one GMR could employ the steady formulation of equation (2.3.6), while a second region includes the transient kernel effects contained in the formulation of (2.3.11). In any case, compatibility must, of course, be maintained across all GMR-to-GMR interfaces. Examples of the mixed GMR formulation are contained in Section 3. This approach also provides for fluid structure interaction which will be explored in Section 2.7.

2.3.4.3 INTEGRATION

The evaluation of the integrals appearing in (2.3.15) is the next process to be examined. Due to the singular nature of the kernel functions $G_{\alpha\beta}, F_{\alpha\beta}$ and $D_{\alpha\beta k}$ considerable care must be exercised during numerical integration. This is particularly true for incompressible viscous flow, in which the final solution is extremely sensitive to errors in integration coefficients. In general, the integration algorithms must be much more sophisticated than those developed for thermoelasticity. In the present implementation, discussed in detail in Honkala (1992), a number of different integration schemes are employed depending upon the order of the kernel singularity, the proximity of the field point ξ to the element, and the size of the element.

Once again consider the following three distinct categories for the surface integrals:

(1) The point ξ does not lie on the element m.

(2) The point ξ lies on the element m, but the kernels involve only weakly singular integrands of the $ln\ r$ type.

(3) The point ξ lies on the element m, and the integral has a strong $\frac{1}{r}$ singularity.

In practical problems involving many elements, it is evident that most of the integration occurring in equation (2.3.15) will be of the Category (1) variety. The integrand is non-singular and standard Gaussian quadrature can be employed. However, for near-singular cases when ξ is close to element m very high order formulas are needed to capture the kernel behavior. For these instances, it is beneficial to identify the point X^o on the element nearest to ξ, and then subdivide the interval of integration about X^o. Within each of the two subsegments a nonlinear transformation is used to further reduce the order of Gaussian quadrature needed for high precision. This nonlinear transformation is similar to that proposed by Mustoe (1984) and Telles (1987), however it should be emphasized that subsegmentation is still required.

Turning next to Category (2), one finds that, unlike elasticity or potential flow, standard Gaussian formulas alone are inadequate. Instead the terms involving $ln\ r$ must be isolated and integrated with special log-weighted Gaussian integration. The remaining non-singular terms comprising $G_{\alpha\beta}$ are then evaluated utilizing standard quadrature.

The strongly singular integrals of Category (3) exist only in the Cauchy principal value sense and cannot be evaluated numerically with sufficient precision. Fortunately, the indirect 'rigid body' or 'equipotential' method, originally developed by Cruse (1974),

is applicable, and leads to the accurate determination of the singular block of the second integral in (2.3.15). The remainder of that integral is non-singular. Consequently, subsegmentation along with standard Gaussian quadrature is adequate.

Similar care is needed for the volume integrals, which involve the kernel $D_{\alpha\beta k}$ containing a $\frac{1}{r}$-type singularity. However, for two-dimensional volume integration, this kernel is only weakly singular, and can be evaluated in the following direct manner. First, the nearest node, say A, in cell l to the point ξ is determined. The cell is then subdivided into triangles radiating from A as shown in Figure 2.3.3. Next, each triangle is mapped onto a unit square. The apex corresponding to A is stretched to form one side of the square. This process essentially eliminates the $\frac{1}{r}$ singularity. Finally, the square is further subsegmented in both radial and circumferential directions depending upon the closeness of ξ and the size of cell l. Standard Gaussian quadrature is applied to each subsegment. This cell integration scheme was based on work by Mustoe (1984) for elastoplasticity. In the present incompressible viscous flow implementation, tolerances have been tightened so that additional subsegmentation is performed, along with higher order quadrature formulas. Additionally, it has been found that circumferential subsegmentation is much more beneficial than the radial breakup.

In time-dependent problems, beyond the first time step, additional integration is required. This integration involves the kernels $G^n_{\alpha\beta}, F^n_{\alpha\beta}$ and $D^n_{\alpha\beta k}$ for $n > 1$. From Table 2.3.1, these are all nonsingular. As a result, a much less sophisticated integration scheme is employed to obtain the required level of accuracy with fewer subsegments and gauss points. If the initial velocities are not uniform, then the nonsingular initial condition integral of equation (2.3.15a) must also be evaluated at each time step. This is accomplished in a manner similar to the integration of $D^n_{\alpha\beta k}$.

Table 2.3.1 - Kernel Singularities

Kernel	Singularity Order
$G^1_{\alpha\beta}$	$ln\ r$
$G^n_{\alpha\beta}$ for $n > 1$	non-singular
$F^1_{\alpha\beta}$	$\frac{1}{r}$
$F^n_{\alpha\beta}$ for $n > 1$	non-singular
$D^1_{\alpha\beta k}$	$\frac{1}{r}$
$D^n_{\alpha\beta k}$ for $n > 1$	non-singular

2.3.4.4 ASSEMBLY

Once the spatial discretization and numerical integration algorithms are completely defined, a system of nonlinear algebraic equations can be developed to permit an approximate solution of the thermoviscous boundary value problem. The method of collocation is employed by writing (2.3.15) at each functional mode.

For each time step N of a transient problem, this nodal collocation process yields

$$\sum_{n=1}^{N} \left[\mathbf{G}^{N-n+1}\mathbf{t}^{n} - \mathbf{F}^{N-n+1}\mathbf{u}^{n} - \mathbf{G}^{N-n+1}\mathbf{t}^{on} + \mathbf{D}^{N-n+1}\sigma^{on}\right] - \mathbf{\Gamma}^{N}\mathbf{u}^{o} = \mathbf{0} \qquad (2.3.17)$$

where

$\mathbf{t}^n$	nodal traction vector for time step n with 3Q components
$\mathbf{u}^n$	nodal velocity vector for time step n with 3P components
$\mathbf{t}^{on}$	nodal convective traction vector for time step n with 3Q components
σ^{on}	nodal convective stress vector for time step n with 6P components
$\mathbf{u}^o$	nodal initial velocity vector with 3P components
$\mathbf{G}^n$	unassembled matrix of size 3P x 3Q calculated from the first integral of (2.3.15) during time step n
$\mathbf{F}^n$	assembled matrix of size 3P x 3P calculated from the second integral of (2.3.15) during time step n, plus the $c_{\alpha\beta}$ contribution in $\mathbf{F}^1$
$\mathbf{D}^n$	assembled matrix of size 3P x 6P calculated from the first volume integral of (2.3.15)
$\mathbf{\Gamma}^N$	assembled matrix of size 3P x 3P calculated from the initial condition integral of (2.3.15)
P	total number of functional nodes
$Q = \sum_{m=1}^{M} A_m$	
A_m	number of functional nodes in element m .

All of the coefficient matrices in (2.3.17) contain independent blocks for each GMR in multiregion problems. However, for any well-posed problem, the boundary conditions and interface relations remove all but 3P unknown components of $\mathbf{u}^N$ and $\mathbf{t}^N$. Furthermore, by solving (2.3.17) at each increment of time, all of the components of $\mathbf{u}^n, \mathbf{t}^n, \mathbf{t}^{on}$ and σ^{on} for $n < N$ are known from previous time steps. Then, (2.3.17) can be rewritten at time $N\Delta\tau$ as

$$\begin{aligned}\mathbf{g}(\mathbf{x}) = {} & \mathbf{A}\mathbf{x}^N - \mathbf{D}^1\sigma^{oN} + \mathbf{G}^1\mathbf{t}^{oN} - \mathbf{B}\mathbf{y}^N \\ & - \sum_{n=1}^{N-1} \left[\mathbf{G}^{N-n+1}\mathbf{t}^{n} - \mathbf{F}^{N-n+1}\mathbf{u}^{n} - \mathbf{G}^{N-n+1}\mathbf{t}^{on} + \mathbf{D}^{N-n+1}\sigma^{on}\right] + \mathbf{\Gamma}^{N}\mathbf{u}^{o} = \mathbf{0}\end{aligned} \qquad (2.3.18)$$

in which

$\mathbf{x}^N$	nodal vector of unknowns with 3P components
$\mathbf{y}^N$	nodal vector of knowns with 3Q components

while $\mathbf{A}$ and $\mathbf{B}$ are the associated coefficient obtained from $\mathbf{F}^1$ and $\mathbf{G}^1$. The $\mathbf{A}$ matrix now includes the compatibility relationships enforced on GMR interfaces. As a result, the GMR blocks in $\mathbf{A}$ are no longer independent, however $\mathbf{A}$ does remain block banded.

The terms included in the summation of (2.3.18) represent the contribution of past events. This, along with the terms $\mathbf{B}\mathbf{y}^N$ and $\mathbf{\Gamma}^N\mathbf{u}^o$, can be simply evaluated once at each time step N with no need for iteration. Let,

$$\mathbf{b}^N = -\mathbf{B}\mathbf{y}^N - \sum_{n=1}^{N-1} \left[\mathbf{G}^{N-n+1}\mathbf{t}^n - \mathbf{F}^{N-n+1}\mathbf{u}^n - \mathbf{G}^{N-n+1}\mathbf{t}^{on} + \mathbf{D}^{N-n+1}\sigma^{on}\right] + \mathbf{\Gamma}^N\mathbf{u}^o. \tag{2.3.19}$$

Then (2.3.18) becomes the following nonlinear set of algebraic equations

$$\mathbf{g}(\mathbf{x}) = \mathbf{A}\mathbf{x}^N - \mathbf{D}^1\sigma^{oN} + \mathbf{G}^1\mathbf{t}^{oN} + \mathbf{b}^N = \mathbf{0}. \tag{2.3.20}$$

A closer examination of $\mathbf{b}^N$ is in order. For example with $N = 1$

$$\mathbf{b}^1 = -\mathbf{B}\mathbf{y}^1 + \mathbf{\Gamma}^1\mathbf{u}^o, \tag{2.3.21a}$$

while for the second time step

$$\mathbf{b}^2 = -\mathbf{B}\mathbf{y}^2 - \mathbf{G}^2\mathbf{t}^1 + \mathbf{F}^2\mathbf{u}^1 + \mathbf{G}^2\mathbf{t}^{o1} - \mathbf{D}^2\sigma^{o1} + \mathbf{\Gamma}^2\mathbf{u}^o \tag{2.3.21b}$$

Obviously, for each step N, one new set of matrices $\mathbf{G}^N, \mathbf{F}^N, \mathbf{D}^N$ and $\mathbf{\Gamma}^N$ must be determined via integration and assembly. Integration, particularly the volume integration needed for $\mathbf{D}^N$ and $\mathbf{T}^N$, can be quite expensive.

As an alternative to the convolution approach defined above, a time marching recurring initial condition algorithm can be employed. This has been utilized by a number of researchers for transient problems of heat conduction, acoustics, and elasticity (Banerjee and Butterfield, 1981). For this latter approach, at time step N the entire contribution of past events is represented by an initial condition integral which utilizes $\mathbf{u}^{N-1}$ as the initial velocity. Thus,

$$\mathbf{g}(\mathbf{x}) = \mathbf{A}\mathbf{x}^N - \mathbf{D}^1\sigma^{oN} + \mathbf{G}^1\mathbf{t}^{oN} + \mathbf{b}^N = \mathbf{0} \tag{2.3.22}$$

with

$$\mathbf{b}^N = -\mathbf{B}\mathbf{y}^N + \mathbf{\Gamma}^1\mathbf{u}^{N-1}. \tag{2.3.23}$$

Obviously, (2.3.22) is identical to (2.3.20). Only the evaluation of $\mathbf{b}^N$ is different. The advantage of the recurring initial condition approach is that no integration is needed beyond the first time step. However, volume integration is required throughout the entire domain because of the presence of $\mathbf{u}^{N-1}$, even for linear problems in which volume integration would not normally be required.

In order to take full advantage of both methods, the present work utilizes the convolution approach in linear regions, and the recurring initial condition algorithm for the remaining nonlinear GMRs which are filled with volume cells. Since $\mathbf{b}^N$ can be computed independently for each GMR, this new dual approach provides no particular difficulty.

2.3.4.5 SOLUTION

An iterative algorithm, along the lines of those traditionally used for BEM elastoplasticity (Banerjee and Butterfield, 1981; Banerjee et al, 1987), can be employed to solve the boundary value problem. However, convergence is usually achieved only at low Reynolds number. More generally the interior equations must be brought into the system matrix, as in (2.3.20), and a full or modified Newton-Raphson algorithm must be employed to obtain solutions even at moderate Reynolds number. (Similar 'variable stiffness' algorithms have also been introduced by Banerjee and Raveendra (1987) and Henry and Banerjee (1988) for elastoplasticity.) Symbolically, at any iteration k,

$$\left[\frac{\partial \mathbf{g}}{\partial \mathbf{x}}(x^l)\right]\left\{\Delta \mathbf{x}^k\right\} = -\left\{\mathbf{g}(\mathbf{x})^k\right\} \tag{2.3.24}$$

where

$$\mathbf{x}^{k+1} = \mathbf{x}^k + \Delta \mathbf{x}^k \tag{2.3.25}$$

and the derivatives on the lefthand side of (2.3.24) are evaluated at $\mathbf{x}^k$. With the full Newton-Raphson approach, $l = k$ and the system matrix must be formed and decomposed at each iteration. The out-of-core solver used in the present implementation was developed originally for elastostatics (Banerjee et al, 1985) from the LINPACK software package (Dongarra et al, 1979), and operates on a submatrix level. Within each submatrix, Gaussian elimination with single pivoting reduces the block to upper triangular form. The final decomposed compacted form of the system matrix is stored in a direct access file for later reuse. Backsubstitution completes the determination of $\Delta \mathbf{x}^k$. Iteration continues until

$$\frac{||(\Delta \mathbf{x}^N)^k||}{||(\mathbf{x}^N)^k||} < \epsilon \tag{2.3.26}$$

where ϵ is a small tolerance, and $||\mathbf{x}||$ is the Euclidean norm of $\mathbf{x}$. For the modified Newton-Raphson algorithm, the system matrix is not formed at every iteration, and only backsubstitution is needed to determine $\Delta \mathbf{x}^k$.

2.3.4.6 CALCULATION OF ADDITIONAL BOUNDARY QUANTITIES

Once the iterative process has converged, a number of additional boundary quantities of interest can be easily calculated. For example, lift and drag can be calculated by numerically integrating the known nodal traction and shape function products over the surface elements of interest. Low order Gaussian quadrature is adequate for this integration, since all the functions are very well behaved.

Furthermore, at each boundary node, the pressure p, stress σ_{ij}, and strain rates $\frac{\partial u_j}{\partial x_i}$ can be determined by simultaneously solving the following relationships:

$$\sigma_{ji}(\xi) n_j(\xi) = N_\omega(\zeta) t_{i\omega} \tag{2.3.27a}$$

$$\sigma_{ij}(\xi) - \mu\left(\frac{\partial u_i}{\partial x_j}(\xi) + \frac{\partial u_j}{\partial x_i}(\xi)\right) + p(\xi) = 0 \tag{2.3.27b}$$

$$\frac{\partial x_j}{\partial \zeta}\frac{\partial u_i}{\partial x_j}(\xi) = \frac{\partial N_\omega}{\partial \zeta} u_{i\omega} \tag{2.3.27c}$$

$$\frac{\sigma_{ii}(\xi)}{2} + p(\xi) = 0. \tag{2.3.27d}$$

It should be emphasized that (2.3.27) represents a set of nine independent equations which are written at the boundary point ξ, and can be solved easily for p, σ_{ij} and $\frac{\partial u_j}{\partial x_i}$ at that point. Afterward, boundary vorticity and dilatation can be obtained, respectively, from

$$\Omega = \frac{\partial u_2}{\partial x_1} - \frac{\partial u_1}{\partial x_2} \tag{2.3.28a}$$

$$\Delta = \frac{\partial u_1}{\partial x_1} + \frac{\partial u_2}{\partial x_2}. \tag{2.3.28b}$$

Of course, for incompressible flow, the dilatation should be zero, but (2.3.28b) can be used as a check.

A comprehensive PATRAN interface has also been developed. Consequently, any of the quantities computed above may be displayed graphically in the form of profiles or contours.

2.3.5 CONCLUDING REMARKS

The formulations presented in this section, based upon Stokes fundamental solutions, are suited primarily for low Reynolds number regimes. For creeping flows, all of the nonlinear terms vanish, resulting in a very efficient, very precise boundary-only solution. The resulting boundary element method is clearly superior to any of the domain based methods for problems of this nature, under both steady and transient conditions.

At somewhat higher velocities, the nonlinear convective effects cannot be ignored. Consequently, the surface integral involving t^o_α and the volume integral containing $\sigma^o_{k\alpha}$ in equations (2.3.6) and (2.3.11) are required. Since volume integration is quite computationally intensive, a boundary element approach becomes less attractive. This is particularly true when discretization is required throughout the domain, as is the case for confined flows. Still, for a given mesh, the boundary element formulation provides a higher degree of accuracy than finite difference or finite element methods, especially in the determination of boundary quantities.

APPENDIX 2.3.1
STEADY KERNEL FUNCTIONS

$$G_{ij} = \frac{1}{4\pi\mu}\left[\frac{y_i y_j}{r^2} - \delta_{ij} ln\ r\right]$$

$$F_{ij} = -\frac{1}{2\pi r}\left[\frac{2y_i y_j y_k n_k}{r^3}\right]$$

$$\frac{\partial G_{ij}}{\partial x_k} = \frac{1}{4\pi\mu r}\left[\frac{\delta_{jk} y_i}{r} + \frac{\delta_{ik} y_j}{r} - \frac{\delta_{ij} y_k}{r} - \frac{2y_i y_j y_k}{r^3}\right]$$

$$G_{\theta\theta} = \frac{1}{2\pi k}\left[ln\ r\right]$$

$$F_{\theta\theta} = \frac{1}{2\pi r}\left[\frac{y_k n_k}{r}\right]$$

$$\frac{\partial G_{\theta\theta}}{\partial x_k} = \frac{1}{2\pi k r}\left[\frac{y_k}{r}\right]$$

$$y_i = x_i - \xi_i$$

$$r^2 = y_i y_i$$

APPENDIX 2.3.2
TIME-DEPENDENT KERNEL FUNCTIONS

$$G_{ij}(\xi - X, t) = \frac{1}{4\pi\mu}\left[\frac{y_i y_j}{r^2}\{s_1(\eta)\} - \delta_{ij}\left\{\frac{s_1(\eta)}{2} - \frac{E_1\left(\frac{\eta^2}{4}\right)}{2}\right\}\right]$$

$$F_{ij}(\xi - X, t) = \frac{1}{2\pi r}\left\{\frac{y_j n_i}{r}\{s_1(\eta) - e^{-\eta^2/4}\} + \frac{y_i n_j}{r}\{s_1(\eta) - H(t)\} + \frac{\delta_{ij} y_k n_k}{r}\{s_1(\eta) - e^{-\eta^2/4}\} - \frac{2 y_i y_j y_k n_k}{r^3}\{2s_1(\eta) - e^{-\eta^2/4}\}\right]$$

$$\frac{\partial G_{ij}}{\partial x_k}(\xi - X, t) = \frac{1}{4\pi\mu r}\left[\frac{\delta_{jk} y_i}{r}\{s_1(\eta)\} + \frac{\delta_{ik} y_j}{r}\{s_1(\eta)\} - \frac{\delta_{ij} y_k}{r}\{2e^{-\eta^2/4} - s_1(\eta)\} - \frac{2 y_i y_j y_k n_k}{r^3}\{2s_1(\eta) - e^{-\eta^2/4}\}\right]$$

where

$$y_i = \xi_i - x_i \qquad r^2 = y_i y_i$$
$$\eta = \frac{r}{(ct)^{1/2}} \qquad c = \mu/\rho$$
$$s_1(\eta) = \frac{4}{\eta^2}(1 - e^{-\eta^2/4})$$
$$E_1(z) = \int_z^\infty \frac{e^{-u}}{u} du.$$

Then,

$$G^n_{ij}(\xi - X) = G_{ij}(\xi - X, n\Delta\tau) \quad \text{for} \quad n = 1$$
$$G^n_{ij}(\xi - X) = G_{ij}(\xi - X, n\Delta\tau) - G_{ij}(\xi - X, (n-1)\Delta\tau) \quad \text{for} \quad n > 1$$

with similar relationships for $F^n_{ij}(\xi - X)$ and $\frac{\partial G^n_{ij}}{\partial x_k}(\xi - X)$.

Figure 2.3.1 Two Dimensional Boundary Elements

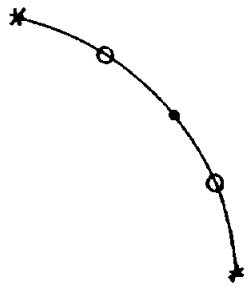

GEOMETRIC NODES (*,•)	3
FUNCTIONAL NODES	
LINEAR (*)	2
QUADRATIC (*,•)	3
QUARTIC (*,•,o)	5

Figure 2.3.2 Two Dimensional Volume Cells

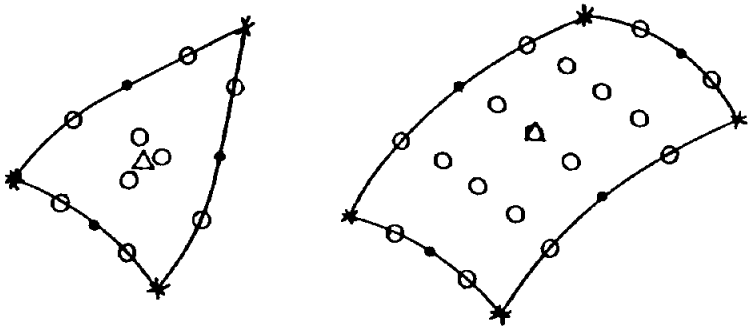

GEOMETRIC NODES (*,·)	6	8
FUNCTIONAL NODES		
LINEAR (*)	3	4
QUADRATIC		
SERENDIPITY (*,·)	6	8
LAGRANGIAN (*,·,Δ)	7	9
QUARTIC (*,·,o)	15	25

Figure 2.3.3 Integration Subsegmentation

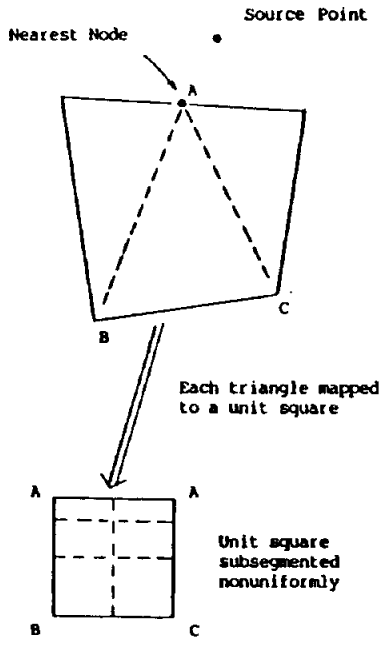

2.4 CONVECTIVE INCOMPRESSIBLE THERMOVISCOUS FLOW

2.4.1 INTRODUCTION

At high fluid velocities, the convective terms in Navier-Stokes equations tend to dominate. As a result, boundary element formulations employing Stokes kernels are inappropriate, since these fundamental solutions model the effects of viscosity but not convection. Instead, more of the physics of the problem must be brought into the linear operator. This concept was clearly understood by Oseen in the early portion of the twentieth century. In his 1927 monograph, Oseen developed exact integral expressions for Navier-Stokes equations using a convective fundamental solution. Unfortunately since this was well before the advent of the computer, he was unable to do much with his formulations beyond some approximate solutions at very low Reynolds number. In the present section, the work of Oseen is resurrected to form the basis for an attractive boundary element method for high speed flows.

2.4.2 GOVERNING EQUATIONS

The differential equations, governing the behavior of an incompressible thermoviscous fluid in the presence of a free stream velocity U_i, can be written:

$$\mu \frac{\partial^2 u_i}{\partial x_j \partial x_j} - \frac{\partial p}{\partial x_i} - \rho U_j \frac{\partial u_i}{\partial x_j} - \rho \frac{\partial u_i}{\partial t} + f_i' = 0, \tag{2.4.1a}$$

$$\frac{\partial u_i}{\partial x_i} = 0, \tag{2.4.1b}$$

$$k \frac{\partial^2 \theta}{\partial x_j \partial x_j} - \rho c_\epsilon U_j \frac{\partial \theta}{\partial x_j} - \rho c_\epsilon \frac{\partial \theta}{\partial t} + \psi' = 0. \tag{2.4.1c}$$

where u_i once again represents the velocity perturbation. In (2.4.1), the effective body forces and sources are defined as

$$f_i' = -\rho u_j \frac{\partial u_i}{\partial x_j} + f_i \tag{2.4.2a}$$

$$\psi' = -\rho c_\epsilon u_j \frac{\partial \theta}{\partial x_j} + \psi. \tag{2.4.2b}$$

These equations are of course identical to those presented in (2.3.4), except that now the convective terms $\rho U_j \partial u_i / \partial x_j$ and $\rho c_\epsilon U_j \partial \theta / \partial x_j$ are included in the linear differential operator.

Fundamental solutions based upon (2.4.1) will contain the character of the flow field at high velocities.

2.4.3 FUNDAMENTAL SOLUTIONS

It is instructive to begin with a look at the fundamental solution of the steady form of the heat equation defined above as (2.4.1c). In a static medium (i.e., $U_i = 0$), the fundamental solution G must satisfy

$$k\frac{\partial^2 G}{\partial x_j \partial x_j} + \delta(x-\xi) = 0 \tag{2.4.3}$$

in which δ is the generalized delta function. The solution to (2.4.3) in two-dimensional space is the well-known potential flow Green's function

$$G(x,\xi) = -\frac{\ln r}{2\pi k} \tag{2.4.4}$$

with

$$y_i = x_i - \xi_i \tag{2.4.5a}$$

$$r^2 = y_i y_i \tag{2.4.5b}$$

Thus, $G(x,\xi)$ represents the temperature response at x due to a unit point heat source at ξ. This response is plotted in the $x_1 - x_2$ plane for a source at the origin in Figure 2.4.1. Radial symmetry is evident.

However, if the medium is moving at velocity U_i, then the fundamental solution G^U must instead satisfy

$$k\frac{\partial^2 G^U}{\partial x_j \partial x_j} - \rho c_\epsilon U_j \frac{\partial G^U}{\partial x_j} + \delta(x-\xi) = 0 \tag{2.4.6}$$

Now, the Green's function (e.g. Carslaw and Jaeger, 1959) is given by

$$G^U(x,\xi) = \frac{e^{-U_k y_k/2\kappa}}{2\pi k} K_o\left[(U_k U_k)^{1/2}\left(\frac{r}{2\kappa}\right)\right] \tag{2.4.7}$$

in which $\kappa = k/\rho c_\epsilon$. This response is plotted in Figures 2.4.2a-d for various magnitudes of an x_1-directional velocity. Obviously, in a moving medium, radial symmetry is lost and a pronounced front-and-back effect develops. That is, at a given distance from the heat source, it is hottest directly downstream.

It should be emphasized that the so-called convective fundamental solution defined in (2.4.7) actualy embodies both the processes of conduction and convection. At low velocity, conduction dominates producing a nearly radially symmetric response. On the other hand, in a high speed medium, the response is concentrated in a very narrow band downstream of the source. Thus, as illustrated in Figure 2.4.2, G^U captures the transition from elliptic toward hyperbolic behavior.

The corresponding convective viscous fundamental solution G^U_{ij} was first presented by Oseen (1911), as the solution to

$$\mu \frac{\partial^2 G^U_{ij}}{\partial x_k \partial x_k} - \frac{\partial G^U_{pj}}{\partial x_i} - \rho U_k \frac{\partial G^U_{ij}}{\partial x_k} + \delta_{ij}\delta(x-\xi) = 0 \tag{2.4.8a}$$

$$\frac{\partial G^U_{kj}}{\partial x_k} = 0. \tag{2.4.8b}$$

The G^U_{ij} tensor is given in explicit form in Appendix 2.4. However, the component G^U_{11}, which represents the velocity in the x_1-direction due to a unit point force in the x_1-direction, is displayed in Figures 2.4.3a-d. For very small U_i, the solution of (2.4.8) approaches the Stokes kernels detailed in Appendix 2.3.1. This is shown in Figure 2.4.3a. Notice that, unlike the heat conduction response of Figure 2.4.2a, the static viscous fundamental solution is not radially symmetric. This is due to the vectorial nature of the flow, and is directly attributed to the $y_i y_j / r^2$ terms in G_{ij}. However, as the flow velocity increases (i.e., Figures 2.4.3b-d), a stronger sense of upstream and downstream develops, and the response once again becomes concentrated in a narrow band ahead of the applied force. At high speed, outside of this band, the response is essentially zero. This behavior is not only important from a physical standpoint, but also can be beneficial in the development of efficient boundary element algorithms.

2.4.4 INTEGRAL REPRESENTATIONS

The convective fundamental solutions depicted in Figures 2.4.2 and 2.4.3 capture the proper character of high Reynolds number incompressible thermoviscous flows, and as a result, can provide the basis for an attractive boundary element formulation. The corresponding integral equations, under steady conditions, can be developed directly from the governing differential equations (2.4.1). This result is,

$$c_{\alpha\beta} u_\alpha = \int_S \left[G^U_{\alpha\beta} t_\alpha - F^U_{\alpha\beta} u_\alpha - G^U_{\alpha\beta} t^{Uo}_\alpha \right] dS + \int_V \left[D^U_{\alpha\beta k} \sigma^{Uo}_{k\alpha} + G^U_{\alpha\beta} f_\alpha \right] dV, \tag{2.4.9}$$

where

$$\sigma^{Uo}_{k\alpha} = [\rho u_k u_i \qquad \rho c_\epsilon u_k \theta] \tag{2.4.10a}$$

$$t^{Uo}_\alpha = \sigma^{Uo}_{k\alpha} n_k. \tag{2.4.10b}$$

the superscript U on the kernel functions is a reminder that these are based upon convective fundamental solutions. All of the kernels appearing in (2.4.9) are detailed in Appendix 2.4. In most cases the body forces, f_α, are either zero or can be accounted for via a particular integral so that the second volume integral in (2.4.9) is not needed.

In examining (2.4.9), it should be noted that the nonlinearities are contained in the surface integral involving $G^U_{\alpha\beta} t^{Uo}_\alpha$ and the remaining volume integral, $D^U_{\alpha\beta k} \sigma^{Uo}_{k\alpha}$. Specifically,

only t_α^{Uo} and $\sigma_{k\alpha}^{Uo}$ are nonlinear, and these are both formed from the product of perturbations. For high speed flows, these perturbations are only significant in the vicinity of objects and in the wake. As a result, volume discretization is only needed in those areas. Elsewhere, the linearized Oseen approximation is adequate.

Equation (2.4.9) is identical to the integral equation developed by Oseen (1927), except for the treatment of the nonlinear convective terms. In deriving (2.4.9), an additional integration-by-parts operation was invoked to completely eliminate the appearance of velocity gradients.

If one is interested in the transient thermoviscous response in a medium with a more or less steady free stream velocity, then a time-dependent formulation is also possible. For this case, the time derivatives are retained in the linear operator, and the following integral equation results:

$$c_{\alpha\beta}u_\alpha = \int_S \left[g_{\alpha\beta}^U * t_\alpha - f_{\alpha\beta}^U * u_\alpha - g_{\alpha\beta}^U * t_\alpha^{Uo}\right] dS$$

$$+ \int_V \left[d_{\alpha\beta k}^U * \sigma_{k\alpha}^{Uo} + g_{\alpha\beta}^U * f_\alpha - g_{\alpha\beta}^U \rho u_\alpha^o\right] dV \qquad (2.4.11)$$

This integral equation and the corresponding fundamental solutions have not appeared in the literature. The functions $g_{\alpha\beta}^U$ are quite involved, but can be expressed in terms of incomplete exponential integrals.

2.4.5 NUMERICAL IMPLEMENTATION

The integral representations for convective thermoviscous flow are quite similar in form to those presented in Section 2.3.3. Consequently, there is a great deal of overlap in the algorithms employed for their respective numerical implementation. At present, the major difference occurs in the schemes utilized for integration.

As discussed previously, the convective fundamental solutions have a much different character than the more familiar Stokes based kernels. The standard boundary element integration schemes are unable to accurately capture the localized nature of the convective kernels, particularly at large Reynolds number. In general, subsegmentation must be much more intense for singular and near-singular cases. For example, in convective near-singular integration, first the location X^o on the element nearest to the load point ξ is identified. Then, a graded subsegmentation pattern is defined about X^o based upon criteria including the distance of ξ to X^o and the free stream velocity. For higher speed flow, smaller subsegments are generated. Gaussian integration order is also typically higher for the convective surface integration. Similar adjustments are required for volume integration as well.

Some progress has been made in the development of alternate integration strategies for singular integration. For example, partial analytical treatment of the G_{ij}^U kernel has proved to be more cost effective. Also, the standard 'rigid body' technique has been

extended to other known solution fields in order to indirectly calculate some of the singular contributions.

However, additional effort is still needed to develop integration algorithms designed specifically for high speed convective kernels. In particular, the response depicted in Figure 2.4.3d must be anticipated. Thus, there is no need to integrate an element which lies outside the narrow band of nonzero response. Furthermore, elements located partially or wholely within the band should be subsegmented accordingly.

The remainder of the numerical implementation follows that discussed in Section 2.3.4. Thus, assembly, solution, and the calculation of additional boundary quantities are accomplished in the same manner as for the Stokes kernel approach. While this is perfectly legitimate, full advantage has not yet been taken of the character of the convective response. For example, at very high speeds, as the behavior becomes hyperbolic, the system equations form a nearly-sequential, banded set. The present assembler and solver, which were designed for elliptic systems, do not recognize this structure, and consequently, are quite inefficient.

APPENDIX 2.4
KERNEL FUNCTIONS

$$G_{ij} = \frac{1}{2\pi\mu}\left[\left(\frac{U_iU_j}{U^2}\right)e^{-\beta}K_o(\alpha) - \frac{c}{U}\left(\frac{U_i}{U}\right)\frac{\partial\phi}{\partial x_j} - \frac{c}{U}\left(\frac{U_j}{U}\right)\frac{\partial\phi}{\partial x_i} + \frac{c}{U}\left(\frac{\delta_{ij}U_\ell}{U}\right)\frac{\partial\phi}{\partial x_\ell}\right]$$

$$G_{pj} = -\frac{1}{2\pi}\left(\frac{1}{r}\right)\left(\frac{y_j}{r}\right)$$

$$F_{ij} = \mu\left(\frac{\partial G_{kj}}{\partial x_i} + \frac{\partial G_{ij}}{\partial x_k}\right)n_k + G_{pj}n_i + \rho U_k G_{ij} n_k$$

$$D_{ijk} = \frac{\partial G_{ij}}{\partial x_k} = \frac{1}{2\pi\mu}\left[-\left(\frac{U_iU_jU_k}{2cU^2}\right)e^{-\beta}K_o(\alpha) - \left(\frac{U}{2c}\right)\left(\frac{U_iU_jy_k}{U^2r}\right)e^{-\beta}K_1(\alpha) - \left(\frac{c}{U}\right)\left(\frac{U_i}{U}\right)\frac{\partial^2\phi}{\partial x_j\partial x_k}\right.$$
$$\left. - \left(\frac{c}{U}\right)\left(\frac{U_j}{U}\right)\frac{\partial^2\phi}{\partial x_i\partial x_k} + \left(\frac{c}{U}\right)\left(\frac{\delta_{ij}U_\ell}{U}\right)\frac{\partial^2\phi}{\partial x_\ell\partial x_k}\right]$$

where

$$y_i = x_i - \xi_i, \qquad r^2 = y_iy_i$$
$$c = \frac{\mu}{\rho} \qquad U^2 = U_iU_i$$
$$\beta = U_ky_k/2c$$
$$\alpha = Ur/2c$$
$$\phi = -ln(\alpha) - e^{-\beta}K_o(\alpha)$$
$$\frac{\partial\phi}{\partial x_i} = -\left(\frac{y_i}{r}\right)\left(\frac{1}{r}\right) + \left(\frac{U}{2c}\right)\left(\frac{y_i}{r}\right)e^{-\beta}K_1(\alpha) + \left(\frac{U_i}{2c}\right)e^{-\beta}K_o(\alpha)$$

$$\frac{\partial^2\phi}{\partial x_i\partial x_j} = -\left(\frac{\delta_{ij}}{r^2}\right) + \left(\frac{2y_iy_j}{r^2}\right) + \left(\frac{U}{2c}\right)\left(\frac{\delta_{ij}}{r} - \frac{2y_iy_j}{r^2} - \frac{U_jy_i}{2cr}\right)e^{-\beta}K_1(\alpha) - \left(\frac{U}{2c}\right)\left(\frac{Uy_iy_j}{2cr^2}\right)e^{-\beta}K_o(\alpha)$$
$$- \left(\frac{U_iU_j}{4c^2}\right)e^{-\beta}K_o(\alpha) - \left(\frac{UU_i}{4c^2}\right)\left(\frac{y_j}{r}\right)e^{-\beta}K_1(\alpha)$$

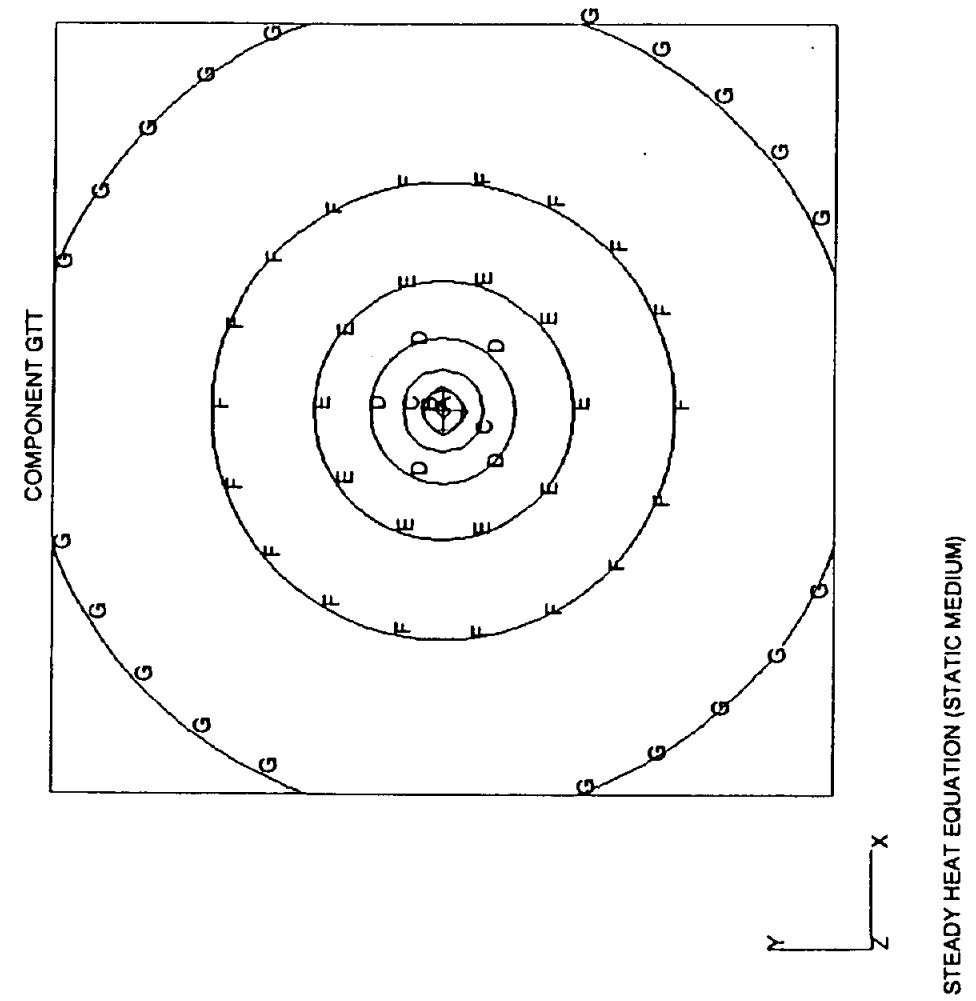

Figure 2.4.1 Kernel for Steady Heat Equation

Figure 2.4.2a Kernel for Convective Heat Equation

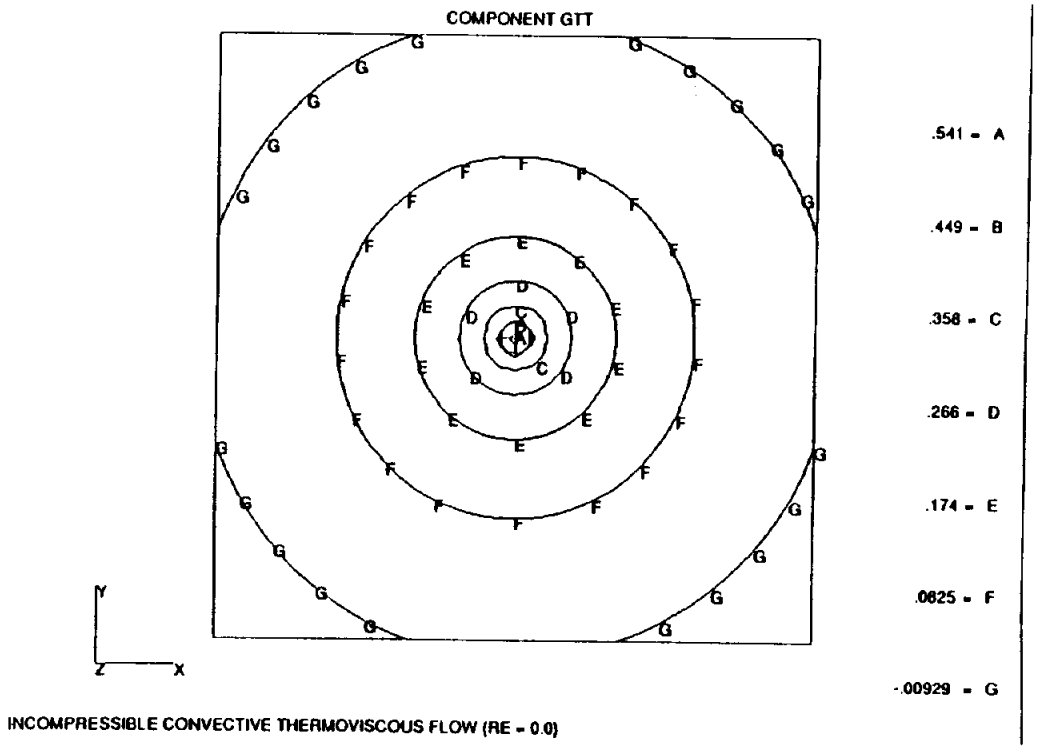

Figure 2.4.2b Kernel for Convective Heat Equation

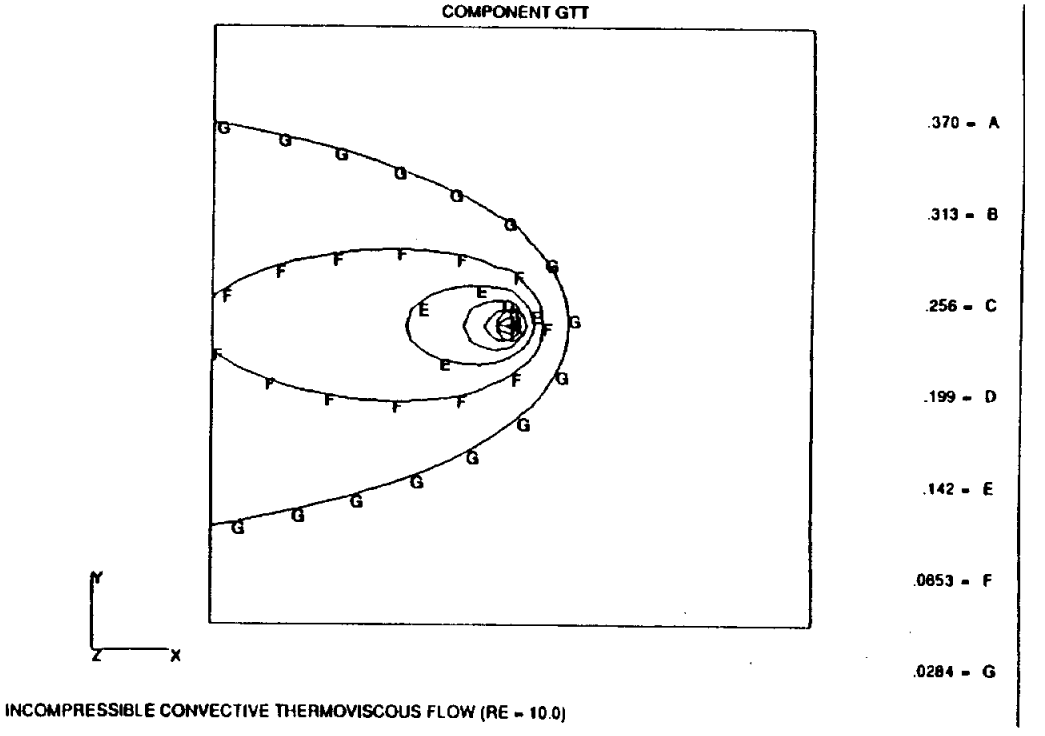

Figure 2.4.2c Kernel for Convective Heat Equation

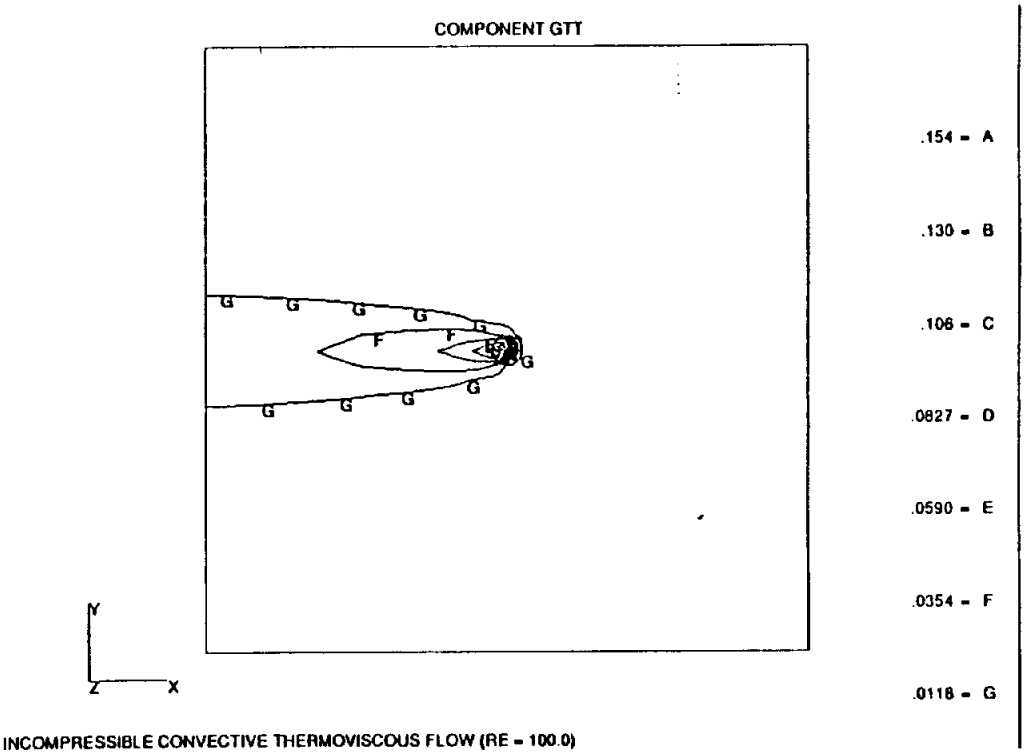

Figure 2.4.2d Kernel for Convective Heat Equation

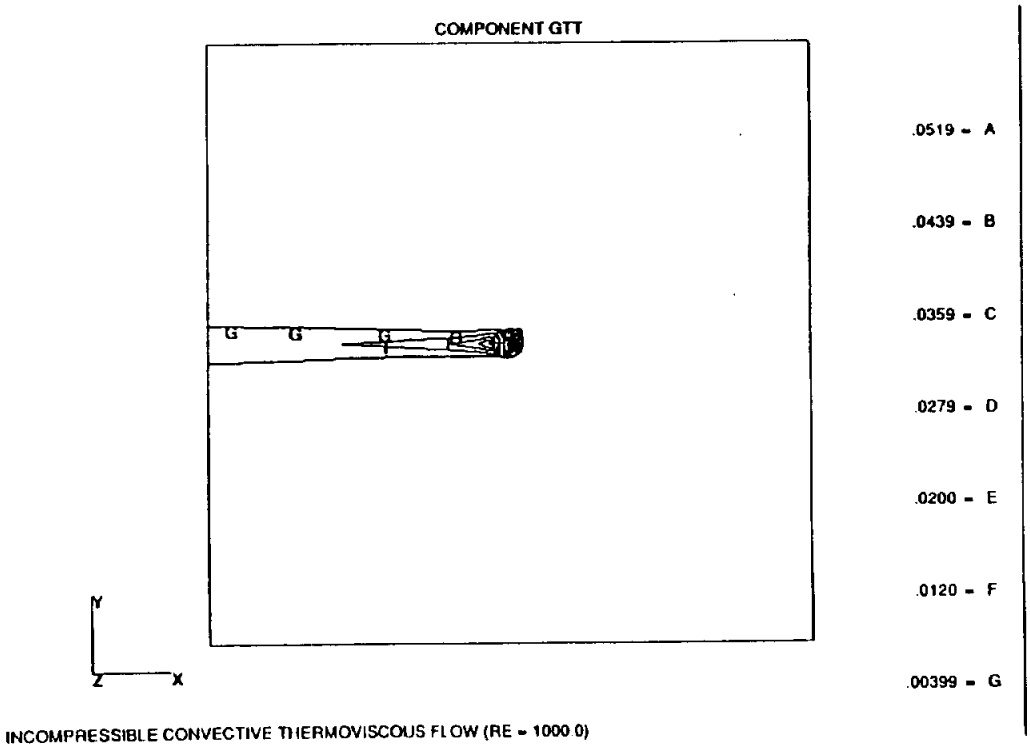

Figure 2.4.3a Kernel for Incompressible Viscous Flow

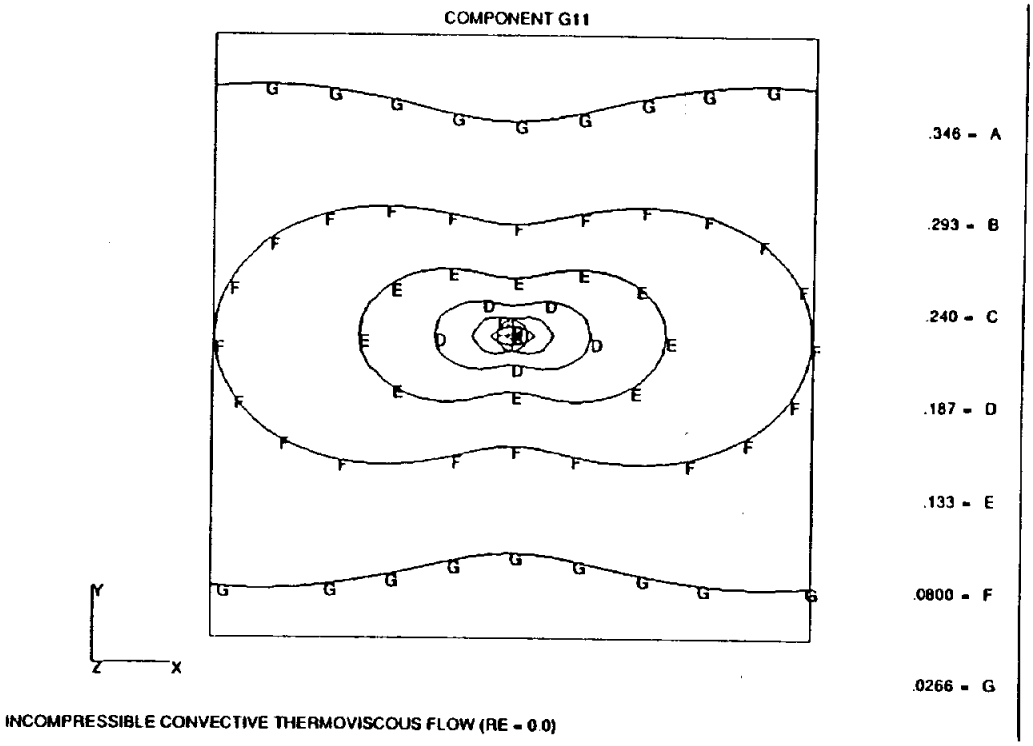

Figure 2.4.3b Kernel for Incompressible Viscous Flow

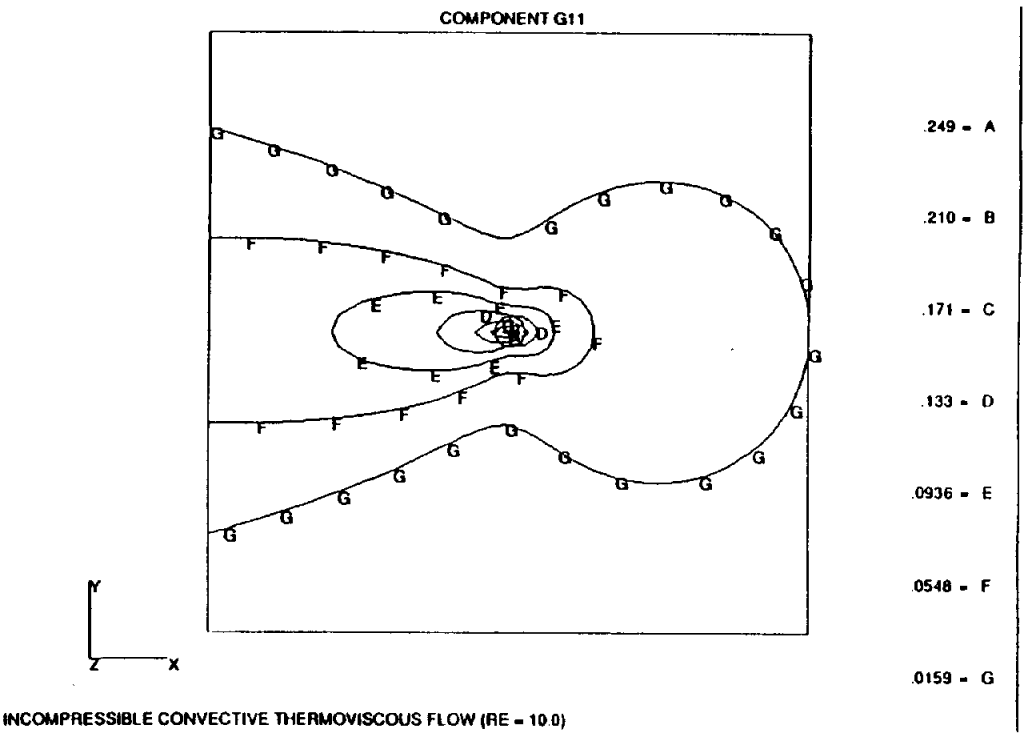

Figure 2.4.3c Kernel for Incompressible Viscous Flow

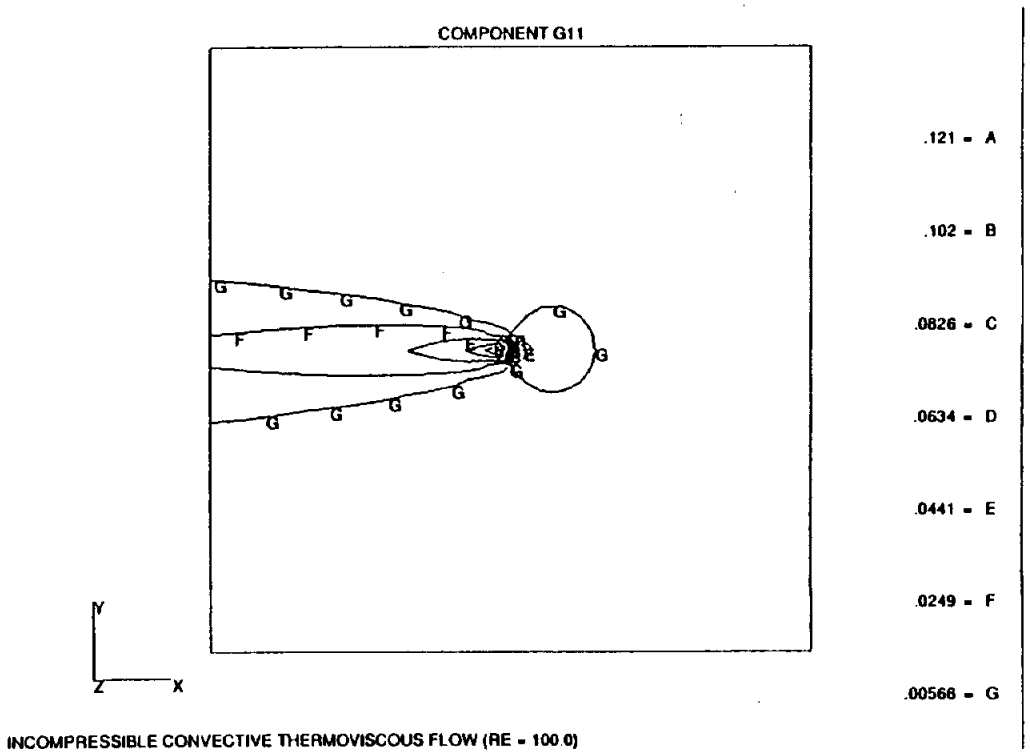

Figure 2.4.3d Kernel for Incompressible Viscous Flow

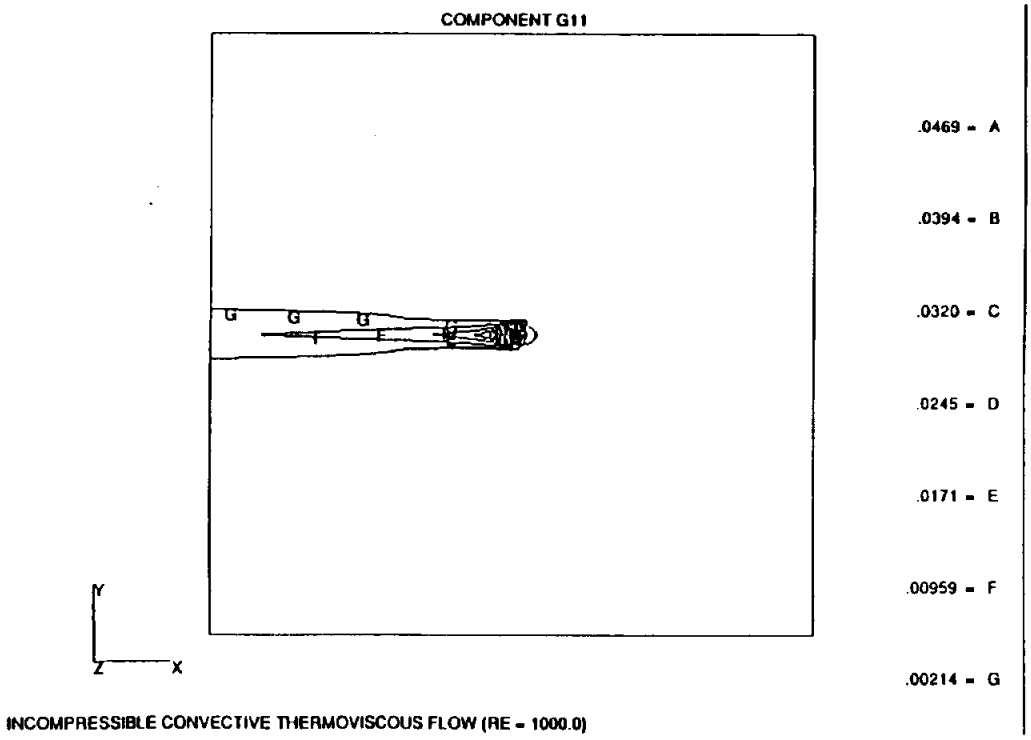

2.5 CONVECTIVE POTENTIAL FLOW

2.5.1 INTRODUCTION

Compressible potential flow is one of the most important fields of aerodynamic analysis. One reason is that for sufficiently large Reynolds numbers the important viscous effects are often confined to an infinitesimal thin boundary layer adjacent to the surface of a body and its wake. Outside the wake and the vortical region near the boundary the flow is essentially irrotational. This fact was first observed by Prandtl in 1904.

The boundary element method is a very useful tool for solving compressible potential flow problems. One of the advantages is that BEM can be easily applied to solve flow problems over complex configurations. A major technical obstacle involved with other methods seems to be the difficulty in generating suitable grids for flows with complex configurations in presence of shock waves. Another advantage of the boundary element method is that the solutions can be obtained by only using surface elements. Results elsewhere can then be in terms of the solutions on surface elements. Thus the boundary element method could be computationally attractive.

In the present section, a reduced equation will be discussed which is valid only in the inviscid and irrotational flow regimes. This formulation requires much less computer time than is needed to solve the full Navier-Stokes equations. In the following sections, the time-dependent governing equation for compressible potential flow is presented, along with fundamental solutions and boundary integral equations. An extensive discussion of the linearized steady state potential flow problem governed by the P-G equation indicates how methodologies have been developed which allow boundary element formulations to be successfully applied to the elliptic (linearized subsonic) and hyperbolic (linearized supersonic) flow problems.

2.5.2 GOVERNING EQUATIONS

The linearized governing differential equation of convective potential flow for isotropic, homogeneous space can be written as

$$\frac{1}{c^2}\frac{D^2\phi}{Dt^2} - \frac{\partial^2\phi}{\partial x_i \partial x_i} = 0\,, \tag{2.5.1}$$

where

ϕ velocity potential defined as $v_i = \frac{\partial \phi}{\partial x_i}$

c local speed of sound

$D/Dt = \partial/\partial t + v_i \partial/\partial x_i$ material time derivative.

After linearization, (2.5.1) becomes

$$\frac{1}{c_o^2}\frac{D_o^2\phi'}{Dt^2} - \frac{\partial^2\phi'}{\partial x_i \partial x_i} = \bar{\psi}\,, \tag{2.5.2}$$

- ϕ' velocity perturbation potential defined as $u_i = \frac{\partial \phi'}{\partial x_i}$
- u_i velocity perturbation
- U_i reference velocity
- c_o speed of sound
- γ ratio of specific heat at constant pressure to that at constant volume
- $\bar{\psi}$ pseudo mass source rate per unit mass which is defined by

$$\bar{\psi} = -\frac{\gamma-1}{c_o^2}\left(\frac{\partial \phi'}{\partial t} + U_i u_i + \frac{1}{2}u^2\right)\frac{\partial u_j}{\partial x_j} - \frac{2}{c_o^2}u_i\frac{\partial u_i}{\partial t} - \frac{2}{c_o^2}\left(U_i u_j + \frac{1}{2}u_i u_j\right)\frac{\partial u_i}{\partial x_j}\,, \tag{2.5.3a}$$

and

$$\frac{D_o}{Dt} = \frac{\partial}{\partial t} + U_i\frac{\partial}{\partial x_i}\,. \tag{2.5.3b}$$

The equation governing compressible potential flow has different character in different flow regimes. For a transient problem, the governing equation is hyperbolic for all Mach numbers and solutions can be obtained using a time marching procedure. The situation is very different when a steady flow is assumed. In this case, the equation is elliptic when the flow is subsonic and hyperbolic when the flow is supersonic. One of the most important distinctive features of supersonic flow is the fact that shock waves occur in the flow field.

2.5.3 FUNDAMENTAL SOLUTIONS

Equation (2.5.2) is a well known convective scalar wave equation. But, the fundamental solution in the convective form does not appear to exist in the literature although some discussions can be found in Goldstein (1976) and Morse and Feshbach (1978).

2.5.3.1 COMPRESSIBLE POTENTIAL FLOW

Consider, first, the effect of an instantaneous point source. Let

$$\bar{\psi} = \delta(x-\xi)\delta(t-\tau)\,. \tag{2.5.4}$$

It is instructive to begin with a look at the fundamental solution in a static medium (i.e. $U_i = 0$). In that case, the fundamental solution g must satisfy

$$\frac{1}{c_o^2}\frac{\partial^2 g}{\partial t^2} - \frac{\partial^2 g}{\partial x_i \partial x_i} = \delta(x-\xi)\delta(t-\tau)\,. \tag{2.5.5}$$

The solution to (2.5.5) is the well-known scalar wave Green's function

$$g(x-\xi,t-\tau)=\begin{cases}\dfrac{\delta(t'-r/c_o)}{4\pi r}\,, & \text{for 3D;}\\[2ex] \dfrac{1}{2\pi}\dfrac{H(t'-r/c_o)}{\sqrt{t'^2-r^2/c_o^2}}\,, & \text{for 2D,}\end{cases}\tag{2.5.6}$$

where

$$\begin{aligned} y_i &= x_i-\xi_i\\ r^2 &= y_iy_i\,.\\ t' &= t-\tau\end{aligned}\tag{2.5.7}$$

Thus, g represents the velocity potential response at location x and time t due to a instantaneous point mass source at ξ and at time τ.

The other fundamental solution that is needed is that due to a unit step mass source acting, again, at point ξ in an infinite medium. This mass source is, then,

$$\bar{\psi}=\delta(x-\xi)H(t)\,.\tag{2.5.8}$$

The response of (2.5.8) can be obtained from (2.5.6) by integrating over τ. Thus,

$$G(x-\xi,t)=\int_0^t g(x-\xi,t-\tau)\,d\tau=\begin{cases}\dfrac{1}{4\pi r}H(t-r/c_o)\,, & \text{for 3D;}\\[2ex] \dfrac{1}{2\pi}H(t-r/c_o)\cosh^{-1}\dfrac{c_ot}{r}\,, & \text{for 2D.}\end{cases}\tag{2.5.9}$$

The steady state response can be derived directly from (2.5.9). Letting $t\to\infty$, this simplifies to

$$G^s(x-\xi)=G(x-\xi,\infty)=\begin{cases}\dfrac{1}{4\pi r}\,, & \text{for 3D;}\\[2ex] -\dfrac{1}{2\pi}\ln r\,, & \text{for 2D.}\end{cases}\tag{2.5.10}$$

2.5.3.2 CONVECTIVE COMPRESSIBLE POTENTIAL FLOW

Now, if the medium is moving at velocity U_i, the fundamental solution g^U must instead satisfy

$$\frac{1}{c_o^2}\frac{D_o^2g^U}{Dt^2}-\frac{\partial^2g^U}{\partial x_i\partial x_i}=\delta(x-\xi)\delta(t-\tau)\,.\tag{2.5.11}$$

Three-dimensional Flow

Performing on (2.5.11) the Laplace transform with respect to τ with homogeneous initial conditions and triple exponential Fourier transform, defined by the relations

$$\bar{f}(x,s)=\mathcal{L}\{f(x,t)\}=\int_0^\infty e^{-st}f(x,t)\,dt\tag{2.5.12a}$$

$$f^*(\alpha,t)=\mathcal{F}\{f(x,t)\}=\iiint_{-\infty}^{\infty}f(x,t)e^{-i\alpha x}\,dV(x)\,,\tag{2.5.12b}$$

with $\alpha x = \alpha_i x_i$, one obtains the following results by assuming a free-stream velocity in the x_1-direction only $(U_1 = U,\ U_2 = U_3 = 0)$

$$\overline{g^{U^*}} = \frac{1}{\alpha^2 + \dfrac{(s + i\alpha_k U_k)^2}{c_o^2}}$$

$$= \begin{cases} \dfrac{1}{-\left(\beta i\alpha_1 - \dfrac{sU_1}{c_o^2\beta}\right)^2 + \alpha_2^2 + \alpha_3^2 + \dfrac{s^2}{c_o^2\beta^2}}\,, & M_\infty < 1\,; \\ \dfrac{1}{\left(\beta i\alpha_1 + \dfrac{sU_1}{c_o^2\beta}\right)^2 + \alpha_2^2 + \alpha_3^2 - \dfrac{s^2}{c_o^2\beta^2}}\,, & M_\infty > 1\,, \end{cases} \tag{2.5.13}$$

with $\alpha^2 = \alpha_i\alpha_i$. Making use of the theorem on convolution for the exponential Fourier transforms defined by the relation

$$f(x,t) = \mathcal{F}^{-1}[f^*(\alpha,t)] = \frac{1}{(2\pi)^{3/2}} \iiint_{-\infty}^{\infty} f^*(\alpha,t) e^{i\alpha x}\, d\alpha\,, \tag{2.5.14}$$

and taking into consideration

$$\mathcal{F}^{-1}\left[\frac{1}{\alpha^2 + k^2}\right] = \frac{1}{4\pi r} e^{-kr}$$

$$\mathcal{F}^{-1}\left[\frac{1}{-\alpha_1^2 + \alpha_2^2 + \alpha_3^2 - k^2}\right] = \frac{1}{2\pi} \frac{H(y_1^2 - (y_2^2 + y_3^2))}{\sqrt{y_1^2 - (y_2^2 + y_3^2)}} \cosh\left(k\sqrt{y_1^2 - (y_2^2 + y_3^2)}\right) \tag{2.5.15}$$

$$\mathcal{F}^{-1}\left[f^*(ci\alpha_i - b)\right] = \frac{1}{c} e^{(b/c)x_i} f\left(\frac{x_i}{c}\right)\,,$$

the Green's function in the Laplace transform domain is given by (for a general free-stream velocity U_i case)

$$\overline{g^U} = \begin{cases} \dfrac{c_o}{4\pi\sqrt{(U_k y_k)^2 + c_o^2\beta^2 r^2}} e^{-sr_o/c_o}\,, & M_\infty < 1; \\ \dfrac{c_o}{2\pi} \dfrac{H\left((U_k y_k)^2 - c_o^2\beta^2 r^2\right)}{\sqrt{(U_k y_k)^2 - c_o^2\beta^2 r^2}} e^{-s\left(\frac{U_k y_k}{c_o^2\beta^2}\right)} \cosh\left(\dfrac{s}{c_o^2\beta^2}\sqrt{(U_k y_k)^2 - c_o^2\beta^2 r^2}\right)\,, & M_\infty > 1, \end{cases} \tag{2.5.16}$$

where

$$r_o = \frac{-U_k y_k + \sqrt{(U_k y_k)^2 + c_o^2\beta^2 r^2}}{c_o\beta^2}\,, \qquad M_\infty < 1\,; \tag{2.5.17a}$$

$$\beta^2 = |1 - M_\infty^2| \qquad \text{is a compressibility parameter}\,; \tag{2.5.17b}$$

$$M_\infty = \frac{U}{c_o} \qquad \text{is the Mach Number}\,. \tag{2.5.17c}$$

It is now possible to perform the inverse Laplace transform on Eqs. (2.5.16)

$$f(x,t) = \mathcal{L}^{-1}\{\bar{f}(x,s)\} = \frac{1}{2\pi i} \int_{c-i\infty}^{c+i\infty} e^{is} \bar{f}(x,s)\, ds\,, \tag{2.5.18}$$

and taking into account that

$$\mathcal{L}^{-1}\{e^{-ks}\} = \delta(t-k)\,, \qquad k>0\,, \tag{2.5.19}$$

the following fundamental solutions in real time and space domain are obtained:

$$g^U(x-\xi,t-\tau) = \begin{cases} \dfrac{c_o}{4\pi}\dfrac{\delta(t'-r_o/c_o)}{\sqrt{(U_k y_k)^2 + c_o^2\beta^2 r^2}}\,, & M_\infty < 1\,; \\ \dfrac{c_o}{4\pi}\dfrac{H(U_k y_k - c_o\beta r)}{\sqrt{(U_k y_k)^2 - c_o^2\beta^2 r^2}}\left[\delta(t'-r_o/c_o)+\delta(t'-r_1/c_o)\right], & M_\infty > 1\,, \end{cases} \tag{2.5.20}$$

where r_o and r_1 are two values of r given by

$$r_{o,1} = \frac{U_k y_k \pm \sqrt{(U_k y_k)^2 - c_o^2\beta^2 r^2}}{c_o\beta^2}\,, \qquad M_\infty > 1\,. \tag{2.5.21}$$

The solution for a unit step source can be obtained from (2.5.20) by integrating over τ, thus:

$$\begin{aligned} G^U(x-\xi,t) &= \int_0^t g^U(x-\xi,t-\tau)\,d\tau \\ &= \begin{cases} \dfrac{c_o}{4\pi}\dfrac{H(t-r_o/c_o)}{\sqrt{(U_k y_k)^2 + c_o^2\beta^2 r^2}}\,, & M_\infty < 1\,; \\ \dfrac{c_o}{4\pi}\dfrac{H(U_k y_k - c_o\beta r)}{\sqrt{(U_k y_k)^2 - c_o^2\beta^2 r^2}}\left[H(t-r_o/c_o)+H(t-r_1/c_o)\right]. & M_\infty < 1. \end{cases} \end{aligned} \tag{2.5.22}$$

The steady state response can be derived from (2.5.22) by letting $t \to \infty$. The result simplifies to:

$$\begin{aligned} G^{Us}(x-\xi) &= G^U(x-\xi,\infty) \\ &= \begin{cases} \dfrac{c_o}{4\pi}\dfrac{1}{\sqrt{(U_k y_k)^2 + c_o^2\beta^2 r^2}}\,, & M_\infty < 1; \\ \dfrac{c_o}{2\pi}\dfrac{H\left(U_k y_k - c_o\beta r\right)}{\sqrt{(U_k y_k)^2 - c_o^2\beta^2 r^2}}\,, & M_\infty > 1\,. \end{cases} \end{aligned} \tag{2.5.23}$$

The nature of the above solutions change substantially depending on whether M_∞ is greater or less than 1. A flow is subsonic if $M_\infty < 1$ and supersonic if $M_\infty > 1$. The governing equation is either elliptic or hyperbolic depending on whether the flow is subsonic or supersonic. For the supersonic case, the surface bounding the region reached by a disturbance starting from a given point is called the Mach surface or characteristic surface which is defined by the Heaviside function in (2.5.23). The properties of supersonic flow described above give it a character that is quite different from that of the subsonic flow. If a subsonic flow meets any obstacle, the presence of this obstacle affects the flow in a space, both upstream and downstream and the effects of the obstacle is zero only asymptotically at an infinite distance from it. A supersonic flow, however, is incident "blindly" on an obstacle; the effect of the latter extends only downstream, and in all the remaining upstream part, the flow does not see the obstacle (Figure 2.5.1).

Finally it is of interest to note that a $1/r$ singularity appears in above equations.

Two-dimensional Flow

Similar to the three-dimensional case, the response for an instantaneous point source is considered first. It is not difficult to get the convective fundamental solution from (2.5.6) by the Galilean transformation $y_i \sim y_i - U_i t'$. Thus,

$$g^U(x-\xi, t-\tau) = \frac{1}{2\pi} \frac{H(t' - r_u/c_o)}{\sqrt{t'^2 - r_u^2/c_o^2}}, \tag{2.5.24}$$

where

$$r_u^2 = (y_i - U_i t')(y_i - U_i t') . \tag{2.5.25}$$

The convective response for a unit step source is

$$G^U(x-\xi, t) = \frac{1}{2\pi} \int_0^t \frac{H(t' - r_u/c_o)}{\sqrt{t'^2 - r_u^2/c_o^2}} d\tau$$

$$= \begin{cases} \dfrac{H(t - r_o/c_o)}{2\pi\beta} \ln \dfrac{c_o^2\beta\sqrt{t^2 - r_u^2/c_o^2} + c_o^2\beta^2 t + U_k y_k}{\sqrt{(U_k y_k)^2 + c_o^2\beta^2 r^2}}, & M_\infty < 1; \\ \dfrac{H(U_k y_k - c_o\beta r)}{2\pi\beta} \left\{ H(t - r_o/c_o) \left[\sin^{-1} \dfrac{c_o^2\beta^2 t - U_k y_k}{\sqrt{(U_k y_k)^2 - c_o^2\beta^2 r^2}} + \dfrac{\pi}{2} \right] \right. & \\ \qquad \left. - H(t - r_1/c_o) \left[\sin^{-1} \dfrac{c_o^2\beta^2 t - U_k y_k}{\sqrt{(U_k y_k)^2 - c_o^2\beta^2 r^2}} - \dfrac{\pi}{2} \right] \right\}, & M_\infty > 1, \end{cases} \tag{2.5.26}$$

in which the variables r_o and r_1 are defined by (2.5.17a) and (2.5.21).

The steady state response can be obtained from (2.5.26). Letting $t \to \infty$, this simiplifies to

$$G^{U_s}(x-\xi) = G^U(x-\xi, \infty)$$

$$= \begin{cases} -\dfrac{1}{2\pi\beta} ln \dfrac{\sqrt{(U_k y_k)^2 + c_o^2\beta^2 r^2}}{c_o\beta}, & M_\infty < 1; \\ \dfrac{1}{2\beta} H(U_k y_k - c_o\beta r), & M_\infty > 1. \end{cases} \tag{2.5.27}$$

In the case of steady two-dimensional flow, the characteristic surfaces will now be replaced by characteristic lines (or simply characteristics) in the plane of the flow. Through any point O in this plane there pass two characteristics (AA' and BB' in Fig 2.5.2), which intersect the stream line through this point at Mach angle α. The downstream branches OA and OB of the characteristics may be said to leave the point O; they bound the region AOB of the flow where perturbations starting from O can take effect.

These functions have a lnr singularity for the subsonic case and are also weakly singular for supersonic flow.

2.5.3.3 INCOMPRESSIBLE POTENTIAL FLOW

For incompressible potential flow, the governing equation is simply

$$\frac{\partial^2 \phi}{\partial x_i \partial x_i} = 0 . \tag{2.5.28}$$

This is the well-known Laplace equation, and the fundamental solutions are

$$\phi = \begin{cases} \dfrac{1}{4\pi r}, & \text{for 3D;} \\ -\dfrac{1}{2\pi} \ln r, & \text{for 2D.} \end{cases} \tag{2.5.29}$$

2.5.4 BOUNDARY INTEGRAL REPRESENTATIONS

2.5.4.1 COMPRESSIBLE POTENTIAL FLOW

The desired integral representation for convective compressible potential flow can be derived directly from the governing differential equation.

The governing equation (2.5.2) must, of course, hold for all points of the flow region at every instant of time. Therefore, the left-hand side of (2.5.2) multiplied by an arbitrary function $\tilde{g}$, and integrated over time and space must remain equal to zero. That is,

$$\int_0^T \int_V \tilde{g} \left[-\frac{1}{c_o^2} \frac{D_o^2 \phi}{Dt^2} + \frac{\partial^2 \phi}{\partial x_i \partial x_i} + \bar{\psi} \right] dV dt = 0 . \tag{2.5.30}$$

Next, the divergence theorem can be applied, repeatedly, to the applicable terms in (2.5.30) to transfer spatial, as well as, temporal derivatives from ϕ to $\tilde{g}$. As a result, equation (2.5.30) is transformed into

$$\begin{aligned} &\int_0^T \int_S \left[\tilde{g} \left(\frac{\partial \phi}{\partial x_i} - \frac{U_i}{c_o^2} \frac{D_o \phi}{Dt} \right) n_i - \left(\frac{\partial \tilde{g}}{\partial x_i} - \frac{U_i}{c_o^2} \frac{D_o \tilde{g}}{Dt} \right) n_i \phi \right] dS dt \\ &+ \int_0^T \int_V \left[\tilde{g} \bar{\psi} \right] dV dt + \frac{1}{c_o^2} \int_V \left[\frac{D_o \tilde{g}}{Dt} \phi \Big|_0^T - \tilde{g} \frac{D_o \phi}{Dt} \Big|_0^T \right] dV \\ &- \int_0^T \int_V \left[\left(\frac{1}{c_o^2} \frac{D_o^2 \tilde{g}}{Dt^2} - \frac{\partial^2 \tilde{g}}{\partial x_i \partial x_i} \right) \phi \right] dV dt = 0 , \end{aligned} \tag{2.5.31}$$

with n_i defined as the unit normal to surface S at x. To complete the derivation of the integral equation for any point ξ interior to S at time τ, the last volume integral appearing in (2.5.31) must reduced to $\phi(\xi, \tau)$. This is accomplished, if

$$\frac{1}{c_o^2} \frac{D_o^2 \tilde{g}}{Dt^2} - \frac{\partial^2 \tilde{g}}{\partial x_i \partial x_i} - \delta(x - \xi) \delta(t - \tau) = 0 . \tag{2.5.32}$$

Green's function $\tilde{g}$ defined by (2.5.32) is the adjoint of the original Green's function presented in Section 2.5.3. That is

$$\tilde{g}(x-\xi, t-\tau) = g^U(\xi - x, \tau - t)\,. \tag{2.5.33}$$

Substituting (2.5.32) and (2.5.33) into (2.5.31) produces the desired integral equation,

$$\begin{aligned} c(\xi)\phi(\xi,\tau) = &\int_0^T\int_S \left[g^U(\xi-x,\tau-t)u_n'(x,t) - f^U(\xi-x,\tau-t)\phi(x,t)\right]\, dS(x)dt \\ &+ \int_0^T\int_V \left[g^U(\xi-x,\tau-t)\bar{\psi}(x,t)\right]\, dV(x)dt \\ &-\frac{1}{c_o^2}\int_V \left[\frac{D_o g^U(\xi-x,\tau)}{Dt}\phi(x,0) - g^U(\xi-x,\tau)\frac{D_o\phi(x,0)}{Dt}\right]\, dV(x)\,, \end{aligned} \tag{2.5.34}$$

where

$$u_n'(x,t) = u_n(x,t) - \frac{U_n}{c_o^2}\frac{D_o\phi(x,t)}{Dt} \tag{2.5.35a}$$

$$f^U(\xi-x,\tau-t) = \frac{\partial g^U(\xi-x,\tau-t)}{\partial n} - \frac{U_n}{c_o^2}\frac{D_o g^U(\xi-x,\tau-t)}{Dt}\,, \tag{2.5.35b}$$

and $c(\xi)$ is constant. When ξ is inside S, $c(\xi) = 1$. If ξ is on the boundary then the values are determined by the relative smoothness of S at ξ. For ξ outside the region V, $c(\xi)$ is zero.

The boundary integral equation (2.5.34) can be rewritten in a more compact notation

$$c\phi = \int_S \left[g^U * u_n' - f^U * \phi\right]\, dS + \int_V \left[g^U * \bar{\psi}\right]\, dV\,. \tag{2.5.36}$$

The symbol $*$ in (2.5.36) once again symbolizes a Riemann convolution integral. If body source is absent and small perturbation approximation is introduced, the volume integral in (2.5.36) no longer remains, which simplifies to

$$c\phi = \int_S [g^U * u_n' - f^U * \phi]\, dS\,. \tag{2.5.37}$$

While for steady conditions this reduces further to

$$c\phi = \int_S \left[G^{Us}u_n' - F^{Us}\phi\right]\, dS\,, \tag{2.5.38}$$

where

$$u_n' = u_n - \frac{U_n U_i}{c_o^2}u_i \tag{2.5.39a}$$

$$F^{Us} = \frac{\partial G^{Us}}{\partial n} - \frac{U_n U_i}{c_o^2}\frac{\partial G^{Us}}{\partial x_i}\,. \tag{2.5.39b}$$

But, generally, it is not convenient to apply boundary values u_n' in solving the physical problems. This topic is discussed later in the next section.

2.5.4.2 INCOMPRESSIBLE POTENTIAL FLOW

A derivation of the integral representation for the incompressible potential theories would follow the same lines as that just presented, and therefore, will not be repeated. That is,

$$\phi = \int_S [g v_n - f\phi]\, dS\,, \tag{2.5.40}$$

where

$$v_n = \frac{\partial \phi}{\partial x_i} n_i \tag{2.5.41a}$$

$$f = \frac{\partial g}{\partial x_i} n_i\,. \tag{2.5.41b}$$

Notice that incompressible potential flow is a steady, non-convective process and with $\bar{\psi} = 0$, the convolution, convective terms and volume integrals vanish in (2.5.40).

2.5.5 NUMERICAL IMPLEMENTATION

2.5.5.1 INTRODUCTION

In this section, a numerical implementation for convective potential flow will be detailed. Unlike the formulations presented in Sections 2.2-2.4, this capability is not available in the current version of BEST-FSI. Instead the implementation was accomplished in a separate single-GMR boundary element code. As a result, some of the generality is not present. However, it is expected that future versions of BEST-FSI will include these two-dimensional steady subsonic and supersonic flow formulations.

2.5.5.2 SPATIAL DISCRETIZATION

The methodology employed for spatial discretization follows that described in Section 2.3. As a result the boundary integral equation for steady state convective compressible potential flow can now be written

$$c(\xi)\phi(\xi) = \sum_{m=1}^{M} \left[\int_{S_m} G(x(\zeta) - \xi) N_\omega(\zeta) u'_{n\omega}\, dS(x(\zeta)) - \int_{S_m} F(x(\zeta) - \xi) N_\omega(\zeta) \phi_\omega\, dS(x(\zeta)) \right]. \tag{2.5.42}$$

This equation is based on small perturbation approximation.

The integrands remaining in (2.5.42) are known in explicit form from the fundamental solutions,

$$G(x-\xi) = G^{U_s}(\xi - x) \tag{2.5.43a}$$

$$F(x-\xi) = \frac{\partial G^{U_s}(\xi - x)}{\partial x_i} n_i(x) - \frac{U_n U_i}{c_o^2} \frac{\partial G^{U_s}(\xi - x)}{\partial x_i} . \tag{2.5.43b}$$

The positioning of the nodal variables outside of the integrals is a key step, then the integrands of (2.5.42) contain only known functions, which can be evaluated numerically.

The following method is applied here to transform u_n' into boundary values u_n and ϕ. The shape function can be used to write

$$u_n'(x) - u_n(x) = -\frac{U_n U_i}{c_o^2} u_i(x) \tag{2.5.44a}$$

$$\frac{\partial N_\omega(\zeta)}{\partial \zeta} \phi_\omega = \frac{\partial x_i}{\partial \zeta} u_i(x) . \tag{2.5.44b}$$

Solving above equations, one obtains

$$u_n(x) = u_i(x) n_i(x) = -\frac{c_o^2}{U_n^2} (u_n'(x) - u_n(x)) - \frac{1}{U_n} (U_2 n_1(x) - U_1 n_2(x)) J^{-1} \frac{\partial N_\omega(\zeta)}{\partial \zeta} \phi_\omega , \tag{2.5.45}$$

in which

$$n_1(x) = J^{-1} \frac{\partial x_2}{\partial \zeta} \tag{2.5.46a}$$

$$n_2(x) = -J^{-1} \frac{\partial x_1}{\partial \zeta} , \tag{2.5.46b}$$

and J is the determinant of the jacobian matrix. Rearranging (2.5.45), one gets

$$u_n'(x) = \left(1 - \frac{U_n^2}{c_o^2}\right) u_n(x) - \frac{U_n}{c_o^2} (U_2 n_1(x) - U_1 n_2(x)) J^{-1} \frac{\partial N_\omega(\zeta)}{\partial \zeta} \phi_\omega . \tag{2.5.47}$$

Substituting (2.5.47) into (2.5.42) produces

$$c\phi = \sum_{m=1}^{M} \left\{ u_{n\omega} \int_{S_m} \left(1 - \frac{U_n^2}{c_o^2}\right) G N_\omega \, dS - \phi_\omega \int_{S_m} \left[F N_\omega + \frac{U_n}{c_o^2} (U_2 n_1 - U_1 n_2) J^{-1} \frac{\partial N_\omega}{\partial \zeta} G \right] dS \right\} \tag{2.5.48}$$

2.5.5.3 INTEGRATION

The evaluation of the integrals appearing in (2.5.48) is the next process to be examined. At present, a difference occurs in the schemes utilized for integration due to the distinctive nature of kernel functions G and F for subsonic and supersonic. Considerable care must be exercised during integration. This is particularly true for supersonic flow, in which the F kernel contains a delta function. Consequently, the integration algorithm must be much more sophisticated than those developed for subsonic flow. In the present implementation, discussed in detail in the next two subsections, a number of different integration schemes are developed depending upon the order of the kernel singularity (Table 2.5.1) and the nature of the kernels involved.

TABLE 2.5.1 Kernel Singularities

Singularity Order

Kernel	Subsonic	Supersonic
G	$\ln r$	$H(r)$
F	$\frac{1}{r}$	$\delta(r)$

Subsonic Flow

The integration schemes for subsonic flow are quite similar to those presented in Section 2.4. Consequently, most common items will not be discussed further. However, analytical integration is discussed in a little more detail due to the nature of the G kernel.

The kernel to be integrated can be written as

$$G(x-\xi) = -\frac{1}{2\pi\beta} ln \frac{\sqrt{(U_k y_k)^2 + \beta^2 c_o^2 r^2}}{c_o \beta}, \qquad M_\infty \leq 1. \tag{2.5.49}$$

The integration of the nearby subsegment of the singular point for the above function can be done by following an analytical scheme. This small subsegment can be considered as a flat line tangential to the singular point. The length of this segment can determined by a limitation of S, say, S^*, i.e.

$$0 \leq S \leq S^*, \tag{2.5.50}$$

so that the desired integral is

$$\int_{S^*} G(x-\xi) N_\omega(\zeta)\, dS(x) = -\frac{1}{2\pi\beta} \int_0^{S^*} (\ln S + A)\, N_\omega(\zeta(S))\, dS, \tag{2.5.51}$$

where

$$A = \ln \sqrt{1 + k^2 M_\infty^2/\beta^2} \qquad \text{is constant,} \tag{2.5.52a}$$

$$k = U_k y_k / U r \qquad \text{is constant for flat segmentation.} \tag{2.5.52b}$$

Case I: Node 1 is Singular Point

The shape functions for a quadratic element can be stated as

$$\begin{aligned} N_1(\zeta(S)) &= 2\left(\zeta - \frac{1}{2}\right)(\zeta - 1) = 2S^2/L^2 - 3S/L + 1 \\ N_2(\zeta(S)) &= -4\zeta(\zeta - 1) = -4S^2/L^2 + 4S/L \\ N_3(\zeta(S)) &= 2\zeta\left(\zeta - \frac{1}{2}\right) = 2S^2/L^2 - S/L, \end{aligned} \tag{2.5.53}$$

where

$$\zeta = S/L, \tag{2.5.54}$$

and L is the length of the element.

Equation (2.5.51) becomes

$$\int_{S^*} G(x-\xi)N_1(\zeta)\,dS = -\frac{1}{2\pi\beta}(2C_2/L^2 - 3C_1/L + C_0) \tag{2.5.55a}$$

$$\int_{S^*} G(x-\xi)N_2(\zeta)\,dS = -\frac{1}{2\pi\beta}(-4C_2/L^2 + 4C_1/L) \tag{2.5.55b}$$

$$\int_{S^*} G(x-\xi)N_3(\zeta)\,dS = -\frac{1}{2\pi\beta}(2C_2/L^2 - C_1/L)\,, \tag{2.5.55c}$$

where

$$C_n = \int_0^{S^*} S^n(\ln S + A)\,dS = \frac{S^{*n+1}}{n+1}\left(\ln S^* + A + \frac{1}{n+1}\right) \qquad n = 0,1,2\,. \tag{2.5.56}$$

The constant k can be expressed as

$$k = (U_2 n_1 - U_1 n_2)/U\,. \tag{2.5.57}$$

Case II: Node 3 is Singular Point

The shape functions for a quadratic element can be stated as

$$\begin{aligned} N_1(\zeta(S)) &= 2\zeta\left(\zeta - \frac{1}{2}\right) = 2S^2/L^2 - S/L \\ N_2(\zeta(S)) &= -4\zeta(\zeta-1) = -S^2/L^2 + 4S/L \\ N_3(\zeta(S)) &= 2\left(\zeta - \frac{1}{2}\right)(\zeta-1) = 2S^2/L^2 - 3S/L + 1\,. \end{aligned} \tag{2.5.58}$$

It is not difficult to get the desired integrals:

$$\int_{S^*} G(x-\xi)N_1(\zeta)\,dS = -\frac{1}{2\pi\beta}(2C_2/L^2 - C_1/L) \tag{2.5.59a}$$

$$\int_{S^*} G(x-\xi)N_2(\zeta)\,dS = -\frac{1}{2\pi\beta}(-4C_2/L^2 + 4C_1/L) \tag{2.5.59b}$$

$$\int_{S^*} G(x-\xi)N_3(\zeta)\,dS = -\frac{1}{2\pi\beta}(2C_2/L^2 - 3C_1/L + C_0)\,. \tag{2.5.59c}$$

But notice here the constant k is

$$k = (U_1 n_2 - U_2 n_1)/U\,. \tag{2.5.60}$$

Case III: Node 2 is Singular Point

In this case, the shape functions for a quadratic element can be stated as

$$\begin{aligned} N_1(\zeta(S)) &= \frac{1}{2}\zeta(\zeta-1) = \frac{1}{2}S^2/L^2 - \frac{1}{2}S/L \\ N_2(\zeta(S)) &= (1-\zeta)(1+\zeta) = 1 - S^2/L^2 \\ N_3(\zeta(S)) &= \frac{1}{2}\zeta(\zeta+1) = \frac{1}{2}S^2/L^2 + \frac{1}{2}S/L\,, \end{aligned} \tag{2.5.61}$$

where

$$\zeta_1 = -S/L_1\,; \qquad \zeta_2 = S/L_2\,, \tag{2.5.62}$$

L_1 distance between node 1 and node 2

L_2 distance between node 2 and node 3.

Substituting (2.5.61) and (2.5.62) into (2.5.51)

$$\int_{S^*} G(x-\xi)N_\omega(\zeta)\,dS = \frac{1}{2\pi\beta}\left\{\int_0^{S^*} G(x-\xi)N_\omega(\zeta_1(S))\,dS + \int_0^{S^*} G(x-\xi)N_\omega(\zeta_2(S))\,dS\right\}, \quad (2.5.63)$$

i.e.,

$$\int_{S^*} G(x-\xi)N_1(\zeta)\,dS = -\frac{1}{2\pi\beta}\left[\frac{1}{2}(C_2^1/L_1^2 + C_1^1/L_1) + \frac{1}{2}(C_2^2/L_2^2 - C_1^2/L_2)\right] \quad (2.5.64a)$$

$$\int_{S^*} G(x-\xi)N_2(\zeta)\,dS = -\frac{1}{2\pi\beta}\left[(1 - c_2^1/L_1^2) + (1 - C_2^2/L_2^2)\right] \quad (2.5.64b)$$

$$\int_{S^*} G(x-\xi)N_3(\zeta)\,dS = -\frac{1}{2\pi\beta}\left[\frac{1}{2}(C_2^1/L_1^2 - C_1^1/L_1) + \frac{1}{2}(C_2^2/L_2^2 + C_1^2/L_2)\right], \quad (2.5.64c)$$

where

$$C_n^i = \int_0^{S^*} s^n(\ln s + A_i)\,dS = \frac{S^{*n+1}}{n+1}\left(\ln S^* + A_i + \frac{1}{n+1}\right). \quad (2.5.65)$$

The constants A_i and k_i are

$$A_i = \ln\sqrt{1 + k_i^2 M_\infty^2/\beta^2} \quad (2.5.66a)$$

$$k_1 = (U_1 n_2 - U_2 n_1)/U\,, \qquad k_2 = (U_2 n_1 - U_1 n_2)/U\,. \quad (2.5.66b)$$

For the F kernel the numerical integration discussed in Section 2.4 together with the indirect 'equipotential' method, is applicable. These lead to the accurate determination of the coefficient involving the F integrals.

Supersonic Flow

For supersonic flow (from Table 2.5.1), the integration of the G kernel is weakly singular. As a result, a much less sophisticated integration scheme can be employed to obtain the required level of accuracy with relatively few subsegments and gauss points.

However, the integration of the F kernel (which is a delta function) must be taken care of properly. The numerical integration is no longer possible and analytical integration must be carried out. In order to explain this scheme easily, the problem is simplified to one involving only x_1-direction free-stream velocity U_1. Thus, the G kernel can be written as

$$G(x-\xi) = \frac{1}{2\beta}\left[H(\beta y_2 - y_1) - H(\beta y_2 + y_1)\right]. \quad (2.5.67)$$

From (2.5.43b), the F kernel can be obtained as:

$$F(x-\xi) = \frac{1}{2}\left[(n_2 + \beta n_1)\delta(y_1 - \beta y_2) - (n_2 - \beta n_1)\delta(y_1 + \beta y_2)\right]. \quad (2.5.68)$$

In above equation the arguments of the delta function $y_1 - \beta y_2$ and $y_1 + \beta y_2$ represent the two characteristic lines of the Mach cone. Thus, for any element m, the required integral can be written as

$$\int_{S_m} F(x-\xi)N_\omega\,dS = \frac{1}{2}\int_{S_m}(n_2 + \beta n_1)N_\omega\delta(y_1 - \beta y_2)\,dS - \frac{1}{2}\int_{S_m}(n_2 - \beta n_1)N_\omega\delta(y_1 + \beta y_2)\,dS. \quad (2.5.69)$$

Only the first integral in the above equation will be examined. To assist in this endeavor, the following two distinct cases can be identified.

(1) The characteristic line does not cross the element m.

(2) The characteristic line crosses the element m.

In the first case, the integral is zero according the definition of the delta function.

Turning next to case (2), the characteristic line and element m may have one or two intersections (for a quadratic element), which can be located by solving the following equation

$$y_1 - \beta y_2 = 0\,. \tag{2.5.70}$$

In the local coordinate system, the above equation becomes

$$a\zeta^2 + b\zeta + c = 0\,. \tag{2.5.71}$$

By imposing the shape function the coordinates y_i can be expressed as

$$y_i = x_i(\zeta) - \xi_i = N_\omega(\zeta) x_{i\omega} - \xi_i\,. \tag{2.5.72}$$

The coefficients of (2.5.71) can be then defined as

$$\begin{aligned} a &= 2z_1 - 4z_2 + 2z_3 \\ b &= -3z_1 + 4z_2 - z_3 \\ c &= z_2 - \eta\,, \end{aligned} \tag{2.5.73}$$

where

$$\begin{aligned} z_\omega &= x_{1\omega} - \beta x_{2\omega} \\ \eta &= \xi_1 - \beta \xi_2\,. \end{aligned} \tag{2.5.74}$$

Of the two roots of equation (2.5.71) ζ_1 and ζ_2, only the solutions $0 \le \zeta_i \le 1$ are relevant. Once the intersections are found, the desired integral is obtained as

$$\frac{1}{2}\int_{S_m} (n_2 + \beta n_1) N_\omega \delta(y_1 - \beta y_2)\, dS = \frac{1}{2a} \sum_{i=1}^{2} [n_2(\zeta_i) + \beta n_1(\zeta_i)]\, N_\omega(\zeta_i) J(\zeta_i) \qquad 0 \le \zeta_i \le 1, \tag{2.5.75}$$

where J is the jacobian (determinant) of the transformation. Following the same procedure, the second integral in (2.5.69) can be determined easily.

Similar to subsonic flow, the singular term of integration of the F kernel can be obtained by the 'equipotential' method.

2.5.5.4 ASSEMBLY

Once the spatial discretization and integration algorithms are completed, a system of linear algebraic equations can be developed to permit an approximate solution of the compressible potential flow problem. The method of collocation is employed by writing (2.5.48) at each functional node:

$$[G]\{u_n\} - [F]\{\phi\} = \{0\}\,, \tag{2.5.76}$$

where

$\{\phi\}$ nodal potential with P components

$\{u_n\}$ nodal normal velocity with Q components

$[F]$ assembled matrix of size $P \times P$ calculated from (2.5.48)

$[G]$ unassembled matrix of size $P \times Q$ calculated from (2.5.48)

P total number of functional nodes

$Q = \sum_{m=1}^{M} A_m$

A_m number of functional nodes in element m.

2.5.5.5 SOLUTION

For subsonic flow, it is a simple operation to rearrange (2.5.76) The known ϕ and u_n values form one vector $\{y\}$ of size $(Q \times 1)$, while the unknown ϕ and u_n values comprise another $P \times 1$ vector $\{x\}$. Whence (2.5.76) can be rewritten as

$$[A]\{x\} - [B]\{y\} = \{0\}, \tag{2.5.77a}$$

which can be solved for $\{x\}$. The result that is all ϕ and u_n components (i.e., both ϕ and u_n on every boundary element) are now known on S.

Because of the hyperbolic nature of the governing equation, the supersonic problem is more like an initial value problem rather than a boundary value problem. Consequently, a marching procedure must be performed in space. Initial data ϕ and $\frac{\partial \phi}{\partial n}$ are prescribed along the line $x = 0$ (see Figure 2.5.3) and the solution is advanced in the x direction subject to wall boundary conditions and an appropriate condition at the upper boundary y_{max}. By using this procedure, the quantities on the boundary can be determined sequentially. Thus the unknown vector $\{x\}$ reduces to $(P - N) \times 1$, where N is the number of points on the initial data surface (inlet surface) for which both ϕ and $\frac{\partial \phi}{\partial n}$ are specified. On the other hand, the values u_n on the outlet surface remain undetermined, because their G-coefficients are all zero. That means that the points at the outlet can only receive influences from other points within the upstream Mach cone. Now the equations can be written as:

$$\begin{bmatrix} a_{(N+1)(N+1)} & 0 & \cdots & 0 \\ a_{(N+2)(N+1)} & a_{(N+2)(N+2)} & \cdots & 0 \\ \vdots & \vdots & \ddots & \vdots \\ a_{P(N+1)} & a_{P(N+2)} & \cdots & a_{PP} \end{bmatrix} \begin{Bmatrix} x_{N+1} \\ x_{N+2} \\ \vdots \\ x_P \end{Bmatrix}$$

$$- \left\{ \begin{bmatrix} b_{(N+1)(N+1)} & 0 & \cdots & 0 \\ b_{(N+2)(N+1)} & b_{(N+2)(N+2)} & \cdots & 0 \\ \vdots & \vdots & \ddots & \vdots \\ b_{P(N+1)} & b_{P(N+2)} & \cdots & b_{PQ} \end{bmatrix} \begin{Bmatrix} y_{N+1} \\ y_{N+2} \\ \vdots \\ y_Q \end{Bmatrix} - \sum_{n=1}^{N} \begin{Bmatrix} a_{(N+1)n} x_n \\ a_{(N+2)n} x_n \\ \vdots \\ a_{Pn} x_n \end{Bmatrix} \right\} = 0. \tag{2.5.77b}$$

These are not simultaneous equations as in the elliptic case, but are successive requiring specification of all boundary quantities at the inlet. The solution therefore does not require

any elimination. The boundary conditions at exit are not required but are determined from the remaining boundary solutions.

2.5.5.6 INTERIOR VALUES

Once equation (2.5.77) is solved, the complete set of primary nodal quantities, $\{\theta\}$ and $\{u_n\}$, is known. Consequently, the response at points within the body can be calculated in a straightforward manner. For any point ξ in the interior, the velocity potential can be determined from (2.5.48) with $c = 1$:

$$\phi = \sum_{m=1}^{M} \left\{ u_{n\omega} \int_{S_m} \left(1 - \frac{U_n^2}{c_o^2}\right) G N_\omega \, dS - \phi_\omega \int_{S_m} \left[F N_\omega + \frac{U_n}{c_o^2}(U_2 n_1 - U_1 n_2) J^{-1} \frac{\partial N_\omega}{\partial \zeta} G \right] dS \right\}. \quad (2.5.78)$$

Meanwhile the boundary integral equation for velocity, can be written

$$u_i(\xi) = \sum_{m=1}^{M} \left[u_{n\omega} \int_{S-m} B_i(x(\zeta) - \xi) \, dS(x(\zeta) - \phi_\omega \int_{S_m} C_i(x(\zeta) - \xi) \, dS(x(\zeta)) \right], \quad (2.5.79)$$

where

$$B_i(x(\zeta) - \xi) = \left(1 - \frac{U_n^2}{c_o^2}\right) \frac{\partial G(x(\zeta) - \xi)}{\partial \xi_i} N_\omega(\zeta) \quad (2.5.80a)$$

$$C_i(x(\zeta) - \xi) = \frac{\partial F(x(\zeta) - \xi)}{\partial \xi_i} N_\omega(\zeta) + \frac{U_n}{c_o^2}(U_2 n_1(x) - U_1 n_2(x)) J^{-1} \frac{\partial N_\omega(\zeta)}{\partial \zeta} \frac{\partial G(x(\zeta) - \xi)}{\partial \xi_i}. \quad (2.5.80b)$$

Actually, for supersonic flow, it is difficult to evaluate C_i since $\frac{\partial F}{\partial x_i}$ is involved. Fortunately, a local finite difference method can be applied.

Equations (2.5.78) and (2.5.79) are valid for interior points, whereas, when ξ is on the boundary, the shape functions can again be used. In this latter case, the velocity potential has the relationship

$$\phi(\xi) = N_\omega(\zeta) \phi_\omega . \quad (2.5.81)$$

Meanwhile the velocity on the boundary satisfies

$$u_n(\xi) = u_i(\xi) n_i(\xi) \quad (2.5.82a)$$

$$\frac{\partial N_\omega(\zeta)}{\partial \zeta} \phi_\omega = \frac{\partial \xi_i}{\partial \zeta} u_i(\xi), \quad (2.5.82b)$$

which can be solved simultaneously for boundary velocity.

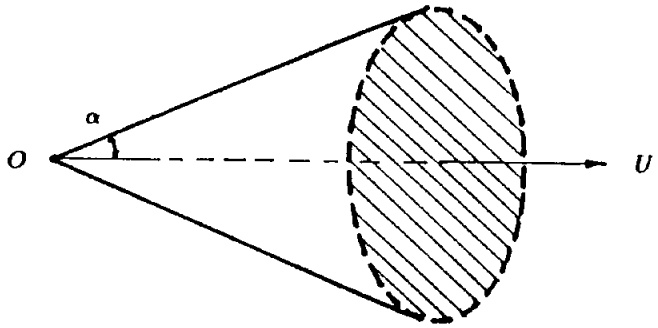

Figure 2.5.1 3D Mach Surface

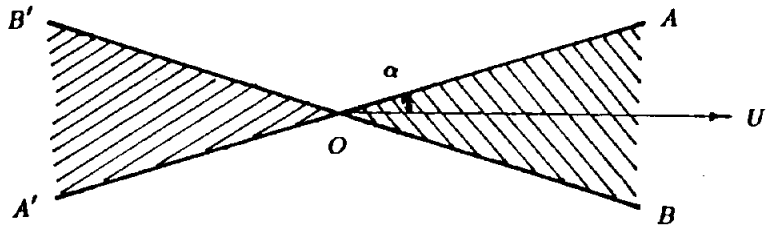

Figure 2.5.2 2D Mach Lines

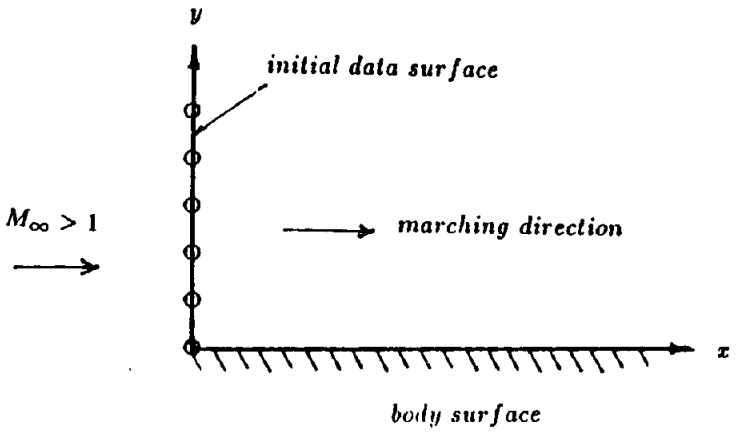

Figure 2.5.3 Coordinate System for Marching Problem

2.6 COMPRESSIBLE THERMOVISCOUS FLOW

2.6.1 INTRODUCTION

Boundary element formulations for convective incompressible flows have been presented in Section 2.4. However for more general high speed flows, compressibility of the fluid must also be considered. In particular, shock-related phenomena that characterizes such flow are not present in the incompressible flow. To correct this deficiency, a compressible thermoviscous integral formulation is presented in this section. It should be note that, while Oseen derived some of the fundamental solutions required for the incompressible case, no such solutions are available for compressible flow. Consequently, considerable time and effort was required to derive these new approximate infinite space Green's functions.

Details of the integral formulations for compressible thermoviscous flow are presented below. Separate subsections present the governing differential equations, the infinite space fundamental solutions and the integral equations.

2.6.2 GOVERNING EQUATIONS

Application of the Principles of Conservation of Mass, Momentum and Energy for a compressible thermoviscous fluid leads to the following differential equations:

$$\frac{D\rho}{Dt} + \rho\frac{\partial v_i}{\partial x_i} - \psi = 0 \tag{2.6.1a}$$

$$\rho\frac{Dv_i}{Dt} - (\lambda+\mu)\frac{\partial^2 v_j}{\partial x_i \partial x_j} - \mu\frac{\partial^2 v_i}{\partial x_j \partial x_j} + \frac{\partial p}{\partial x_i} - f_i = 0 \tag{2.6.1b}$$

$$\rho c_p\frac{D\theta}{Dt} - k\frac{\partial^2\theta}{\partial x_i \partial x_i} - \frac{Dp}{Dt} + \frac{p}{\rho}\psi - \Phi - \phi = 0\,, \tag{2.6.1c}$$

where

- v_i local velocity vector
- ρ mass density
- p thermodynamic pressure
- θ thermodynamic temperature
- λ, μ coefficients of viscosity
- c_p specific heat at constant pressure
- k thermal conductivity
- ψ mass source rate per unit volume
- f_i body force vector
- ϕ heat source rate per volume

D/Dt material time derivative defined as $\frac{D}{Dt} = \frac{\partial}{\partial t} + v_i \frac{\partial}{\partial x_i}$,
and Φ is the viscous dissipation defined by

$$\Phi = \tau_{ij} \frac{\partial v_i}{\partial x_j}, \tag{2.6.2}$$

where for compressible flow

$$\tau_{ij} = \mu \left(\frac{\partial v_i}{\partial x_j} + \frac{\partial v_j}{\partial x_i} \right) + \lambda \delta_{ij} \frac{\partial v_k}{\partial x_k}. \tag{2.6.3}$$

By introducing reference values for each of the primary variables and the perturbations except for temperature θ, the governing (2.6.1) can be rewritten as

$$\frac{D_o \tilde{\rho}}{Dt} + \rho_o \frac{\partial u_i}{\partial x_i} - \bar{\psi} = 0 \tag{2.6.4a}$$

$$\rho_o \frac{D_o u_i}{Dt} - (\lambda + \mu) \frac{\partial^2 u_j}{\partial x_i \partial x_j} - \mu \frac{\partial^2 u_i}{\partial x_j \partial x_j} + \frac{\partial \tilde{p}}{\partial x_i} - \bar{f}_i = 0 \tag{2.6.4b}$$

$$\rho_o c_p \frac{D_o \theta}{Dt} - k \frac{\partial^2 \theta}{\partial x_i \partial x_i} - \frac{D_o \tilde{p}}{Dt} - \bar{\phi} = 0, \tag{2.6.4c}$$

in which

$$\bar{\psi} = -u_i \frac{\partial \tilde{\rho}}{\partial x_i} - \tilde{\rho} \frac{\partial u_i}{\partial x_i} + \psi \tag{2.6.5a}$$

$$\bar{f}_i = -\rho u_j \frac{\partial u_i}{\partial x_j} - \tilde{\rho} \frac{D_o u_i}{Dt} + f_i \tag{2.6.5b}$$

$$\bar{\phi} = -\rho c_p u_i \frac{\partial \theta}{\partial x_i} - \tilde{\rho} c_p \frac{D_o \theta}{Dt} + u_i \frac{\partial \tilde{p}}{\partial x_i} - \frac{p}{\rho} \psi + \Phi + \phi, \tag{2.6.5c}$$

and

$$\frac{D_o}{Dt} = \frac{\partial}{\partial t} + U_i \frac{\partial}{\partial x_i}, \tag{2.6.6}$$

U_i, ρ_o, ρ_o constant reference variables

$u_i, \tilde{p}, \tilde{\rho}$ perturbations.

An alternative formulation for the mass conservation equation (2.6.4a) can be developed noting that speed of sound $c = \sqrt{\frac{dp}{d\rho}}$ depends on the relationship between pressure and density. Thus the second equation of (2.6.4) becomes

$$\rho_o \frac{D_o u_i}{Dt} - (\lambda + \mu) \frac{\partial^2 u_j}{\partial x_i \partial x_j} - \mu \frac{\partial^2 u_i}{\partial x_j \partial x_j} + c^2 \frac{\partial \tilde{\rho}}{\partial x_i} = \bar{f}_i. \tag{2.6.4b'}$$

Differentiating (2.6.4b') with respect to x_i, one obtains

$$\frac{D_o}{Dt} \left(\rho_o \frac{\partial u_i}{\partial x_i} \right) - \eta \frac{\partial^2}{\partial x_j \partial x_j} \left(\rho_o \frac{\partial u_i}{\partial x_i} \right) + c^2 \frac{\partial^2 \tilde{\rho}}{\partial x_i \partial x_i} = \frac{\partial \bar{f}_i}{\partial x_i}, \tag{2.6.7}$$

in which $\eta = (\lambda + 2\mu)/\rho_o$.

Substituting (2.6.4a) into (2.6.7), the governing equation for density is obtained as

$$\frac{1}{c^2} \frac{D_o^2 \tilde{\rho}}{Dt^2} - \frac{\partial^2 \tilde{\rho}}{\partial x_i \partial x_i} - \frac{\eta}{c^2} \frac{\partial^2}{\partial x_i \partial x_i} \left(\frac{D_o \tilde{\rho}}{Dt} \right) = \frac{1}{c^2} \left[\frac{D_o}{Dt} - (\lambda + 2\mu) \frac{\partial^2}{\partial x_i \partial x_i} \right] \bar{\psi} - \frac{1}{c^2} \frac{\partial \bar{f}_i}{\partial x_i}. \tag{2.6.8}$$

Once again, the relationship between pressure and density ($c^2 = \frac{dp}{d\rho}$) is applied in (2.6.8). The resulting governing equation for pressure then becomes

$$\frac{1}{c^2}\frac{D_o^2\tilde{p}}{Dt^2} - \frac{\partial^2\tilde{p}}{\partial x_i \partial x_i} - \frac{\eta}{c^2}\frac{\partial^2}{\partial x_i \partial x_i}\left(\frac{D_o\tilde{p}}{Dt}\right) = \left[\frac{D_o}{Dt} - (\lambda+2\mu)\frac{\partial^2}{\partial x_i \partial x_i}\right]\tilde{\psi} - \frac{\partial \bar{f}_i}{\partial x_i}\,. \tag{2.6.9}$$

The final form of the governing differential equations for compressible thermoviscous flow can now be rewritten as

$$\frac{1}{c^2}\frac{D_o^2\tilde{p}}{Dt^2} - \frac{\partial^2\tilde{p}}{\partial x_i \partial x_i} - \bar{\Omega} = 0 \tag{2.6.10a}$$

$$\rho_o\frac{D_o u_i}{Dt} - (\lambda+\mu)\frac{\partial^2 u_j}{\partial x_i \partial x_j} - \mu\frac{\partial^2 u_i}{\partial x_j \partial x_j} + \frac{\partial\tilde{p}}{\partial x_i} - \bar{f}_i = 0 \tag{2.6.10b}$$

$$\rho_o c_p\frac{D_o\theta}{Dt} - k\frac{\partial^2\theta}{\partial x_i \partial x_i} - \frac{D_o\tilde{p}}{Dt} - \bar{\phi} = 0\,, \tag{2.6.10c}$$

where

$$\bar{\Omega} = \left[\frac{D_o}{Dt} - (\lambda+2\mu)\frac{\partial^2}{\partial x_i \partial x_i}\right]\tilde{\psi} - \frac{\partial \bar{f}_i}{\partial x_i} + \frac{\eta}{c^2}\frac{\partial^2}{\partial x_i \partial x_i}\left(\frac{D_o\tilde{p}}{Dt}\right)\,. \tag{2.6.11}$$

Note here, the third term which is the viscous effect in the pressure equation is included in body source $\bar{\Omega}$ since its contribution can be assumed to be small (the coefficient $\frac{\eta}{c^2}$ is small). Now, the first two equations of (2.6.10) are one way coupled. The first equation is independent of the others, while the mass and momentum balance operators are coupled by the inclusion of both velocity (u_i) and pressure ($\tilde{p}$). The derivation of the fundamental solutions and integral formulation based upon equations (2.6.10) are detailed in the following sections.

2.6.3 FUNDAMENTAL SOLUTIONS

Consider, first, the coupled set of equations (2.6.10a) and (2.6.10b). The first equation now is just the scalar wave equation for which the fundamental solution is presented in Section 2.5.3. However, the equations (2.6.10b) require further investigation. Introduce the Helmholz decomposition of the velocity and body force, such that

$$u_i = \frac{\partial w}{\partial x_i} + e_{ijk}\frac{\partial W_k}{\partial x_j} \qquad \text{with} \quad \frac{\partial W_i}{\partial x_i} = 0 \tag{2.6.12a}$$

$$\bar{f}_i = \frac{\partial f}{\partial x_i} + e_{ijk}\frac{\partial F_k}{\partial x_j} \qquad \text{with} \quad \frac{\partial F_i}{\partial x_i} = 0\,. \tag{2.6.12b}$$

Then, (2.6.10b) becomes

$$\frac{\partial}{\partial x_i}\left[\rho_o\frac{D_o w}{Dt} - (\lambda+2\mu)\frac{\partial^2 w}{\partial x_j \partial x_j} + \tilde{p} - f\right] + e_{ikl}\frac{\partial}{\partial x_k}\left[\rho_o\frac{D_o W_l}{Dt} - \mu\frac{\partial^2 W_l}{\partial x_j \partial x_j} - F_l\right] = 0\,. \tag{2.6.13}$$

For generality, the bracketed terms must vanish independently. Thus

$$\rho_o\frac{D_o w}{Dt} - (\lambda+2\mu)\frac{\partial^2 w}{\partial x_i \partial x_i} + \tilde{p} - f = 0 \tag{2.6.14a}$$

$$\rho_o\frac{D_o W_i}{Dt} - \mu\frac{\partial W_i}{\partial x_j \partial x_j} - F_i = 0\,. \tag{2.6.14b}$$

Notice that equation (2.6.14b) is completely independent of w and $\tilde{p}$, and, consequently can be solved separately. In fact, this is the vortical component of flow, which is dominated by viscosity and convection. This component behaves in an identical manner for both compressible and incompressible flow. On the other hand, the dilatational component must respond elastically within a convective medium, i.e.

$$u_i = u_i^{(vort)} + u_i^{(dil)}\,, \tag{2.6.15}$$

where

$$u_i^{(vort)} = e_{ijk}\frac{\partial W_k}{\partial x_j} = u_i^{(incomp)} \tag{2.6.16a}$$

$$u_i^{(dil)} = \frac{\partial w}{\partial x_i}\,. \tag{2.6.16b}$$

Combining appropriate derivatives of (2.6.10a), (2.6.14a) and (2.6.10c), yields the following differential equations for w and θ:

$$\left(\frac{1}{c^2}\frac{D_o^2}{Dt^2} - \frac{\partial^2}{\partial x_i \partial x_i}\right)\left[\frac{1}{\eta}\frac{D_o}{Dt} - \frac{\partial^2}{\partial x_j \partial x_j}\right] w = \frac{1}{\lambda+2\mu}\left(\frac{1}{c^2}\frac{D_o^2}{Dt^2} - \frac{\partial^2}{\partial x_i \partial x_i}\right) f - \frac{1}{\lambda+2\mu}\bar{\Omega} \tag{2.6.17a}$$

$$\left(\frac{1}{c^2}\frac{D_o^2}{Dt^2} - \frac{\partial^2}{\partial x_i \partial x_i}\right)\left(\frac{1}{\kappa}\frac{D_o}{Dt} - \frac{\partial^2}{\partial x_k \partial x_k}\right)\theta = \frac{1}{k}\frac{D_o\bar{\Omega}}{Dt} + \frac{1}{k}\left(\frac{1}{c^2}\frac{D_o^2}{Dt^2} - \frac{\partial^2}{\partial x_i \partial x_i}\right)\bar{\phi}\,. \tag{2.6.17b}$$

Actually, the solutions of (2.6.17) that are required for the boundary element formulation are those due to instantaneous point mass sources and point forces. Furthermore, the pressure response and the velocity field corresponding to these sources and forces must be determined at same time. In all cases, the results can be determined directly from the solution of the equation

$$\left(\frac{1}{c^2}\frac{D_o^2}{Dt^2} - \frac{\partial^2}{\partial x_i \partial x_i}\right)\left(\frac{1}{\eta}\frac{D_o}{Dt} - \frac{\partial^2}{\partial x_j \partial x_j}\right)\left(\frac{1}{\kappa}\frac{D_o}{Dt} - \frac{\partial^2}{\partial x_k \partial x_k}\right)\beta_U - \delta(x-\xi)\delta(t-\tau) = 0\,, \tag{2.6.18}$$

where the scalar variable β_U is introduced along with the usual generalized delta function (δ). The subscript, U, is merely a reminder that β_U is a uniformly moving medium solution. Consequently, the fundamental solutions of the equation (2.6.10) can be obtained from the variable β_U

$$\frac{\partial^2 g_{ij}^{U(dil)}}{\partial x_k \partial x_k} = \frac{1}{\lambda+2\mu}\left(\frac{1}{c^2}\frac{D_o^2}{Dt^2} - \frac{\partial^2}{\partial x_k \partial x_k}\right)\left(\frac{1}{\kappa}\frac{D_o}{Dt} - \frac{\partial^2}{\partial x_j \partial x_j}\right)\frac{\partial^2 \beta_U}{\partial x_i \partial x_j} \tag{2.6.19a}$$

$$g_{ip}^U = -\frac{1}{\lambda+2\mu}\left(\frac{1}{\kappa}\frac{D_o}{Dt} - \frac{\partial^2}{\partial x_k \partial x_k}\right)\frac{\partial \beta_U}{\partial x_i} \tag{2.6.19b}$$

$$g_{\theta p}^U = \frac{1}{k}\left(\frac{1}{\eta}\frac{D_o}{Dt} - \frac{\partial^2}{\partial x_i \partial x_i}\right)\frac{D_o \beta_U}{Dt} \tag{2.6.19c}$$

$$g_{\theta\theta}^U = \frac{1}{k}\left(\frac{1}{c^2}\frac{D_o^2}{Dt^2} - \frac{\partial^2}{\partial x_i \partial x_i}\right)\left(\frac{1}{\eta}\frac{D_o}{Dt} - \frac{\partial^2}{\partial x_j \partial x_j}\right)\beta_U \tag{2.6.19d}$$

In a condensed notation, equation (2.6.18) can be written as

$$L\beta_U - \delta(x-\xi)\delta(t-\tau) = 0\,. \tag{2.6.20}$$

For solving the above equation, the Laplace transform with respect to t and triple exponential Fourier transform with respect x are applied again, which leads to

$$\overline{L^*}\,\overline{\beta_U}^* - 1 = 0\,. \tag{2.6.21}$$

Now $\bar{L}^*$ is a algebraic function

$$\overline{L}^* = \left[\alpha^2 + \frac{(s+i\alpha_k U_k)^2}{c^2}\right]\left[\alpha^2 + \frac{s+i\alpha_k U_k}{\eta}\right]\left[\alpha^2 + \frac{s+i\alpha_k U_k}{\kappa}\right]. \tag{2.6.22}$$

The result in the transform domain is obviously

$$\overline{\beta_U}^* = \frac{1}{\overline{L}^*} = \frac{1}{\left[\alpha^2 + \frac{(s+i\alpha_k U_k)^2}{c^2}\right]\left[\alpha^2 + \frac{s+i\alpha_k U_k}{\eta}\right]\left[\alpha^2 + \frac{s+i\alpha_k U_k}{\kappa}\right]}. \tag{2.6.23}$$

Backsubstituting the above equation into (2.6.19), the corresponding fundamental solutions in the transform domain can be obtained as:

$$\begin{aligned}\overline{\left(g_{ij}^{U(dil)}\right)}^* &= -\frac{1}{(\lambda+2\mu)}\frac{(i\alpha_i)(i\alpha_j)}{\alpha^2}\left[\alpha^2 + \frac{s+i\alpha_k U_k}{\kappa}\right]\left[\alpha^2 + \frac{(s+i\alpha_k U_k)^2}{c^2}\right]\overline{\beta_U}^* \\ &= -\frac{1}{\lambda+2\mu}\frac{(i\alpha_i)(i\alpha_j)}{\alpha^2\left[\alpha^2 + \frac{s+i\alpha_k U_k}{\eta}\right]}\end{aligned} \tag{2.6.24a}$$

$$\begin{aligned}\overline{\left(g_{ip}^{U}\right)}^* &= -\frac{1}{\lambda+2\mu}\left[\alpha^2 + \frac{s+i\alpha_k U_k}{\kappa}\right](i\alpha_i)\overline{\beta_U}^* \\ &= -\frac{1}{\lambda+2\mu}\frac{i\alpha_i}{\left[\alpha^2 + \frac{s+i\alpha_k U_k}{\eta}\right]\left[\alpha^2 + \frac{(s+i\alpha_k U_k)^2}{c^2}\right]}\end{aligned} \tag{2.6.24b}$$

$$\begin{aligned}\overline{\left(g_{\theta p}^{U}\right)}^* &= \frac{1}{k}(s+i\alpha_k U_k)\left[\alpha^2 + \frac{s+i\alpha_k U_k}{\eta}\right]\overline{\beta_U}^* \\ &= \frac{1}{k}\frac{s+i\alpha_k U_k}{\left[\alpha^2 + \frac{(s+i\alpha_k U_k)^2}{c^2}\right]\left[\alpha^2 + \frac{s+i\alpha_k U_k}{\kappa}\right]}\end{aligned} \tag{2.6.24c}$$

$$\begin{aligned}\overline{\left(g_{\theta\theta}^{U}\right)}^* &= \frac{1}{k}\left[\alpha^2 + \frac{(s+i\alpha_k U_k)^2}{c^2}\right]\left[\alpha^2 + \frac{s+i\alpha_k U_k}{\eta}\right]\overline{\beta_U}^* \\ &= \frac{1}{k}\frac{1}{\alpha^2 + \frac{s+i\alpha_k U_k}{\kappa}}\,.\end{aligned} \tag{2.6.24d}$$

The response for unit step body forces and sources can be obtained from the above solutions by multipling by a factor $\frac{1}{s}$. That is,

$$\overline{\left(G_{\alpha\beta}^{U}\right)}^* = \frac{1}{s}\overline{\left(g_{\alpha\beta}^{U}\right)}^*\,. \tag{2.6.25}$$

The steady state solutions in the Fourier transform domain can be obtained from (2.6.24) by letting $s \to 0$. Thus,

$$(G^{Us}_{\alpha\beta})^* = \overline{\left(g^U_{\alpha\beta}\right)}^*_{s=0}. \tag{2.6.26}$$

2.6.3.1 UNCONVECTIVE COMPRESSIBLE FLOW

Governing Equations

Before the Oseen's kernels are introduced, it is easy to start from the corresponding Stokes' kernels. The entire contribution of the convective terms are considered as effective body forces and sources. Thus, the governing equations (2.6.10) become

$$\frac{1}{c^2}\frac{\partial^2 \tilde{p}}{\partial t^2} - \frac{\partial^2 \tilde{p}}{\partial x_i \partial x_i} - \bar{\Omega} = 0 \tag{2.6.27a}$$

$$\rho_o \frac{\partial u_i}{\partial t} - (\lambda+\mu)\frac{\partial^2 u_j}{\partial x_i \partial x_j} - \mu \frac{\partial^2 u_i}{\partial x_j \partial x_j} + \frac{\partial \tilde{p}}{\partial x_i} - \bar{f}_i = 0 \tag{2.6.27b}$$

$$\rho_o c_p \frac{\partial \theta}{\partial t} - k\frac{\partial^2 \theta}{\partial x_i \partial x_i} - \frac{\partial \tilde{p}}{\partial t} - \bar{\phi} = 0\,, \tag{2.6.27c}$$

where

$$\bar{\Omega} = \left[\frac{\partial}{\partial t} - (\lambda+2\mu)\frac{\partial^2}{\partial x_i \partial x_i}\right]\bar{\psi} - \frac{\partial \bar{f}_i}{\partial x_i} \tag{2.6.28a}$$

$$\bar{f}_i = -\rho_o v_j \frac{\partial u_i}{\partial x_j} - \tilde{\rho}\frac{Du_i}{Dt} + f_i \tag{2.6.28b}$$

$$\bar{\psi} = -v_i \frac{\partial \tilde{\rho}}{\partial x_i} - \tilde{\rho}\frac{\partial u_i}{\partial x_i} + \psi \tag{2.6.28c}$$

$$\bar{\phi} = -\rho_o c_p v_i \frac{\partial \theta}{\partial x_i} - \tilde{\rho} c_p \frac{D_o \theta}{Dt} + v_i \frac{\partial \tilde{p}}{\partial x_i} - \frac{p}{\rho}\psi + \Phi + \phi\,. \tag{2.6.28e}$$

The fundamental solutions of the above equations in Laplace and Fourier transform domains can be obtained from (2.6.24) by letting $U_i = 0$, i.e.

$$\overline{\left(g^{U(dil)}_{ij}\right)}^* = -\frac{1}{\lambda+2\mu}\frac{(i\alpha_i)(i\alpha_j)}{\alpha^2\left(\alpha^2 + \frac{s}{\eta}\right)} \tag{2.6.29a}$$

$$\overline{\left(g^U_{ip}\right)}^* = -\frac{1}{\lambda+2\mu}\frac{i\alpha_i}{\left(\alpha^2+\frac{s}{\eta}\right)\left(\alpha^2+\frac{s^2}{c^2}\right)} \tag{2.6.29b}$$

$$\overline{\left(g^U_{\theta p}\right)}^* = \frac{1}{k}\frac{s}{\left(\alpha^2+\frac{s^2}{c^2}\right)\left(\alpha^2+\frac{s}{\kappa}\right)} \tag{2.6.29c}$$

$$\overline{\left(g^U_{\theta\theta}\right)}^* = \frac{1}{k}\frac{1}{\alpha^2+\frac{s}{\kappa}}\,. \tag{2.6.29d}$$

Three-dimensional Flow

Taking the inversions of the exponential Fourier transform and Laplace transform, and also, taking into consideration

$$\mathcal{L}^{-1}\mathcal{F}^{-1}\left[\frac{1}{s\alpha^2}\right] = \frac{H(t)}{4\pi r}$$

$$\mathcal{L}^{-1}\mathcal{F}^{-1}\left[\frac{1}{\alpha^2+\frac{s}{k}}\right] = \frac{1}{8\sqrt{k\pi^3 t^3}}e^{-r^2/4kt}$$

$$\mathcal{L}^{-1}\mathcal{F}^{-1}\left[\frac{1}{s}\frac{1}{\alpha^2+\frac{s}{k}}\right] = \frac{1}{4\pi r}erfc\frac{r}{2\sqrt{kt}}$$

$$\mathcal{L}^{-1}\mathcal{F}^{-1}\left[\frac{1}{s-\frac{c^2}{k}}\frac{1}{\alpha^2+\frac{s}{k}}\right] = \frac{1}{4\pi r}\alpha_k(r,t) \tag{2.6.30}$$

$$\mathcal{L}^{-1}\mathcal{F}^{-1}\left[\frac{1}{s}\frac{1}{\alpha^2+\frac{s^2}{c^2}}\right] = \frac{1}{4\pi r}H(t-r/c)$$

$$\mathcal{L}^{-1}\mathcal{F}^{-1}\left[\frac{1}{s-\frac{c^2}{k}}\frac{1}{\alpha^2+\frac{s^2}{c^2}}\right] = \frac{1}{4\pi r}H(t-r/c)e^{\frac{c^2}{k}(t-r/c)},$$

where

$$\alpha_k(r,t) = \frac{1}{2}e^{c^2t/k}\left[e^{-cr/k}erfc\frac{r-ct}{2\sqrt{kt}} + e^{cr/k}erfc\frac{r+ct}{2\sqrt{kt}}\right], \tag{2.6.31}$$

the solution can be written as

$$g_{ij}^{(dil)}(x-\xi,t-\tau) = \frac{\partial^2\phi_\eta(r,t')}{\partial x_i \partial x_j} \tag{2.6.32a}$$

$$g_{ip}(x-\xi,t-\tau) = \frac{1}{\rho_o}\frac{\partial}{\partial x_i}\left\{\frac{1}{4\pi r}\left[erfc\frac{r}{2\sqrt{\eta t'}} - \alpha_\eta(r,t') - H(t'-r/c)\left(1-e^{\frac{c^2t'}{\eta}(t'-r/c)}\right)\right]\right\} \tag{2.6.32b}$$

$$g_{\theta p}(x-\xi,t-\tau) = \frac{c^2}{4\pi k r}\left[\alpha_\kappa(r,t') - H(t'-r/c)e^{\frac{c^2}{\kappa}(t-r/c)}\right] \tag{2.6.32c}$$

$$g_{\theta\theta}(x-\xi,t-\tau) = \frac{1}{8\rho_o c_p(\pi\kappa t')^{3/2}}e^{-r^2/4\kappa t'}, \tag{2.6.32d}$$

where

$$\phi_\eta(r,t) = -\frac{1}{4\pi\rho_o r}erf\frac{r}{2\sqrt{\eta t}} \tag{2.6.33a}$$

$$t' = t-\tau. \tag{2.6.33b}$$

Similarly, the solutions for unit step body forces and sources can be obtained via equation (2.6.25). Taking into account that

$$\mathcal{L}^{-1}\mathcal{F}^{-1}\left[\frac{1}{s^2\alpha^2}\right] = \frac{t}{4\pi r}$$

$$\mathcal{L}^{-1}\mathcal{F}^{-1}\left[\frac{1}{s^2}\frac{1}{\alpha^2+\frac{s}{k}}\right] = \frac{1}{4\pi r}4ti^2erfc\frac{r}{2\sqrt{kt}} \tag{2.6.34}$$

$$\mathcal{L}^{-1}\mathcal{F}^{-1}\left[\frac{1}{s^2}\frac{1}{\alpha^2+\frac{s^2}{c^2}}\right] = \frac{1}{4\pi r}H(t-r/c)(t-r/c),$$

one obtains

$$G_{ij}^{(dil)}(x-\xi,t) = \frac{\partial \Phi_\eta}{\partial x_i \partial x_j} \tag{2.6.35a}$$

$$G_{ip}(x-\xi,t) = \frac{\eta}{c^2\rho_o}\frac{\partial}{\partial x_i}\left\{\frac{1}{4\pi r}\left[erfc\frac{r}{2\sqrt{\eta t}} + 4\frac{c^2 t}{\eta} i^2 erfc\frac{r}{2\sqrt{\eta t}} - \alpha_\eta(r,t) - H(t-r/c)\left(\frac{c^2}{\eta}(t-r/c) + 1 - e^{\frac{c^2}{\eta}(t-r/c)}\right)\right]\right\} \tag{2.6.35b}$$

$$G_{\theta p}(x-\xi,t) = \frac{1}{4\pi\rho_o c_p r}\left[\alpha_\kappa(r,t) - erfc\frac{r}{2\sqrt{\kappa t}} - H(t-r/c)\left(e^{\frac{c^2}{\kappa}(t-r/c)} - 1\right)\right] \tag{2.6.35c}$$

$$G_{\theta\theta}(x-\xi,t) = \frac{1}{4\pi k r} erfc\frac{r}{2\sqrt{\kappa t}}, \tag{2.6.35d}$$

where

$$\Phi_\eta(r,t) = -\frac{t}{4\pi\rho_o r}\left(1 - 4i^2 erfc\frac{r}{2\sqrt{kt}}\right). \tag{2.6.36}$$

The corresponding steady state response is given by

$$G_{ij}^{s\,(dil)}(x-\xi) = G_{ij}^{(dil)}(x-\xi,\infty) = \frac{\partial^2 \Phi_\eta^s}{\partial x_i \partial x_j} \tag{2.6.37a}$$

$$G_{ip}^s(x-\xi) = G_{ip}(x-\xi,\infty) = \frac{\partial \Phi_\eta^s}{\partial x_i} \tag{2.6.37b}$$

$$G_{\theta p}^s(x-\xi) = G_{\theta p}(x-\xi,\infty) = 0 \tag{2.6.37c}$$

$$G_{\theta\theta}^s(x-\xi) = G_{\theta\theta}(x-\xi,\infty) = \frac{1}{4\pi k r}, \tag{2.6.37d}$$

where

$$\Phi_\eta^s(r) = \frac{r}{8\pi(\lambda+2\mu)}. \tag{2.6.38}$$

Two-dimensional Flow

Similar to three-dimensions, subjecting (2.6.29) to the inverse exponential Fourier transform and Laplace transforms by taking into consideration

$$\begin{aligned}
&\mathcal{L}^{-1}\mathcal{F}^{-1}\left[\frac{1}{s\alpha^2}\right] = \frac{H(t)}{2\pi}\ln r \\
&\mathcal{L}^{-1}\mathcal{F}^{-1}\left[\frac{1}{\alpha^2+\frac{s}{k}}\right] = \frac{1}{4\pi t}e^{-r^2/4kt} \\
&\mathcal{L}^{-1}\mathcal{F}^{-1}\left[\frac{1}{s}\frac{1}{\alpha^2+\frac{s}{k}}\right] = \frac{1}{4\pi}E_1\left(\frac{r^2}{4kt}\right) \\
&\mathcal{L}^{-1}\mathcal{F}^{-1}\left[\frac{1}{s-\frac{c^2}{k}}\frac{1}{\alpha^2+\frac{s}{k}}\right] = \frac{1}{2\pi}\gamma_k(r,t) \\
&\mathcal{L}^{-1}\mathcal{F}^{-1}\left[\frac{1}{s}\frac{1}{\alpha^2+\frac{s^2}{c^2}}\right] = \frac{1}{2\pi}H(t-r/c)\cosh^{-1}\frac{ct}{r} \\
&\mathcal{L}^{-1}\mathcal{F}^{-1}\left[\frac{1}{s-\frac{c^2}{k}}\frac{1}{\alpha^2+\frac{s^2}{c^2}}\right] = \frac{1}{2\pi}H(t-r/c)\omega_k(r,t),
\end{aligned} \tag{2.6.39}$$

where

$$\gamma_k(r,t) = \frac{1}{2}e^{c^2t/k}\int_0^{c^2t/k}\frac{1}{\tau}e^{-\tau-c^2r^2/4k^2\tau}\,d\tau = \frac{1}{2}e^{c^2t/k}\left[K_o\left(\ln\frac{2ct}{r},\frac{cr}{k}\right)+K_o\left(\frac{cr}{k}\right)\right] \tag{2.6.40a}$$

one obtains

$$H(t-r/c)\omega_k(r,t) = e^{c^2t/k}\int_0^{c^2t/k}e^{-\tau}\frac{H(\tau-cr/k)}{\sqrt{\tau^2-\left(\frac{cr}{k}\right)^2}}\,d\tau = H(t-r/c)e^{c^2t/k}K_o\left(\cosh\frac{ct}{r},\frac{cr}{k}\right). \tag{2.6.40b}$$

In the above, $K_o(\alpha,\beta)$ is incomplete MacDonald function and $K_o(\alpha)$ is the modified Bessel function. The solution then becomes

$$g_{ij}^{(dil)}(x-\xi,t-\tau) = \frac{\partial^2\phi_\eta(r,t')}{\partial x_i\partial x_j} \tag{2.6.41a}$$

$$g_{ip}(x-\xi,t-\tau) = \frac{1}{2\pi\rho_o}\frac{\partial}{\partial x_i}\left\{\frac{1}{2}E_1\left(\frac{r^2}{4\eta t'}\right)-\gamma_\eta(r,t')-H(t'-r/c)\left[\cosh^{-1}\frac{ct'}{r}-\omega_\eta(r,t')\right]\right\} \tag{2.6.41b}$$

$$g_{\theta p}(x-\xi,t-\tau) = \frac{c^2}{2\pi k}\left[\gamma_\kappa(r,t')-H(t'-r/c)\omega(r,t')\right] \tag{2.6.41d}$$

$$g_{\theta\theta}(x-\xi,t-\tau) = \frac{1}{4\pi kt'}e^{r^2/4\kappa t'}, \tag{2.6.41e}$$

where

$$\phi_\eta(r,t) = \frac{1}{2\pi\rho_o}\left[\ln r+\frac{1}{2}E_1\left(\frac{r^2}{4\eta t}\right)\right]. \tag{2.6.42}$$

Similarly, the fundamental solutions for unit step body forces and body sources can be obtained using (2.6.25) and taking into consideration

$$\begin{aligned}
&\mathcal{L}^{-1}\mathcal{F}^{-1}\left[\frac{1}{s^2\alpha^2}\right] = \frac{t}{2\pi}\ln r\\
&\mathcal{L}^{-1}\mathcal{F}^{-1}\left[\frac{1}{s^2}\frac{1}{\alpha^2+\frac{s}{k}}\right] = \frac{t}{4\pi}\left[E_1\left(\frac{r^2}{4kt}\right)-E_2\left(\frac{r^2}{4kt}\right)\right]\\
&\mathcal{L}^{-1}\mathcal{F}^{-1}\left[\frac{1}{\frac{s^2}{c^2}}\frac{1}{\alpha^2+s^2}\right] = \frac{1}{2\pi}H(t-r/c)\left[t\cosh^{-1}\frac{ct}{r}-\sqrt{t^2-r^2/c^2}\right],
\end{aligned} \tag{2.6.43}$$

Thus,

$$G_{ij}^{(dil)}(x-\xi,t) = \frac{\partial^2\Phi_\eta}{\partial x_i\partial x_j} \tag{2.6.44a}$$

$$\begin{aligned}
G_{ip}(x-\xi,t) = \frac{\eta}{2\pi c^2\rho_o}\frac{\partial}{\partial x_i}\Bigg\{&\frac{1}{2}E_1\left(\frac{r^2}{4\eta t}\right)-\gamma_\eta(r,t)+\frac{c^2t}{2\eta}\left[E_1\left(\frac{r^2}{4\eta t}\right)-E_2\left(\frac{r^2}{4\eta t}\right)\right]\\
&-H(t-r/c)\left[\frac{c^2t}{\eta}\cosh^{-1}\frac{ct}{r}-\sqrt{t^2-r^2/c^2}+\cosh^{-1}\frac{ct}{r}-\omega_\eta(r,t)\right]\Bigg\}
\end{aligned} \tag{2.6.44b}$$

$$G_{\theta p}(x-\xi,t)=\frac{1}{2\pi\rho_o c_p}\left[\gamma_\kappa(r,t)-\frac{1}{2}E_1\left(\frac{r^2}{4\kappa t}\right)-H(t-r/c)\left(\omega_\kappa(r,t)-\cosh^{-1}\frac{ct}{r}\right)\right] \quad (2.6.44c)$$

$$G_{\theta\theta}(x-\xi,t)=\frac{1}{4\pi k}E_1\left(\frac{r^2}{4\kappa t}\right), \quad (2.6.44d)$$

where

$$\Phi_\eta(r,t)=\frac{t}{4\pi\rho_o}\left[2lnr+E_1\left(\frac{r^2}{4\eta t}\right)-E_2\left(\frac{r^2}{4\eta t}\right)\right]. \quad (2.6.45)$$

The corresponding steady state response is

$$G_{ij}^{s\,(dil)}(x-\xi)=G_{ij}(x-\xi,\infty)=\frac{\partial^2\Phi_\eta^s}{\partial x_i\partial x_j} \quad (2.6.46a)$$

$$G_{ip}^{s}(x-\xi)=G_{ip}(x-\xi,\infty)=\frac{\partial\Phi_\eta^s}{\partial x_i} \quad (2.6.46b)$$

$$G_{\theta p}^{s}(x-\xi)=G_{\theta p}(x-\xi,\infty)=0 \quad (2.6.46c)$$

$$G_{\theta\theta}^{s}(x-\xi)=G_{\theta\theta}(x-\xi,\infty)=-\frac{1}{2\pi}\ln r, \quad (2.6.46d)$$

where

$$\Phi_\eta^s(r)=-\frac{1}{8\pi(\lambda+2\mu)}r^2(\ln r-1). \quad (2.6.47)$$

2.6.3.2 CONVECTIVE COMPRESSIBLE FLOW

Governing Equations

In operator notation, the governing equations for compressible thermoviscous flow (2.6.10) are simply

$$L_{\alpha\beta}^U u_\beta+\bar{f}_\alpha=0, \quad (2.6.48)$$

in which

$$u_\beta=\{u_i,\ p,\ \theta\}^T \quad (2.6.49a)$$

$$\bar{f}_\beta=\{\bar{f}_i,\ \bar{\Omega},\ \bar{\phi}\}^T, \quad (2.6.49b)$$

The subscript i varies from one to three for three-dimensional and one to two for two-dimensional problems, respectively. Meanwhile, the linearized differential operator $L_{\alpha\beta}^U$ is defined by

$$L_{\alpha\beta}^U=\begin{bmatrix} L_{ij}^U & L_{ip}^U & L_{i\theta}^U \\ L_{pj}^U & L_{pp}^U & L_{p\theta}^U \\ L_{\theta j}^U & L_{\theta p}^U & L_{\theta\theta}^U \end{bmatrix}$$

$$=\begin{bmatrix} -\delta_{ij}\rho_o\dfrac{D_o}{Dt}+(\lambda+\mu)\dfrac{\partial^2}{\partial x_i\partial x_j}+\delta_{ij}\mu\dfrac{\partial^2}{\partial x_k\partial x_k} & -\dfrac{\partial}{\partial x_i} & 0 \\ 0 & -\dfrac{1}{c^2}\dfrac{D_o^2}{Dt^2}+\dfrac{\partial^2}{\partial x_i\partial x_i} & 0 \\ 0 & -\dfrac{D_o}{Dt} & -\rho_o c_p\dfrac{D_o}{Dt}+k\dfrac{\partial^2}{\partial x_i\partial x_i} \end{bmatrix}. \quad (2.6.50)$$

The superscript U denotes that convective terms are involved in the differential operator.

The fundamental solutions in Laplace and Fourier transform domain were presented in (2.6.24). Meanwhile the fundamental solutions for unit step body forces and sources can be obtained from (2.6.25).

The steady state solutions in the Fourier transform domain are

$$\left(G_{ij}^{U*(dil)}\right)^* = -\frac{1}{\lambda+2\mu}\frac{(i\alpha_i)(i\alpha_j)}{\alpha^2\left[\alpha^2+\frac{i\alpha_k U_k}{\eta}\right]} \tag{2.6.51a}$$

$$\left(G_{ip}^{U*}\right)^* = -\frac{1}{\lambda+2\mu}\frac{i\alpha_i}{\left[\alpha^2+\frac{i\alpha_k U_k}{\eta}\right]\left[\alpha^2+\frac{(i\alpha_k U_k)^2}{c^2}\right]} \tag{2.6.51b}$$

$$\left(G_{\theta p}^{U*}\right)^* = \frac{1}{k}\frac{i\alpha_k U_k}{\left[\alpha^2+\frac{(i\alpha_k U_k)^2}{c^2}\right]\left[\alpha^2+\frac{i\alpha_k U_k}{\kappa}\right]} \tag{2.6.51c}$$

$$\left(G_{\theta\theta}^{U*}\right)^* = \frac{1}{k}\frac{1}{\alpha^2+\frac{i\alpha_k U_k}{\kappa}}. \tag{2.6.51d}$$

Three-dimensional Flow

It is not difficult to get the convective fundamental solutions for instantaneous body force and source from (2.6.32) by introducing a Galilean coordinate transform:

$$g_{ij}^{U(dil)}(x-\xi,t-\tau) = \frac{\partial^2\phi_\eta(r_u,t')}{\partial x_i\partial x_j} \tag{2.6.52a}$$

$$g_{ip}^{U}(x-\xi,t-\tau) = \frac{1}{\rho_o}\frac{\partial}{\partial x_i}\left\{\frac{1}{4\pi r_u}\left[erfc\frac{r_u}{2\sqrt{\eta t'}} - \alpha_\eta(r_u,t') - H(t'-r_u/c)\left(1-e^{\frac{c^2t'}{\eta}(t'-r_u/c)}\right)\right]\right\} \tag{2.6.52b}$$

$$g_{\theta p}^{U}(x-\xi,t-\tau) = \frac{c^2}{4\pi k r_u}\left[\alpha_\kappa(r_u,t') - H(t'-r_u/c)e^{\frac{c^2}{\kappa}(t'-r_u/c)}\right] \tag{2.6.52c}$$

$$g_{\theta\theta}^{U}(x-\xi,t-\tau) = \frac{1}{8\rho_o c_p(\pi\kappa t')^{3/2}}e^{-r_u^2/4\kappa t'}, \tag{2.6.52d}$$

where

$$r_u^2 = (y_i - U_i t')(y_i - U_i t'). \tag{2.6.53}$$

The solutions for unit step body forces and sources can be obtained from (2.6.52) by integrating over τ or performing the inversion of Fourier and Laplace transform on (2.6.25). By taking into consideration

$$\mathcal{L}^{-1}\mathcal{F}^{-1}\left[\frac{1}{s\left(\alpha^2+\frac{s+i\alpha_k U_k}{k}\right)}\right]$$
$$= \frac{1}{8\pi r}e^{U_k y_k/2k}\left[e^{-Ur/2k}erfc\frac{r-Ut}{2\sqrt{kt}} + e^{Ur/2k}erfc\frac{r+Ut}{2\sqrt{kt}}\right]$$

$$\mathcal{L}^{-1}\mathcal{F}^{-1}\left[\frac{i\alpha_i}{s}\frac{1}{\alpha^2\left(\alpha^2+\frac{s+i\alpha_k U_k}{k}\right)}\right]$$

$$= \frac{1}{8\pi U r}\left\{\frac{U_i r - U y_i}{Ur - U_k y_k}\left[1 - e^{-(Ur-U_k y_k)/2k} erfc\frac{r-Ut}{2\sqrt{kt}} - \frac{r-Ut}{r_u} erf\frac{r_u}{2\sqrt{kt}}\right]\right.$$

$$\left. + \frac{U_i r + U y_i}{Ur + U_k y_k}\left[1 - e^{(Ur+U_k y_k)/2} erfc\frac{r+Ut}{2\sqrt{kt}} - \frac{r+Ut}{r_u} erf\frac{r_u}{2\sqrt{kt}}\right]\right\}$$

$$\mathcal{L}^{-1}\mathcal{F}^{-1}\left[\frac{i\alpha_i}{s(s+i\alpha_k U_k)}\frac{1}{\alpha^2+\frac{s+i\alpha_k U_k}{k}}\right]$$

$$= \frac{1}{8\pi U r}\left\{\frac{U_i r - U y_i}{Ur - U_k y_k}\left[e^{-(Ur-U_k y_k)/2k} erfc\frac{r-Ut}{2\sqrt{kt}} - \frac{r-Ut}{r_u} erfc\frac{r_u}{2\sqrt{kt}}\right]\right.$$

$$\left. + \frac{U_i r + U y_i}{Ur + U_k y_k}\left[e^{(Ur+U_k y_k)/k2} erfc\frac{r+Ut}{2\sqrt{kt}} - \frac{r+Ut}{r_u} erfc\frac{r_u}{2\sqrt{kt}}\right]\right\}$$

$$\mathcal{L}^{-1}\mathcal{F}^{-1}\left[\frac{1}{s(s+i\alpha_k U_k - \frac{c^2}{k})}\frac{1}{\alpha^2+\frac{s+i\alpha_k U_k}{k}}\right]$$

$$= \frac{1}{4\pi}\int_0^t \alpha_k(r_u,\tau)\,d\tau$$

$$\mathcal{L}^{-1}\mathcal{F}^{-1}\left[\frac{1}{s(s+i\alpha_k U_k)}\frac{1}{\alpha^2+\frac{(s+i\alpha_k U_k)^2}{c^2}}\right]$$

$$= \frac{H(1-M)}{4\pi U} H(t - r_o/c)\ln\frac{Ur_u + U^2 t - U_k y_k}{Ur_o + U^2 r_o/c - U_k y_k}$$

$$+ \frac{H(M-1)}{4\pi U} H(U_k y_k - c\beta r)\times$$

$$\times\left[H(t-r_o/c)\ln\frac{Ur_u + U^2 t - U_k y_k}{Ur_o + U^2 r_o/c - U_k y_k} - H(t-r_1/c)\ln\frac{Ur_u + U^2 t - U_k y_k}{Ur_1 + U^2 r_1/c - U_k y_k}\right]$$

$$\mathcal{L}^{-1}\mathcal{F}^{-1}\left[\frac{1}{s(s+i\alpha_k U_k - \frac{c^2}{k})}\frac{1}{\alpha^2+\frac{(s+i\alpha_k U_k)^2}{c^2}}\right]$$

$$= \int_0^t \frac{H(\tau - r_u/c)}{4\pi r_u} e^{\frac{c^2}{k}(\tau - r_u/c)}\,d\tau\,, \qquad (2.6.54)$$

one obtains

$$G_{ij}^{U(dil)}(x-\xi,t) = \frac{\partial^2 \Phi_\eta^U}{\partial x_i \partial x_j} = -\frac{\partial \psi_{i\eta}}{\partial x_j} \qquad (2.6.55a)$$

$$G_{ip}^{U}(x-\xi,t) = \frac{1}{8\pi\rho_o U r}\left\{\frac{U_i r - U y_i}{Ur - U_k y_k}\left[e^{-(Ur-U_k y_k)/2\eta} erfc\frac{r-Ut}{2\sqrt{\eta t}} - \frac{r-Ut}{r_u} erfc\frac{r_u}{2\sqrt{\eta t}}\right]\right.$$

$$+\frac{U_i r+U y_i}{Ur+U_k y_k}\left[e^{(Ur+U_k y_k)/2\eta}erfc\frac{r+Ut}{2\sqrt{\eta t}}-\frac{r+Ut}{r_u}erfc\frac{r_u}{2\sqrt{\eta t}}\right]\Bigg\}$$

$$-\frac{1}{4\pi\rho_o U}\frac{\partial}{\partial x_i}\Bigg\{H(1-M)H(t-r_o/c)\ln\frac{Ur_u+U^2t-U_k y_k}{Ur_o+U^2r_o/c-U_k y_k}$$

$$+H(M-1)H(U_k y_k-c\beta r)\times$$

$$\times\left[H(t-r_o/c)\ln\frac{Ur_u+U^2t-U_k y_k}{Ur_o+U^2r_o/c-U_k y_k}-H(t-r_1/c)\ln\frac{Ur_u+U^2t-U_k y_k}{Ur_1+U^2r_1/c-U_k y_k}\right]$$

$$+U\int_0^t\left[\alpha_\eta(r_u,\tau)-\frac{1}{r_u}H(\tau-r_u/c)e^{\frac{c^2}{\eta}(\tau-r_u/c)}\right]d\tau\Bigg\} \qquad (2.6.55b)$$

$$G^U_{\theta p}(x-\xi,t)=\frac{1}{4\pi kU}\Bigg\{H(1-M)H(t-r_u/c)\ln\frac{Ur_u+U^2t-U_k y_k}{Ur_o+U^2r_o/c-U_k y_k}$$

$$+H(M-1)H(U_k y_k-c\beta r)\times$$

$$\left[H(t-r_o/c)\ln\frac{Ur_u+U^2t-U_k y_k}{Ur_o+U^2r_o/c-U_k y_k}-H(t-r_1/c)\ln\frac{Ur_u+U^2t-U_k y_k}{Ur_1+U^2r_1/c-U_k y_k}\right]$$

$$+U\int_0^t\left[\alpha_\eta(r_u,\tau)-\frac{1}{r_u}H(\tau-r_u/c)e^{\frac{c^2}{\eta}(\tau-r_u/c)}\right]d\tau\Bigg\} \qquad (2.6.55c)$$

$$G^U_{\theta\theta}(x-\xi,t)=\frac{1}{8\pi kr}e^{U_k y_k/2\kappa}\left[e^{Ur/2\kappa}erfc\frac{r-Ut}{2\sqrt{\kappa t}}+e^{Ur/2\kappa}erfc\frac{r+Ut}{2\sqrt{\kappa t}}\right], \qquad (2.6.55d)$$

where

$$\Phi^U_\eta(x-\xi,t)=-\frac{1}{4\pi\rho_o}\int_0^t\frac{1}{r_u}erf\frac{r_u}{2\sqrt{\eta(t-\tau)}}d\tau \qquad (2.6.56a)$$

$$\psi_{i\eta}(x-\xi,t)=\frac{1}{8\pi\rho_o Ur}\Bigg\{\frac{U_i r-U y_i}{Ur-U_k y_k}\left[1-e^{-(Ur-U_k y_k)/2\eta}erfc\frac{r-Ut}{2\sqrt{\eta t}}-\frac{r-Ut}{r_u}erf\frac{r_u}{2\sqrt{\eta t}}\right]$$

$$+\frac{U_i r+U y_i}{Ur+U_k y_k}\left[1-e^{(Ur+U_k y_k)/2\eta}erfc\frac{r+Ut}{2\sqrt{\eta t}}-\frac{r+Ut}{r_u}erfc\frac{r_u}{2\sqrt{\eta t}}\right]\Bigg\} \qquad (2.6.56b)$$

$$r_o=\begin{cases}\dfrac{-U_k y_k+\sqrt{(U_k y_k)^2+c^2\beta^2r^2}}{c\beta^2}, & M<1;\\ \dfrac{U_k y_k-\sqrt{(U_k y_k)^2-c^2\beta^2r^2}}{c\beta^2}, & M>1\end{cases} \qquad (2.6.56c)$$

$$r_1=\frac{U_k y_k+\sqrt{(U_k y_k)^2-c^2\beta^2r^2}}{c\beta^2} \qquad (5.56d)$$

$$\beta^2=|1-M^2| \qquad (2.6.56e)$$

$$M=\frac{U}{c}\qquad \text{is Mach Number.} \qquad (2.6.56f)$$

The corresponding steady state solutions can be obtained from (2.6.51) by taking into

consideration

$$\mathcal{F}^{-1}\left[\frac{1}{i\alpha_k U_k}\frac{1}{\alpha^2}\right] = -\frac{1}{4\pi U}\ln\frac{Ur - U_k y_k}{2}$$

$$\mathcal{F}^{-1}\left[\frac{1}{\alpha^2 + \dfrac{i\alpha_k U_k}{k}}\right] = \frac{1}{4\pi r}e^{(U_k y_k - Ur)/2k}$$

$$\mathcal{F}^{-1}\left[\frac{1}{i\alpha_k U_k}\frac{1}{\alpha^2 + \dfrac{i\alpha_k U_k}{k}}\right] = \frac{1}{4\pi U}E_1\left(\frac{Ur - U_k y_k}{2k}\right)$$

$$\mathcal{F}^{-1}\left[\frac{1}{i\alpha_k U_k - \dfrac{c^2}{k}}\frac{1}{\alpha^2 + \dfrac{i\alpha_k U_k}{k}}\right] = \frac{1}{4\pi U}P_k \qquad (2.6.57)$$

$$\mathcal{F}^{-1}\left[\frac{1}{i\alpha_k U_k}\frac{1}{\alpha^2 + \dfrac{(i\alpha_k U_k)^2}{c^2}}\right] = \frac{1}{4\pi U}F$$

$$\mathcal{F}^{-1}\left[\frac{1}{i\alpha_k U_k - \dfrac{c^2}{k}}\frac{1}{\alpha^2 + \dfrac{(i\alpha_k U_k)^2}{c^2}}\right] = \frac{1}{4\pi c}Q_k\,,$$

where

$$F(x-\xi) = \begin{cases} \sinh^{-1}\dfrac{U_k y_k}{\beta\sqrt{U^2 r^2 - (U_k y_k)^2}}\,, & M < 1\,; \\ 2H(U_k y_k - c\beta r)\cosh^{-1}\dfrac{U_k y_k}{\beta\sqrt{U^2 r^2 - (U_k y_k)^2}}\,, & M > 1\,. \end{cases} \qquad (2.6.58a)$$

$$P_k(x-\xi) = e^{U_k y_k/kM^2}\int\frac{1}{R}e^{-\left(\frac{c}{M}-\frac{U}{2}\right)x/k - UR/2k}\,dx \qquad (2.6.58b)$$

$$Q_k(x-\xi) = \begin{cases} T_k\,, & M < 1; \\ 2H(U_k y_k - c\beta r)T_k\,, & M > 1\,; \end{cases} \qquad (2.6.58c)$$

$$T_k(x-\xi) = e^{U_k y_k/kM^2}\int\frac{e^{-cx/kM}}{\sqrt{x^2 + \frac{1-M^2}{M^2}R^2}}\,dx \qquad (2.6.58d)$$

$$R = \sqrt{x^2 + \frac{U^2 r^2 - (U_k y_k)^2}{U^2}} \qquad (2.6.58e)$$

$$x = \frac{U_k y_k}{U}\,. \qquad (2.6.58f)$$

Thus,

$$G_{ij}^{U_s(dil)}(x-\xi) = G_{ij}^{U(dil)}(x-\xi,\infty) = \frac{\partial^2\Phi_\eta^{U_s}}{\partial x_i\partial x_j} \qquad (2.6.59a)$$

$$G_{ip}^{U_s}(x-\xi) = G_{ip}(x-\xi,\infty) = \frac{1}{4\pi\rho_o U}\frac{\partial}{\partial x_i}\left[E_1\left(\frac{Ur - U_k y_k}{2\eta}\right) - P_\eta + Q_\eta - F\right] \qquad (2.6.59b)$$

$$G^{Us}_{\theta p}(x-\xi) = G^{U}_{\theta p}(x-\xi,\infty) = \frac{c}{4\pi kM}\left[P_\kappa - Q_\kappa\right] \tag{2.6.59c}$$

$$G^{Us}_{\theta\theta}(x-\xi) = G^{U}_{\theta\theta}(x-\xi,\infty) = \frac{1}{4\pi kr}e^{(U_k y_k - Ur)/2\kappa}, \tag{2.6.59d}$$

where

$$\Phi^{Us}_{\eta} = \frac{1}{4\pi\rho_o U}\left[\ln\frac{Ur - U_k y_k}{2\eta} + E_1\left(\frac{Ur - U_k y_k}{2\eta}\right)\right]. \tag{2.6.60}$$

Two-dimensional Flow

The convective fundamental solutions for an pulse body force and source can be obtained from (2.6.41) by Galilean coordinate transform:

$$g^{U(dil)}_{ij}(x-\xi,t-\tau) = \frac{\partial^2\phi_\eta(r_u,t')}{\partial x_i\partial x_j} \tag{2.6.61a}$$

$$g^{U}_{ip}(x-\xi,t-\tau) = \frac{1}{2\pi\rho_o}\frac{\partial}{\partial x_i}\left\{\frac{1}{2}E_1\left(\frac{r_u^2}{4\eta t'}\right) - \gamma_\eta(r_u,t') - H(t'-r_u/c)\left[\cosh^{-1}\frac{ct'}{r_u} - \omega_\eta(r_u,t')\right]\right\} \tag{2.6.61b}$$

$$g^{U}_{\theta p}(x-\xi,t-\tau) = \frac{c^2}{2\pi k}\left[\gamma_\kappa(r_u,t') - H(t'-r_u/c)\omega_\kappa(r_u,t')\right] \tag{2.6.61c}$$

$$g^{U}_{\theta\theta}(x-\xi,t-\tau) = \frac{1}{4\pi kt'}e^{r_u^2/4\kappa t'}, \tag{2.6.61d}$$

where the functions γ_α, ω_α and ϕ_α were defined in (2.6.40) and (2.6.42), respectively.

The convective solutions for unit step body force and source can be obtained from (2.6.61) by integrating over τ. That is,

$$G^{U(dil)}_{ij}(x-\xi,t) = \frac{1}{4\pi(\lambda+2\mu)}\left(\delta_{ij} - \frac{U_iU_j}{U^2}\right)e^{U_k y_k/2\eta}\psi_\eta(r,t) - \left(\delta_{ij}\frac{U_k}{U}\frac{\partial\phi'_\eta}{\partial x_k} - \frac{U_i}{U}\frac{\partial\phi'_\eta}{\partial x_j} - \frac{U_j}{U}\frac{\partial\phi'_\eta}{\partial x_i}\right) \tag{2.6.62a}$$

$$G^{U}_{ip}(x-\xi,t) = \int_0^t g^{U}_{ip}(x-\xi,\tau)\,d\tau \tag{2.6.62b}$$

$$G^{U}_{\theta p}(x-\xi,t) = \int_0^t g^{U}_{\theta p}(x-\xi,\tau)\,d\tau \tag{2.6.62c}$$

$$G^{U}_{\theta\theta}(x-\xi,t) = \frac{1}{4\pi k}e^{U_k y_k/2\kappa}\psi_\kappa(r,t), \tag{2.6.62d}$$

where

$$\phi'_\eta(x-\xi,t) = \frac{1}{2\pi\rho U}\left[ln\frac{r}{r_u} + \frac{1}{2}e^{U_k y_k/2\eta}\psi_\eta(r,t) - \frac{1}{2}E_1\left(\frac{r_u^2}{4\eta t}\right)\right]$$

$$\psi_\eta(r,t) = K_o\left(\frac{Ur}{2\eta}\right) + K_o\left(ln\frac{Ut}{r},\frac{Ur}{2\eta}\right) \tag{2.6.63}$$

$$\psi_\kappa(r,t) = K_o\left(\frac{Ur}{2\kappa}\right) + K_o\left(ln\frac{Ut}{r},\frac{Ur}{2\kappa}\right)$$

The steady state solutions can be obtained by taking into consideration that

$$\mathcal{F}^{-1}\left[\frac{1}{\alpha^2+\frac{i\alpha_k U_k}{k}}\right]=\frac{1}{2\pi}e^{U_k y_k/2k}K_o\left(\frac{Ur}{2k}\right)$$

$$\mathcal{F}^{-1}\left[\frac{1}{i\alpha_k U_k}\frac{1}{\alpha^2+\frac{i\alpha_k U_k}{k}}\right]=\frac{1}{2\pi U}P_{ko}$$

$$\mathcal{F}^{-1}\left[\frac{i\alpha_i}{i\alpha_k U_k}\frac{1}{\alpha^2+\frac{i\alpha_k U_k}{k}}\right]=\frac{U_i}{2\pi U^2}e^{U_k y_k/2k}K_o\left(\frac{Ur}{2k}\right)-\frac{1}{4\pi kU}\left(Uy_i-\frac{U_i}{U}U_k y_k\right)P_{k1}$$

$$\mathcal{F}^{-1}\left[\frac{1}{i\alpha_k U_k-\frac{c^2}{k}}\frac{1}{\alpha^2+\frac{i\alpha_k U_k}{k}}\right]=\frac{1}{2\pi U}Q_{ko}$$

$$\mathcal{F}^{-1}\left[\frac{i\alpha_i}{i\alpha_k U_k-\frac{c^2}{k}}\frac{1}{\alpha^2+\frac{i\alpha_k U_k}{k}}\right]=\frac{U_i}{2\pi U^2}\left[e^{U_k y_k/2k}K_o\left(\frac{Ur}{2k}\right)+\frac{U}{kM^2}Q_{ko}\right]$$
$$-\frac{1}{4\pi kU}\left(Uy_i-\frac{U_i}{U}U_k y_k\right)Q_{k1}$$

$$\mathcal{F}^{-1}\left[\frac{1}{\alpha^2+\frac{(i\alpha_k U_k)^2}{c^2}}\right]=\begin{cases}-\frac{1}{2\pi\beta}\ln\frac{\sqrt{(U_k y_k)^2+c^2\beta^2 r^2}}{c\beta}\,, & M<1\,;\\ \frac{1}{2\pi}H(U_k y_k-c\beta r)\,, & M>1\,.\end{cases}$$

$$\mathcal{F}^{-1}\left[\frac{i\alpha}{i\alpha_k U_k}\frac{1}{\alpha^2+\frac{(i\alpha_k U_k)^2}{c^2}}\right]=\frac{U_i}{U^2}\mathcal{F}^{-1}\left[\frac{1}{\alpha^2+\frac{(i\alpha_k U_k)^2}{c^2}}\right]$$
$$-\frac{H(1-M)}{2\pi U}\frac{Uy_i-\frac{U_i}{U}U_k y_k}{\sqrt{U^2r^2-(U_k y_k)^2}}\tan^{-1}\frac{U_k y_k}{\beta\sqrt{U^2r^2-(U_k y_k)^2}}$$

$$\mathcal{F}^{-1}\left[\frac{1}{i\alpha_k U_k-\frac{c^2}{k}}\frac{1}{\alpha^2+\frac{(i\alpha_k U_k)^2}{c^2}}\right]=\frac{k}{c^2}\mathcal{F}^{-1}\left[\frac{1}{\alpha^2+\frac{(i\alpha_k U_k)^2}{c^2}}\right]$$
$$+\frac{H(1-M)k}{2\pi c^2\beta}e^{U_k y_k/kM^2}\Im\left(e^{\frac{i\beta}{kM^2}\sqrt{U^2r^2-(U_k y_k)^2}}E_1\left(-\frac{U_k y_k}{kM^2}+\frac{i\beta}{kM^2}\sqrt{U^2r^2-(U_k y_k)^2}\right)\right)$$

$$\mathcal{F}^{-1}\left[\frac{i\alpha_i}{i\alpha_k U_k-\frac{c^2}{k}}\frac{1}{\alpha^2+\frac{(i\alpha_k U_k)^2}{c^2}}\right]$$
$$=\frac{H(1-M)}{2\pi U}\left[\frac{U_i}{\beta U}e^{U_k y_k/kM^2}\Re\left(e^{\frac{i\beta}{kM^2}\sqrt{U^2r^2-(U_k y_k)^2}}E_1\left(-\frac{U_k y_k}{U^2}+\frac{i\beta}{kM^2}\sqrt{U^2r^2-(U_k y_k)^2}\right)\right)\right.$$
$$\left.+\frac{Uy_i-\frac{U_i}{U}U_k y_k}{\sqrt{U^2r^2-(U_k y_k)^2}}e^{U_k y_k/kM^2}\Im\left(e^{\frac{i\beta}{kM^2}\sqrt{U^2r^2-(U_k y_k)^2}}E_1\left(-\frac{U_k y_k}{U^2}+\frac{i\beta}{kM^2}\sqrt{U^2r^2-(U_k y_k)^2}\right)\right)\right],$$

(2.6.64)

where $\Re(z)$ and $\Im(z)$ are the real part and imaginary part of z, respectively, and

$$
\begin{aligned}
P_{ko} &= \int e^{Ux/2k} K_o\left(\frac{UR}{2k}\right) dx \\
P_{k1} &= \int \frac{1}{R} e^{Ux/2k} K_1\left(\frac{UR}{2k}\right) dx \\
Q_{ko} &= e^{U_k y_k/kM^2} \int e^{(U/2k - c/kM)x} K_o\left(\frac{UR}{2k}\right) dx \\
Q_{k1} &= e^{U_k y_k/kM^2} \int \frac{1}{R} e^{(U/2k - c/kM)x} K_1\left(\frac{UR}{2k}\right) dx \\
R &= \sqrt{x^2 + \frac{U^2 r^2 - (U_k y_k)^2}{U^2}} \\
x &= \frac{U_k y_k}{U},
\end{aligned}
\tag{2.6.65}
$$

Thus,

$$
\begin{aligned}
G_{ij}^{Us(dil)}(x-\xi) &= \frac{1}{2\pi(\lambda+2\mu)}\left(\delta_{ij} - \frac{U_i U_j}{U^2}\right) e^{U_k y_k/2\eta} K_o\left(\frac{Ur}{2\eta}\right) \\
&\quad - \left(\delta_{ij}\frac{U_k}{U}\frac{\partial \phi_\eta^s}{\partial x_k} - \frac{U_i}{U}\frac{\partial \phi_\eta^s}{\partial x_j} - \frac{U_j}{U}\frac{\partial \phi_\eta^s}{\partial x_i}\right)
\end{aligned}
\tag{2.6.66a}
$$

$$
\begin{aligned}
G_{ip}^{Us}(x-\xi) &= -\frac{1}{2\pi\rho_o k U}\left[\frac{U_i}{M^2} Q_{\eta o} + \frac{1}{2}\left(U y_i - \frac{U_i}{U} U_k y_k\right)(P_{\eta 1} - Q_{\eta 1})\right] - \frac{U_i}{\rho_o U^2} G_{pp}^{Us}(x-\xi) \\
&\quad + \frac{H(1-M)}{2\pi\rho_o U}\left\{ e^{U_k y_k/\eta M^2} \Re\left(e^{\frac{i\beta}{\eta M^2}\sqrt{U^2r^2-(U_k y_k)^2}} E_1\left(-\frac{U_k y_k}{\eta M^2} + \frac{i\beta}{\eta M^2}\sqrt{U^2 r^2 - (U_k y_k)^2}\right)\right)\right. \\
&\quad + \frac{U y_i - \frac{U_i}{U} U_k y_k}{\sqrt{U^2 r^2 - (U_k y_k)^2}}\left[\tan^{-1}\frac{U_k y_k}{\beta\sqrt{U^2 r^2 - (U_k y_k)^2}}\right. \\
&\quad \left.\left. + e^{U_k y_k/\eta M^2} \Im\left(e^{\frac{i\beta}{\eta M^2}\sqrt{U^2r^2-(U_k y_k)^2}} E_1\left(-\frac{U_k y_k}{\eta M^2} + \frac{i\beta}{\eta M^2}\sqrt{U^2 r^2 - (U_k y_k)^2}\right)\right)\right]\right\}
\end{aligned}
\tag{2.6.66b}
$$

$$
\begin{aligned}
G_{\theta p}^{Us}(x-\xi) &= \frac{c}{2\pi k M} Q_{\kappa o} + \frac{1}{\rho_o c_p} G_{pp}^{Us}(x-\xi) \\
&\quad - \frac{H(1-M)}{2\pi\rho_o c_p \beta} e^{U_k y_k/\kappa M^2} \Im\left(e^{\frac{i\beta}{\kappa M^2}\sqrt{U^2r^2-(U_k y_k)^2}} E_1\left(-\frac{U_k y_k}{\kappa M^2} + \frac{i\beta}{\kappa M^2}\sqrt{U^2 r^2 - (U_k y_k)^2}\right)\right)
\end{aligned}
\tag{2.6.66c}
$$

$$
G_{\theta\theta}^{us}(x-\xi) = \frac{1}{2\pi k} e^{U_k y_k/2\kappa} K_o\left(\frac{Ur}{2\kappa}\right), \tag{2.6.66d}
$$

where

$$
\phi_\eta^s(x-\xi) = \frac{1}{2\pi\rho U}\left[ln r + e^{U_k y_k/2\eta} K_o\left(\frac{Ur}{2\eta}\right)\right]. \tag{5.67}
$$

Since the algebraic form of these two-dimensional kernels is complicated it is best to examine the behavior graphically. For this exercise, a forty-by-forty grid of sampling points

was generated as shown in Figure 2.6.1. The source point is fixed at the origin, located as the central point in the grid. The character of the kernel is displayed in Figures 2.6.2-2.6.7.

First, the component G_{11} is plotted for various free stream velocities, expressed in terms of Mach numbers, in Figure 2.6.2. (Note that G_{11} is the velocity in the x_1-direction at the sampling point due to a unit point force in the x_1-direction at the origin.) For very small U_i, the solution of (2.6.66a) approaches the Stokes kernels as illustrated in Figure 2.6.2a. As the magnitude of the free stream velocity increases (*i.e.*, Figures 2.6.2b-d), a pronounced sense of flow direction becomes evident with the nonzero response concentrated in a narrow band behind the applied force. However, the response is always a near-hyperbolic behavior in a quickly moving stream. This behavior is not only important from a physical standpoint, but also can be beneficial in the development of an efficient boundary element algorithm.

On the other hand, the character of G_{pp}, representing the pressure response due to a unit source, is much different. At a zero Mach number, the pressure is radially symmetric as seen in Figure 2.6.4a. Increasing the Mach number to 0.9 produces a transition to the, by now, familiar convective form. However, at $M = 1$, the field suddenly becomes singular. Figure 2.6.4c shows a distinctive Mach cone at $M = 1.1$. It should be noted that the analytical kernels produce absolutely straight lines defining the cone. Unfortunately, the graphics package is unable to accurately portray the discontinuity. As the Mach number increases further, the included angle of the cone decreases. The response at $M = 8$ is displayed in Figure 2.6.4d.

Figure 2.6.3 shows the coupling term G_{p1}, which measures the pressure due to unit point force in the x_1-direction. This term also exhibits the shock-related Mach cone.

Finally, Figure 2.6.7 shows the heat transfer fundamental solution defined in (2.6.66d). It should be emphasized that the so-called convective fundamental solution actually embodies both the processes of conduction and convection. At low velocity, conduction dominates producing a nearly radially symmetric response. On the other hand, in a high speed medium, the response is concentrated in a very narrow band downstream of the source. Thus, as illustrate in Figure 2.6.7, $G^{Us}_{\theta\theta}$ captures the transition from elliptic toward hyperbolic behavior.

2.6.4 BOUNDARY INTEGRAL REPRESENTATIONS

The desired integral representation can be derived directly from the differential equations of transient convective compressible thermoviscous flow.

The governing equations (2.6.48) multiplied by an arbitrary function $\tilde{g}_{\alpha\gamma}$, and integrated over time and space, must remain equal to zero. That is,

$$< \tilde{g}_{\alpha\gamma}, L^U_{\alpha\beta}u_\beta + \tilde{f}_\alpha >= \int_0^T \int_V \tilde{g}_{\alpha\gamma}(L^U_{\alpha\beta}u_\beta + \tilde{f}_\alpha)\, dV\, dt = 0\,, \tag{2.6.68}$$

where the standard notation for the inner product of two functions has been introduced.

Returning to the explicit forms of the differential operators, this becomes

$$\int_o^T\int_V \left\{ \tilde{g}_{i\gamma}\left[-\rho_o\frac{D_o u_i}{Dt}+(\lambda+\mu)\frac{\partial^2 u_j}{\partial x_i\partial x_j}+\mu\frac{\partial^2 u_i}{\partial x_j\partial x_j}-\frac{\partial u_p}{\partial x_i}+\bar{f}_i\right] \right.$$
$$+\tilde{g}_{p\gamma}\left[-\frac{1}{c^2}\frac{D_o^2\tilde{p}}{Dt^2}+\frac{\partial^2\tilde{p}}{\partial x_i\partial x_i}+\bar{f}_p\right] \qquad (2.6.69)$$
$$\left.+\tilde{g}_{\theta\gamma}\left[-\rho_o c_p\frac{D_o u_\theta}{Dt}+k\frac{\partial^2 u_\theta}{\partial x_i\partial x_i}+\frac{D_o u_p}{Dt}+\bar{f}_\theta\right]\right\} dV\,dt=0\,,$$

Next, the divergence theorem can be applied repeatedly to applicable terms in (2.6.69) to transfer spatial as well as temporal derivatives from u_β to $\tilde{g}_{\alpha\gamma}$. Thus the first term of (2.6.69) becomes

$$\int_o^T\int_V \left\{ \tilde{g}_{i\gamma}\left[-\rho_o\frac{D_o u_i}{Dt}+(\lambda+\mu)\frac{\partial^2 u_j}{\partial x_i\partial x_j}+\mu\frac{\partial^2 u_i}{\partial x_j\partial x_j}-\frac{\partial u_p}{\partial x_i}+\bar{f}_i\right]\right\} dV\,dt$$
$$=\int_0^T\int_S \left\{ \tilde{g}_{i\gamma}\left[\lambda\frac{\partial u_j}{\partial x_j}n_i+\mu\left(\frac{\partial u_i}{\partial x_j}+\frac{\partial u_j}{\partial x_i}\right)n_j-u_p n_i\right]\right.$$
$$\left.-\left[\lambda\frac{\partial\tilde{g}_{j\gamma}}{\partial x_j}n_i+\mu\left(\frac{\partial\tilde{g}_{i\gamma}}{\partial x_j}+\frac{\partial\tilde{g}_{j\gamma}}{\partial x_i}\right)n_j+\rho_o U_n\tilde{g}_{i\gamma}\right]u_i\right\} dS\,dt \qquad (2.6.70)$$
$$+\int_0^T\int_V\{\tilde{g}_{i\gamma}\bar{f}_i\}\,dV\,dt-\int_V\{\rho_o\tilde{g}_{i\gamma}u_i|_0^T\}\,dV$$
$$+\int_0^T\int_V\left\{\left[\rho_o\frac{D_o\tilde{g}_{i\gamma}}{Dt}+(\lambda+\mu)\frac{\partial^2\tilde{g}_{j\gamma}}{\partial x_i\partial x_j}+\mu\frac{\partial^2\tilde{g}_{i\gamma}}{\partial x_j\partial x_j}\right]u_i+\left[\frac{\partial\tilde{g}_{i\gamma}}{\partial x_i}\right]u_p\right\}dV\,dt\,;$$

the second term is

$$\int_0^T\int_V\left\{\tilde{g}_{p\gamma}\left[-\frac{1}{c^2}\frac{D_o^2 u_p}{Dt^2}+\frac{\partial^2 u_p}{\partial x_i\partial x_i}+\bar{f}_p\right]\right\}dS\,dt$$
$$=\int_0^T\int_S\left\{\tilde{g}_{p\gamma}\left[\frac{\partial u_p}{\partial n}-\frac{U_n}{c^2}\frac{D_o u_p}{Dt}\right]-\left[\frac{\partial\tilde{g}_{p\gamma}}{\partial n}-\frac{U_n}{c^2}\frac{D_o\tilde{g}_{p\gamma}}{Dt}\right]u_p\right\}dS\,dt$$
$$+\int_0^T\int_V\{\tilde{g}_{p\gamma}\bar{f}_p\}\,dV\,dt-\frac{1}{c^2}\int_V\left\{\tilde{g}_{p\gamma}\frac{D_o u_p}{Dt}|_0^T-\frac{D_o\tilde{g}_{p\gamma}}{Dt}u_p|_0^T\right\}dV \qquad (2.6.71)$$
$$+\int_0^T\int_V\left\{\left[-\frac{D_o^2\tilde{g}_{p\gamma}}{Dt^2}+c_o^2\frac{\partial^2\tilde{g}_{p\gamma}}{\partial x_i\partial x_i}\right]u_p\right\}dV\,dt\,;$$

the third term is

$$\int_0^T\int_V\left\{\tilde{g}_{\theta\gamma}\left[-\rho_o c_p\frac{D_o u_\theta}{Dt}+k\frac{\partial^2 u_\theta}{\partial x_i\partial x_i}+\frac{D_o u_p}{Dt}+\bar{f}_\theta\right]\right\}$$
$$=\int_0^T\int_S\left\{\tilde{g}_{\theta\gamma}\left[k\frac{\partial u_\theta}{\partial x_i}n_i-\rho_o c_p U_n u_\theta-\frac{\partial u_p}{\partial n}+U_n u_p\right]-\left[k\frac{\partial\tilde{g}_{\theta\gamma}}{\partial x_i}n_i\right]u_\theta\right\}dV\,dt$$
$$+\int_0^T\int_V\{\tilde{g}_{\theta\gamma}\bar{f}_\theta\}\,dV\,dt-\int_V\{\rho_o c_p\tilde{g}_{\theta\gamma}u_\theta|_0^T-\tilde{g}_{\theta\gamma}u_p|_0^T\}\,dV \qquad (2.6.72)$$
$$+\int_0^T\int_V\left\{\left[\rho_o c_p\frac{D_o\tilde{g}_{\theta\gamma}}{Dt}+k\frac{\partial^2\tilde{g}_{\theta\gamma}}{\partial x_i\partial x_i}\right]u_\theta-\left[\frac{D_o\tilde{g}_{\theta\gamma}}{Dt}\right]u_p\right\}dV\,dt\,.$$

Combining equations (2.6.70), (2.6.71) and (2.6.72), equation (2.6.69) becomes

$$
\begin{aligned}
&\int_0^T\int_V \left\{ \tilde{g}_{i\gamma}\left[\lambda\frac{\partial u_j}{\partial x_j}n_i+\mu\left(\frac{\partial u_i}{\partial x_j}+\frac{\partial u_j}{\partial x_i}\right)n_j-u_p n_i\right]\right.\\
&\qquad -\left[\lambda\frac{\partial \tilde{g}_{j\gamma}}{\partial x_j}n_i+\mu\left(\frac{\partial \tilde{g}_{i\gamma}}{\partial x_j}+\frac{\partial \tilde{g}_{j\gamma}}{\partial x_i}\right)n_j+\rho_o U_n\tilde{g}_{i\gamma}\right]u_i\\
&\qquad +\tilde{g}_{p\gamma}\left[\frac{\partial u_p}{\partial n}-\frac{U_n}{c^2}\frac{D_o u_p}{Dt}\right]-\left[\frac{\partial \tilde{g}_{p\gamma}}{\partial n}-\frac{U_n}{c^2}\frac{D_o\tilde{g}_{p\gamma}}{Dt}\right]u_p\\
&\qquad \left.+\tilde{g}_{\theta\gamma}\left[k\frac{\partial u_\theta}{\partial n}-\rho_o c_p U_n u_\theta-\frac{\partial u_p}{\partial n}+U_n u_p\right]-\left[k\frac{\partial \tilde{g}_{\theta\gamma}}{\partial n}\right]u_\theta\right\}dS\,dt\\
&+\int_0^T\int_V\{\tilde{g}_{i\gamma}\bar{f}_i+\tilde{g}_{p\gamma}\bar{f}_p+\tilde{g}_{\theta\gamma}\bar{f}_\theta\}\,dV\,dt\\
&\quad -\int_V\left\{\rho_o\tilde{g}_{i\gamma}u_i|_0^T+\frac{1}{c^2}\frac{D_o\tilde{g}_{p\gamma}}{Dt}u_p|_0^T-\frac{1}{c^2}\tilde{g}_{p\gamma}\frac{D_o u_p}{Dt}|_0^T+\rho_o c_p\tilde{g}_{\theta\gamma}u_\theta|_0^T-\tilde{g}_{\theta\gamma}u_p|_0^T\right\}dV\\
&+\int_0^T\int_V\left\{\left[\rho_o\frac{D_o\tilde{g}_{i\gamma}}{Dt}+(\lambda+\mu)\frac{\partial^2\tilde{g}_{j\gamma}}{\partial x_i\partial x_j}+\mu\frac{\partial^2\tilde{g}_{i\gamma}}{\partial x_j\partial x_j}\right]u_i\right.\\
&\qquad +\left[\frac{\partial\tilde{g}_{i\gamma}}{\partial x_i}-\frac{1}{c^2}\frac{D_o^2\tilde{g}_{p\gamma}}{Dt^2}+\frac{\partial^2\tilde{g}_{p\gamma}}{\partial x_i\partial x_i}-\frac{D_o\tilde{g}_{\theta\gamma}}{Dt}\right]u_p\\
&\qquad \left.+\left[\rho_o c_p\frac{D_o\tilde{g}_{\theta\gamma}}{Dt}+k\frac{\partial^2\tilde{g}_{\theta\gamma}}{\partial x_i\partial x_i}\right]u_\theta\right\}dV\,dt=0\,,
\end{aligned}
\tag{2.6.73}
$$

or

$$
\begin{aligned}
&\int_0^T\int_S\left\{\left[\tilde{g}_{i\gamma}t_i-\tilde{f}_{i\gamma}u_i\right]+[\tilde{g}_{p\gamma}t_p-\tilde{g}_{p\gamma}u_p]+[\tilde{g}_{\theta\gamma}t_\theta-\tilde{g}_{\theta\gamma}u_\theta]\right\}dS\,dt\\
&+\int_0^T\int_V\{\tilde{g}_{i\gamma}\bar{f}_i+\tilde{g}_{p\gamma}\bar{f}_p+\tilde{g}_{\theta\gamma}\bar{f}_\theta\}\,dV\,dt\\
&\quad -\int_V\left\{\rho_o\tilde{g}_{i\gamma}+\frac{1}{c^2}\frac{D_o\tilde{g}_{p\gamma}}{Dt}u_p|_0^T-\frac{1}{c^2}\tilde{g}_{p\gamma}\frac{D_o u_p}{Dt}|_0^T+\rho_o c_p\tilde{g}_{\theta\gamma}u_\theta|_0^T\right\}dV\\
&+\int_0^T\int_V\left\{\left[\rho_o\frac{D_o\tilde{g}_{i\gamma}}{Dt}+(\lambda+\mu)\frac{\partial^2\tilde{g}_{j\gamma}}{\partial x_i\partial x_j}+\mu\frac{\partial^2\tilde{g}_{i\gamma}}{\partial x_j\partial x_j}\right]u_i\right.\\
&\qquad +\left[\frac{\partial\tilde{g}_{i\gamma}}{\partial x_i}-\frac{1}{c^2}\frac{D_o^2\tilde{g}_{p\gamma}}{Dt^2}+\frac{\partial^2\tilde{g}_{p\gamma}}{\partial x_i\partial x_i}-\frac{D_o\tilde{g}_{\theta\gamma}}{Dt}\right]u_p\\
&\qquad \left.+\left[\rho_o c_p\frac{D_o\tilde{g}_{\theta\gamma}}{Dt}+k\frac{\partial^2\tilde{g}_{\theta\gamma}}{\partial x_i\partial x_i}\right]u_\theta\right\}dV\,dt=0\,.
\end{aligned}
\tag{2.6.73$'$}
$$

where

$$t_i=\lambda\frac{\partial u_j}{\partial x_j}n_i+\mu\left(\frac{\partial u_i}{\partial x_j}+\frac{\partial u_j}{\partial x_i}\right)n_j-u_p n_i \tag{2.6.74a}$$

$$t_p=\frac{\partial u_p}{\partial n}-\frac{U_n}{c^2}\frac{D_o u_p}{Dt} \tag{2.6.74b}$$

$$t_\theta=k\frac{\partial u_\theta}{\partial n}-\rho_o c_p U_n u_\theta-\frac{\partial u_p}{\partial n}+U_n u_p \tag{2.6.74c}$$

$$\tilde{f}_{i\gamma}=\lambda\frac{\partial\tilde{g}_{j\gamma}}{\partial x_j}n_i+\mu\left(\frac{\partial\tilde{g}_{i\gamma}}{\partial x_j}+\frac{\partial\tilde{g}_{j\gamma}}{\partial x_i}\right)n_j+\rho_o U_n\tilde{g}_{i\gamma} \tag{2.6.74d}$$

$$\tilde{f}_{p\gamma} = \frac{\partial \tilde{g}_{p\gamma}}{\partial n} - \frac{U_n}{c^2}\frac{D_o \tilde{g}_{p\gamma}}{Dt} \tag{2.6.74e}$$

$$\tilde{f}_{\theta\gamma} = k\frac{\partial \tilde{g}_{\theta\gamma}}{\partial n}\,. \tag{2.6.74f}$$

In order to complete the derivation of the integral equation for the perturbed velocity and temperature at any point ξ, interior to S, at time $\tau < T$, the last volume integral in (2.6.73) must be reduced to $-u_\gamma(\xi,\tau)$. This is accomplished, if

$$< \tilde{L}_{\beta\alpha}\tilde{g}_{\alpha\gamma}, u_\beta >= -u_\gamma(\xi,\tau)\,, \tag{2.6.75}$$

or after making use of the properties of the delta function

$$\tilde{L}_{\beta\alpha}\tilde{g}_{\alpha\gamma} + \delta_{\beta\gamma}\delta(x-\xi)\delta(t-\tau) = 0\,, \tag{2.6.76}$$

where the differential operator $\tilde{L}_{\beta\alpha}$ has the definition

$$\tilde{L}_{\beta\alpha} = \begin{bmatrix} \tilde{L}_{ji} & \tilde{L}_{jp} & \tilde{L}_{j\theta} \\ \tilde{L}_{pi} & \tilde{L}_{pp} & \tilde{L}_{p\theta} \\ \tilde{L}_{\theta i} & \tilde{L}_{\theta p} & \tilde{L}_{\theta\theta} \end{bmatrix}$$

$$= \begin{bmatrix} \delta_{ji}\rho\dfrac{D_o}{Dt} + (\lambda+\mu)\dfrac{\partial^2}{\partial x_i \partial x_j} + \delta_{ji}\mu\dfrac{\partial^2}{\partial x_k \partial x_k} & 0 & 0 \\ \dfrac{\partial}{\partial x_i} & -\dfrac{1}{c^2}\dfrac{D_o^2}{Dt^2} + \dfrac{\partial^2}{\partial x_i \partial x_i} & -\dfrac{D_o}{Dt} \\ 0 & 0 & \rho c_p\dfrac{D_o}{Dt} + k\dfrac{\partial^2}{\partial x_i \partial x_i} \end{bmatrix}. \tag{2.6.77}$$

Formally, $\tilde{L}_{\alpha\beta}$ is called the adjoint of the original compressible thermoviscous flow operator $L^U_{\alpha\beta}$ in (2.6.50), and $\tilde{g}_{\alpha\gamma}$ defined by (2.6.76) is the adjoint Green's function. This function $\tilde{g}_{\alpha\gamma}$ can be obtained simply by transposing the fundamental solution $g^U_{\alpha\beta}$ presented in the previous section. That is,

$$\tilde{g}_{\alpha\gamma}(x-\xi, t-\tau) = g^U_{\gamma\alpha}(\xi - x, \tau - t) \tag{2.6.78a}$$

$$\tilde{f}_{\alpha\gamma}(x-\xi, t-\tau) = f^U_{\gamma\alpha}(\xi - x, \tau - t)\,. \tag{2.6.78b}$$

Substituting (2.6.78) into (2.6.73) produces the desired integral equation,

$$c_{\alpha\beta}u_\beta = \int_S [g^U_{\alpha\beta} * t_\beta - f^U_{\alpha\beta} * u_\beta]\, dS + \int_V [g^U_{\alpha\beta} * \bar{f}_\beta]\, dV\,, \tag{2.6.79}$$

in which, for simplicity, the initial conditions have been assumed zero. The $*$ in (2.6.79) once again symbolizes a Riemann convolution integral.

2.6.5 CONCLUDING REMARKS

In this section, new fundamental solutions were derived for compressible thermoviscous convective and unconvective flows for both three-dimensional and two-dimensional; steady and unsteady cases. The contour plots of Figures 2.6.2 through 2.6.7 suggest that this latest effort has produced physically meaningful kernel functions.

Although the numerical implementation of the compressible formulation has not yet been undertaken, some of the characteristics of the boundary element approach should be noted: For high speed flows, the nonlinearities will once again be concentrated in a thin layer near the surface and in the wake. Thus, all of the discussion concerning high *Re* incompressible flow is valid here as well. Furthermore, with the compressibility comes the hyperbolic phenomenon of shock. In a boundary element approach, the discontinuity can be captured analytically through the fundamental solution. It is not necessary to use a mesh to model the, generally unknown, location of the shock front. This is a distinct advantage for boundary elements over the domain-based methods.

Figure 2.6.1 Grid For Fundamental Solution Contour Plots

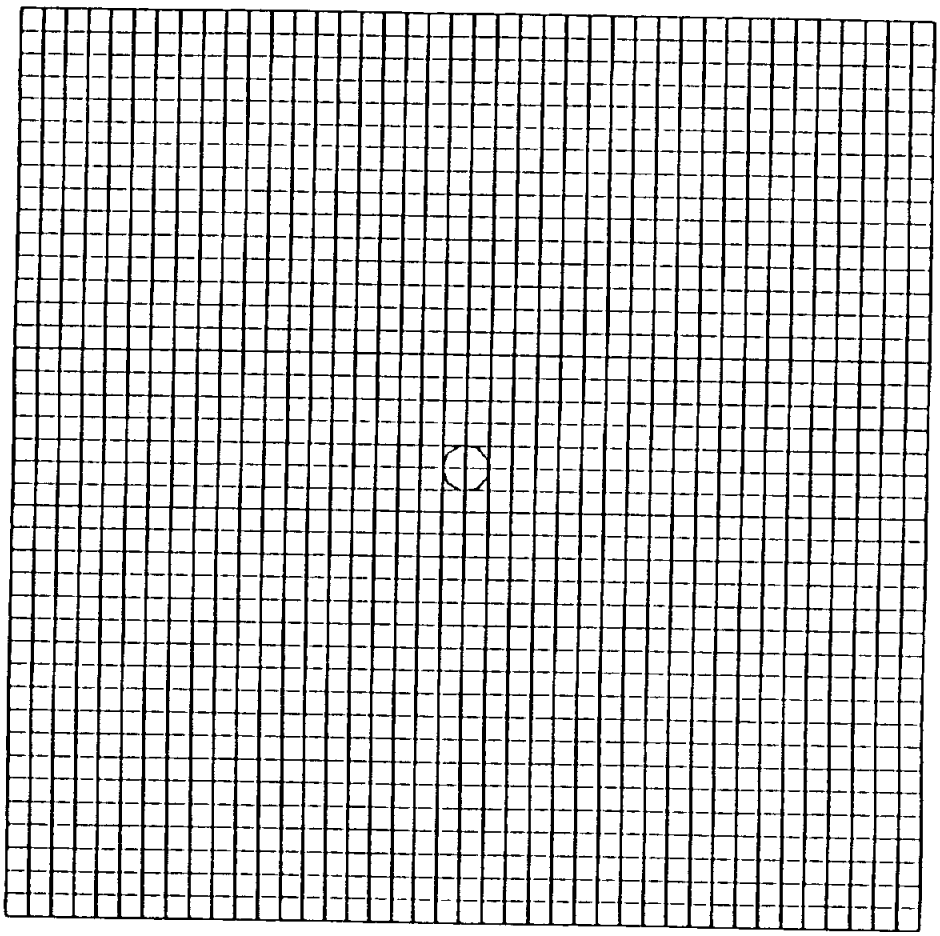

Figure 2.6.2 Fundamental Solution G_{11}

Figure 2.6.2(a)

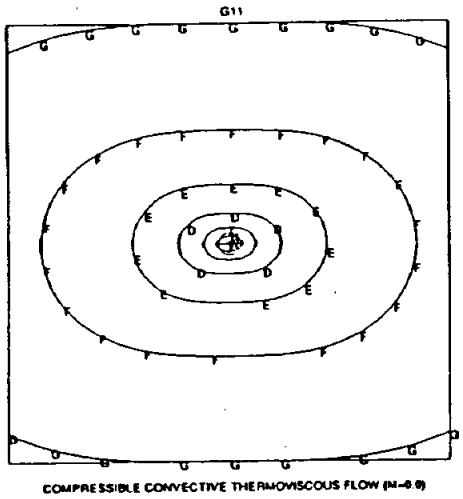

Figure 2.6.2(c)

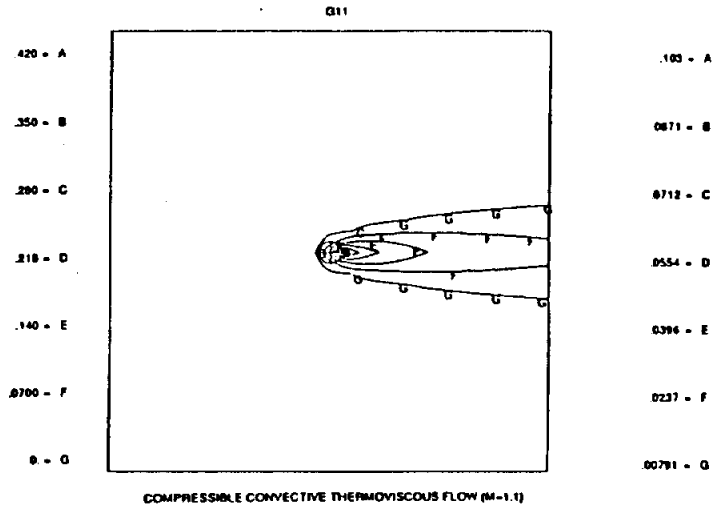

Figure 2.6.2(b)

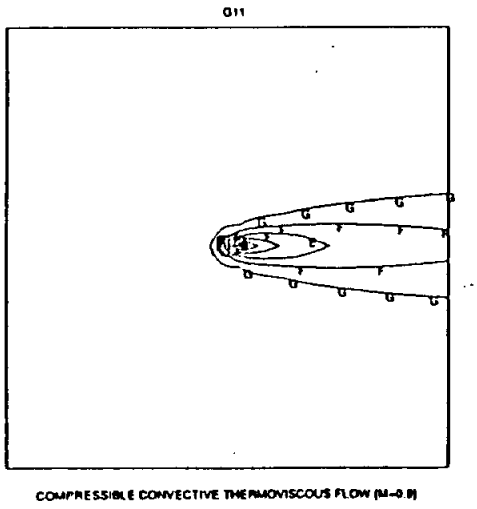

Figure 2.6.2(d)

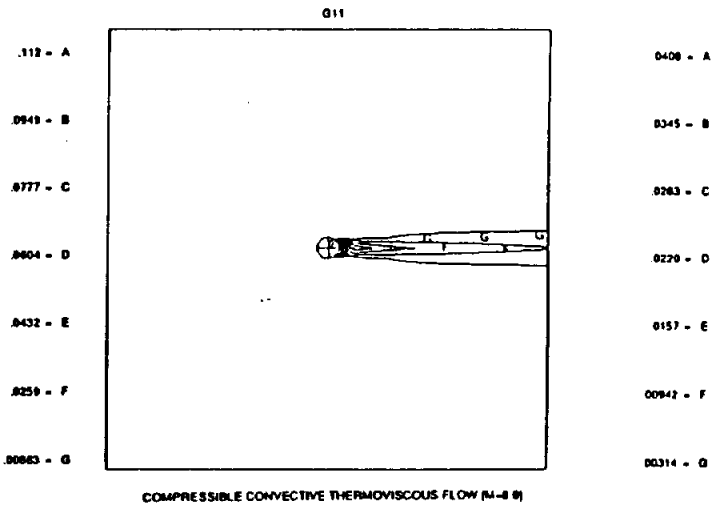

C-2

Figure 2.6.3 Fundamental Solution G_{1p}

Figure 2.6.3(*a*)

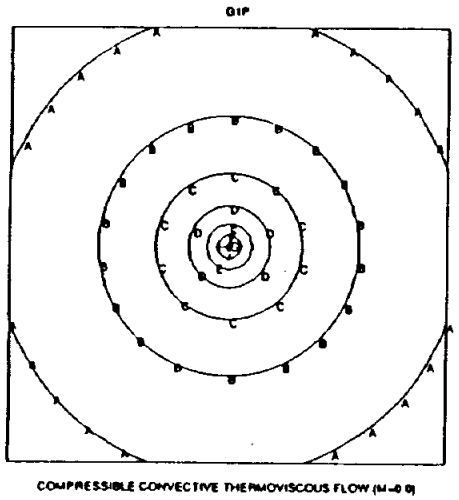

Figure 2.6.3(*c*)

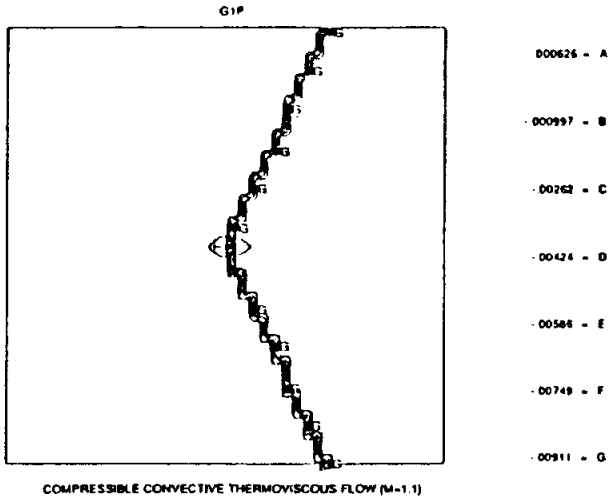

Figure 2.6.3(*b*)

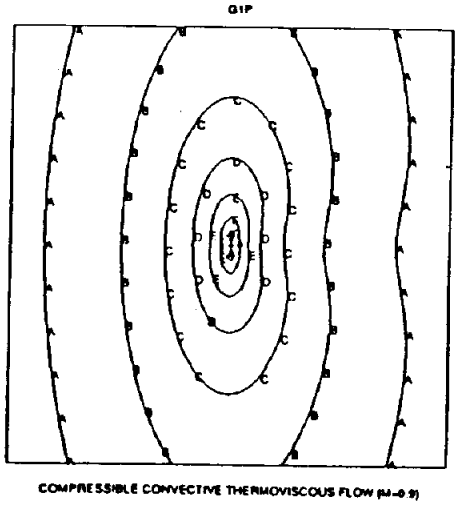

Figure 2.6.3(*d*)

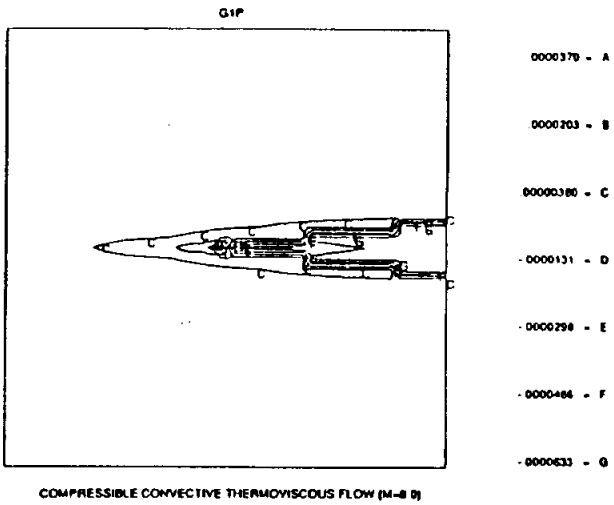

Figure 2.6.4 Fundamental Solution G_{pp}

Figure 2.6.4(a)

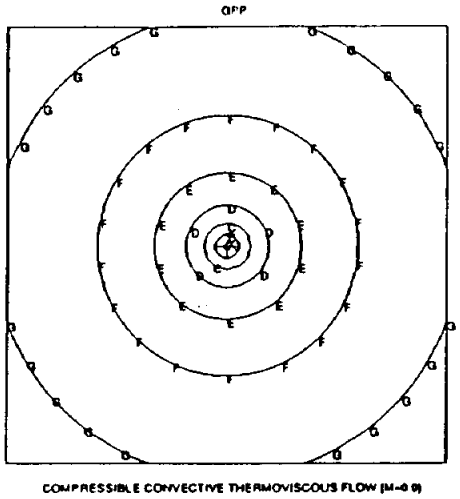

Figure 2.6.4(c)

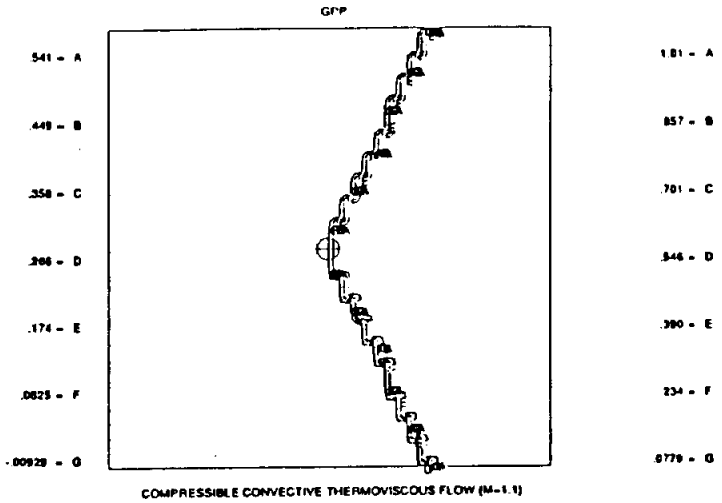

Figure 2.6.4(b)

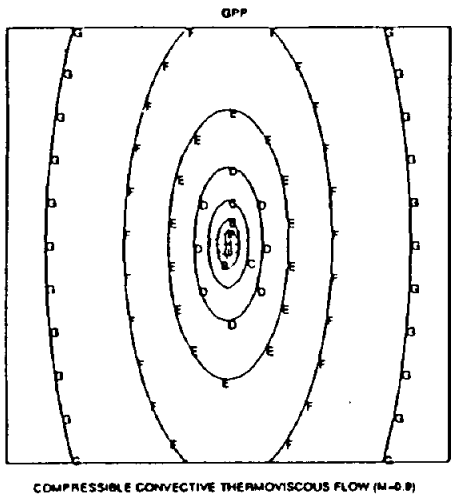

Figure 2.6.4(d)

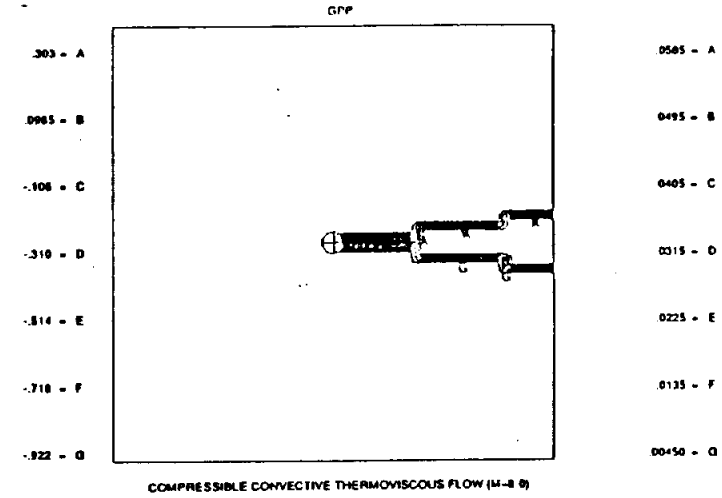

Figure 2.6.5 Fundamental Solution $G_{\theta 1}$

Figure 2.6.5(a)

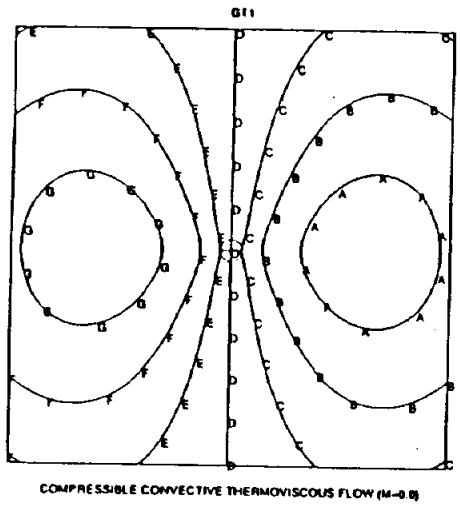

Figure 2.6.5(c)

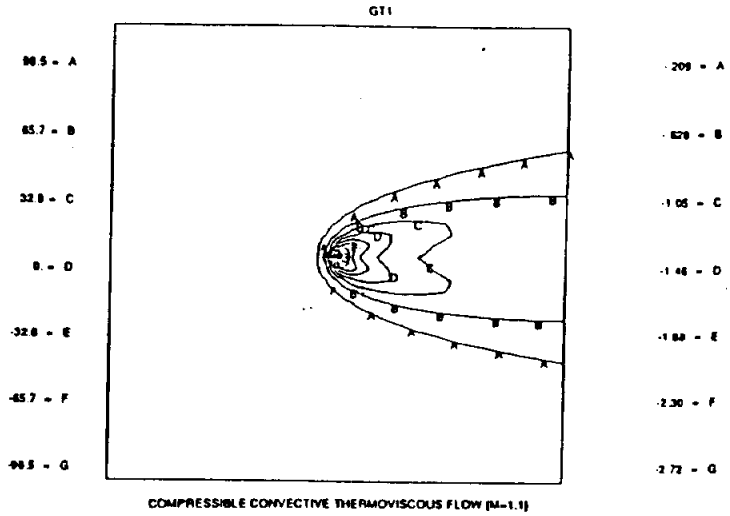

Figure 2.6.5(b)

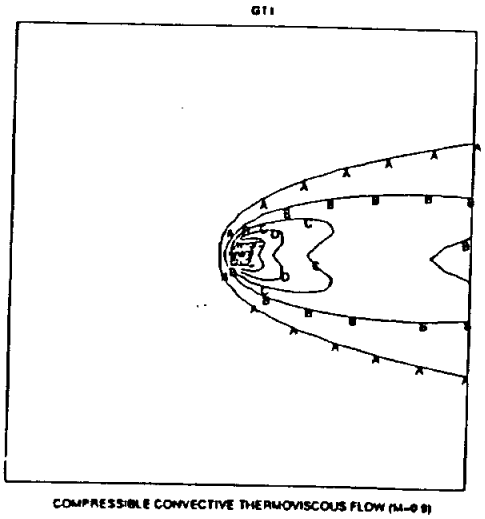

Figure 2.6.5(d)

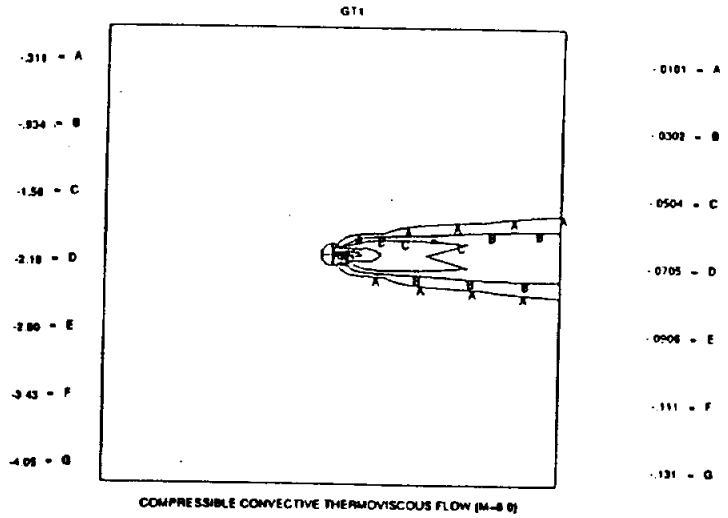

Figure 2.6.6 Fundamental Solution $G_{\theta p}$

Figure 2.6.6(a)

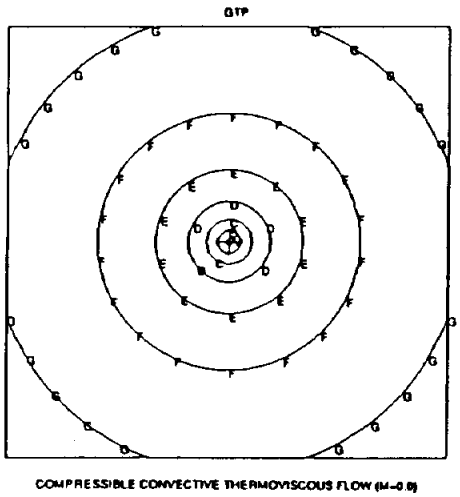

Figure 2.6.6(c)

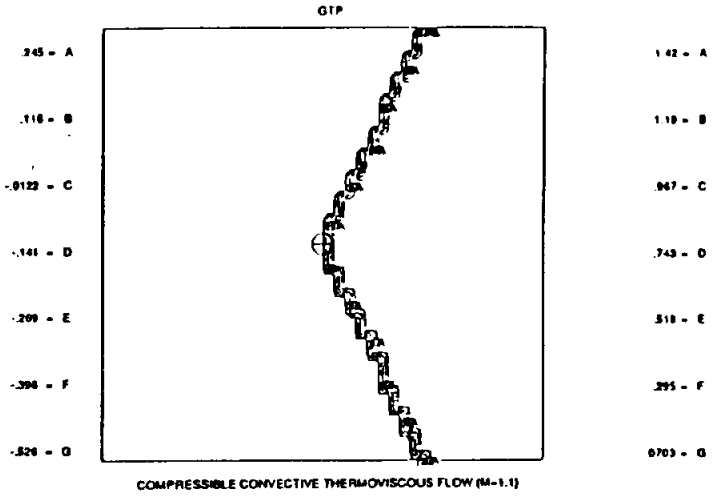

Figure 2.6.6(b)

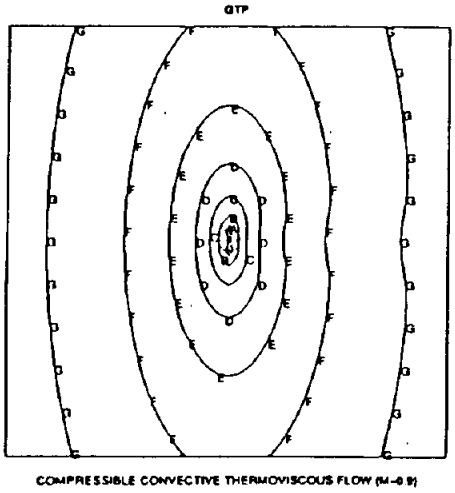

Figure 2.6.6(d)

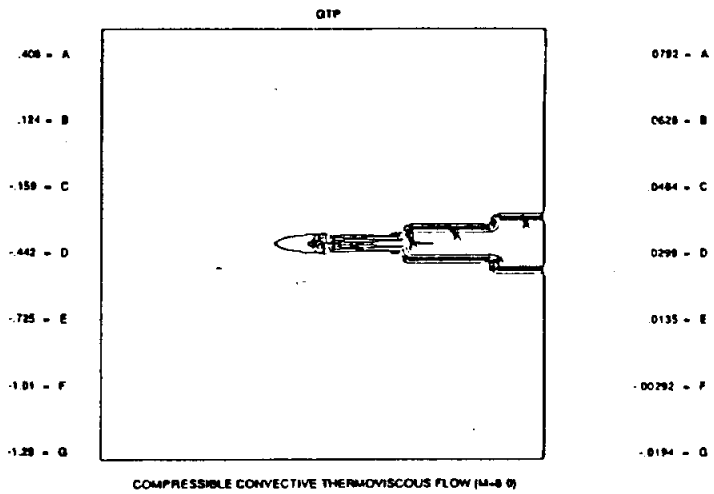

Figure 2.6.7 Fundamental Solution $G_{\theta\theta}$

Figure 2.6.7(a)

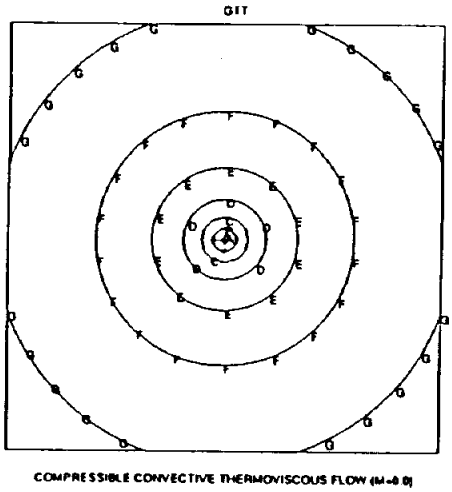

Figure 2.6.7(c)

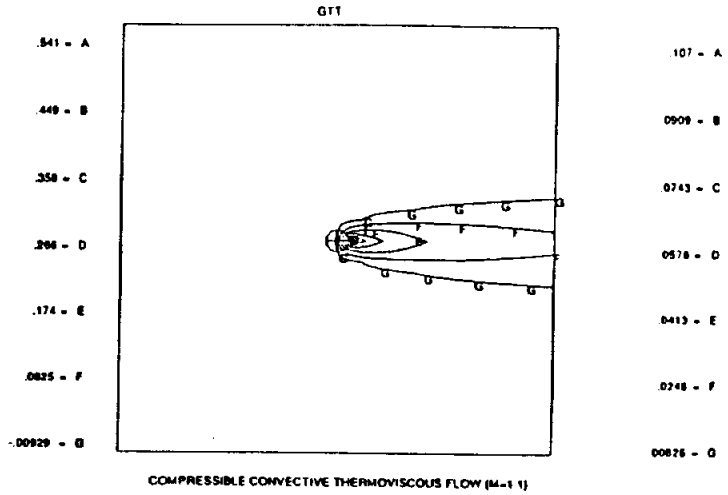

Figure 2.6.7(b)

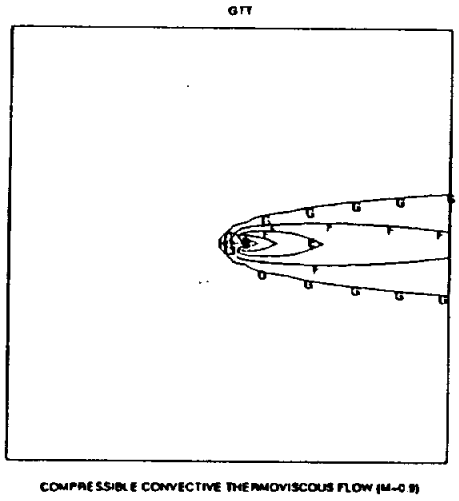

Figure 2.6.7(d)

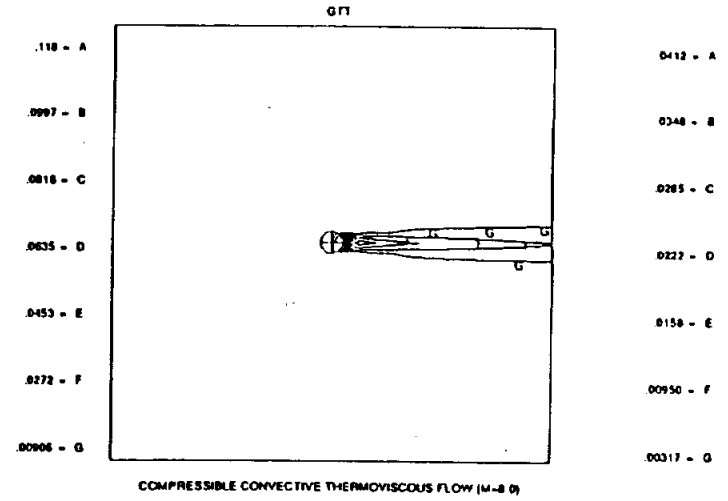

2.7 FLUID-STRUCTURE INTERACTION

2.7.1 INTRODUCTION

In the previous sections, boundary element formulations have been developed separately for a thermoelastic structural component and for a thermoviscous fluid. However, the ultimate goal of this ongoing grant is to develop a single computer program to determine the temperatures, deformation and stresses of a component exposed to a hot gas flow path, without the need for experimentally determined ambient fluid temperatures and film coefficients. While further work is still required for the fluid phase, sufficient progress has been made to demonstrate the utility of the overall concept. Consequently, in this section, problems of fluid-structure interaction will be examined.

2.7.2 FORMULATION

The Geometric Modeling Region (GMR) provides the vehicle for achieving interaction between the solid and fluid. Recall that it is possible to employ fluid formulations in different GMRs. Now, some of the regions will use the thermoelastic solid boundary element model, while others utilize one of the thermoviscous fluid formulations. Compatibility must be enforced across all GMR interfaces, no matter which model is used for adjoining regions. A boundary element approach is ideal for these problems, since the integral equations are written directly on the interfacial surfaces.

For demonstration purposes, consider the problem of flow past a blade as sketched in Figure 2.7.1. The blade itself is labeled GMR1, and is modeled as a thermoelastic solid. A boundary mesh is all that is required for this structure. Surrounding the blade is a thin layer of cells. This is a nonlinear thermoviscous fluid region, named GMR2, in which the complete Navier-Stokes equations are solved. GMR2 is enclosed by inner and outer surfaces composed of boundary elements. The mesh utilized for the inner surface of GMR2 matches that employed for the blade in GMR1. Finally, the outer region GMR3, which extends to infinity, employs the convective Oseen kernels. The boundary element model for GMR3 consists merely of the surface elements required to describe the interface to GMR2. Since no cells are present, the nonlinear volume and surface integrals are ignored. Thus, an approximation is introduced. However, as mentioned previously, outside of the boundary layer and wake these nonlinear contributions are negligible. (Recall that each region is the counterpart of a substructure or superelement commonly used in the finite element technology, however GMR1 and GMR3 do not require any volume discretization.)

The interface between GMR2 and GMR3 poses no particular problem. Total velocity and temperature from both regions are equated at each interface node, while the tractions

and flux must be equal in magnitude but of opposite direction. The latter conditions for the compatibility of traction and flux are also true for the solid-fluid interface between GMR1 and GMR2. Total temperature must, of course, be equal on this interface as well. However, the solid integral formulations of Section 2.2 are written in terms of displacement, while those for fluids use velocity. Consequently, a change in variable must be introduced to ensure complete interface compatibility. For that purpose, consider the following matrix form of the integral equation for a thermoviscous fluid:

$$\begin{bmatrix} c_{ij} & 0 \\ 0 & c_{\theta\theta} \end{bmatrix}^T \begin{Bmatrix} v_i \\ \theta \end{Bmatrix} = \begin{bmatrix} G_{ij} & 0 \\ 0 & G_{\theta\theta} \end{bmatrix}^T \begin{Bmatrix} t_i \\ q \end{Bmatrix} - \begin{bmatrix} F_{ij} & 0 \\ 0 & F_{\theta\theta} \end{bmatrix}^T \begin{Bmatrix} v_i \\ \theta \end{Bmatrix} + \begin{Bmatrix} R_j \\ R_\theta \end{Bmatrix}. \tag{2.7.1}$$

The contributions from nonlinearities and past time steps are all contained in R_β, as are any terms associated with the translation from perturbed velocity to total velocity v_i. Meanwhile, a similar expression written for a thermoelastic solid becomes

$$\begin{bmatrix} c_{ij} & 0 \\ 0 & c_{\theta\theta} \end{bmatrix}^T \begin{Bmatrix} u_i \\ \theta \end{Bmatrix} = \begin{bmatrix} G_{ij} & 0 \\ G_{\theta j} & G_{\theta\theta} \end{bmatrix}^T \begin{Bmatrix} t_i \\ q \end{Bmatrix} - \begin{bmatrix} F_{ij} & 0 \\ F_{\theta j} & F_{\theta\theta} \end{bmatrix}^T \begin{Bmatrix} u_i \\ \theta \end{Bmatrix} + \begin{Bmatrix} R_j \\ R_\theta \end{Bmatrix}, \tag{2.7.2}$$

where u_i is the total displacement. This must be rewritten in terms of total velocity v_i, where

$$v_i = \frac{\partial u_i}{\partial \tau}. \tag{2.7.3}$$

After invoking properties of the convolution integrals that are present in the original integral equation (2.2.2), the appropriate representation for the solid can be written

$$\begin{bmatrix} c_{ij} & 0 \\ 0 & c_{\theta\theta} \end{bmatrix}^T \begin{Bmatrix} v_i \\ \theta \end{Bmatrix} = \begin{bmatrix} \hat{G}_{ij} & 0 \\ \hat{G}_{\theta j} & G_{\theta\theta} \end{bmatrix}^T \begin{Bmatrix} t_i \\ q \end{Bmatrix} - \begin{bmatrix} F_{ij} & 0 \\ \hat{F}_{\theta j} & F_{\theta\theta} \end{bmatrix}^T \begin{Bmatrix} v_i \\ \theta \end{Bmatrix} + \begin{Bmatrix} \hat{R}_j \\ \hat{R}_\theta \end{Bmatrix}, \tag{2.7.4}$$

in which $\hat{G}_{ij}, \hat{G}_{\theta j}$ and $\hat{F}_{\theta j}$ are now modified kernel functions and $\hat{R}_\beta$ is the corresponding right-hand-side contribution. However, at this point, the fluid formulation (2.7.1) and the solid formulation (2.7.4) are completely compatible, and are in an ideal form to solve quite general interaction problems.

2.7.3 NUMERICAL IMPLEMENTATION

The boundary element code, BEST-FSI, was generalized so that any combination of solid and fluid regions could be accommodated. Also, the modified thermoelastic kernels of equation (2.7.4) were implemented. The entire BEST-FSI input is free format and keyword driven. Output is provided on a region-by-region basis, and thus contains only information pertinent to the region type. Displacements, temperatures, stresses and strains are detailed for solid GMRs, while velocities, temperatures, stresses, pressures, strain rates and vorticities are output for fluid regions. In all cases, a complete PATRAN interface is available, so that any quantities can be plotted.

Figure 2.7.1 Fluid-Structure Interaction Conceptional Model

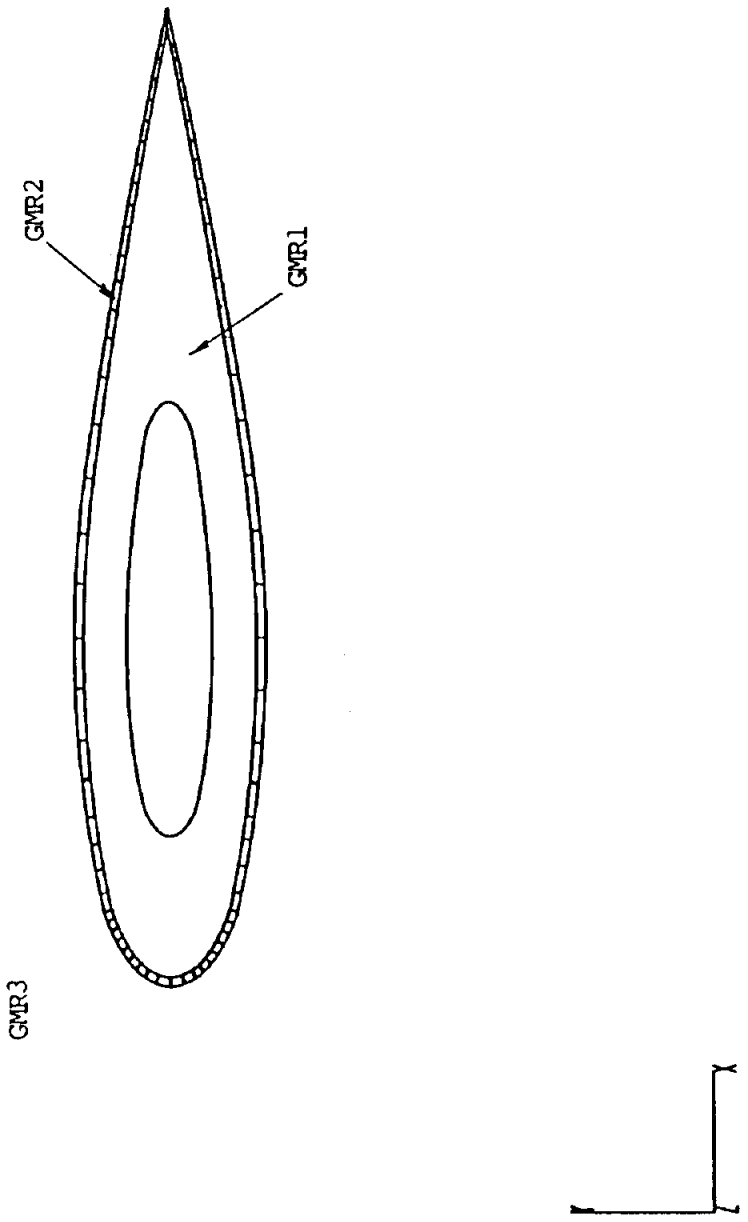

3.0 APPLICATIONS

3.1 INTRODUCTION

Boundary element formulations were detailed in the previous section for the analysis of thermoelastic solids and thermoviscous fluids. In this section, these new formulations are applied to solve numerous example problems. The individual subsections correspond to those presented in Section 2. (Thus, Section 2.4 and 3.4 both concern convective incompressible thermoviscous flow.)

It should be noted that all of these numerical applications were completed on a Sun SPARC workstation. Results presented in Sections 3.2, 3.3, 3.4, and 3.7 were obtained with BEST-FSI. On the other hand, convective potential flow results provided in Section 3.5 were obtained by executing a separate single-region boundary element code. The convective potential flow and compressible thermoviscous flow formulations are not yet available in BEST-FSI.

3.2 THERMOELASTIC DEFORMATION

3.2.1 SUDDEN HEATING OF ALUMINUM BLOCK

As a first example, transient heating of an aluminum block is examined under plane strain conditions. The block, shown in Figure 3.2.1, initially rests in thermodynamic equilibrium at zero temperature. Then, suddenly, the face at $Y = 1.0$ in. is elevated to 100°F, while the remaining three faces are insulated and restrained against normal displacements. Thus, only axial deformation in the Y–direction is permitted. Naturally, as the diffusive process progresses, temperature builds along with the lateral stresses σ_{xx} and σ_{zz}. To complete the specification of the problem, the following standard set of material properties are used to characterize the aluminum:

$$E = 10 \times 10^6 psi, \qquad \nu = 0.33,$$
$$\alpha = 13 \times 10^{-6}/^oF,$$
$$k = 25 \text{in.lb./sec.in.}^oF, \qquad \rho c_\epsilon = 200 \text{in.lb./in.}^3{}^oF.$$

The two-dimensional boundary element idealization consists of the simple four element, eight node model included in Figure 3.2.1. A time step of 0.4 sec. is selected, corresponding to a non-dimensional time step of 0.5. Additionally, a finite element analysis of this same problem was conducted using a modified thermal version of the computer code CRISP (Gunn and Britto, 1984). The finite element model is also a two-dimensional plane strain representation, however, sixteen linear strain quadrilaterals are placed along the diffusion length. In the FE run, a time step of 0.2 sec. is employed.

Temperatures, displacements, and stresses are compared in Table 3.2.1. Notice that the boundary element analysis, with only one element in the flow direction, produces a better time-temperature history than does a sixteen element FE analysis with a smaller time step. Both methods exhibit greatest error during the initial stages of the process. This is the result of the imposition of a sudden temperature change. Meanwhile, the comparison of the overall axial displacement indicates agreement to within 3% for the BE analysis and 5% for the FE run. A steady-state analysis via both methods produces the exact answer to three digit accuracy. The last comparison, in the table, involves lateral stresses at an integration point in the FE model. The boundary element results are quite good throughout the range, however, the FE stresses exhibit considerable error, particularly during the initial four seconds. Actually, these finite element stress variations are not unexpected in light of the errors present in the temperature and displacement response. Recall that in the standard finite element process, stresses are computed on the basis of numerical differentiation of the displacements, whereas in boundary elements, the stresses at interior points are obtained directly from a discretized version of an exact integral equation. Consequently, the BE interior stress solution more nearly coincides with the actual response.

Table 3.2.1

Sudden Heating of Aluminum Block

Time (sec.)	Temperature (°F) at $Y = 0$			Axial Displacement (μ in.) at $Y = 1.0$			Lateral Stress (ksi) at $Y = 0.5312$		
	Exact	FE	BEM	Exact	FE	BEM	Exact	FE	BEM
0.8	4.7	3.4	3.8	910	860	920	-5.6	-3.9	-5.4
1.6	22.0	19.8	20.7	1290	1250	1320	-9.1	-7.7	-9.2
2.4	38.3	36.4	37.7	1570	1540	1610	-11.3	-10.3	-11.7
3.2	51.5	50.0	51.5	1780	1760	1840	-13.1	-12.2	-13.5
4.0	61.9	60.7	62.2	1950	1930	2000	-14.4	-13.8	-14.8
4.8	70.1	69.1	70.5	2090	2070	2130	-15.5	-15.0	-15.9
5.6	76.5	75.7	76.9	2200	2180	2230	-16.3	-15.9	-16.7
6.4	81.5	80.9	81.9	2280	2270	2310	-17.0	-16.7	-17.3
7.2	85.5	84.9	85.8	2340	2330	2370	-17.5	-17.2	-17.8
8.0	88.6	88.2	88.8	2400	2390	2410	-17.9	-17.7	-18.1

Figure 3.2.1

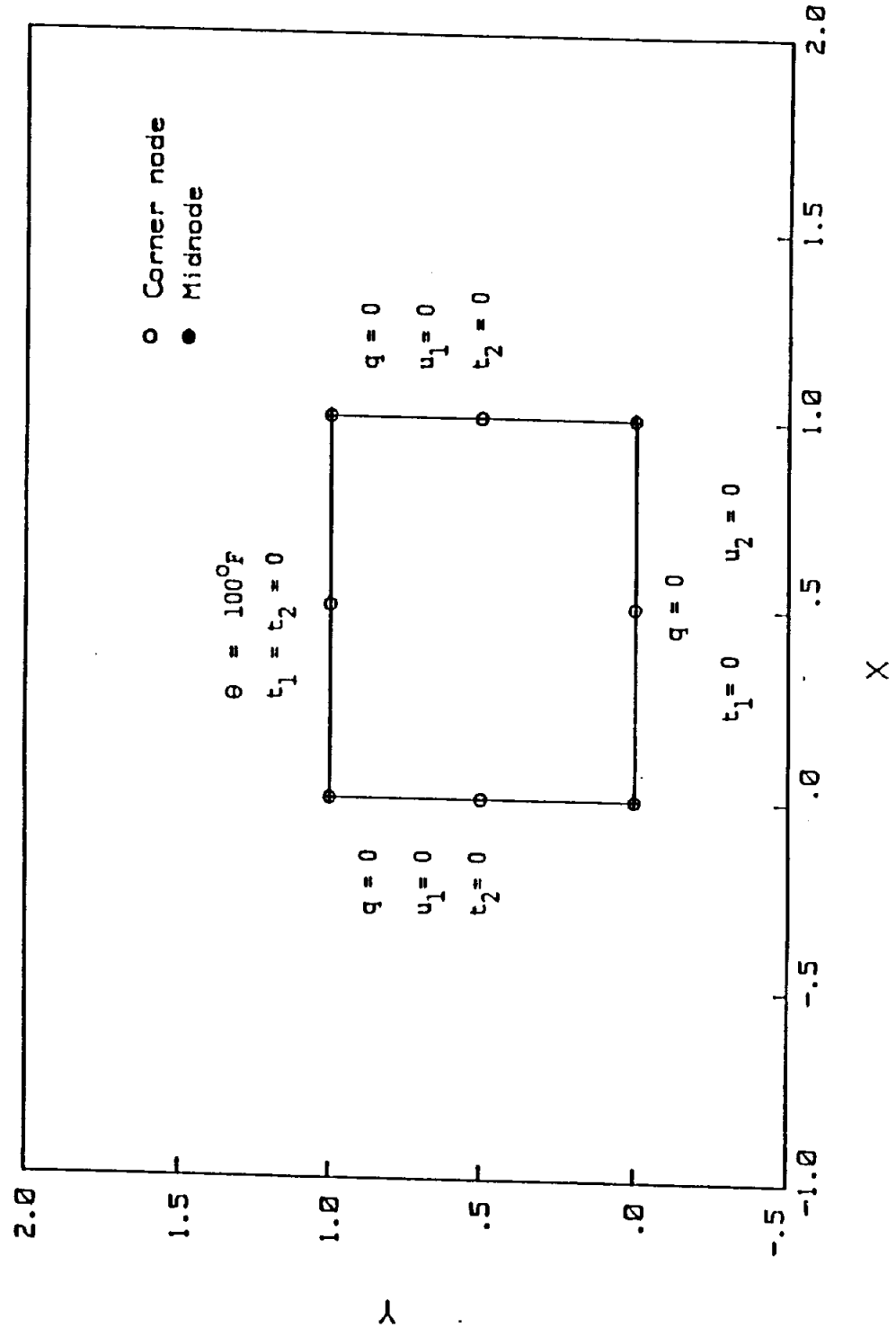
ALUMINUM BLOCK
Problem Definition
o Corner node
● Midnode
θ = 100°F
t1 = t2 = 0
q = 0
u1 = 0
t2 = 0
q = 0
u2 = 0
t1 = 0
q = 0
u1 = 0
t2 = 0
q = 0
2.0
1.5
1.0
.5
.0
-.5
-1.0
Y
X

3.2.2 CIRCULAR DISK

Next, transient thermal stresses in a circular disc are investigated. The disc of radius 'a' initially rests at zero uniform temperature. The top and bottom surfaces are thermally insulated, and all boundaries are completely free of mechanical constraint. Then, suddenly, at time zero, the temperature of the entire outer edge (i.e., $r = a$) is elevated to unity and, subsequently, maintained at that level.

The boundary element model of the disc with unit radius is shown in Figure 3.2.2. Only four quadratic elements are employed, along with quarter symmetry. Ten interior points are also included strictly to monitor response. In addition, the following non-dimensionalized material properties are arbitrarily selected for the plane stress analysis:

$$E = 1.333 \qquad \rho c_e = 1.0$$
$$\nu = 0.333 \qquad k = 1.0$$
$$\alpha = 0.75$$

Results obtained under quasistatic conditions for a time step of 0.005 are compared, in Figures 3.2.3, 3.2.4 and 3.2.5, to the analytical solution presented in Timoshenko and Goodier (1970). Notice that temperatures, as well as radial and tangential stresses are accurately determined via the boundary element analysis. In particular from Figure 3.2.5, even the tangential stress on the outer edge is faithfully reproduced. An extremely fine finite element mesh would be required to obtain a comparable level of accuracy, particularly, for the surface stresses.

Figure 3.2.2

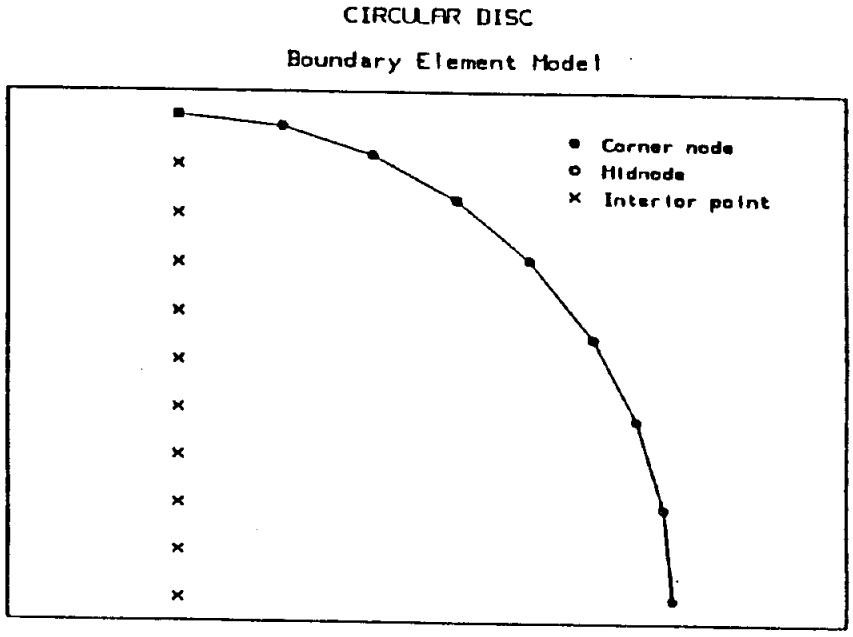

Figure 3.2.3

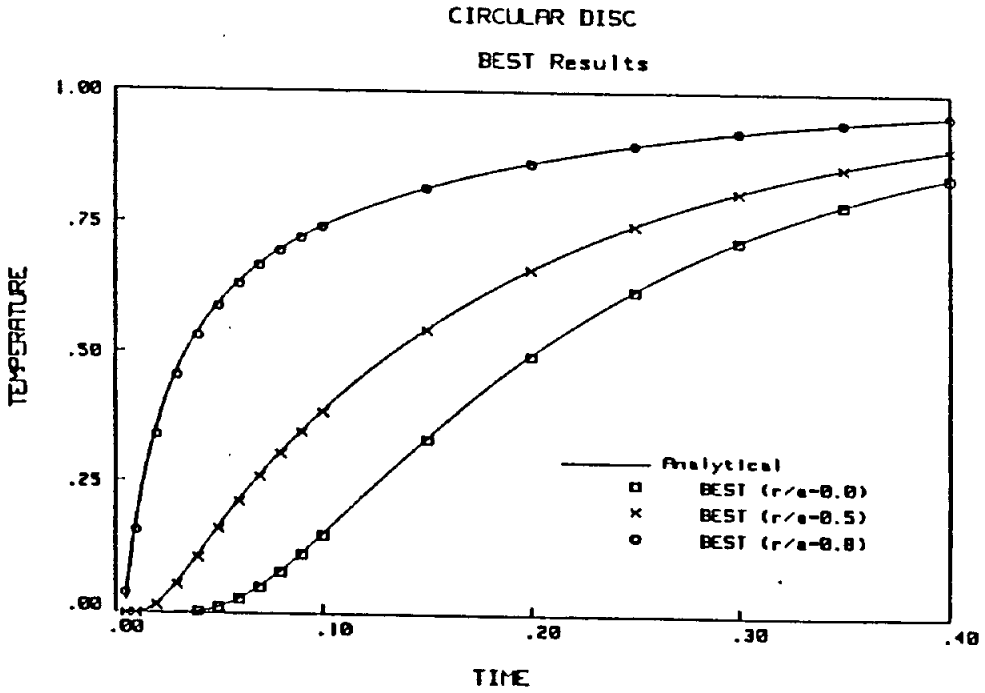

Figure 3.2.4

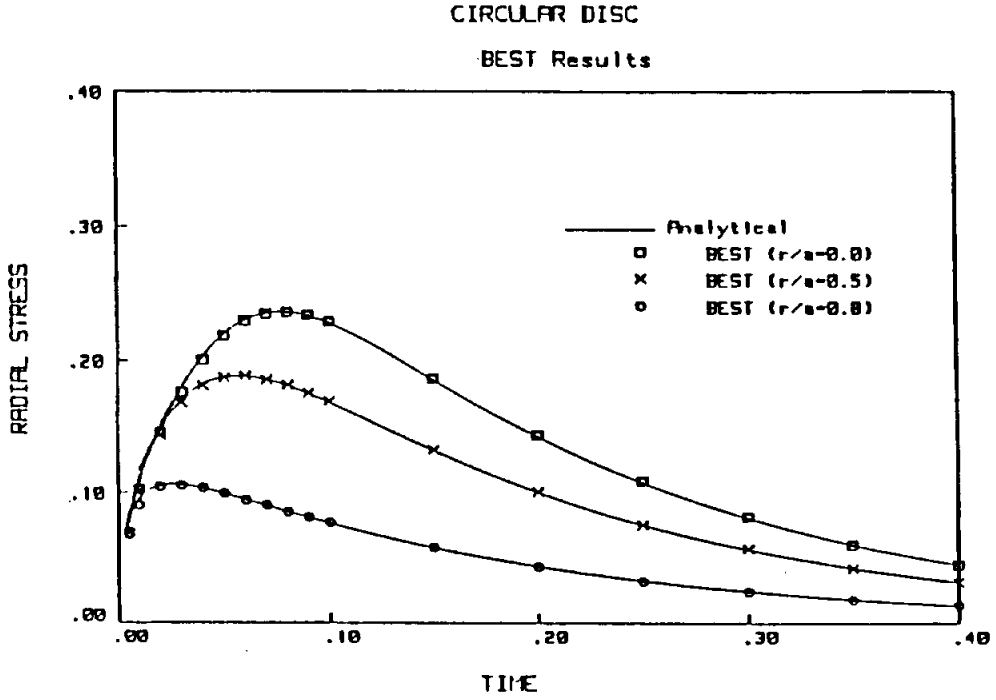

Figure 3.2.5

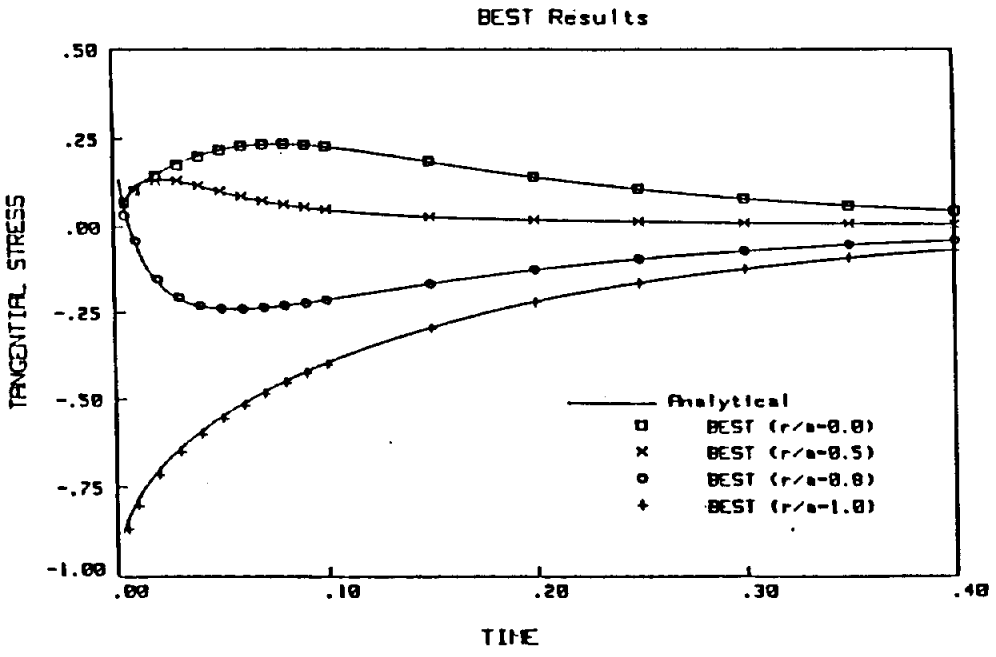

3.3 INCOMPRESSIBLE THERMOVISCOUS FLOW

3.3.1 CONVERGING CHANNEL

The two-dimensional incompressible flow through a converging channel also possesses a well known analytical solution which is purely radial (Millsaps and Pohlhausen, 1953). A comprehensive finite element study of this problem has been made by Gartling et al (1977).

The boundary element model is shown in Figure 3.3.1. The mesh contains 96 cells and is divided into two regions. The boundary conditions were modeled using an exact specification of the boundary conditions appearing in the analytical solution (Fig. 3.3.1). Viscosity is unity, and tractions and density are incremented to reach higher Reynolds numbers. The Reynolds number for this problem is defined as

$$R_e = \frac{\rho R_i V_2(R_i)}{\nu} \tag{3.3.1}$$

where $V_2(R_i)$ is the maximum velocity in the region, which is -24.0 for the problem solved here.

Figure 3.3.2 illustrates the results for two Reynolds numbers, indicating good accuracy along the entire width of the channel. Not only are the velocities accurate, but the pressures and tractions are very accurate also.

It has been observed that finite element versions of this problem have several peculiarities which prevent the analytical solution from being reproduced. First of all, since velocities are often specified at the inlet and at the wall and centerline, ambiguous boundary condition specification results. Also, typically a parabolic "fully developed" velocity profile is usually specified at the inlet. However, the nonlinear solution has a flattened velocity distribution across the width of the channel (see Fig. 3.3.2). Hence, the analytical solution cannot be reproduced exactly if the "fully developed" profile is specified at the inlet. Also, the finite element modelers of this problem usually leave out the traction distribution at the exit and specify zero tractions there. This also gives rise to non-radial flow.

The reason for so much interest in the converging flow problem is that it is one of the few problems possessing an analytical solution. However, by specifying a model which does not correspond to this problem, as in the finite element case, one cannot accurately compare results to the analytical solution. Any such comparisons are merely qualitative. In this light, the boundary element model here has utilized an exact model of the boundary condition and a meaningful comparison can be made.

Figure 3.3.1 Converging Channel - Problem Definition

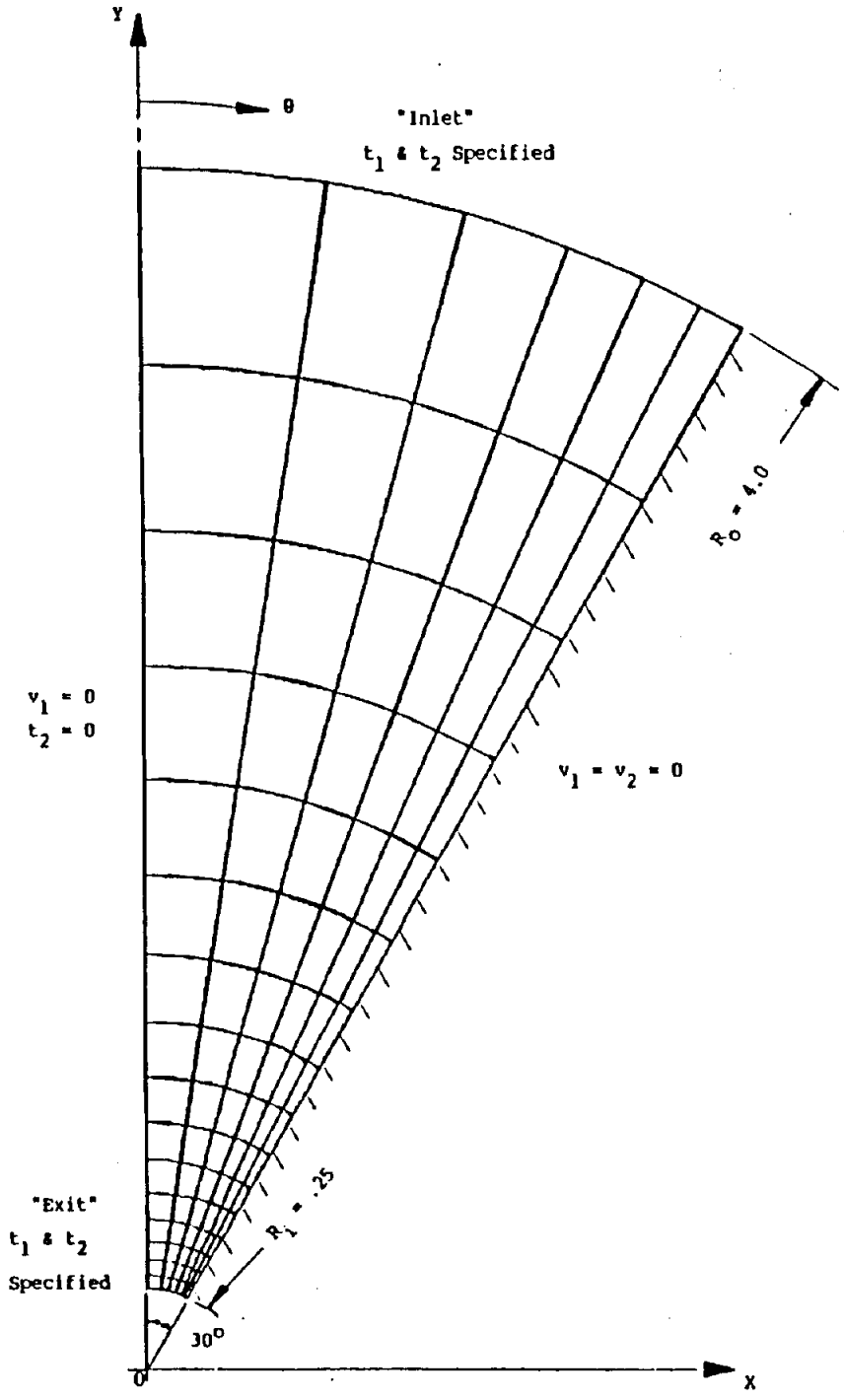

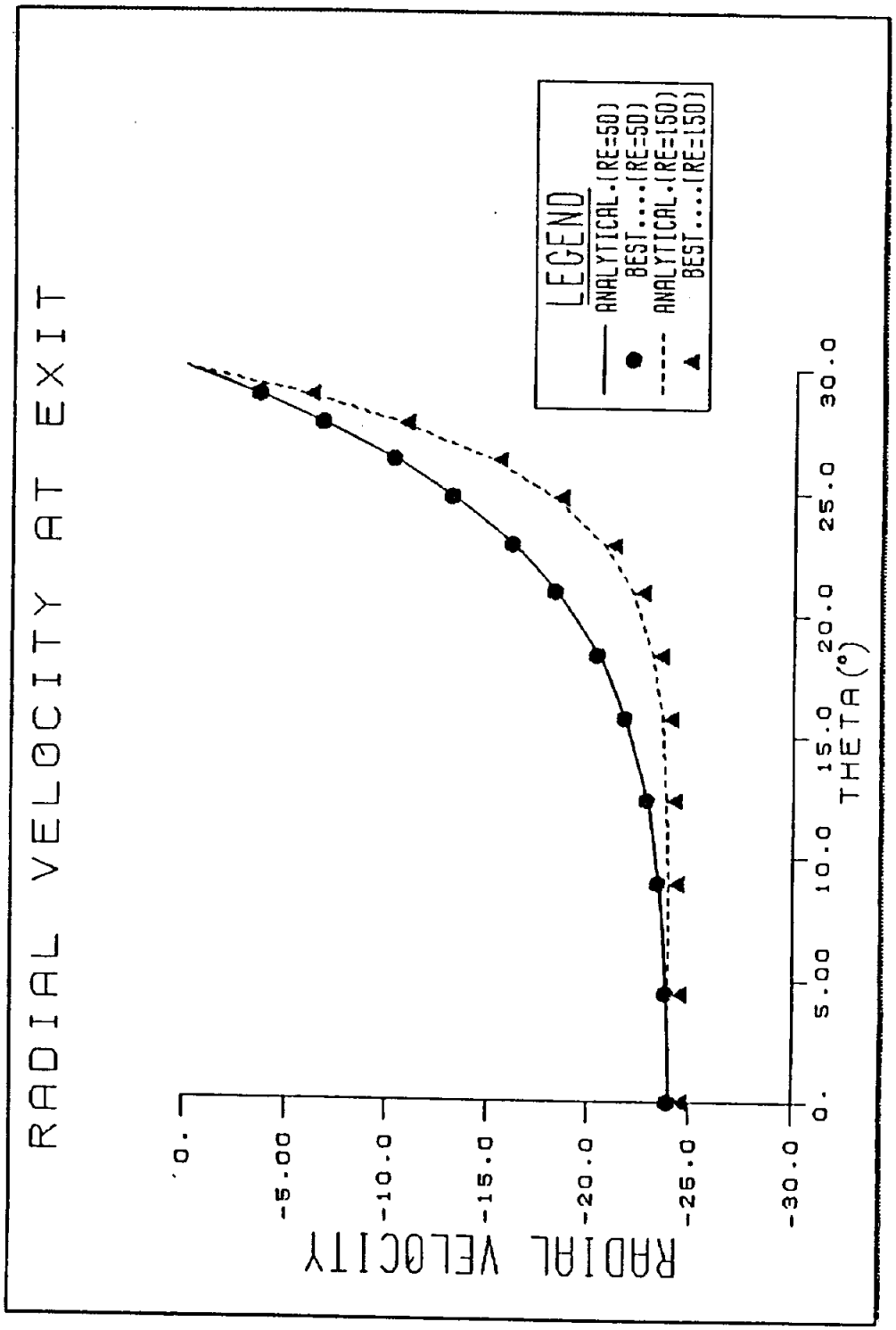

Figure 3.3.2 Converging Channel - Radial Velocity

3.3.2 TRANSIENT COUETTE FLOW

Consider as the first transient analysis the case of developing Couette flow between two plates, parallel to the x-z plane, a distance h apart. Initially, both of the plates, as well as the fluid, are at rest. Then, beginning at time $t = 0$, the bottom plate is moved continuously with velocity V in the x-direction. Due to the no-slip condition at the fluid-plate interface, Couette flow begins to develop as the vorticity diffuses. Eventually, when steady conditions prevail, the x-component of the velocity assumes a linear profile.

The following exact solution to this unsteady problem is provided by Schlicting (1955):

$$v_x(y,t) = V\left\{\sum_{n=0}^{\infty} erfc[2n\eta_1 + \eta] - \sum_{n=0}^{\infty} erfc[2(n+1)\eta_1 - \eta]\right\} \tag{3.3.2a}$$

$$v_y(y,t) = 0 \tag{3.3.2b}$$

where

$$\eta = \frac{y}{(4\mu t/\rho)^{1/2}} \qquad \eta_1 = \frac{h}{(4\mu t/\rho)^{1/2}} \tag{3.3.3a,b}$$

$$erfc(z) = 1 - erf(z) = 1 - \frac{2}{\pi^{1/2}}\int_o^z e^{-\gamma^2} d\gamma. \tag{3.3.3c}$$

All of the nonlinear terms vanish, since both v_y and $\partial v_x/\partial x$ are zero.

The two-dimensional boundary element model, utilized for this problem, is displayed in Figure 3.3.3. Four quadratic surface elements are employed, with one along each edge of the domain. A number of sampling points are included strictly to monitor response. Notice that the region of interest is arbitrarily truncated at the planes $x = 0$ and $x = \ell$. All of the boundary conditions are also shown in Figure 3.3.3. For the presentation of BEST-FSI results, all quantities are normalized. Thus,

$$Y = \frac{y}{h} \tag{3.3.4a}$$

$$T = \frac{\alpha t}{h^2} \tag{3.3.4b}$$

and the horizontal velocity is v_x/V. Figure 3.3.4 provides the velocity profiles at four different times, using a time step $\Delta T = 0.025$ and the convolution approach. There is some error present at small times near the top plate, where the velocity is nearly zero. Results at $Y = 0.5$ versus time are shown in Figure 3.3.5 for several values of the time step. Obviously, the correlation improves with a reduction in time step and $\Delta T = 0.025$ provides accurate velocities throughout the time history. However, even for a very large time step, the BEST-FSI solution shows no signs of instability. Error, evident in the initial portion, diminishes with time, and all values of ΔT produce the correct steady response. Further reduction of ΔT beyond 0.025 yields little benefit. Instead, mesh refinement in the y-direction is needed, primarily to capture the short time behavior. Figure 3.3.6 shows the BEST-FSI results for a model with just two, equal length, elements along each vertical side. The correlation

with the analytical solution is now excellent. The time step selected for the refined model was based upon the general recommendation that

$$\Delta T \cong \frac{0.05\ell_{min}^2}{c}, \tag{3.3.5}$$

where ℓ_{min} is the length of the smallest element.

The convolution approach, defined by equation (2.3.18), was used to obtain the results presented in Figures 3.3.4-3.3.6. Alternatively, the recurring initial condition algorithm can be invoked. In that case, complete volume discretization is required even for this linear problem. For the model of Figure 3.3.4, a single volume cell connecting the eight nodes is all that is required. The BEST-FSI results for different values of ΔT are shown in Figure 3.3.7. The solutions are good for the two smaller time step magnitudes, however there is a slight degradation in accuracy from the convolution results.

Interestingly, the solution in (3.3.2a) is identical to that for one-dimensional transient heat conduction in an insulated rod with one end maintained at temperature V, while the other remains at zero. However, in a corresponding boundary element analysis, the numerical integrations defined in (2.3.15a) must be calculated much more precisely for unsteady viscous flow than for heat conduction in order to obtain comparable levels of accuracy.

Figure 3.3.3

TRANSIENT COUETTE FLOW

Boundary Element Model

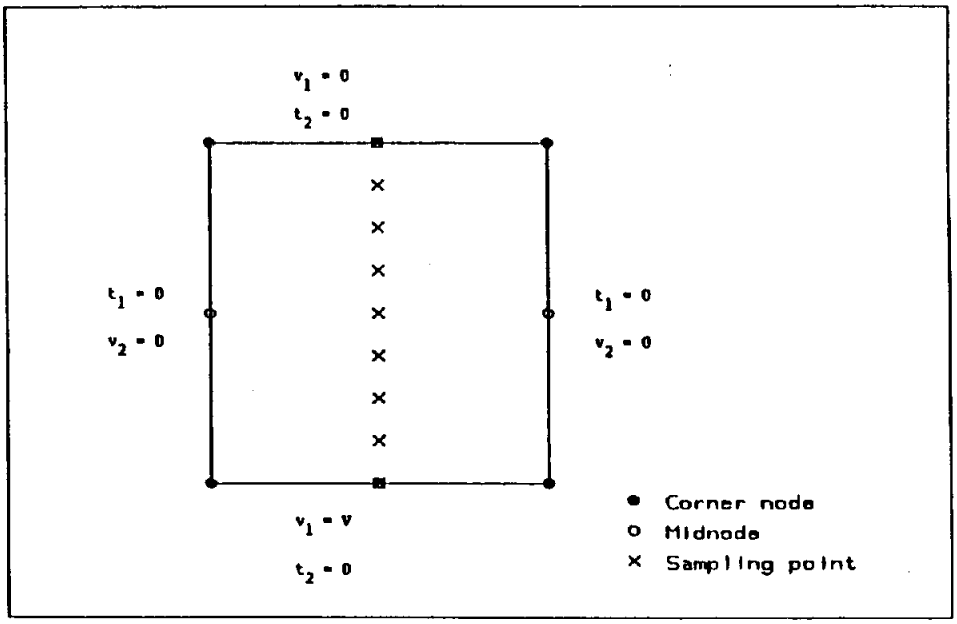

Figure 3.3.4

TRANSIENT COUETTE FLOW

Velocity Profile

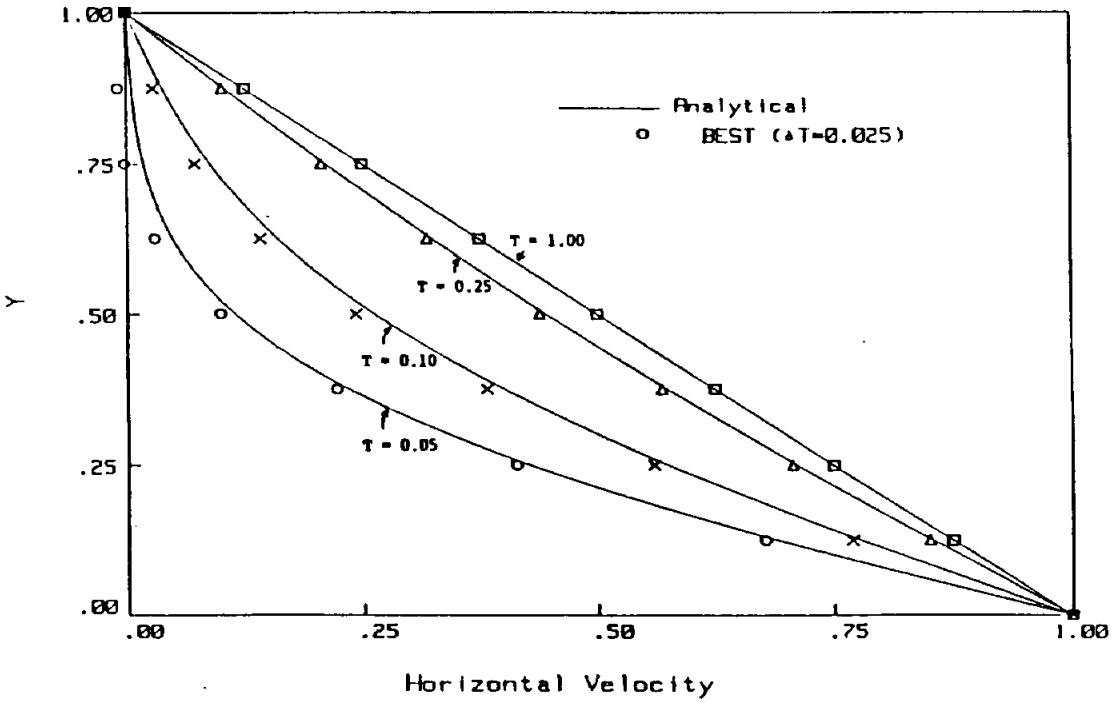

Figure 3.3.5

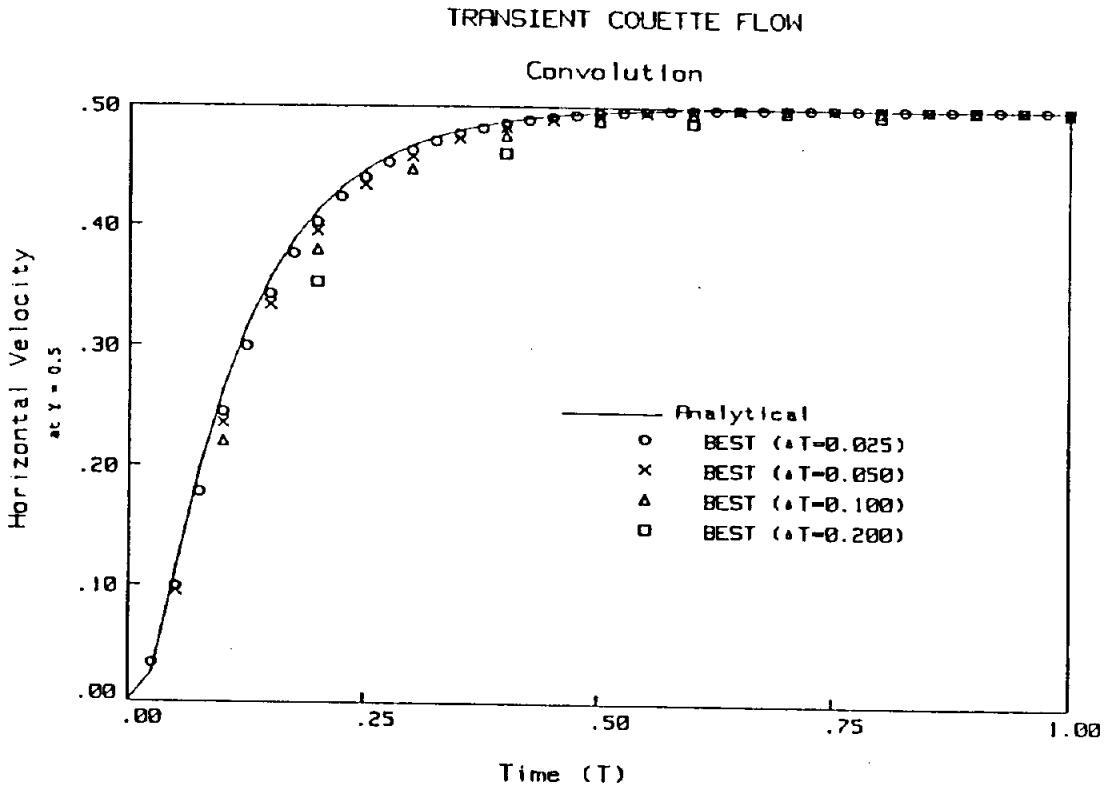

Figure 3.3.6

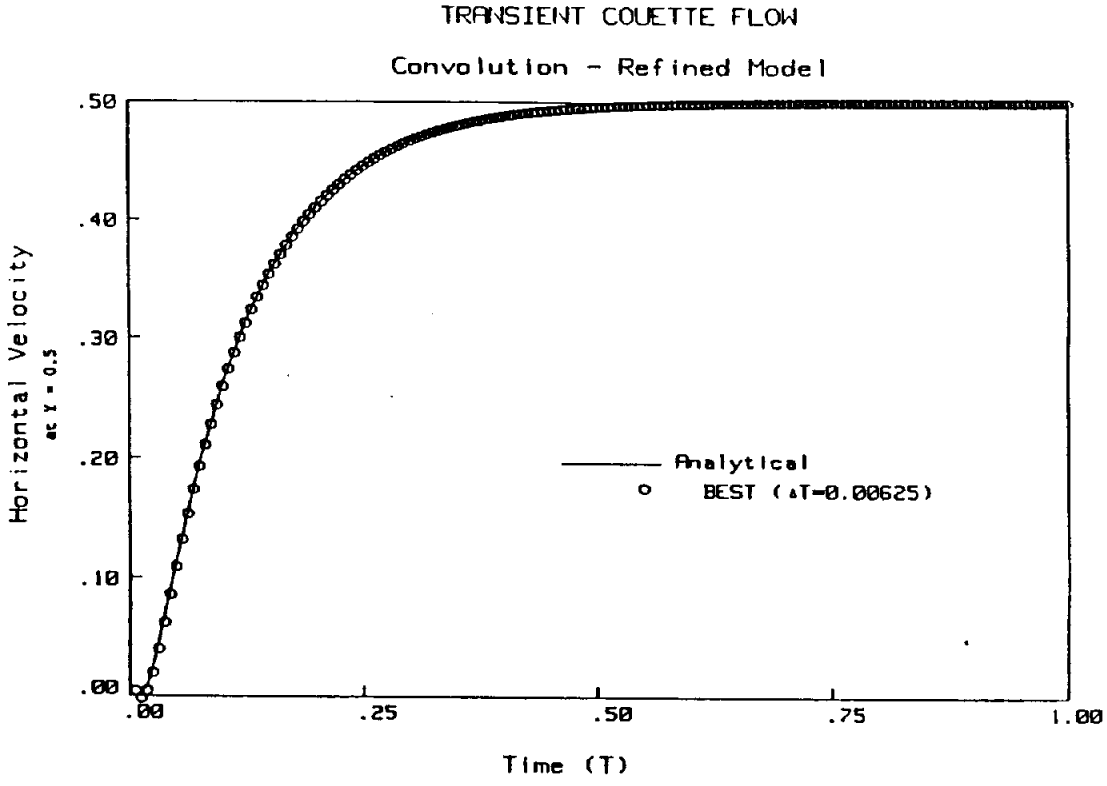

Figure 3.3.7

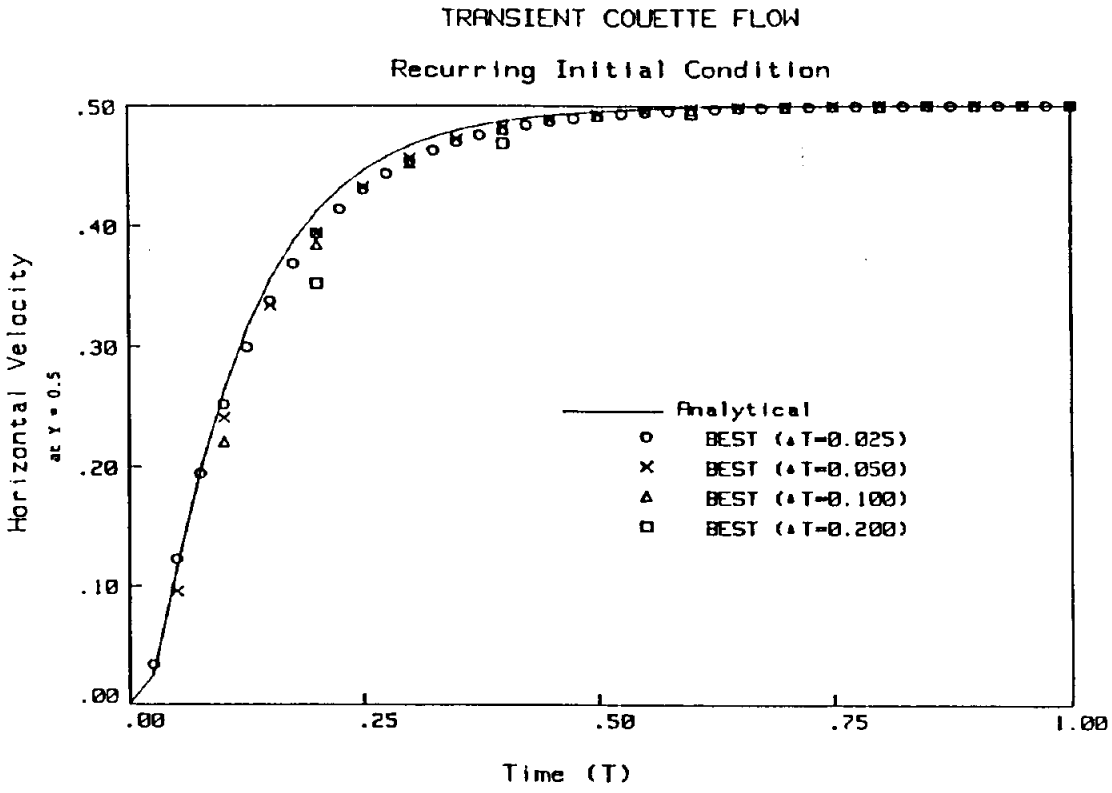
TRANSIENT COUETTE FLOW
Recurring Initial Condition
Horizontal Velocity
at Y = 0.5
.50
.40
.30
.20
.10
.00
.00
.25
.50
.75
1.00
Time (T)
Analytical
BEST (ΔT=0.025)
BEST (ΔT=0.050)
BEST (ΔT=0.100)
BEST (ΔT=0.200)

3.3.3 FLOW BETWEEN ROTATING CYLINDERS

As the next example, the developing flow between rotating cylinders is analyzed. The inner cylinder of radius r_i is stationary, while the outer concentric cylinder with radius r_o is given a tangential velocity V, beginning abruptly at time zero. The steady solution appears in Schlicting (1955). However, even for the transient case, the flow is purely circumferential. Thus, the governing Navier-Stokes equations reduce to

$$\mu\left(\frac{\partial^2 v_\theta}{\partial r^2}+\frac{1}{r}\frac{\partial v_\theta}{\partial r}-\frac{v_\theta}{r^2}\right)-\rho\frac{\partial v_\theta}{\partial t}=0 \tag{3.3.6a}$$

$$-\frac{\partial p}{\partial r}+\frac{v_\theta^2}{r}=0 \tag{3.3.6b}$$

in polar coordinates (r,θ,z). As discussed in Batchelor (1967), separation of variables can be used to obtain the following solution (Honkala, 1992)

$$v_r(r,t)=0 \tag{3.3.7a}$$

$$v_\theta(r,t)=c_1 r+\frac{c_2}{r}+\sum_{n=1}^{\infty}D_n\{J_1(\lambda_n r)Y_1(\lambda_n r_o)-Y_1(\lambda_n r)J_1(\lambda_n r_o)\}e^{-\lambda_n^2 \alpha t} \tag{3.3.7b}$$

where

$$c_1=\frac{V r_o}{r_o^2-r_i^2} \qquad c_2=-c_1 r_i^2 \tag{3.3.8a,b}$$

$$D_n=\frac{\pi^2}{2}\frac{\lambda_n J_1^2(\lambda_n r_i)}{J_1^2(\lambda_n r_i)-J_1^2(\lambda_n r_o)}\{Y_1(\lambda_n r_o)F_{1n}+J_1(\lambda_n r_o)F_{2n}\} \tag{3.3.8c}$$

$$F_{1n}=-c_1[r_o^2 J_2(\lambda_n r_o)-r_i^2 J_2(\lambda_n r_i)]+c_2[J_o(\lambda_n r_o)-J_o(\lambda_n r_i)] \tag{3.3.8d}$$

$$F_{2n}=c_1[r_o^2 Y_2(\lambda_n r_o)-r_i^2 Y_2(\lambda_n r_i)]-c_2[Y_o(\lambda_n r_o)-Y_o(\lambda_n r_i)] \tag{3.3.8e}$$

and λ_n is the nth root of the equation

$$J_1(\lambda r_i)Y_1(\lambda r_o)-J_1(\lambda r_o)Y_1(\lambda r_i)=0. \tag{3.3.9}$$

Figure 3.3.8 depicts the boundary element model representing the region between the two cylinders. A thirty degree segment is isolated, with cyclic symmetry boundary conditions imposed along the edges $\theta=0°$ and $\theta=30°$. The inner radius is unity, while an outer radius of two is assumed. Unit values are also taken for the viscosity, density and V. The model consists of six quadratic elements and two quadratic cells. The cells, of course, are not needed for linear analysis utilizing the convolution approach.

Results of the BEST-FSI analysis are compared to the exact solution in Figure 3.3.9 for convolution and in Figure 3.3.10 for the recurring initial condition algorithm. In both diagrams, results with and without the nonlinear convective terms are plotted. The results are quite good throughout the time history with the convolution approach, while some noticeable error is present at early times for the recurring initial condition solutions. The linear and nonlinear velocity profiles are nearly identical, as expected from the exact

solution expressed in (3.3.7b). However, unlike the previous example, the nonlinear terms do not simply vanish from the integral equation written in cartesian form. Instead, the nonlinear surface and volume integrals must combine in the proper manner to produce the correct solution. Consequently, this problem provides a good test for the entire BEM formulation.

Relative run times are shown in Table 3.3.1 for the different analysis types. Obviously, the nonlinear convolution approach is very expensive, since this involves volume integration at each time step. As a result, in the general implementation, convolution is only utilized in linear GMRs.

Table 3.3.1 - Flow Between Rotating Cylinders (Run Time Comparisons)

Analysis Type	Time Marching Algorithm	Relative CPU Time
Linear	Convolution	1.0
Nonlinear	Convolution	25.8
Linear	Recurring Initial Condition	1.5
Nonlinear	Recurring Initial Condition	1.8

Figure 3.3.8

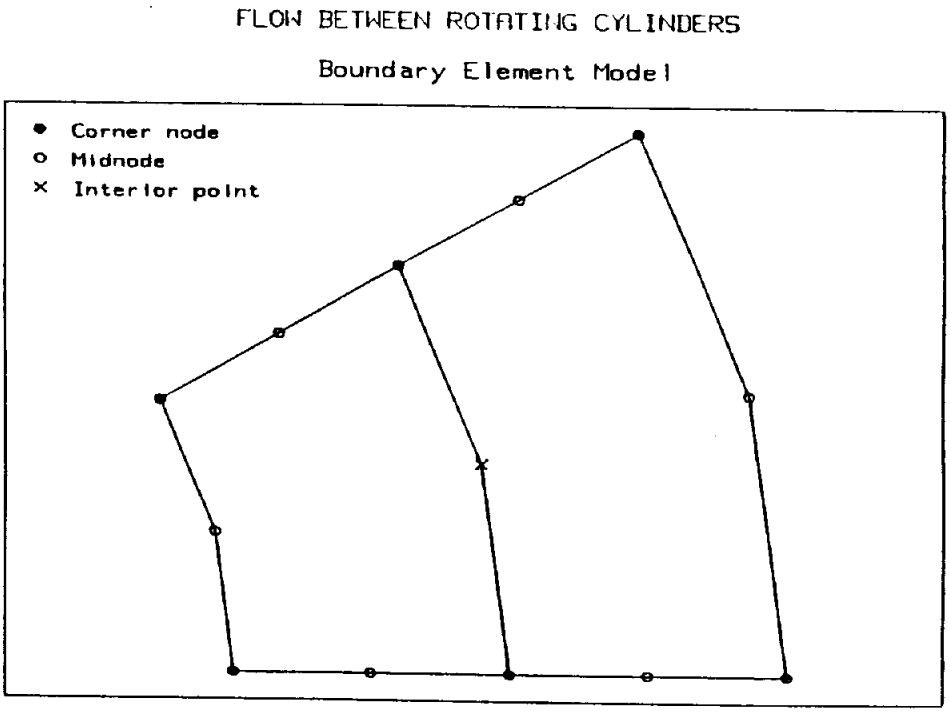
FLOW BETWEEN ROTATING CYLINDERS
Boundary Element Model
Corner node
Midnode
Interior point

Figure 3.3.9

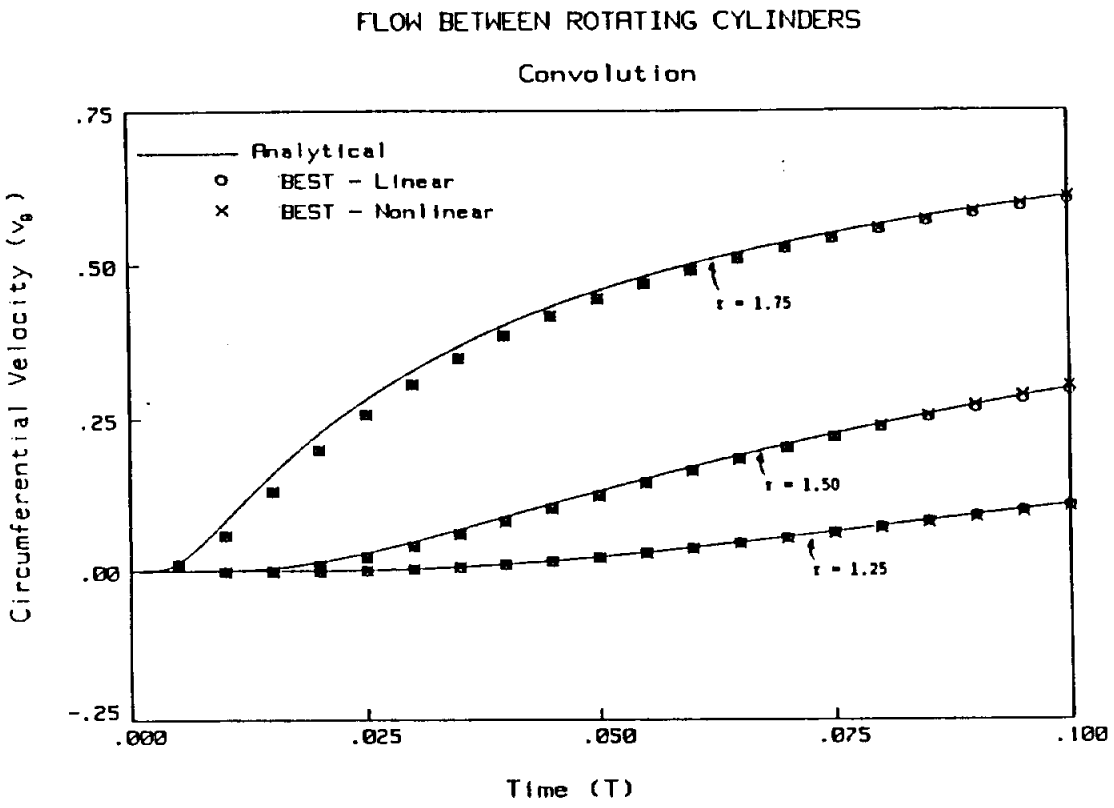

Figure 3.3.10

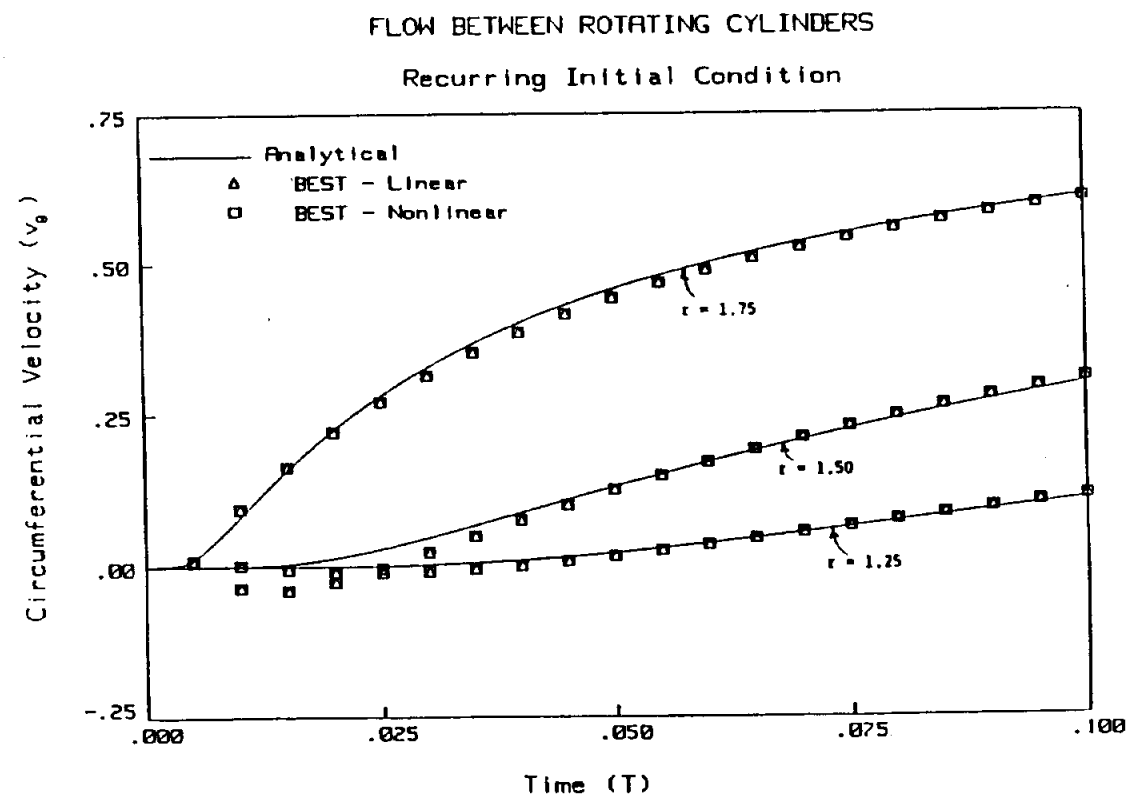

3.3.4 DRIVEN CAVITY FLOW

The two-dimensional driven cavity has become the standard test problem for incompressible computational fluid dynamics codes. In a way, this is unfortunate because of the ambiguities in the specification of the boundary conditions. However, numerous results are available for comparison purposes.

The incompressible fluid of uniform viscosity is confined within a unit square region. The fluid velocities on the left, right and bottom sides are fixed at zero, while a uniform nonzero velocity is specified in the x-direction along the top edge. Thus, in the top corners, the x-velocity is not clearly defined. To alleviate this difficulty in the present analysis, the magnitude of this velocity component is tapered to zero at the corners.

Results are presented for the four region, 324 cell boundary element model shown in Figure 3.3.11. Notice that a higher level of refinement is used near the edges. Spatial plots of the resulting velocity vectors are displayed in Figures 3.3.12a and b for Reynolds numbers (Re) of 400 and 1000, respectively. Notice that, in particular, the shift of the vortical center follows that described by Burggraf (1966) in his classic paper. A more quantitative examination of the results can be found in Figure 3.3.13 where the horizontal velocities on the vertical centerline obtained from the present BEST-FSI analysis are compared to those of Ghia et al (1982). It is assumed that the latter solutions are quite accurate since the authors employed a 129 by 129 finite difference grid. As is apparent, from the figure, all of the solutions are in excellent agreement. Finally, it should be noted that the simple iterative algorithm fails to converge much beyond $Re = 100$. Beyond that range the use of a Newton-Raphson type algorithm is imperative.

In this driven cavity problem, complete volume discretization is required, since the nonlinear convective terms are nonzero throughout the entire domain. As a result, the evaluation of the volume integrals appearing in (2.3.6) is computationally expensive due to the singular nature of the kernels. Consequently, it is important to investigate the relative merits of a boundary element approach. To aid in this study, a finite element formulation was developed based primarily on the work of Gartling et al (1977). This finite element implementation (Honkala, 1992) utilizes a penalty function approach for incompressibility, along with a Newton-Raphson solution algorithm. An identical sixty-four lagrangian cell model was selected for both the boundary element and finite element analysis. Results are plotted in Figure 3.3.14 for $Re = 100$. The boundary element results, though more expensive, are significantly more accurate. In fact, at this level of refinement, the finite element results show some oscillation. Clearly, for a given mesh, the boundary integral formulation captures more of the physics.

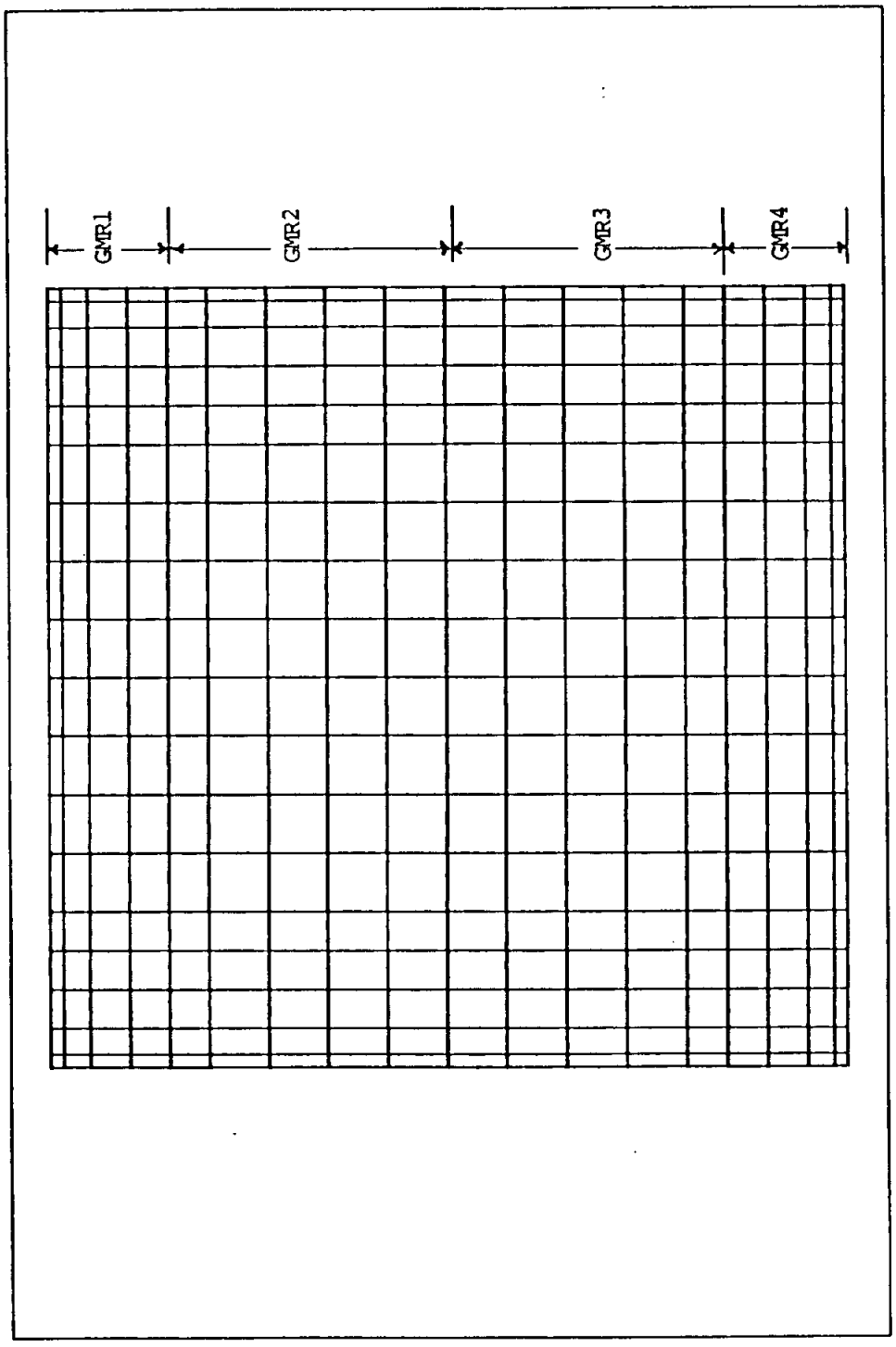
DRIVEN CAVITY - FOUR REGION MODEL
Boundary Element Model
GMR1
GMR2
GMR3
GMR4

Figure 3.3.11

Figure 3.3.12 Driven Cavity - Velocity Vectors

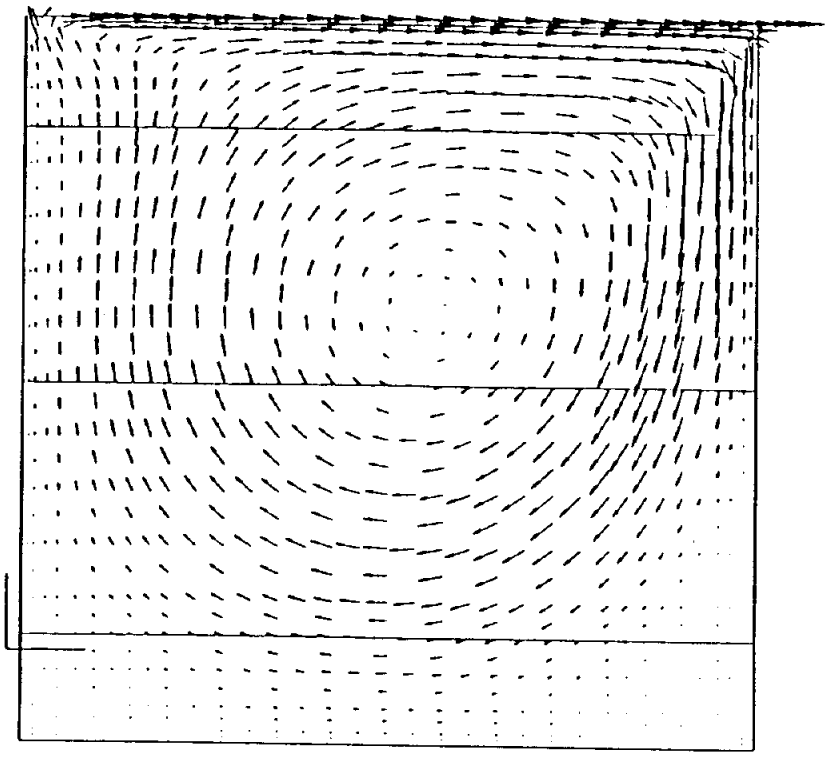

a) Re =400

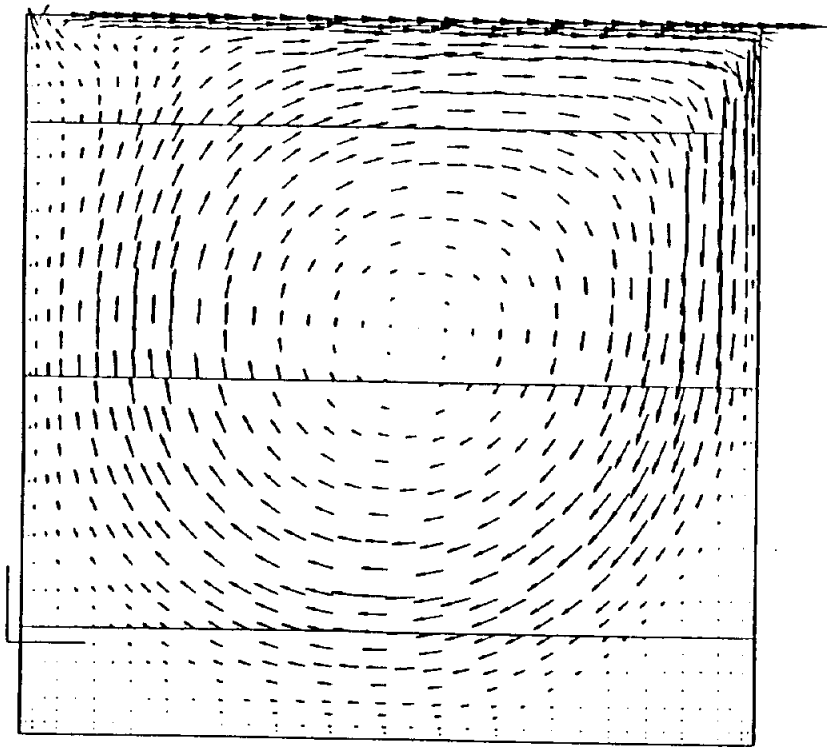

b) Re =1000

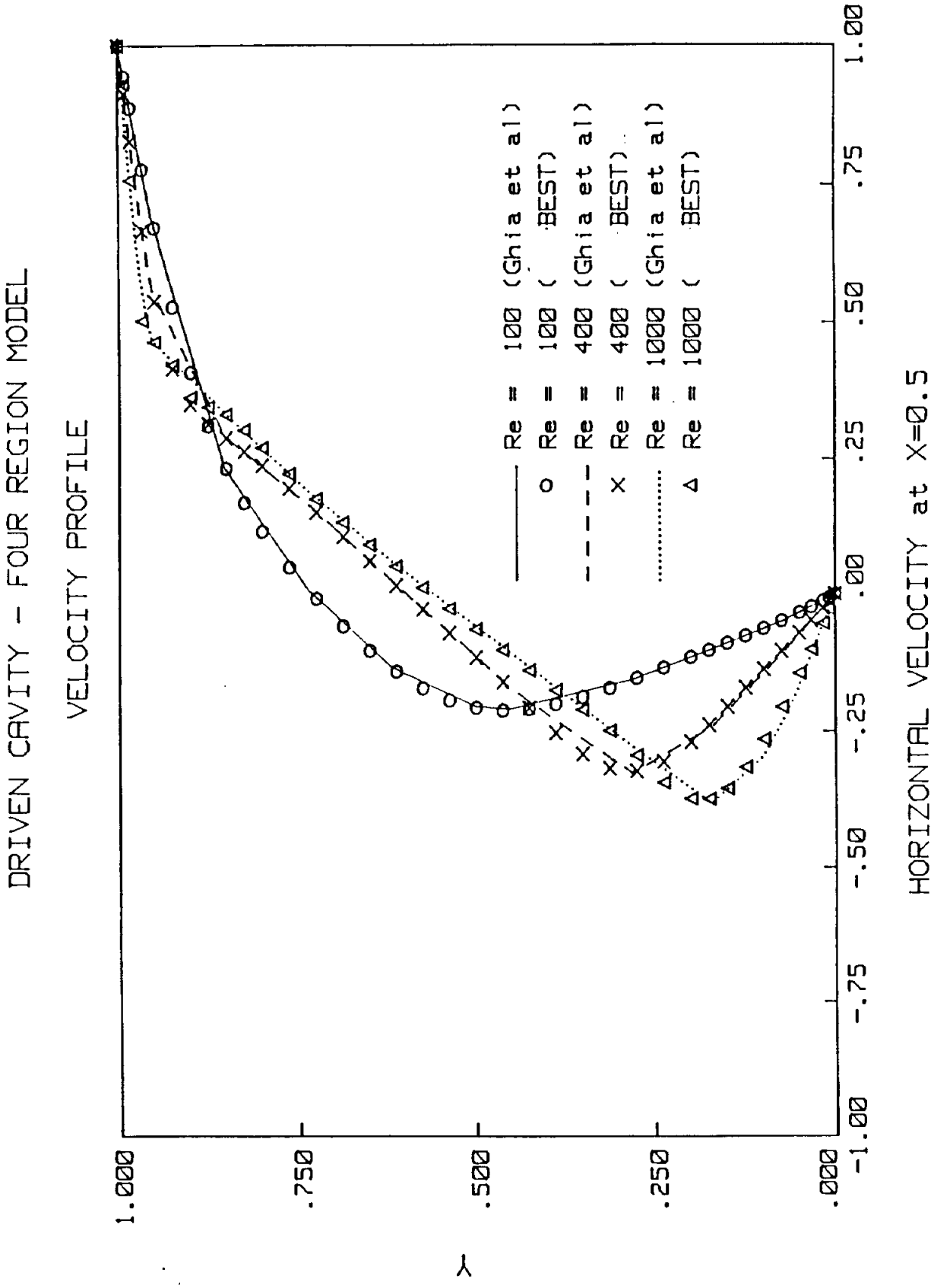
DRIVEN CAVITY - FOUR REGION MODEL
VELOCITY PROFILE
HORIZONTAL VELOCITY at X=0.5
Re = 100 (Ghia et al)
Re = 100 (BEST)
Re = 400 (Ghia et al)
Re = 400 (BEST)
Re = 1000 (Ghia et al)
Re = 1000 (BEST)
1.00
.75
.50
.25
.00
-.25
-.50
-.75
-1.00
1.000
.750
.500
.250
.000
Y

Figure 3.3.13

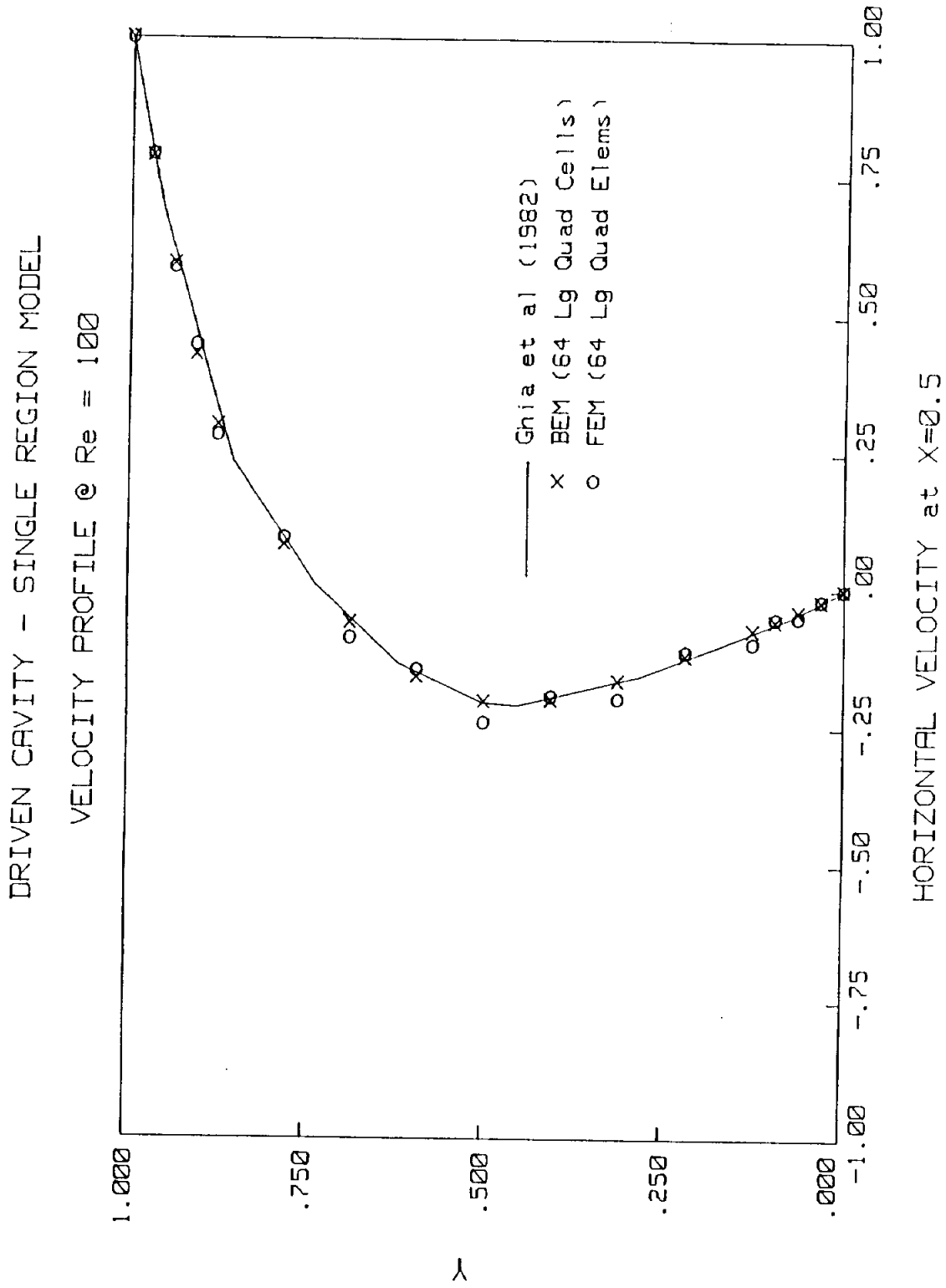
DRIVEN CAVITY - SINGLE REGION MODEL
VELOCITY PROFILE @ Re = 100
Ghia et al (1982)
BEM (64 Lg Quad Cells)
FEM (64 Lg Quad Elems)
HORIZONTAL VELOCITY at X=0.5
Y
1.000
.750
.500
.250
.000
-1.00
-.75
-.50
-.25
.00
.25
.50
.75
1.00

Figure 3.3.14

3.3.5 TRANSIENT DRIVEN CAVITY FLOW

The next example involves the initiation of flow in the same square cavity. An incompressible fluid of uniform density and viscosity is at rest within a unit square region. The velocities of the vertical sides and the bottom are fixed at zero throughout time. At time zero, the horizontal velocity of the top edge is suddenly raised to a value of 1000 and maintained at that level. A gradual transition of velocities is introduced near the top corners to provide continuity.

The four region, 324 cell model shown in Figure 3.3.15 is employed for the boundary element analysis. The resulting velocity vector plots at several times are shown in Figure 3.3.16 for this case having a Reynolds number of 1000. The recurring condition algorithm was used. As in the previous two time-dependent examples, the results lead directly to the steady solution after a sufficient number of time steps. This steady solution correlates closely with the results of Ghia et al (1982).

It should be noted that Tosaka and Kakuda (1987) have run the transient driven cavity at $Re = 10,000$. However, their results show signs of instability even at relatively small times, and are compared to the steady solution of Ghia et al which also is not correct at this much higher Reynolds number. A valid solution in this Re range would necessitate the use of an extremely refined mesh, far beyond that employed by Tosaka and Kakuda or Ghia et al.

Figure 3.3.15 Transient Driven Cavity - Boundary Element Model

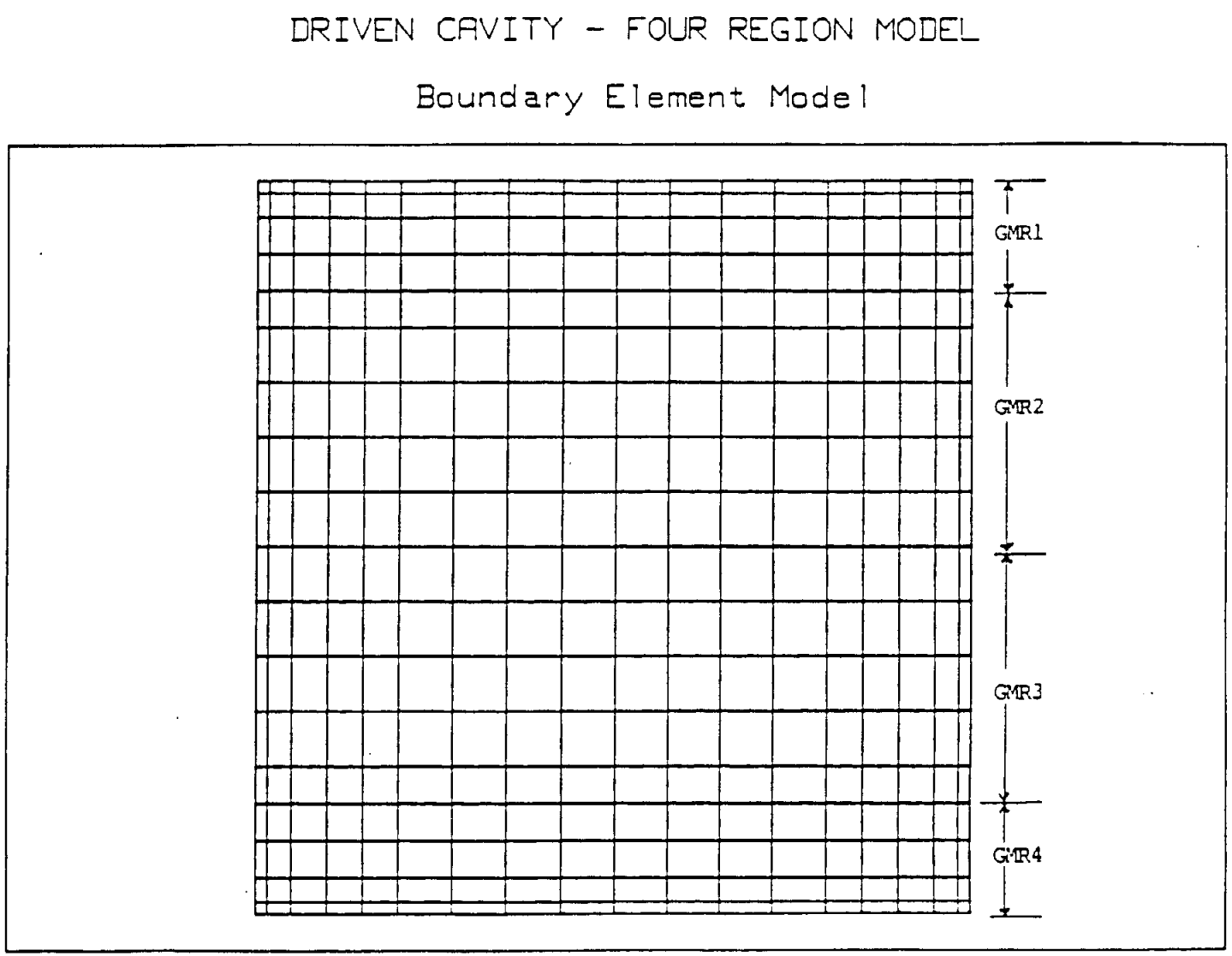

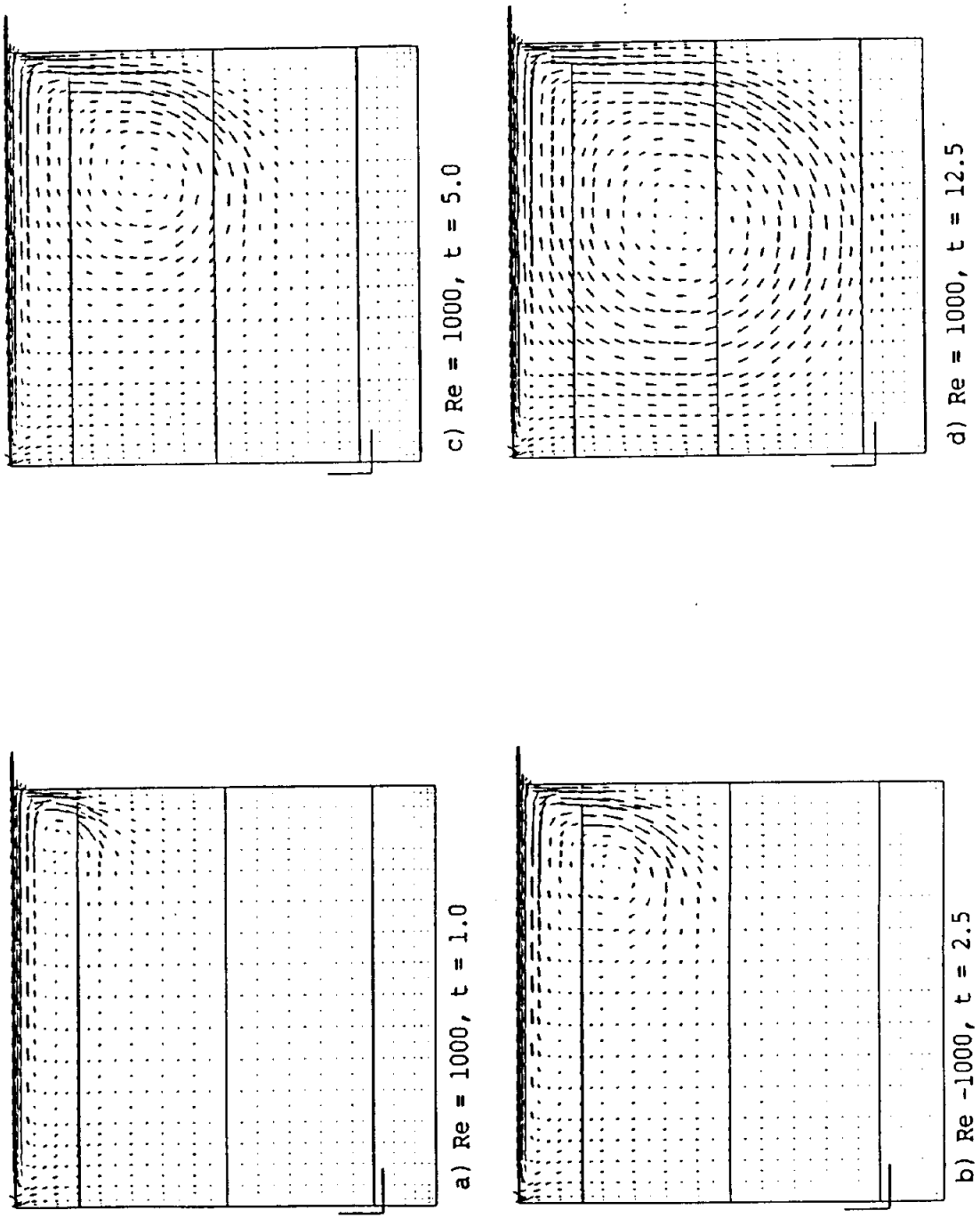

Figure 3.3.16 Transient Driven Cavity - Velocity Vectors

3.4 CONVECTIVE INCOMPRESSIBLE THERMOVISCOUS FLOW

3.4.1 BURGERS FLOW

The classic uniaxial linear Burgers problem provides an excellent test of the convective thermoviscous formulations. The incompressible fluid flows in the x-direction with uniform velocity U. Meanwhile, the y-component of the velocity and temperature are specified as U_o and T_o, respectively, at inlet. Both are zero at the outlet. The length of the flow field is L. The analytical solution (Schlicting, 1955) is

$$V_y = \zeta U_o$$

$$T = \zeta T_o$$

where

$$\zeta = \left\{1 - exp\left[R_L\left(\frac{x}{L} - 1\right)\right]\right\} / \{1 - exp[-R_L]\}$$

with $R_L = UL$.

The boundary element model employs eighteen quadratic surface elements encompassing the rectangular domain. The elements are graded, providing a very fine discretization near the exit, where V_y and T vary substantially for large R_L. Results are shown in Figure 3.4.1 for the thermal problem and in Figure 3.4.2 for the viscous problem. Excellent correlation with the analytical solution is obtained in both instances for this boundary-only analysis, even for the highly convective case of R_L = 1000. The portion of the flow field just ahead of the outlet is examined more closely in Figure 3.4.3. The convective Oseen solution obviously produces a precise solution. This problem can also be solved by utilizing the Stokes kernels and volume cells. As seen in Figure 3.4.3, this latter approach is not quite as accurate. It should be noted that traditionally finite difference and finite element methods have a difficult time dealing with the convective terms present in this problem. Generally, ad hoc upwinding techniques must be introduced to produce stable, accurate solutions. On the other hand, with the convective boundary element approach the kernel functions contain an analytical form of upwinding. As a result, very precise BEM results can be obtained.

Figure 3.4.1

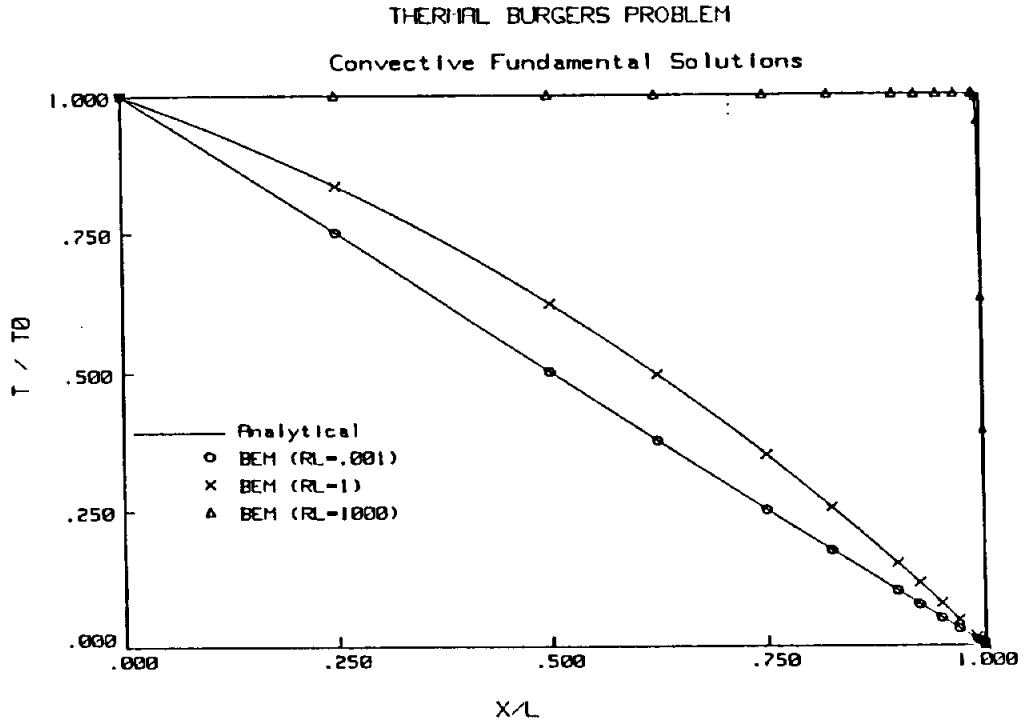

Figure 3.4.2

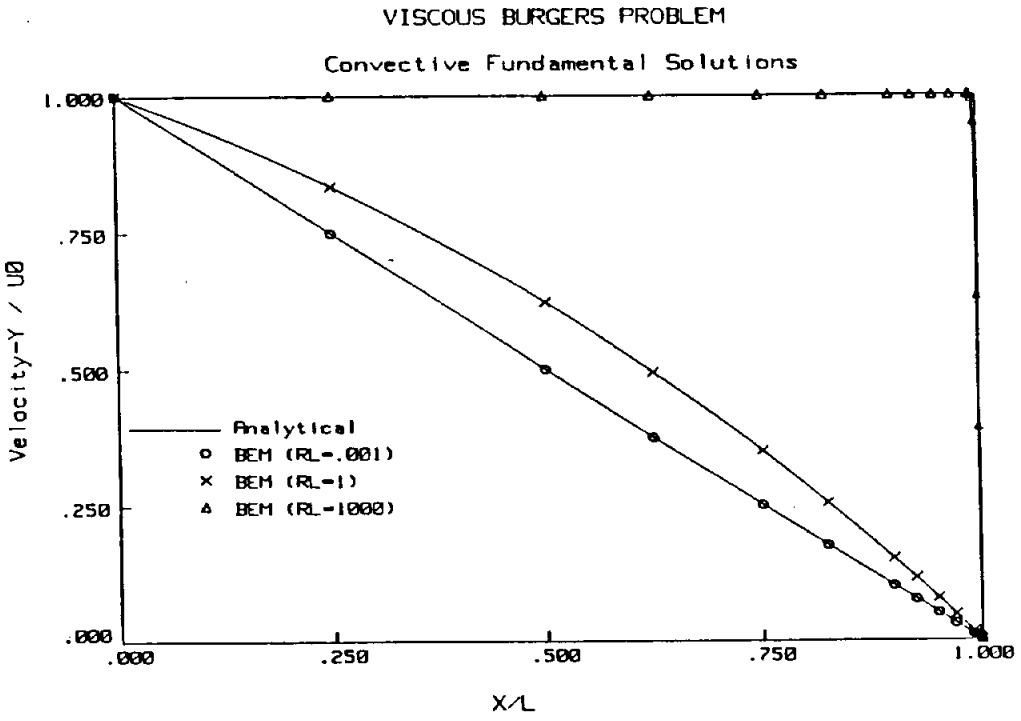

Figure 3.4.3

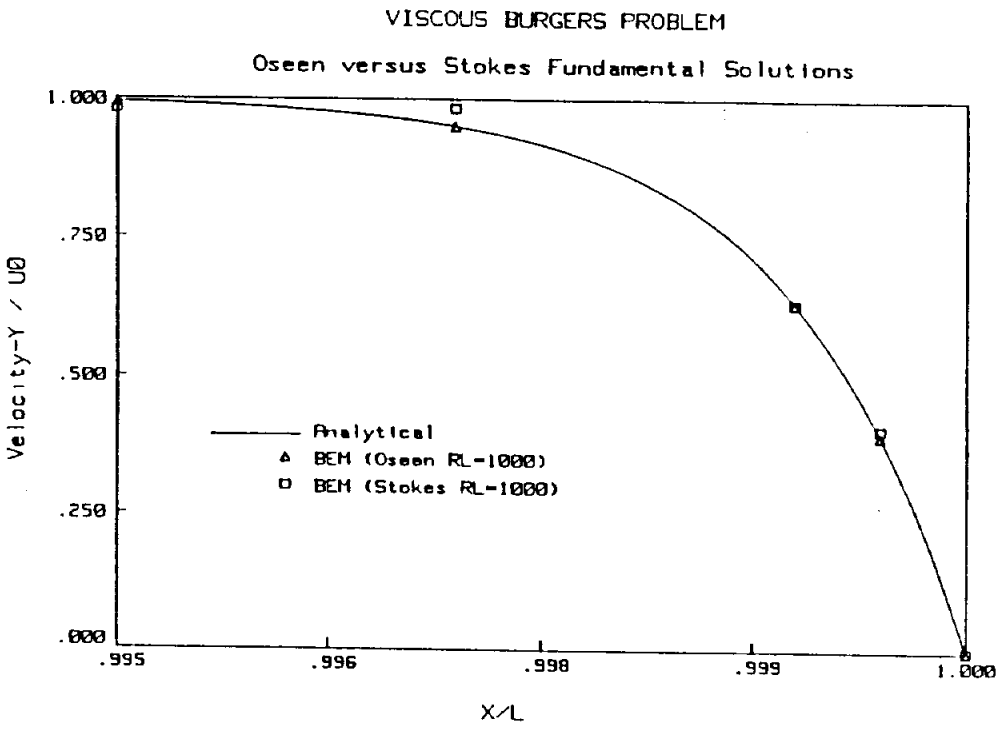
VISCOUS BURGERS PROBLEM
Oseen versus Stokes Fundamental Solutions
1.000
.750
.500
.250
.000
Velocity-Y / U0
Analytical
BEM (Oseen RL=1000)
BEM (Stokes RL=1000)
.995
.996
.998
.999
1.000
X/L

3.4.2 FLOW OVER A CYLINDER

As the next convective fluids example, the oft-studied case of incompressible flow over a circular cylinder is considered. Initially for this problem, both the steady convective and non-convective formulations are utilized in the same analysis. The boundary element model is displayed in Figure 3.4.4. Note that half-symmetry is imposed. In the inner region, the Stokes kernels are employed along with a complete volume discretization. Thus, the complete Navier-Stokes equations are represented. The outer region uses the Oseen kernels with a boundary-only formulation. The small non-linear contributions that would be present in the outer region away from the cylinder are ignored. For those more familiar with finite elements, each region can be thought of as a substructure or superelement. However, the outer region does not require a volume mesh.

The steady-state velocity vector plot at $Re = 40$ is shown in Figure 3.4.5. The recirculating zone, behind the cylinder, is clearly visible. Additionally, the resulting drag coefficient (C_D) of 1.8 obtained from the BE analysis is within the band of experimental scatter as presented by Panton (1984) for the circular cylinder.

Similarly, a transient analysis can be conducted. Now a full mesh as shown in Figure 3.4.6 is employed. The inner region uses a time-dependent nonlinear Stokes formulation, while linear Oseen kernels provide the basis for the outer infinite region. Results are shown in Figure 3.4.7a for $Re = 100$ at a time for which the flow is nearly fully developed. Meanwhile, Figure 3.4.7b present the solution at the same time, but with a different angle of attack for the oncoming fluid. The results are virtually identical. This illustrates the relative insensitivity of boundary element solutions to the cell discretization pattern. The reason for this behavior, which is particularly important in modeling hyperbolic phenomena, is that so much of the boundary element formulation is analytical. Another item to note from these results is the completely symmetric flow patterns that were obtained. Asymmetry would have to be induced by perturbing either the geometry, the free stream velocity or the boundary conditions.

While all of this is encouraging, the development of a simplified procedure involving far less volume discretization is desirable. For example, a completely linear Oseen analysis, which ignores all nonlinear convective terms in both regions, produces a very similar solution, except in the vicinity of the cylinder. Vector plots from the nonlinear analysis and the boundary-only linear Oseen analysis are superimposed in Figure 3.4.8. Although it is difficult to distinguish between the two analyses in that plot, both produce a recirculatory zone behind the cylinder. Thus, the main features of the problem are captured by the boundary-only analysis. However, the linear solution, in general, overstates the velocities and velocity gradients in the neighborhood of the cylinder. Consequently, a drag coefficient of 3.4 is calculated, which is much higher than that found experimentally. This trend, of overpredicting the experimental drag, continues even to much higher Reynolds numbers as shown in Figure 3.4.9. Qualitatively, however, the behavior of the BEM Oseen solution is consistent with the experimental curve for Reynolds Numbers up to 100,000.

A much improved solution can be obtained by introducing a row of cells encompassing

the cylinder. The full nonlinear Navier-Stokes equations are solved within this inner region which includes an inner and outer ring of surface elements. Exterior to the outer ring is a linear Oseen region. This exterior region consists simply of one matching ring of surface elements. Its volume extends outward to infinity, where the velocity reaches its free stream value. Figure 3.4.10 illustrates a typical mesh, along with the resulting velocity vectors. As Reynolds number is increased, the significant nonlinear effects concentrate nearer to the cylinder, so that the thickness of the inner region may be reduced. Figure 3.4.9 also displays the drag obtained by utilizing just a single row of cells. Results are quite encouraging.

Figure 3.4.4

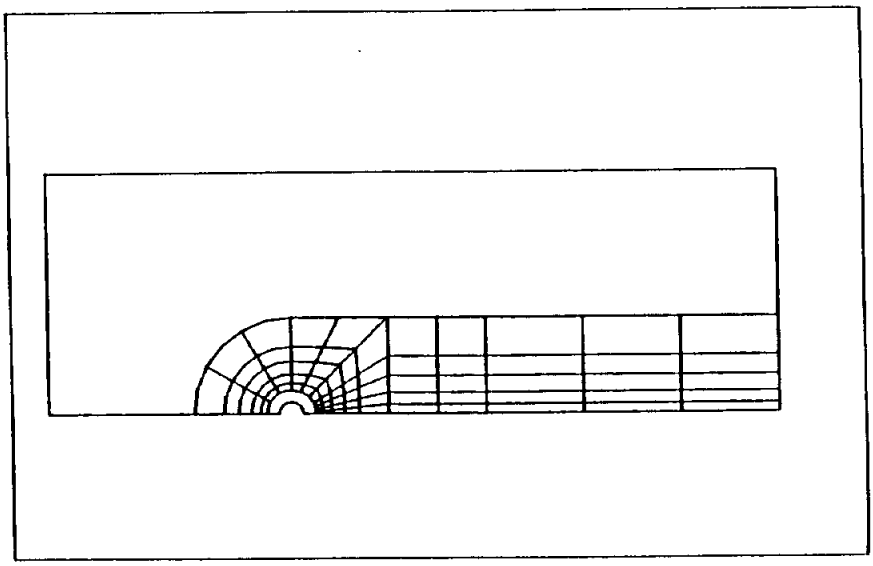

Figure 3.4.5

FLOW OVER A CYLINDER
VELOCITY VECTORS AT Re = 40

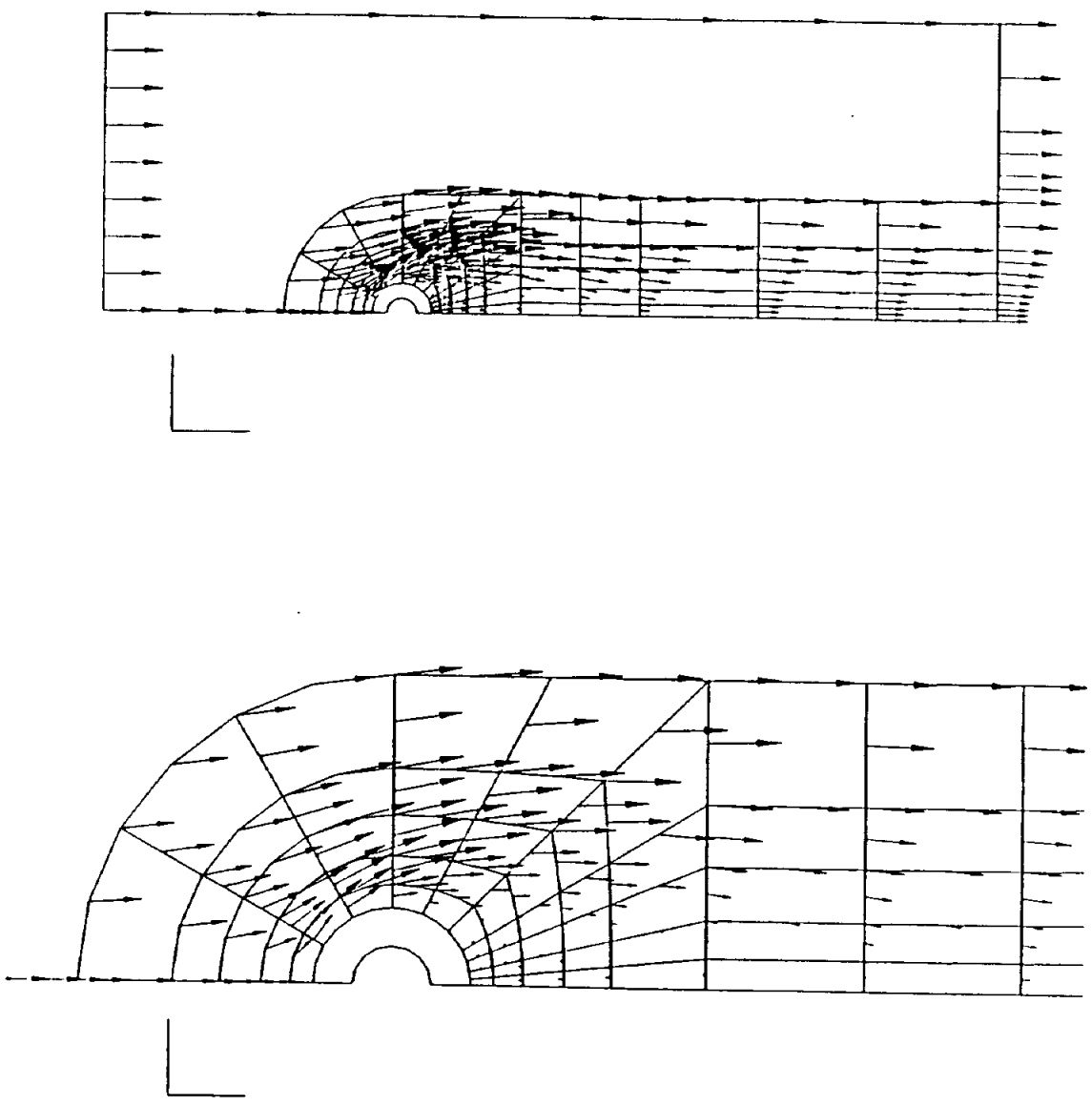

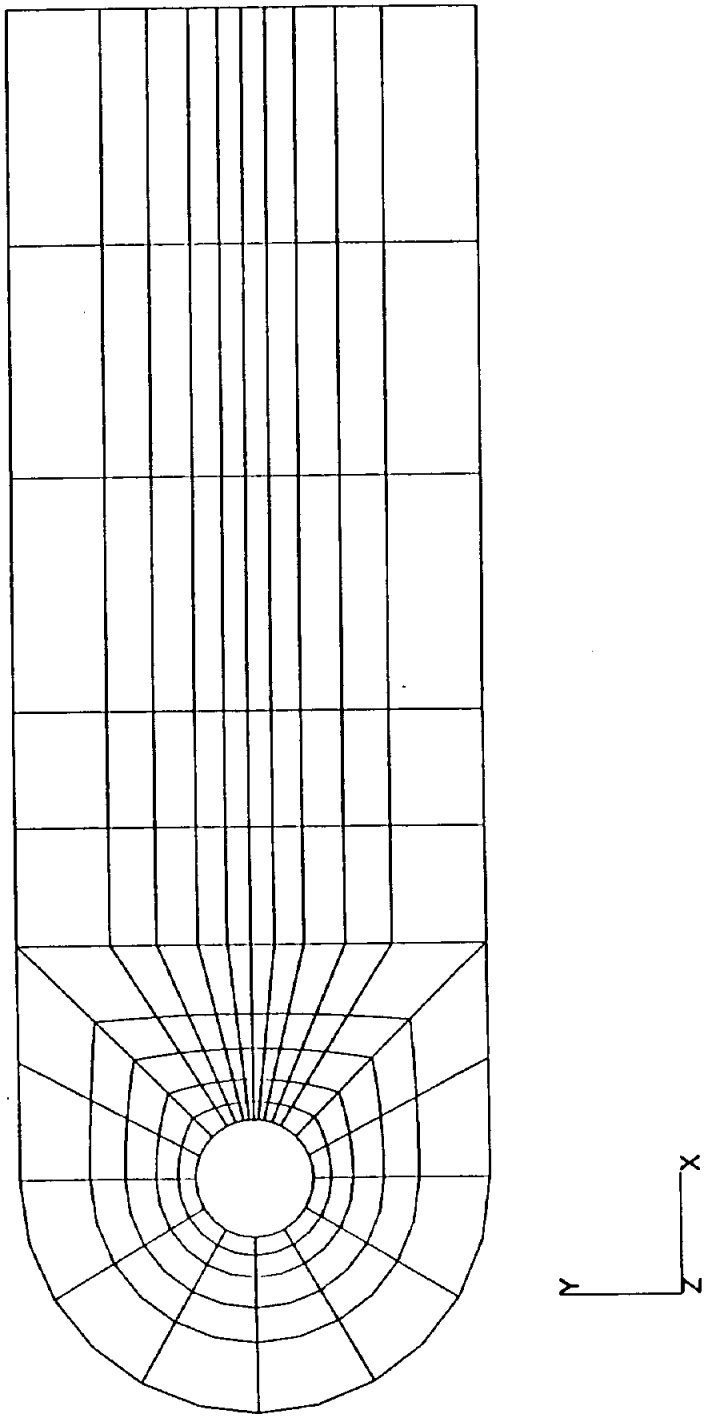

Figure 3.4.6 FLOW OVER A CYLINDER - FULL MESH

Figure 3.4.7a FULL CYLINDER (ANGLE OF ATTACK = 0^{O})

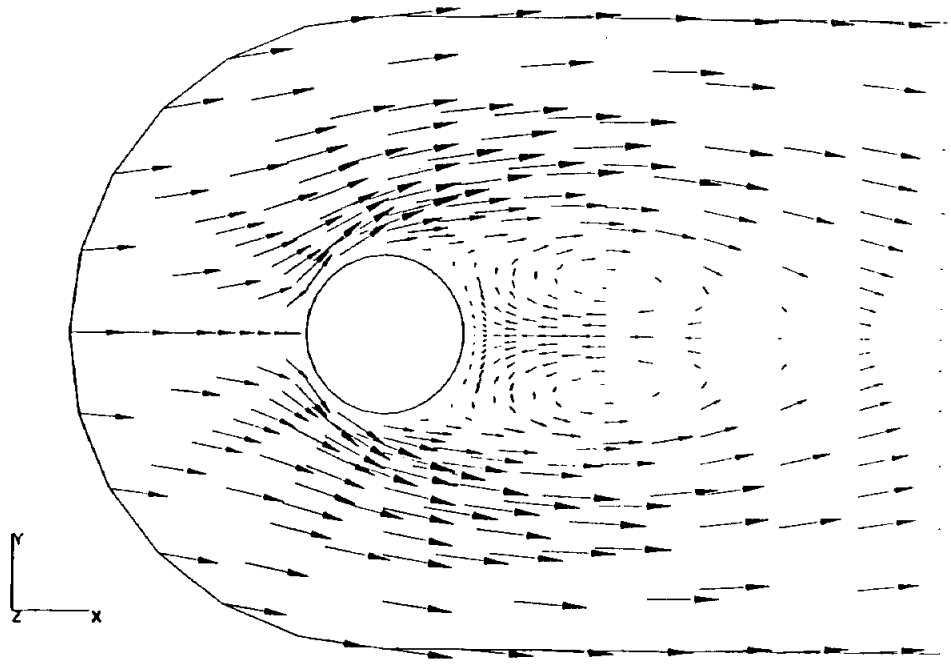

Figure 3.4.7b FULL CYLINDER (ANGLE OF ATTACK = 10^{O})

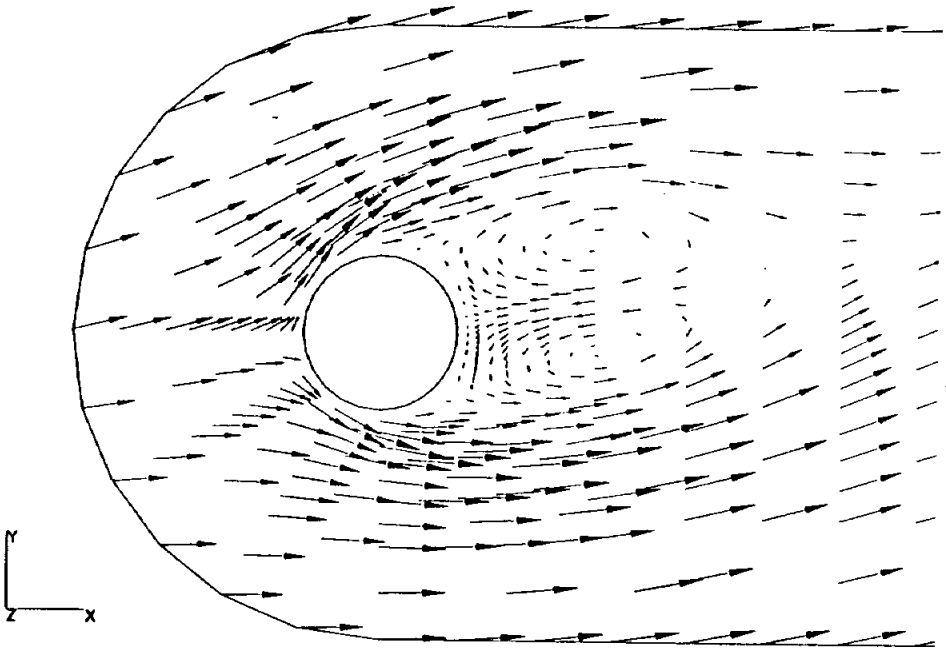

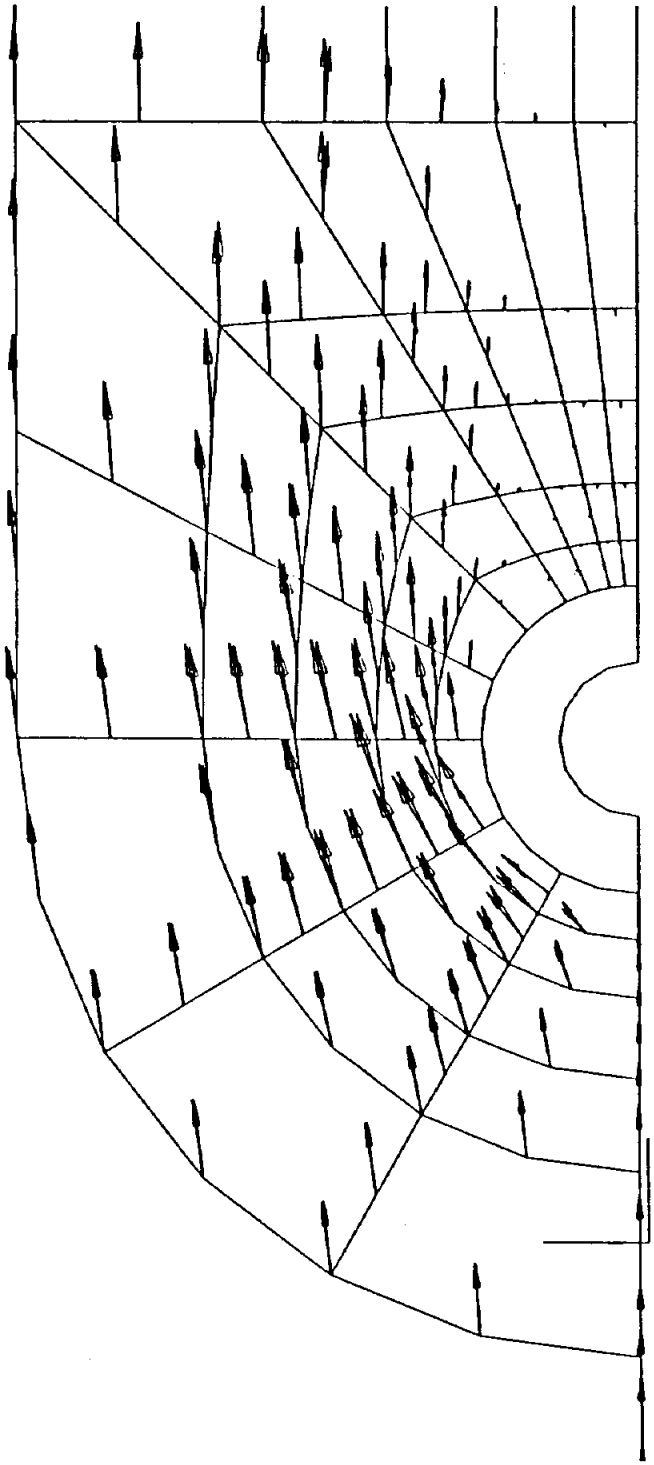

Figure 3.4.8

FLOW OVER A CYLINDER

NONLINEAR SOLUTION VERSUS LINEAR OSEEN SOLUTION

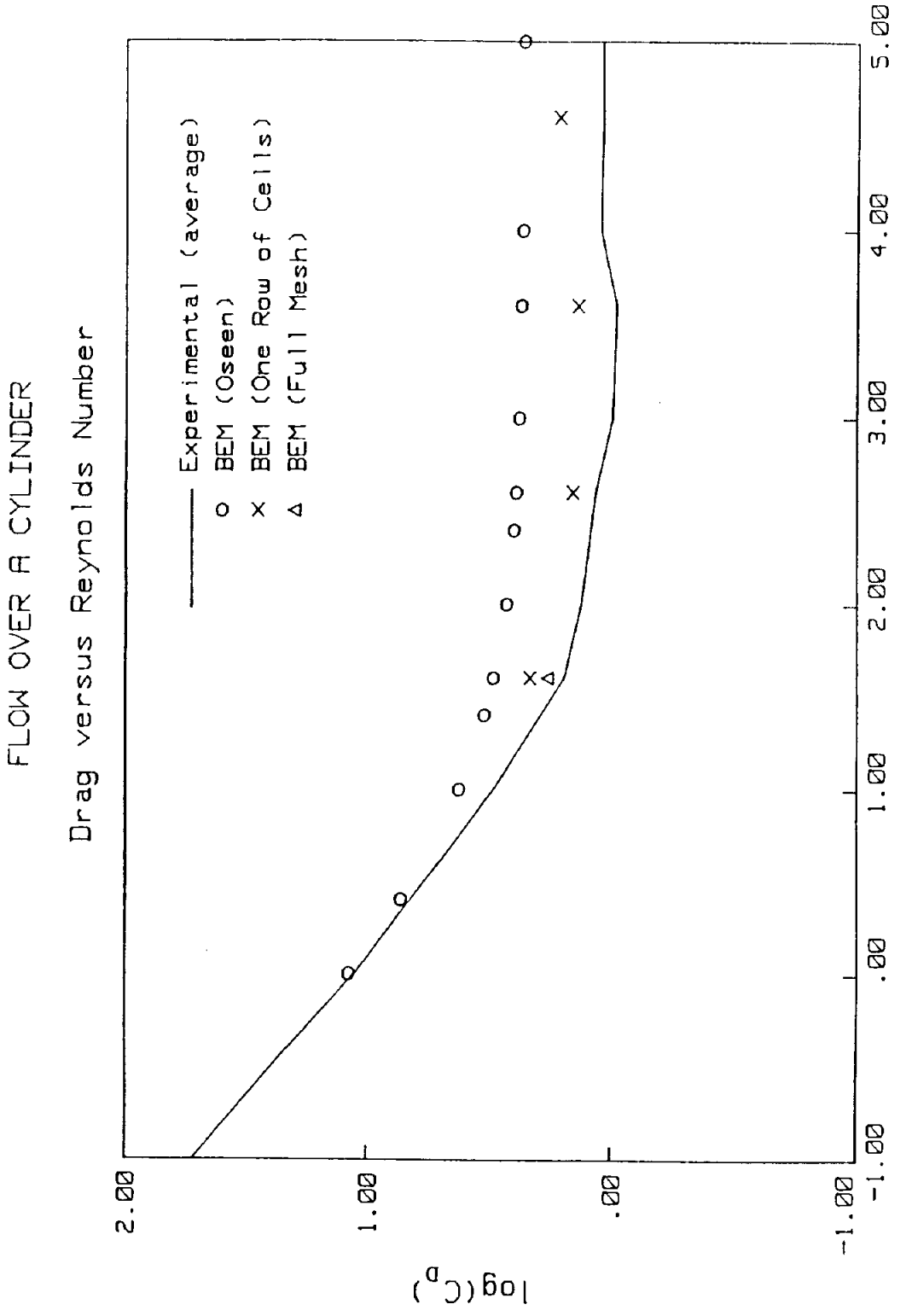
FLOW OVER A CYLINDER
Drag versus Reynolds Number
Experimental (average)
BEM (Oseen)
BEM (One Row of Cells)
BEM (Full Mesh)
log(C_D)
log(Re)
2.00
1.00
.00
-1.00
-1.00
.00
1.00
2.00
3.00
4.00
5.00

Figure 3.4.9

Figure 3.4.10

FLOW OVER A CYLINDER

NONLINEAR SOLUTION WITH A SINGLE ROW OF CELLS

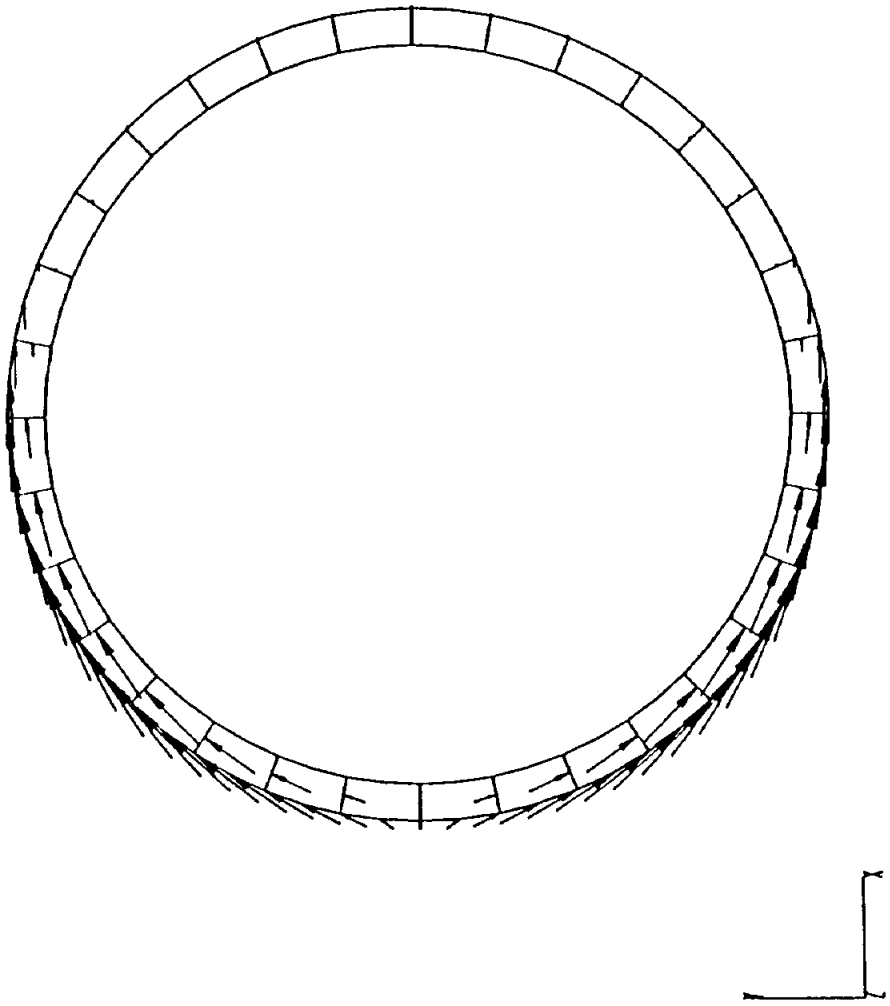

3.4.3 FLOW PAST AIRFOILS

For illustrative purposes, a boundary-only thermoviscous analysis was conducted for convective flow around a pair of NACA-0018 airfoils. The boundary element model of the blades is shown in Figure 3.4.11. A hot fluid at unit temperature flows from left to right with a unit magnitude of the free stream velocity. Meanwhile, the airfoils are assumed to be stationary with their outer surface maintained at zero temperature.

It should be emphasized that this problem was run as a boundary-only analysis, however, a number of sampling points were included in the fluid surrounding the airfoils in order to graphically portray the response. First the thermal solution is examined. Figure 3.4.12a depicts the temperature distribution in the fluid at a Peclet (Pe) number of ten, where $Pe = UL/\kappa$, with fluid velocity U, thermal diffusivity κ and airfoil chord length L. Meanwhile, Figures 3.4.12b-d show the response at progressively higher Peclet number. At $Pe = 10000$, quartic surface elements were required in order to obtain an accurate solution. The strong convective character is quite noticeable at larger Pe as the effect of the cold airfoils is swept downstream. Also, in Figures 3.4.12c and d there is virtually no interaction between the airfoils. This type of behavior is expected from a physical standpoint. It occurs in the analysis because of the banded nature of the convective fundamental solutions illustrated previously (e.g., Figure 2.4.2). However, interaction will take place if the angle of attack is altered. Figure 3.4.12e shows the response at a 30° angle for $Pe = 1000$.

The velocity distribution around the airfoils follows a similar pattern. For these results displayed in Figure 3.4.13, Reynolds number is defined by $Re = \rho UL/\mu$. In these plots, the magnitude of the velocity, obtained from a boundary-only solution, is contoured. These results feature somewhat more interaction particularly upstream of the airfoils. It should be emphasized that even though a linearized solution algorithm is employed the so-called phenomenon of boundary layer separation can still occur. Figure 3.4.14 focuses on the rear portion of the upper blade. The contour line demarks the transition from positive to negative streamwise velocity, and thus very nearly identifies the point of separation.

Next, a second row of blades is added. The modeling effort for this extension is quite trivial, since there is actually no discretization required beyond that needed to describe the airfoil surfaces. For this problem, four vertical sections of one hundred sampling points were included for display purposes. Velocity vectors across those sections are plotted in Figures 3.4.15 and 3.4.16 for Reynolds numbers of 10000 and 100000, respectively. The vertical spacing between the airfoils increases as one examines a through c in these two diagrams. The velocity profiles are noticeably affected by that spacing. However, in all of the plots significant velocity gradients are present. It is interesting to consider the level of refinement that would be necessary in a domain based finite difference or finite element analysis in order to capture similar gradients.

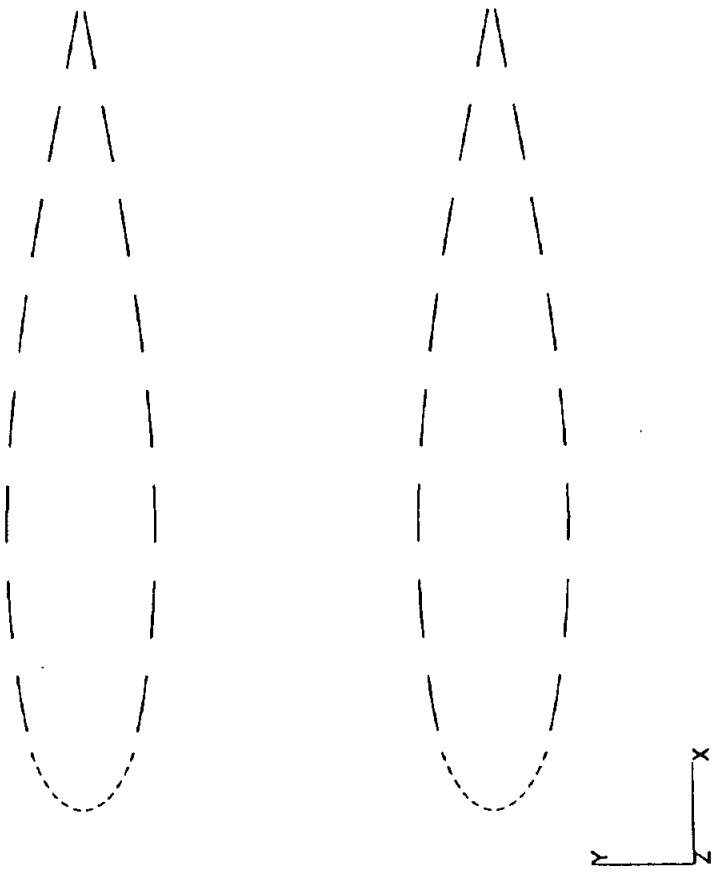

Figure 3.4.11

NACA-0018 AIRFOILS - BOUNDARY ELEMENT MODEL

W/SHRINK ELEMENTS OPTION

Figure 3.4.12a

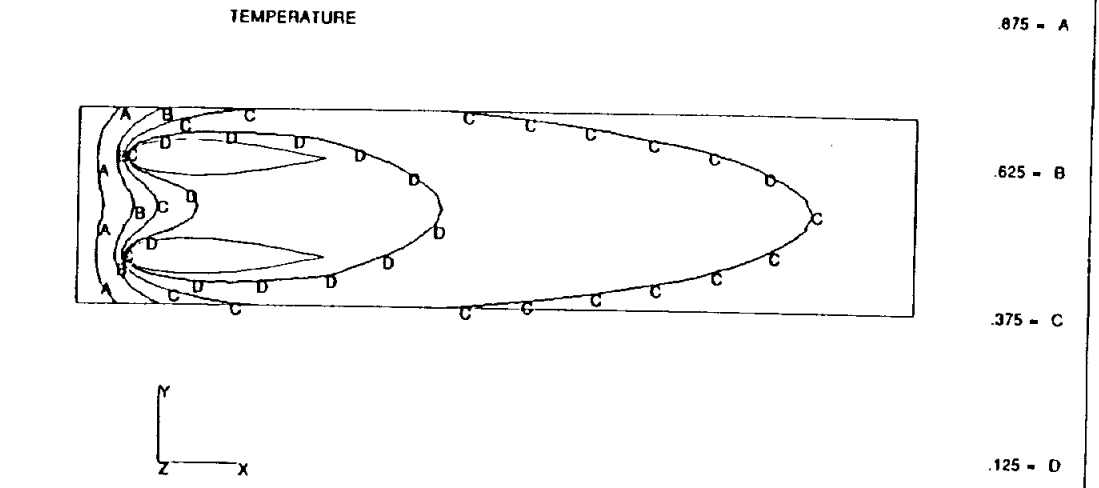

CONVECTIVE THERMOVISCOUS FLOW (RE,PE =10, ANGLE = 0)

Figure 3.4.12b

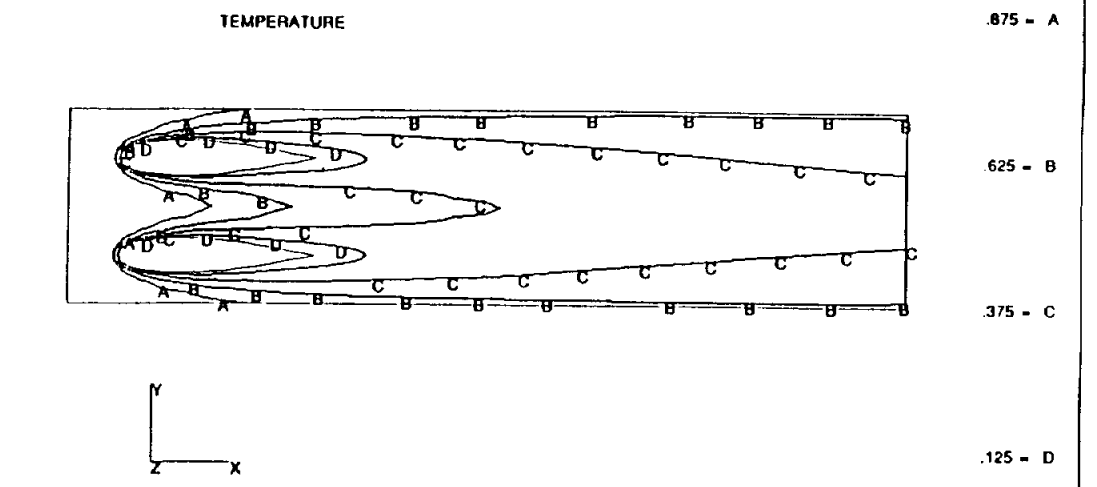

CONVECTIVE THERMOVISCOUS FLOW (RE,PE =100, ANGLE = 0)

Figure 3.4.12c

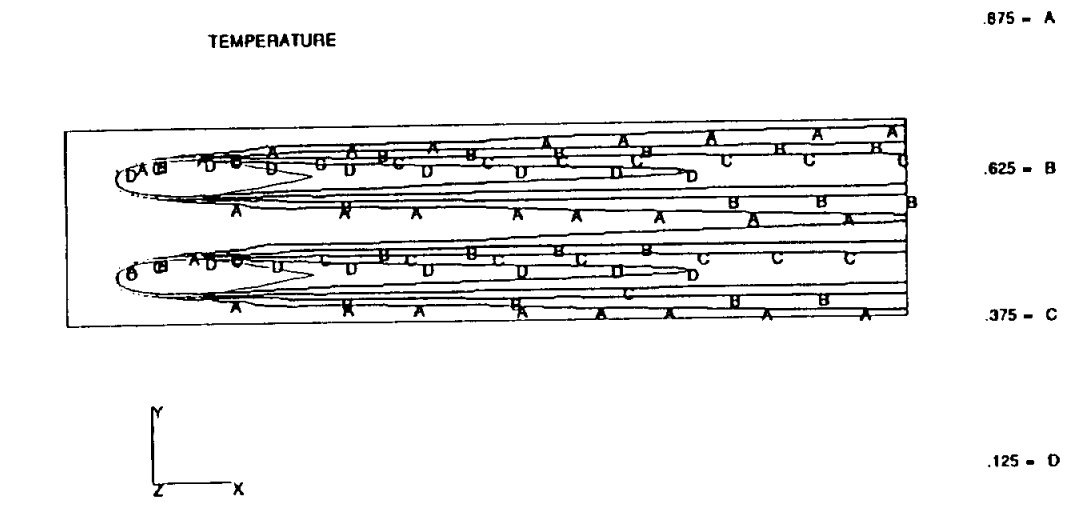

CONVECTIVE THERMOVISCOUS FLOW (RE,PE =1000, ANGLE = 0)

Figure 3.4.12d

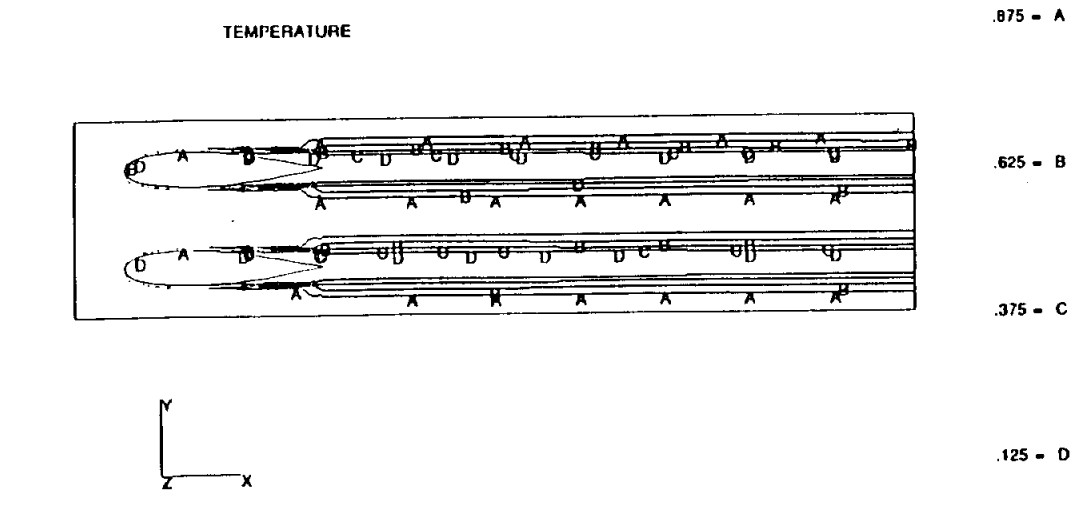

CONVECTIVE THERMOVISCOUS FLOW (RE,PE =10000, ANGLE = 0)

Figure 3.4.12e

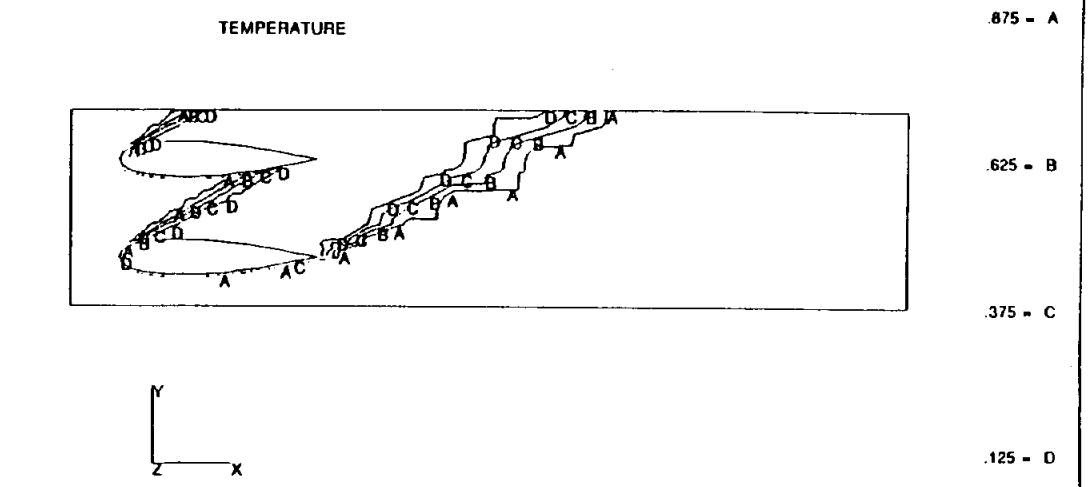

Figure 3.4.13a

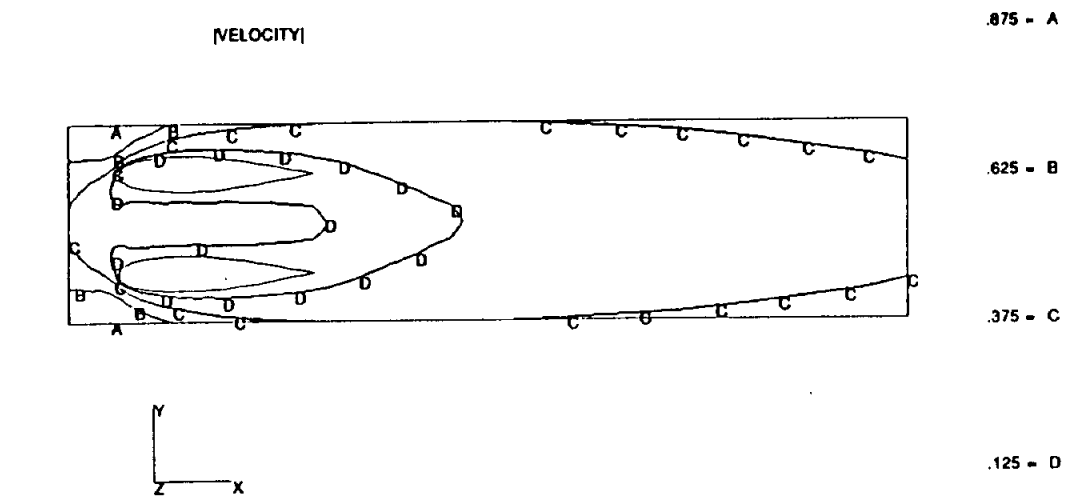

CONVECTIVE THERMOVISCOUS FLOW (RE,PE =10, ANGLE = 0)

Figure 3.4.13b

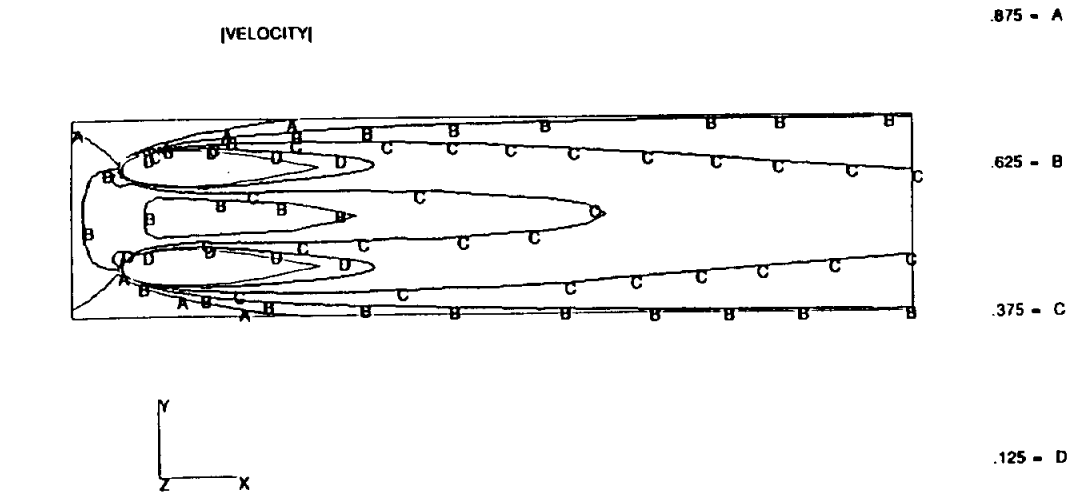

CONVECTIVE THERMOVISCOUS FLOW (RE,PE =100, ANGLE = 0)

Figure 3.4.13c

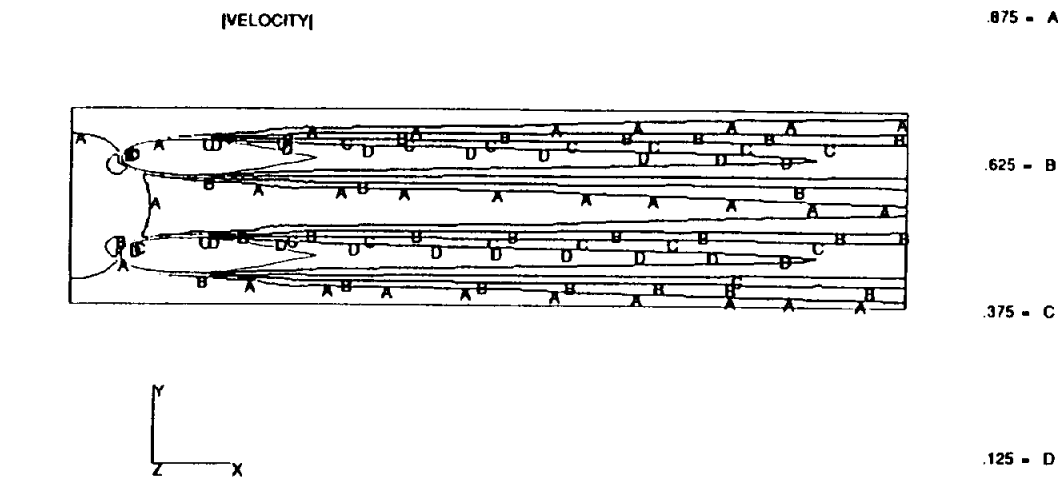

CONVECTIVE THERMOVISCOUS FLOW (RE,PE =1000, ANGLE = 0)

Figure 3.4.13d

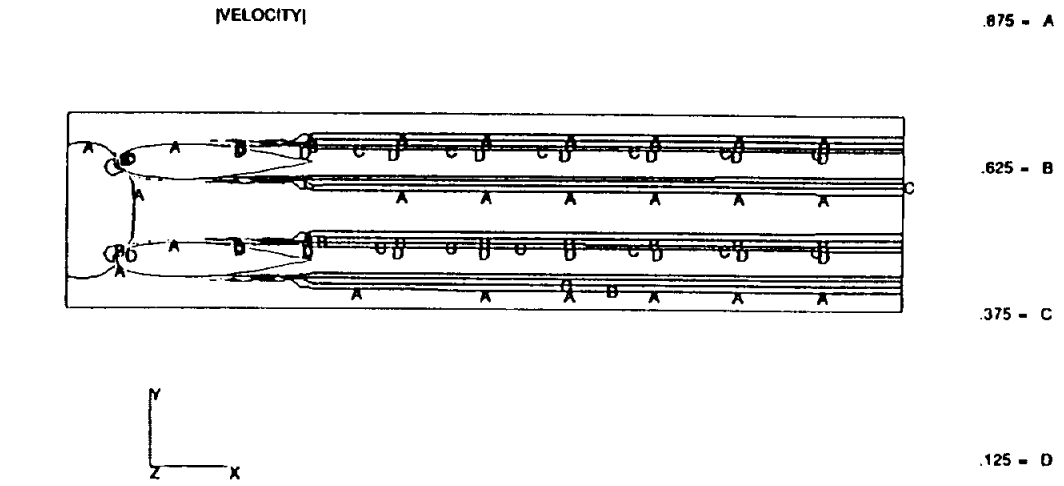

CONVECTIVE THERMOVISCOUS FLOW (RE,PE =10000, ANGLE = 0)

Figure 3.4.13e

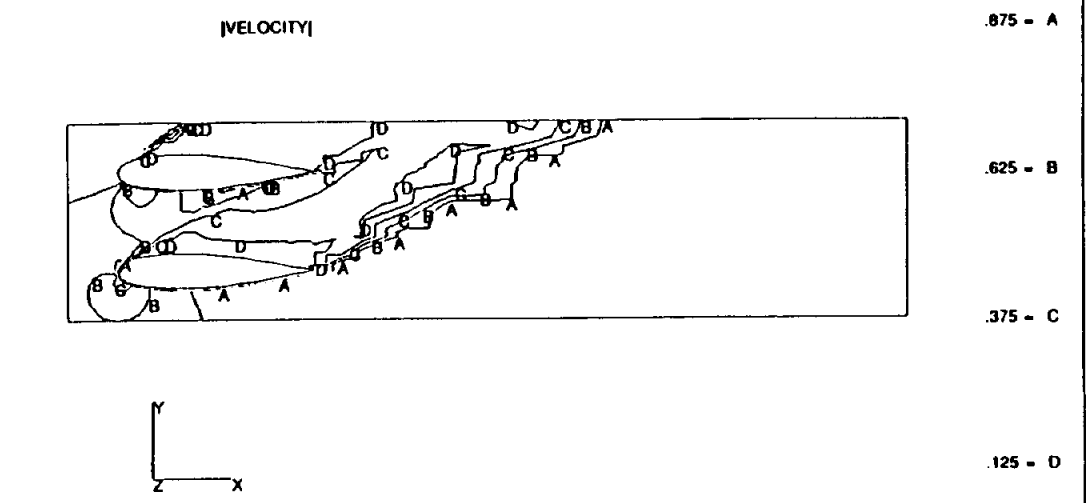

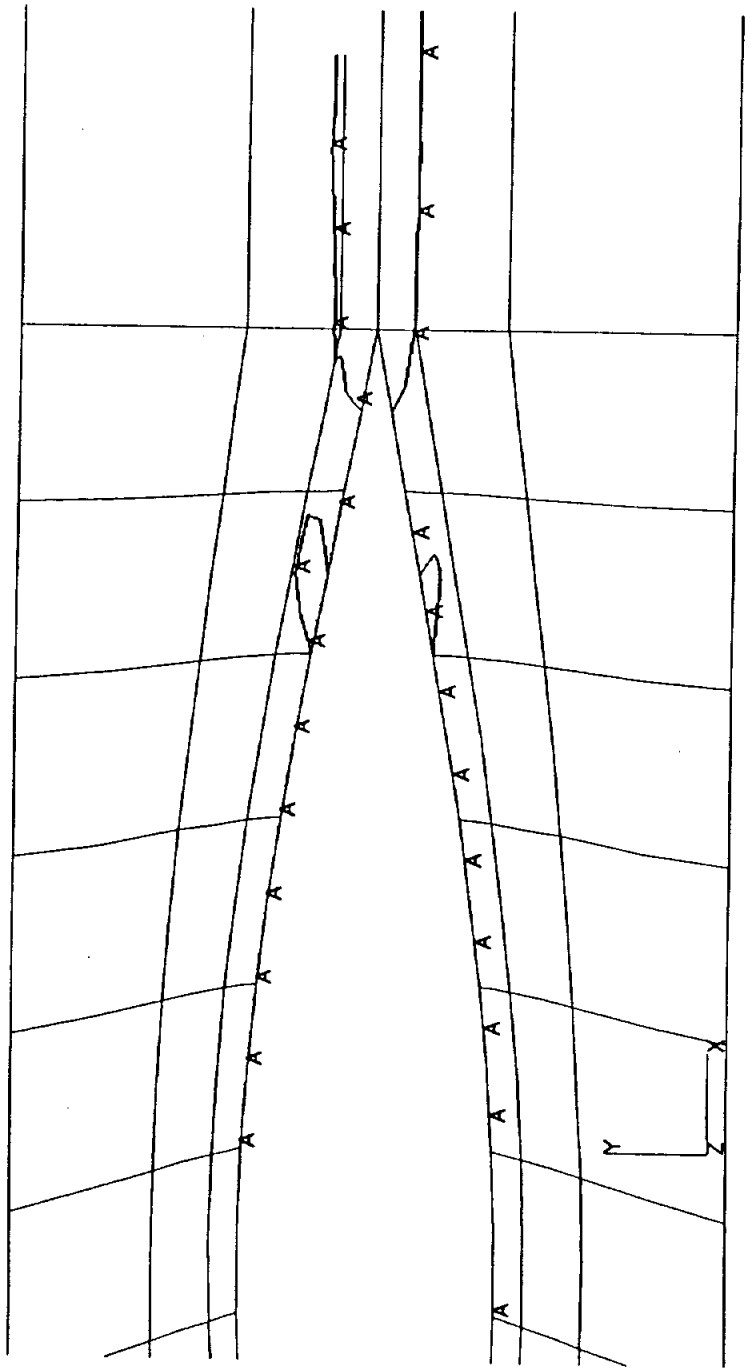

Figure 3.4.14 BOUNDARY LAYER SEPARATION

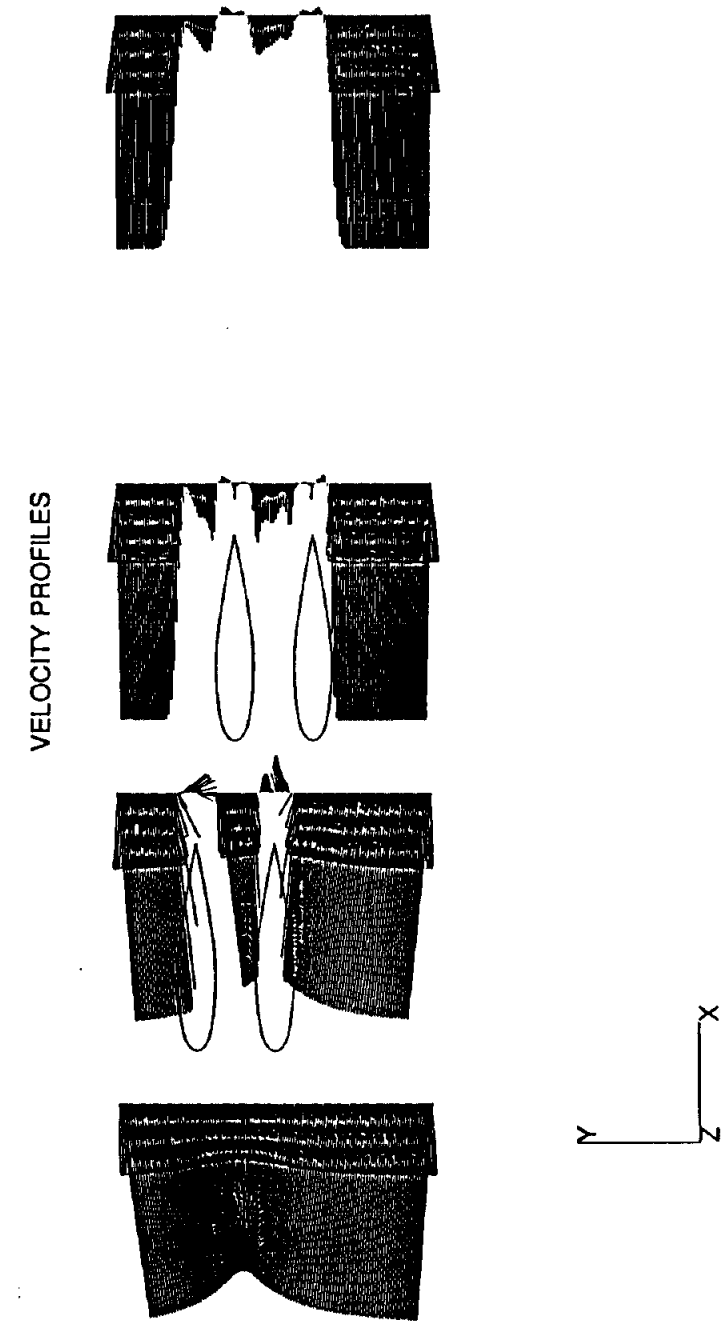

Figure 3.4.15a

Figure 3.4.15b

NACA-0018 AIRFOILS (RE = 10000; ANGLE = 0)

VELOCITY PROFILES

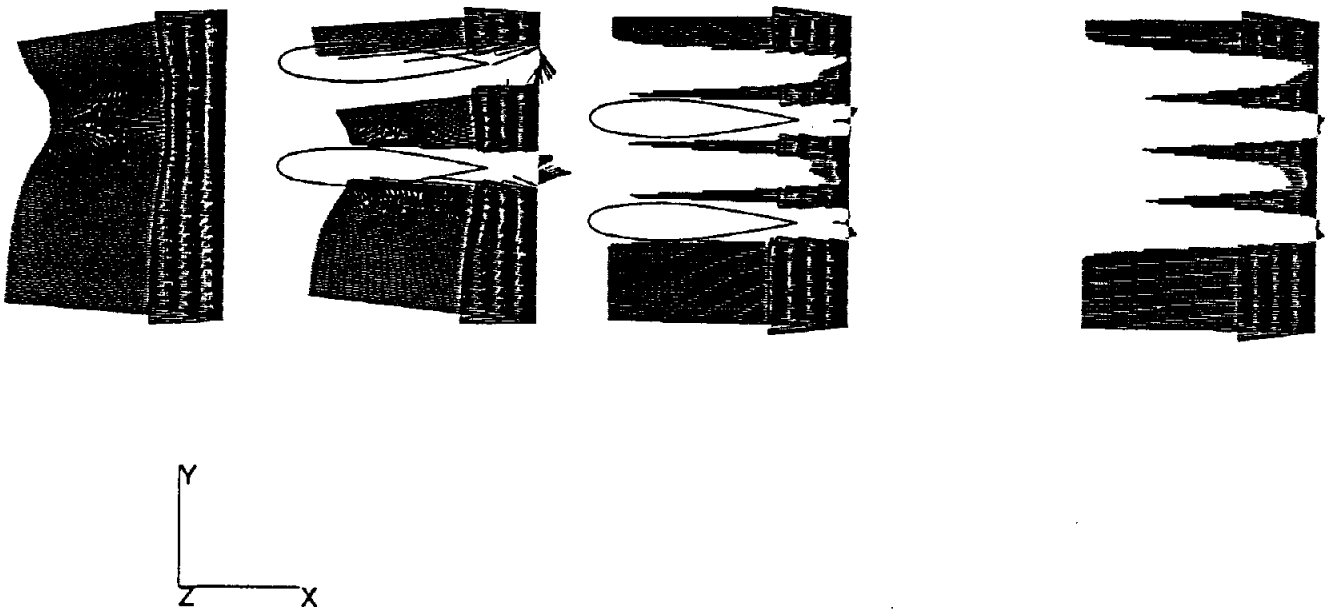

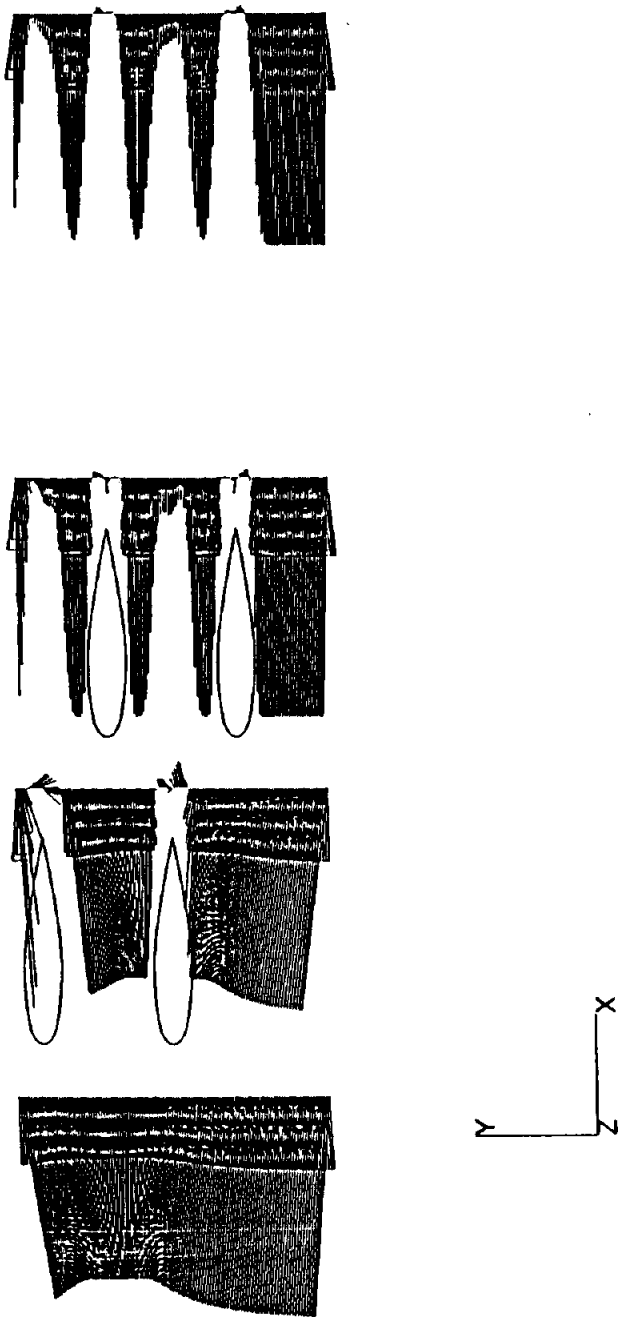

Figure 3.4.15c

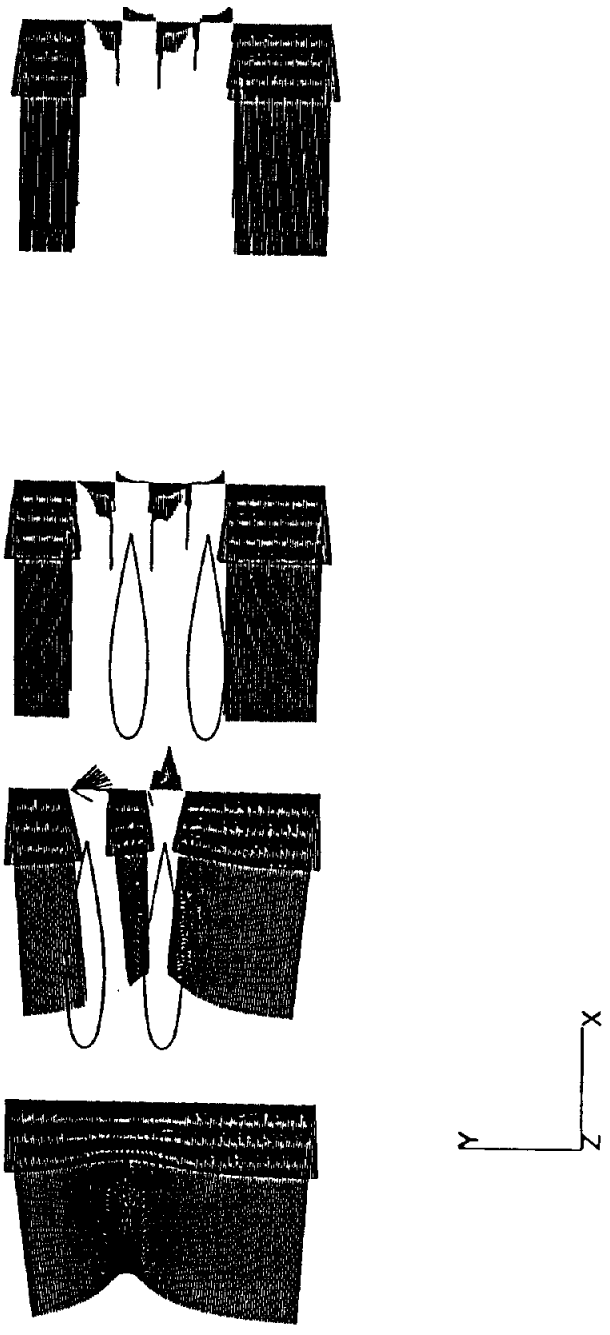

Figure 3.4.16a

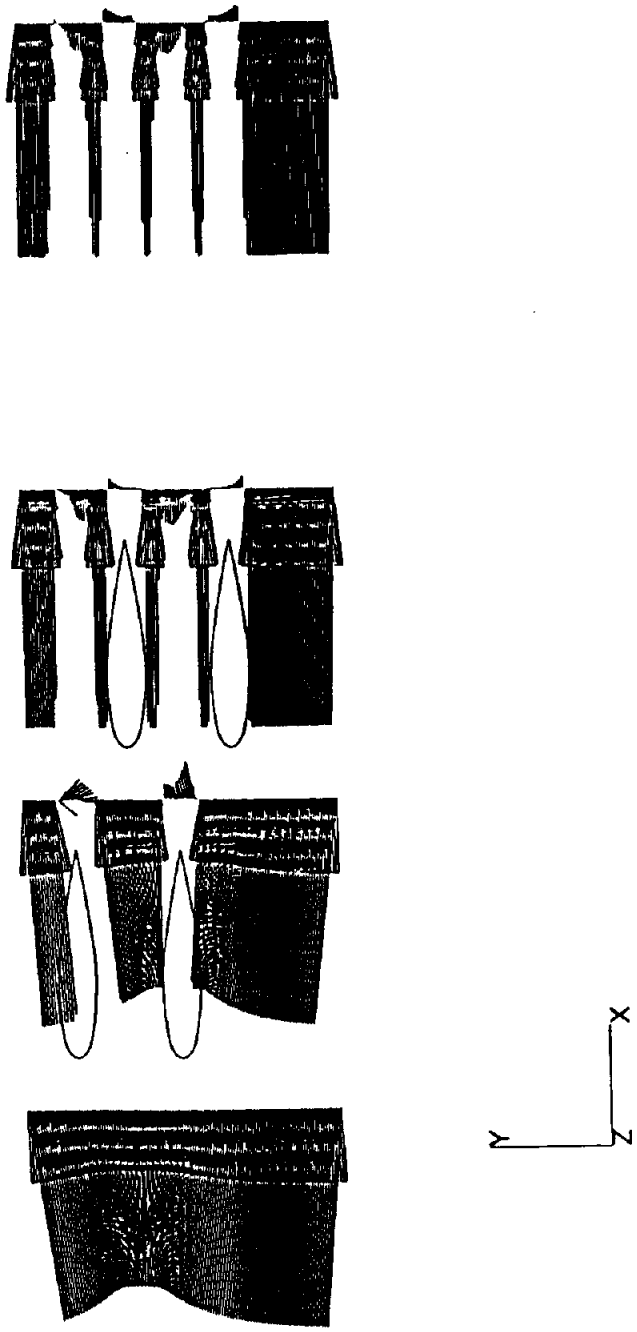

Figure 3.4.16b

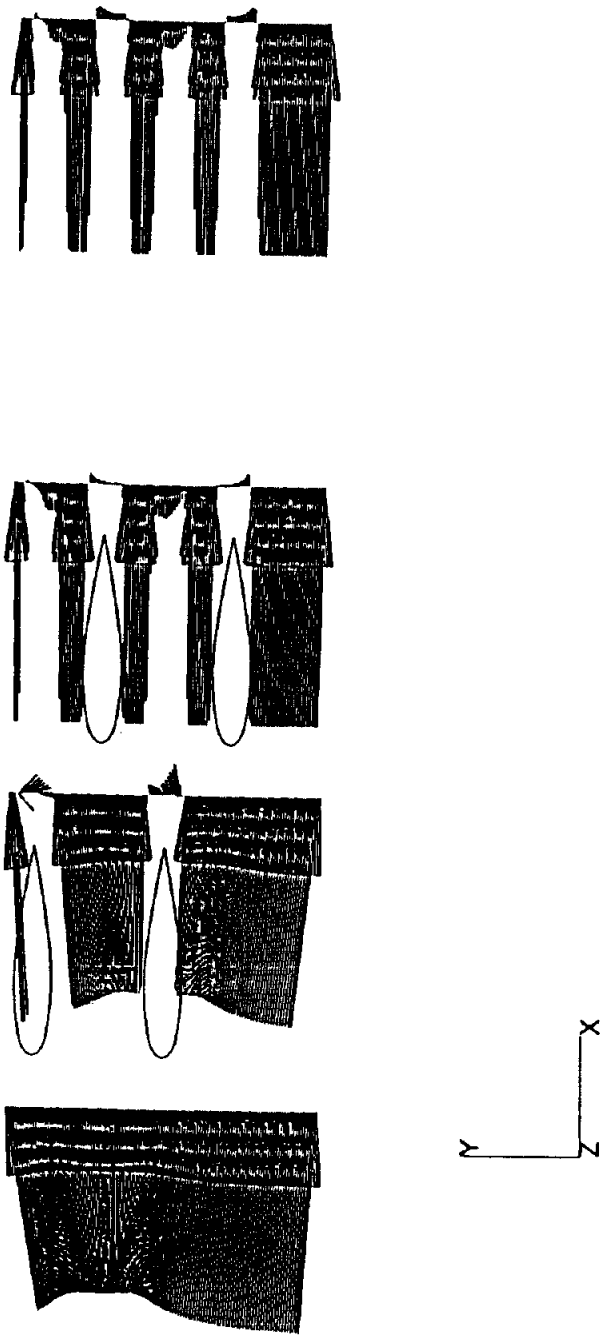

Figure 3.4.16c

3.5 CONVECTIVE POTENTIAL FLOW

3.5.1 ONE-DIMENSIONAL WAVE PROPAGATION

The uniaxial linear acoustic wave problem provides an excellent test of the convective compressible potential flow formulations. The variables ϕ and $\frac{\partial \phi}{\partial n}$ are specified as ϕ_o and $-u_o$, respectively, at the inlet. Both are undefined at the outlet. The length of the flow field is L. The analytical solution is then simply

$$\phi = \phi_o + u_o x \tag{3.5.1a}$$

$$\frac{\partial \phi}{\partial x} = u_o . \tag{3.5.1b}$$

The boundary element model utilized here employs six quadratic elements encompassing rectangular domain. Results are shown in Figure 3.5.1. As can be seen, excellent correlation with the analytical solution is obtained for this initial problem.

Figure 3.5.1 One-dimensional Wave Propagation

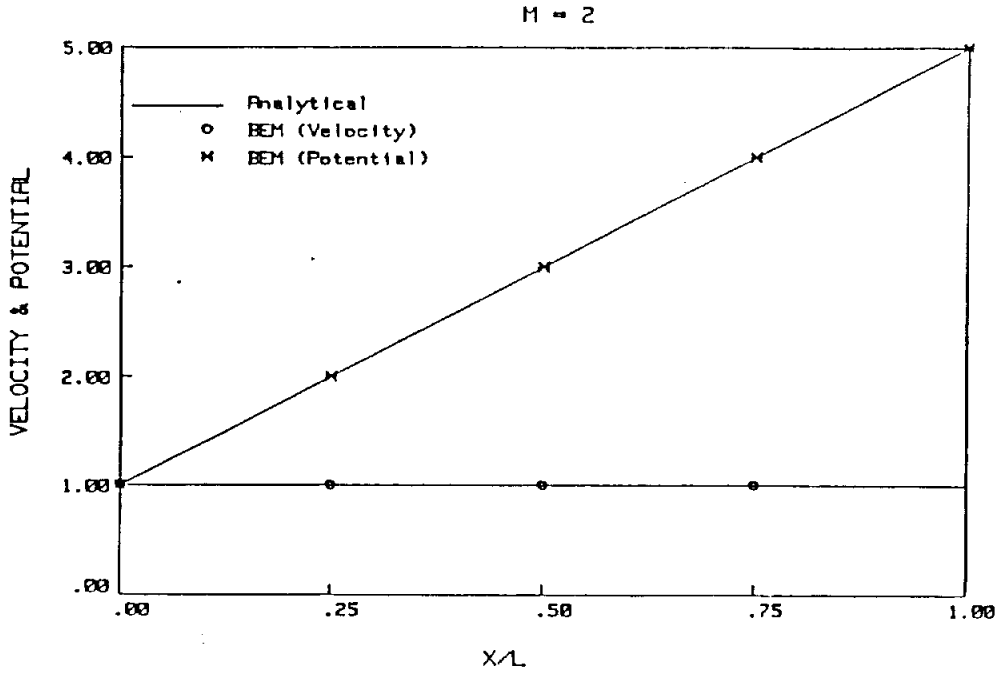

3.5.2 FLOW OVER A WEDGE

Consider some examples of flow produced by a two-dimensional wedge (half angle $\theta = 15°$) moving at a Mach number of $M_\infty = 0.1, 2.0$. The wedge and the associated flow are shown in Figure 3.5.2, while the BEM model with half symmetry is displayed in Figure 3.5.3. At a large distance from the wedge, the unperturbed flow will generally be assumed to be uniform and directed along the x_1-axis, i.e.

$$v_i = U_i \qquad or \qquad u_i = 0 \tag{3.5.2a}$$

$$\phi' = 0\,. \tag{3.5.2b}$$

On the other hand the velocity components normal to the surface of wedge are equal to zero, i.e.

$$v_n = 0 \qquad or \qquad u_n = -U_n\,. \tag{3.5.3}$$

with the tangential component at the wedge left unspecified.

For the subsonic case ($M_\infty = 0.1$), the maximum velocity occurs at the outlet where the smallest cross section exists as shown in Figures 3.5.4 and 3.5.5. For the supersonic case ($M_\infty = 2.0$), the flow is conical. This means that flow properties along rays from vertex of the wedge are constant. The boundary conditions are the surface tangency requirement at the wedge surface and freestream conditions outside the shock wave. With the marching procedure, the wedge-flow problem can be solved without difficulty. The application of boundary conditions however requires careful consideration. There must be enough space included in the computational domain so that the shock wave can form naturally and not be affected by the boundary conditions which are maintained at y_{max}. The result is shown in Figure 3.5.6 to 3.5.10. The "shock front" is inclined at the Mach angle $\alpha = \sin^{-1}(1/M_\infty)$ to the x axis. It is interesting to note that the velocity of flow behind the "shock front" decreases. The air suddenly slows down and compresses. The velocity gradient is perpendicular to the shock line, i.e., is at angle α to the y axis (Figure 3.5.11). Excellent correlation with the analytical solution is obtained for this linear problem. Figure 3.5.9 shows the discontinuity of the pressure waves. The pressure coefficient C_p is calculated on the basis of the 'exact isentropic' relation between the pressure and the external surface speed. It should be noted that u_i here is assumed to be much smaller than U_i otherwise the small perturbation approximation would not be sufficient to compute the motion. One difficulty which immediately arises is that the Mach angle for the air in the region behind "shock front" is appreciably different from the Mach angle for air in the region in front of shock line whenever the speed v differs appreciably in the two regions. The question then arises: What should be the angle between the x axis and the Mach line dividing two regions? Should it be the angle $\alpha = \sin^{-1}(1/M_\infty)$ appropriate for the front region or the angle appropriate for the air in the back region (which is greater than α)? Detailed study of an exact solution indicates that the angle between the x axis and the actual "shock front" is intermediate between the two discussed in the previous sentence and that the air as it flows across this front undergoes a practically instantaneous change of state to a

new speed, density, and pressure appropriate to the back region. This explains why in the linearized solution, the front angle is less than those from finite element nonlinear solutions (Zienkiewicz and Taylor, 1991; Brueckner and Heinrich, 1991). So, in problems involving perturbations which are not small, for more exact representation, the volume integral for non-linear terms should be taken into consideration.

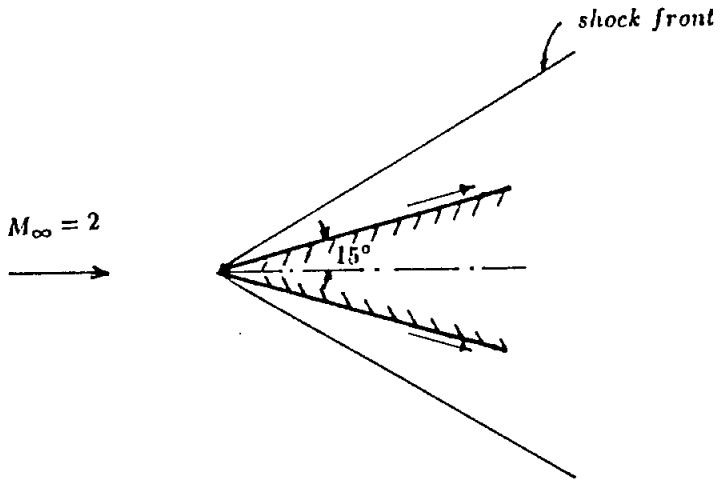

Figure 3.5.2 Wedge Flow with Attached Shock

Figure 3.5.3 Mesh of Wedge Problem

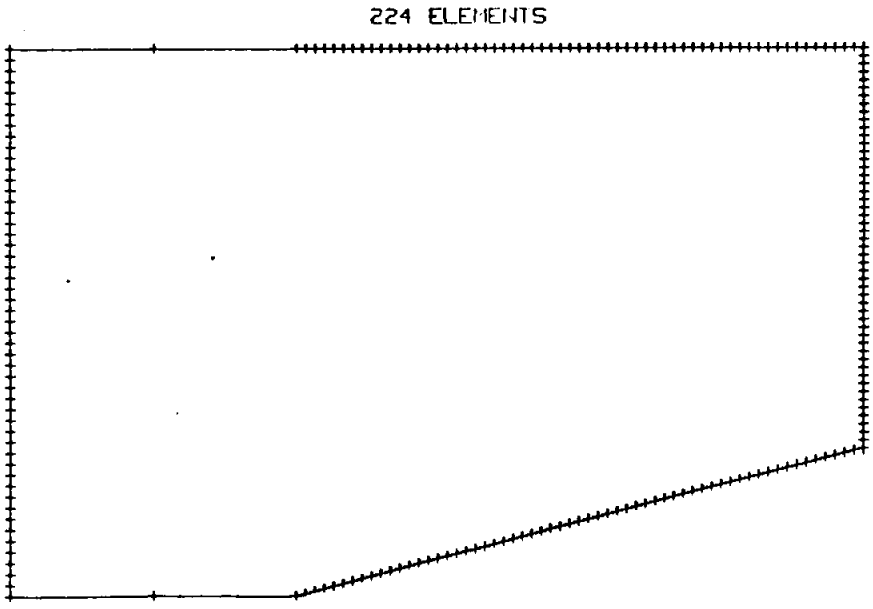

Figure 3.5.4 Subsonic Wedge Flow - Velocity Vectors

$M_\infty = 0.1$

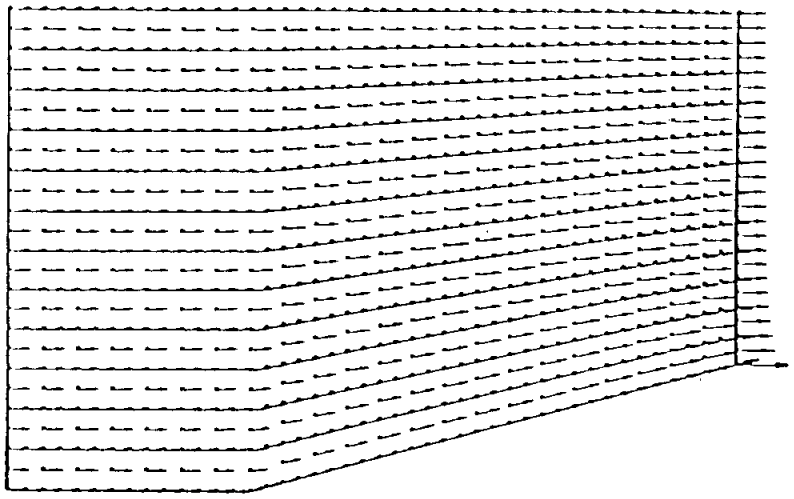

Figure 3.5.5 Subsonic Wedge Flow - Mach Contours

$M_\infty = 0.1$

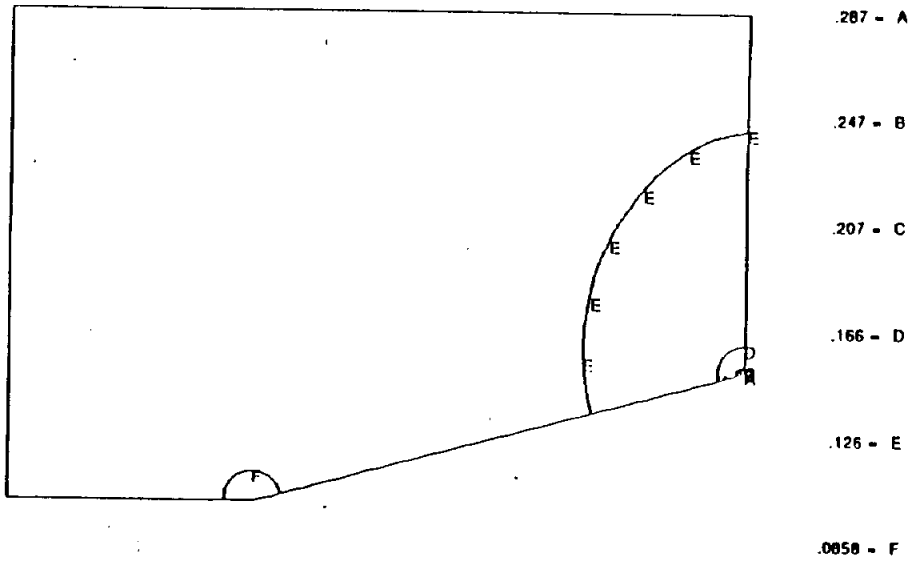

Figure 3.5.6 Wedge Flow - Potential Contours

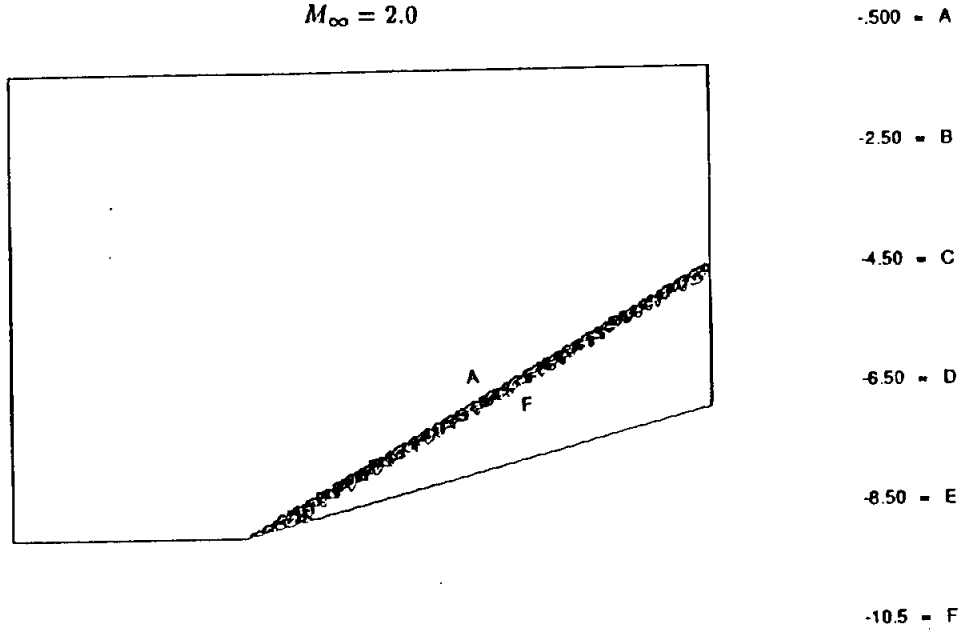

Figure 3.5.7 Wedge flow - Potential Distribution

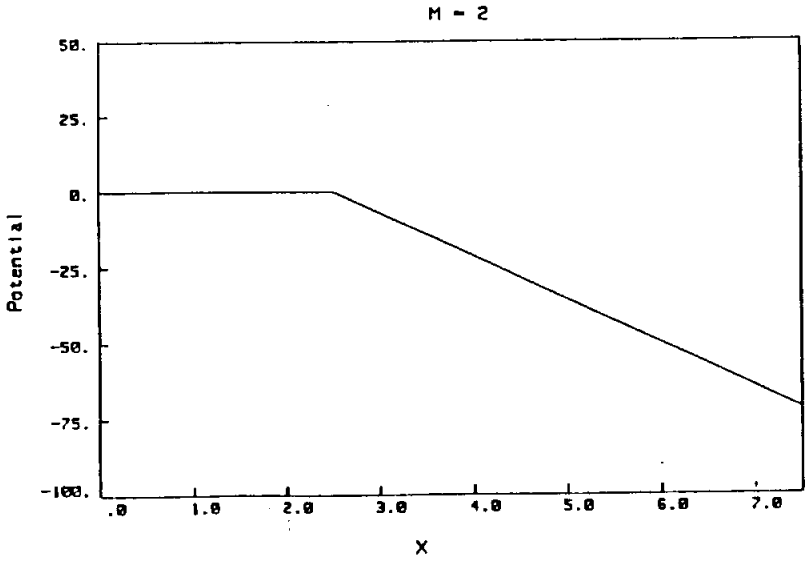

Figure 3.5.8 Supersonic Wedge Flow - Mach Contours

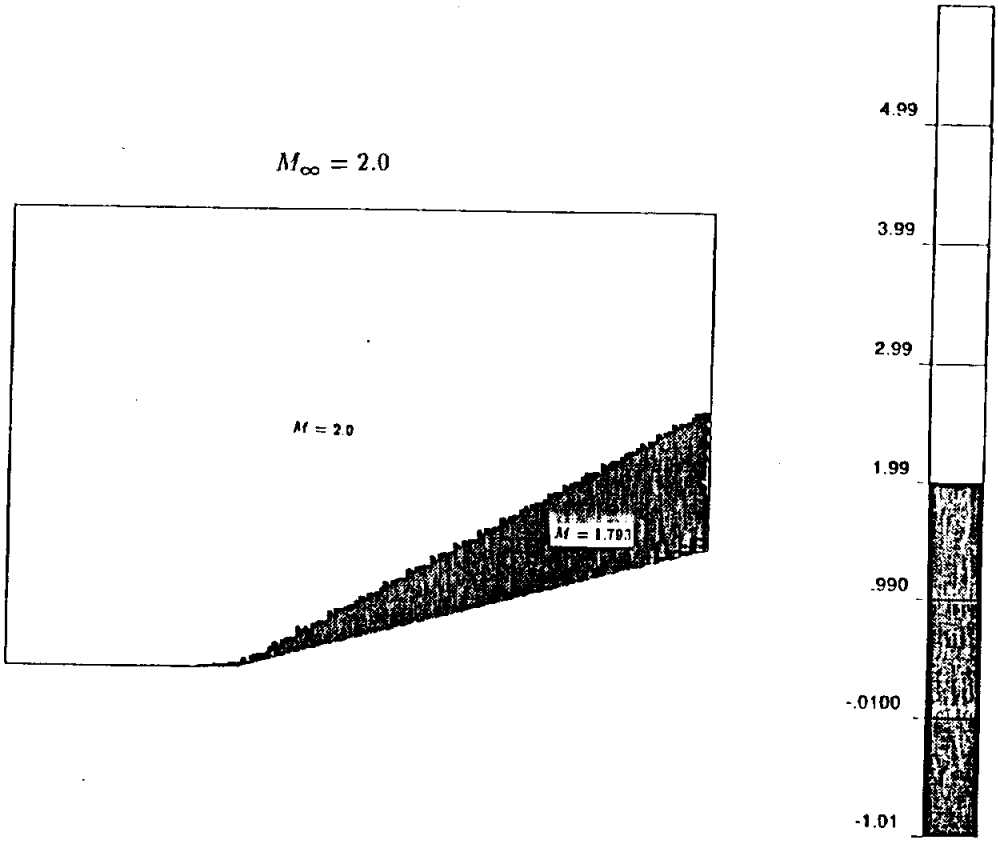

Figure 3.5.9 Wedge Flow - Pressure Coefficient Distribution

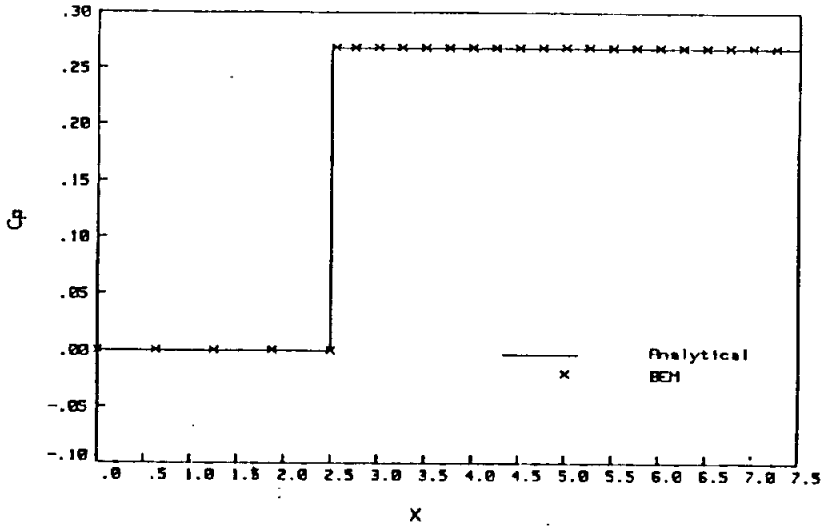

Figure 3.5.10 Supersonic Wedge flow - Velocity Vectors

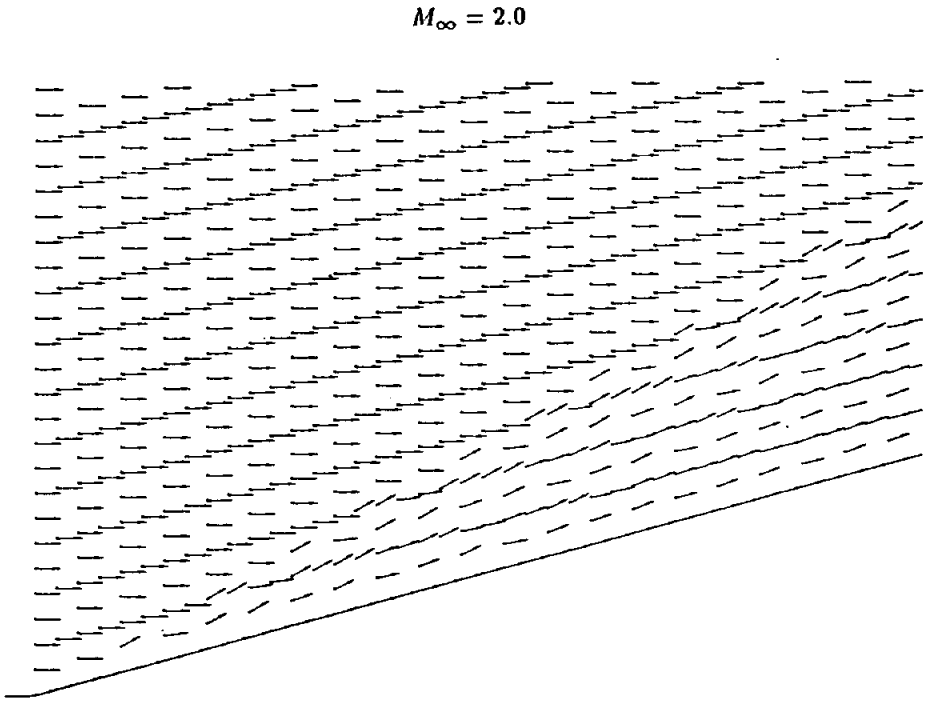

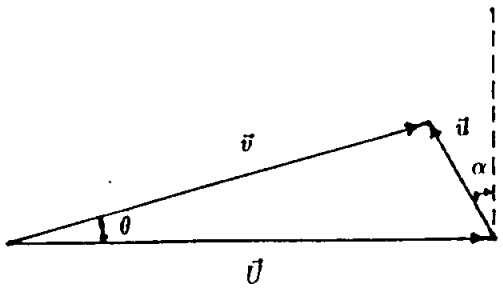

$$M = M_\infty \frac{\cos\alpha}{\cos(\alpha+\theta)}; \quad u_1 = U\frac{\sin\alpha\sin\theta}{\cos(\alpha+\theta)}.$$

Figure 3.5.11 Supersonic Wedge Flow - Vector Diagram

3.5.3 FLOW THROUGH A CHANNEL

In the next example, the supersonic flow in a channel with compression and expansion ramps is solved. The mesh and boundary condition for the case $M_\infty = 1.3$ are given in Figure 3.5.12. It can be seen that for the subsonic case at $M_\infty = 0.1$, the maximum velocity is located at the narrowest section as shown in Figures 3.5.13 and 3.5.14.

Steady-state potential and local Mach number contours for the supersonic case obtained using a marching procedure are shown in Figures 3.5.15 and 3.5.16, respectively. All clearly show the generation of an oblique shock wave at the compression ramp, its reflection off the top wall of the channel and its interaction with the expansion shock produced by the downstream ramp. The velocity vectors calculated in this region of flow are shown in Figure 3.5.17 and further illustrate the effects described above.

Finally, in Figure 3.5.18 and 3.5.19, the potential and pressure coefficient distribution along both upper and lower surface are displayed. Similarly to the wedge flow problem, excellent results have been obtained for the linearized case.

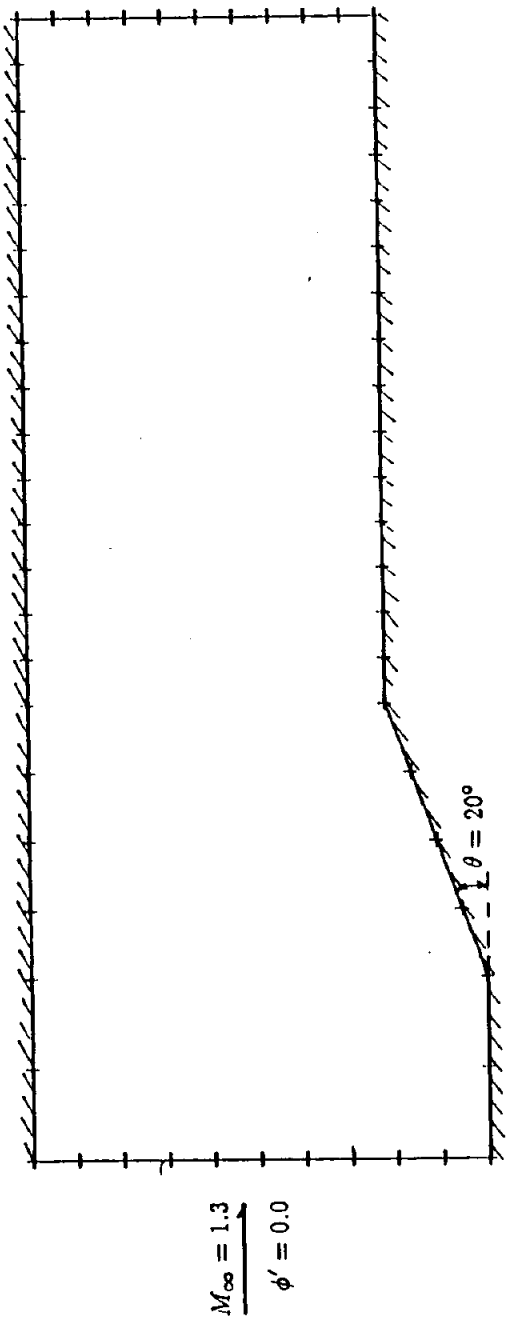

Figure 3.5.12 Mesh of Channel Flow

Figure 3.5.13 Subsonic Channel Flow - Velocity Vectors

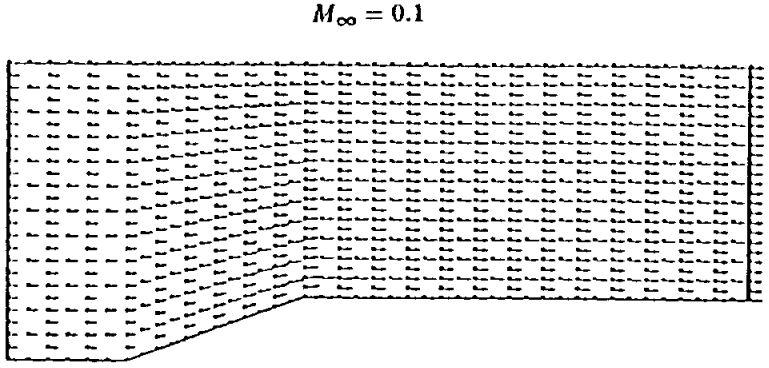

Figure 3.5.14 Subsonic Channel Flow - Mach Contours

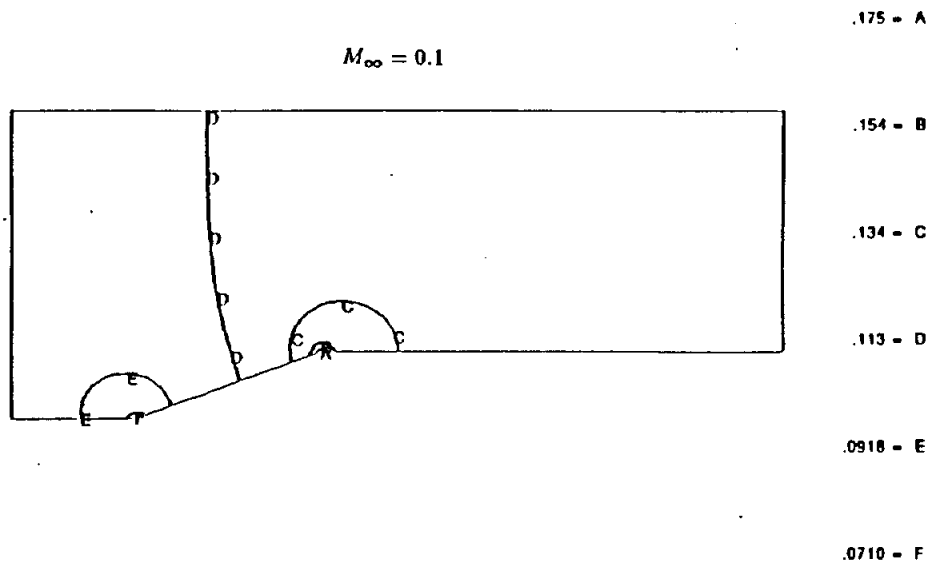

Figure 3.5.15 Channel Flow - Potential Contours

$M_\infty = 1.3$

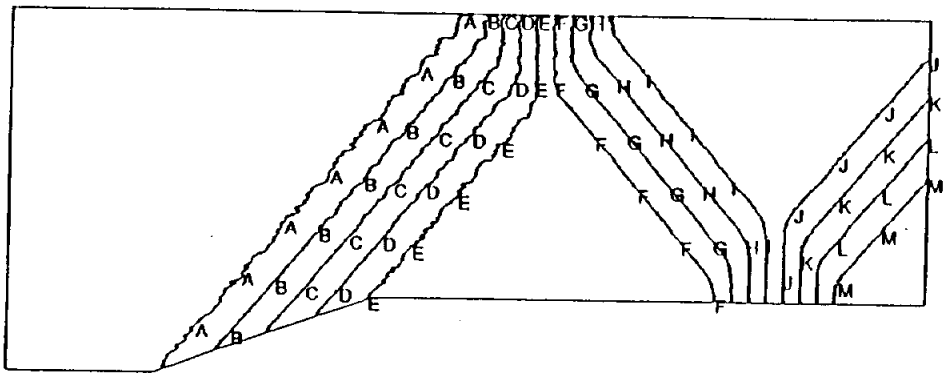

-.700 = A
-4.50 = B
-8.30 = C
-12.1 = D
-15.9 = E
-19.7 = F
-23.5 = G
-27.3 = H
-31.1 = I
-34.9 = J
-38.7 = K
-42.5 = L
-46.3 = M
-50.1 = N
-53.9 = O

Figure 3.5.16 Supersonic Channel Flow - Mach Contours

$M_\infty = 1.3$

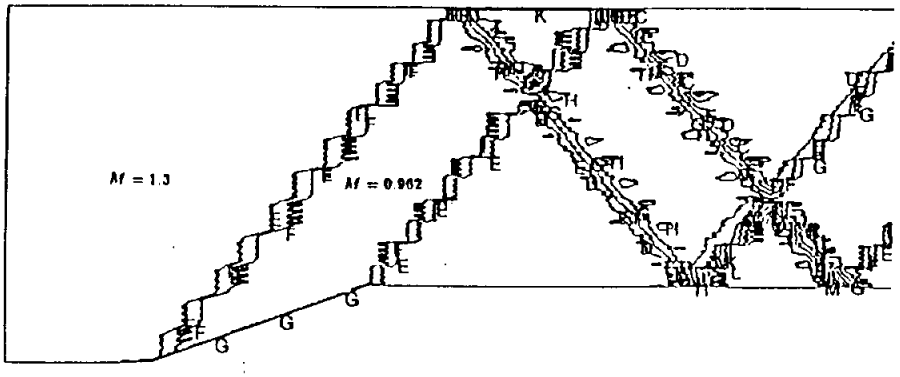

1.65 = A
1.55 = B
1.45 = C
1.34 = D
1.24 = E
1.14 = F
1.03 = G
.932 = H
.829 = I
.726 = J
.623 = K
.520 = L
.418 = M
.315 = N

Figure 3.5.17 Supersonic Channel Flow - Velocity Vectors

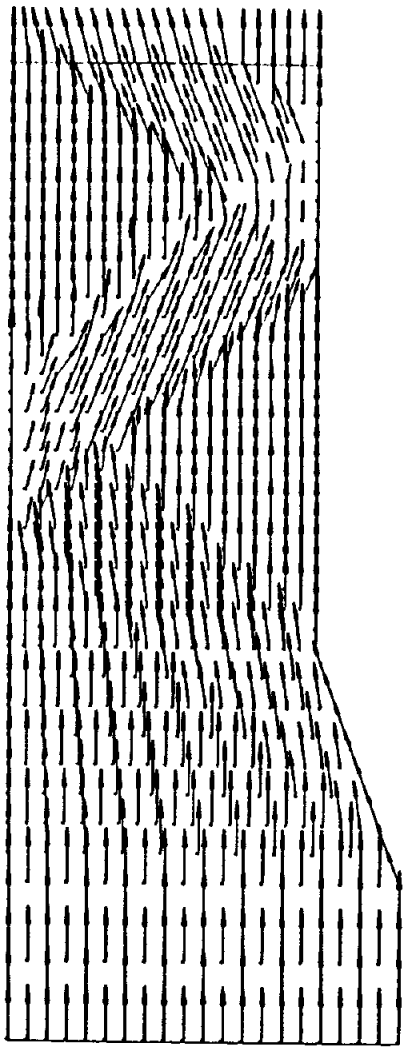

Figure 3.5.18 Channel Flow - Potential Distribution

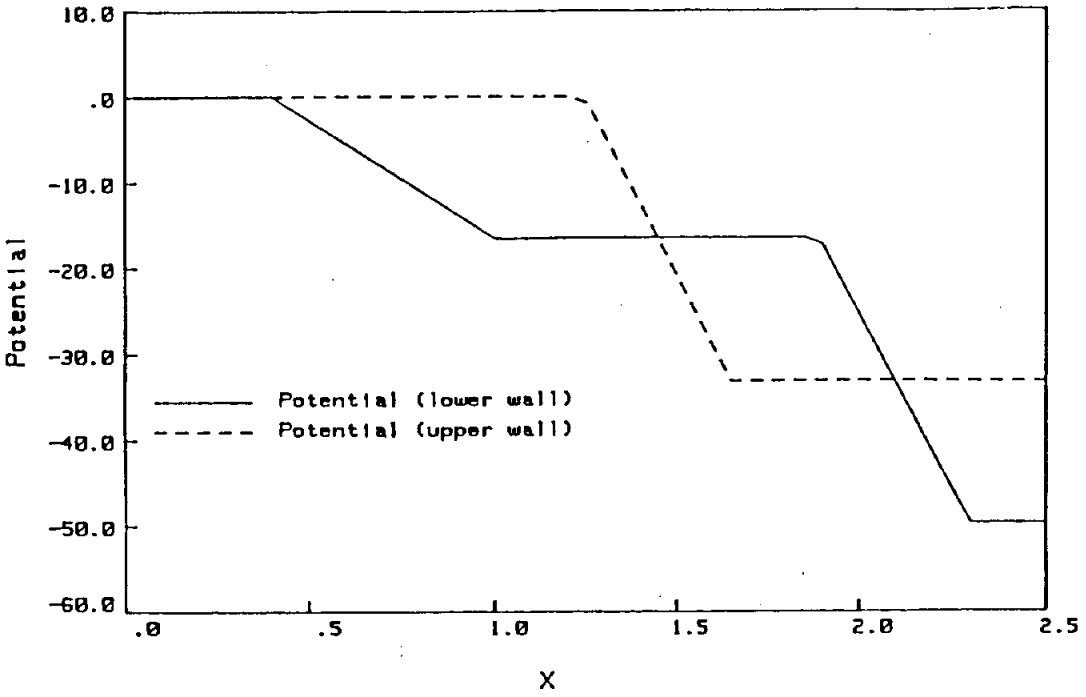

Figure 3.5.19 Channel Flow - Pressure Coefficient Distribution

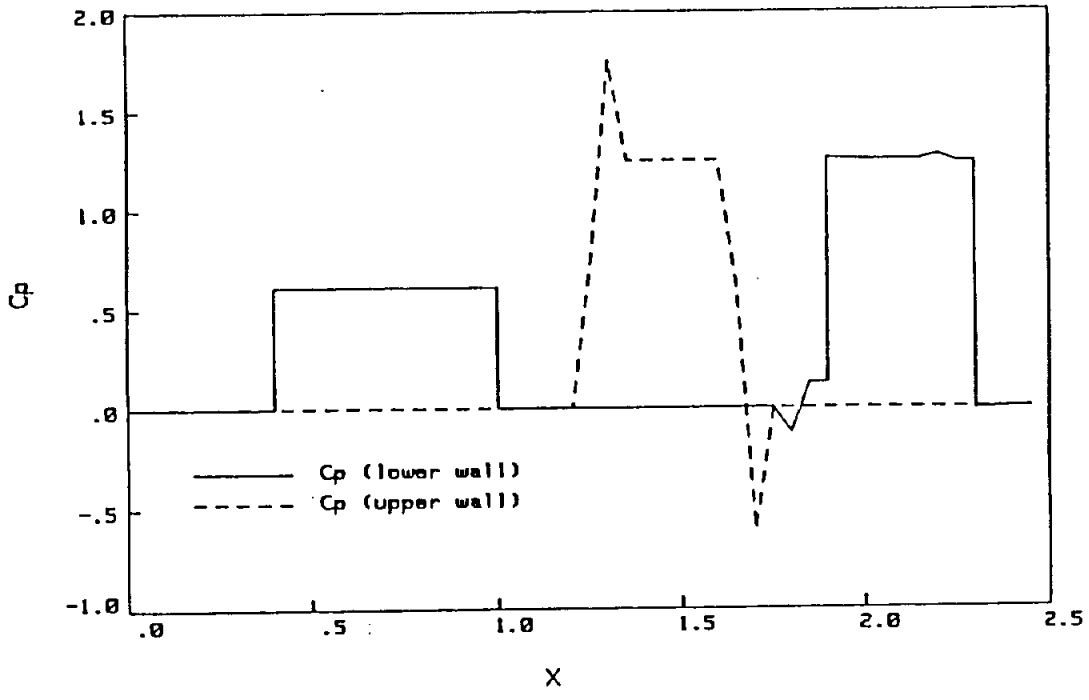

3.5.4 FLOW AROUND A CYLINDER

Attention is next confined to the case of steady state flow around a circular cylinder, in a frame of reference fixed with the cylinder. For transonic flows (the Mach number M is very close to unity), the linearized equation of perturbation potential is not applicable. Neither is the above BEM because the transonic flow is a truly nonlinear problem, and the P-G equation is not valid. For the subsonic case, the flow lines are similar to those of heat transfer. For the supersonic case (M_∞=3), the mesh needs to be refined behind the cylinder in order to capture the shock. The shock front, shown in Figures 3.5.20 and 3.5.21, emanates from the cylinder. In front of the shock wave, the flow is uniform: behind it, the flow is modified. The surface of the shock wave extends to infinity, and at a great distance from the cylinder, the shock is weak. It intersects the incident steamlines at an angle approaching the Mach angle. The velocity shock is a band which includes compression and expansion regions as shown in Figure 3.5.21.

Figure 3.5.20 Supersonic Cylinder Flow - Potential Contours

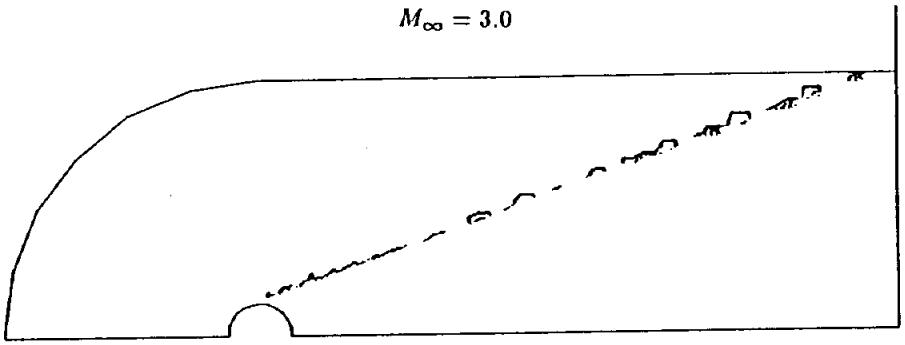

Figure 3.5.21 Supersonic Cylinder Flow - Mach Contours

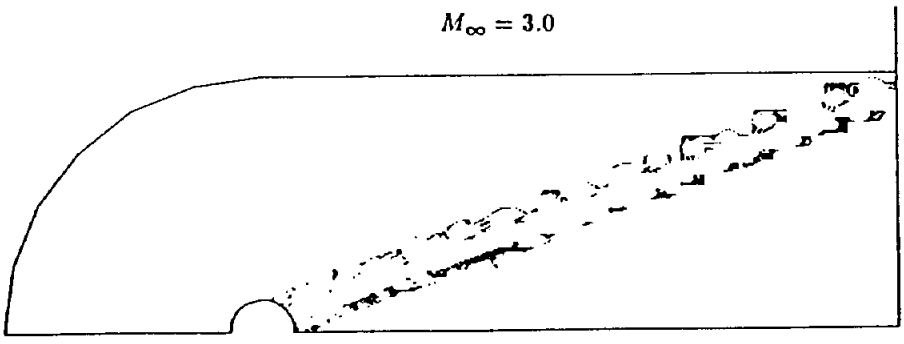

3.6 COMPRESSIBLE THERMOVISCOUS FLOW

The compressible thermoviscous flow formulations detailed in Section 2.4 have not as yet been implemented in a boundary element code. Application examples will be included in future releases of this manual.

3.7 FLUID-STRUCTURE INTERACTION

3.7.1 STEADY RESPONSE OF A THICK CYLINDER

For the first example, a thick-walled stainless steel cylinder rests under plane strain conditions in a stream of hot gas. The cylinder has an outer diameter of 1.0 in. and a thickness of 0.125 in. The inner surface of the cylinder is maintained at a temperature of 0°F, while the gas temperature in the free stream is 1000°F. The following thermoelastic properties are assumed for the solid cylinder

$$E = 29. \times 10^6 psi, \qquad \nu = 0.30$$
$$\alpha = 9.6 \times 10^{-6} \text{in./in.}^\circ F$$
$$k = 6.48 \text{ in.lb./sec.in.}^\circ F$$
$$\rho = 7.34 \times 10^{-4} \text{lb.sec.}^2/\text{in.}^4 \qquad c_\epsilon = 3.83 \times 10^5 \text{in.lb.in./lb.sec.}^{2\circ} F.$$

Additionally, the thermoviscous properties of the hot gas are taken as

$$\mu = 5.30 \times 10^{-9} \text{lb.sec/in.}^2$$
$$k = 7.28 \times 10^{-3} \text{in.lb./sec.in.}^\circ F$$
$$\rho = 3.69 \times 10^{-8} \text{lb.sec.}^2/\text{in.}^4 \qquad c_p = 9.49 \times 10^5 \text{in.lb.in./lb.sec.}^{2\circ} F.$$

Fluid velocities of 144 in./sec., 1440 in./sec. and 14400 in./sec., corresponding to Reynolds Numbers of $10^3, 10^4$ and 10^5, are examined. In all cases, the hot gas flows from left to right, and only the steady response is considered.

At $Re = 1000$, the maximum temperature in the cylinder is only 98°F, and the peak compressive axial stress is 36 ksi. However, when the fluid velocity is increased to attain an $Re = 10,000$ a much more significant response is obtained. The temperature contours are shown in Figure 3.7.1a, the deformed shape is depicted in Figure 3.7.1b, and Figure 3.7.1c illustrates the axial stress distribution. It should be noted that in Figure 3.7.1b the deformation has been scaled by a factor of 100. The effects of convection are quite evident in all three diagrams. With Reynolds number increased to 100,000 these effects become even more pronounced, as seen in Figures 3.7.2. Now the peak metal temperature has reached 918°F.

Figure 3.7.1 STEADY RESPONSE OF A THICK CYLINDER (Re = 10,000)

a) Temperature

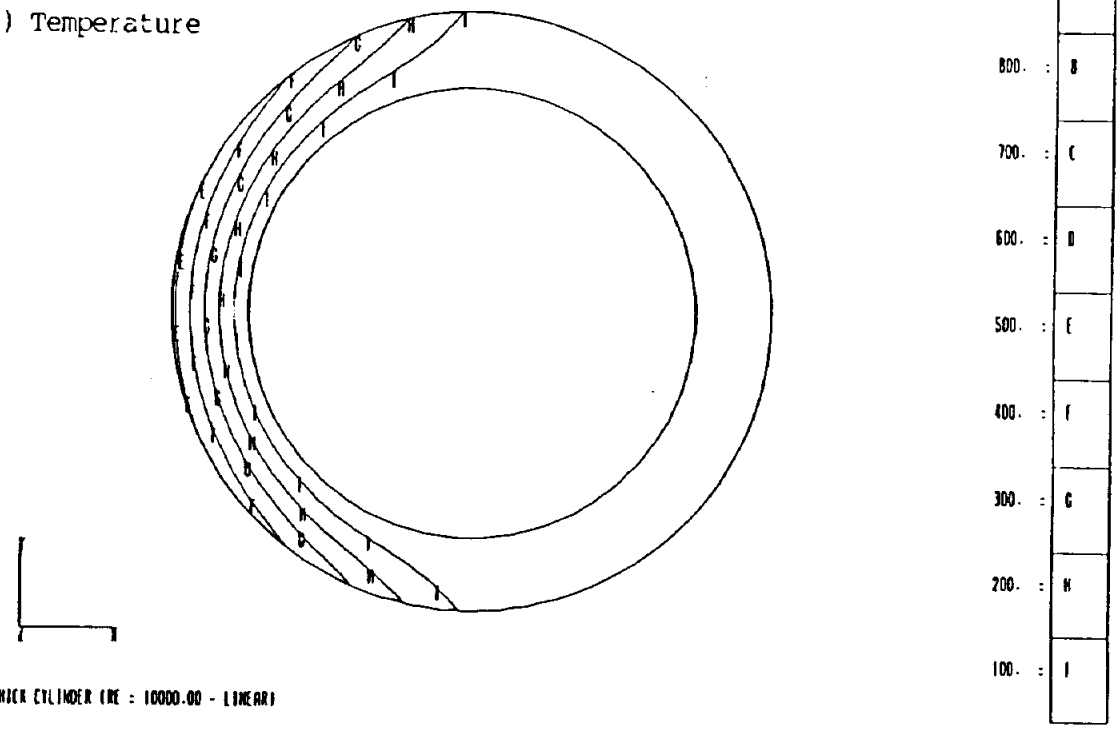

OSEEN FLOW AROUND A THICK CYLINDER (RE = 10000.00 - LINEAR)

b) Deformed Shape

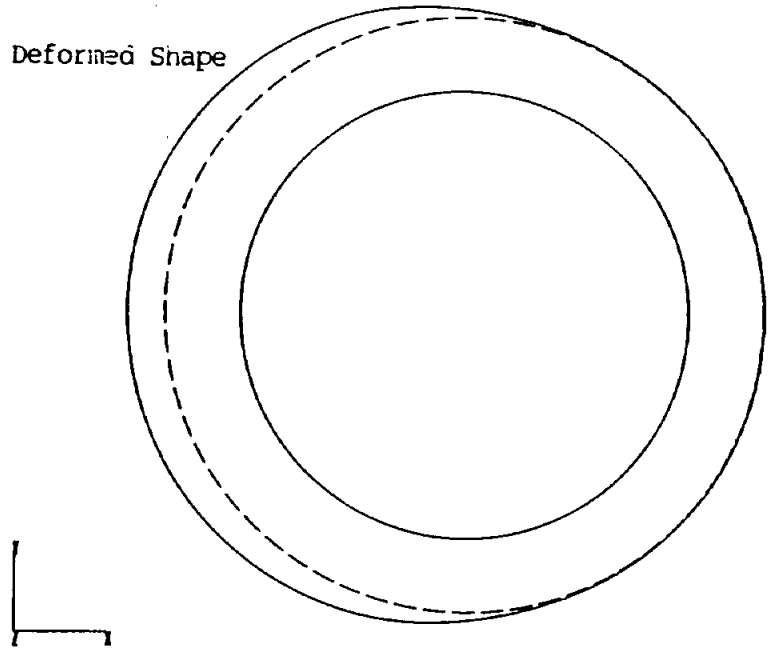

OSEEN FLOW AROUND A THICK CYLINDER (RE = 10000.00 - LINEAR)

Figure 3.7.1 STEADY RESPONSE OF A THICK CYLINDER (Re = 10,000)

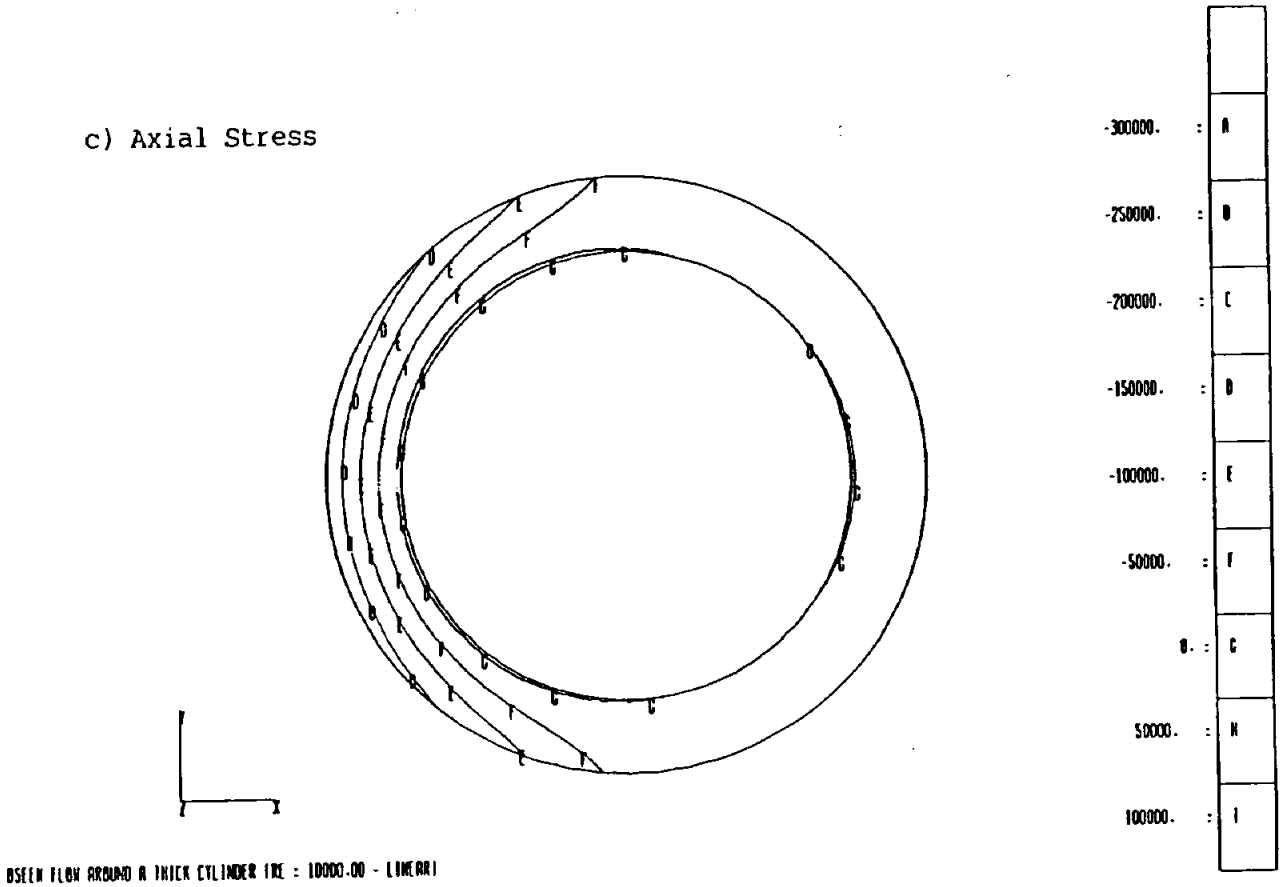

Figure 3.7.2 STEADY RESPONSE OF A THICK CYLINDER (Re =100,000)

a) Temperature

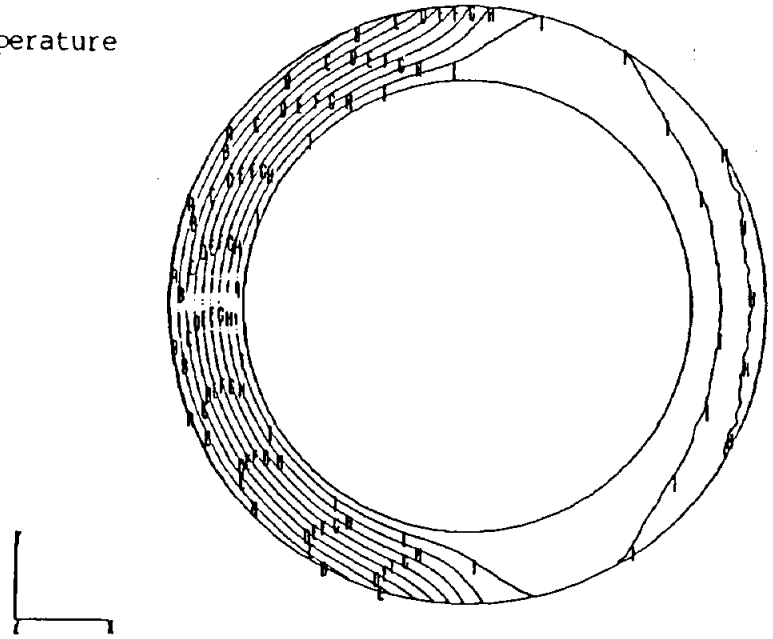

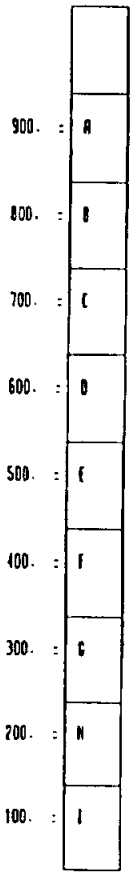

OSEEN FLOW AROUND A THICK CYLINDER (RE : 100000.00 - LINEAR)

b) Deformed Shape

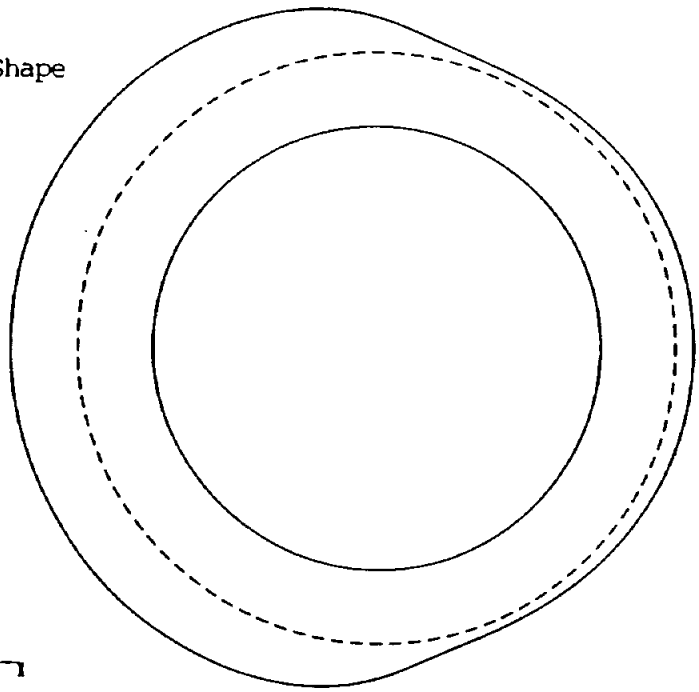

OSEEN FLOW AROUND A THICK CYLINDER (RE : 100000.00 - LINEAR)

Figure 3.7.2 STEADY RESPONSE OF A THICK CYLINDER (Re = 100,000)

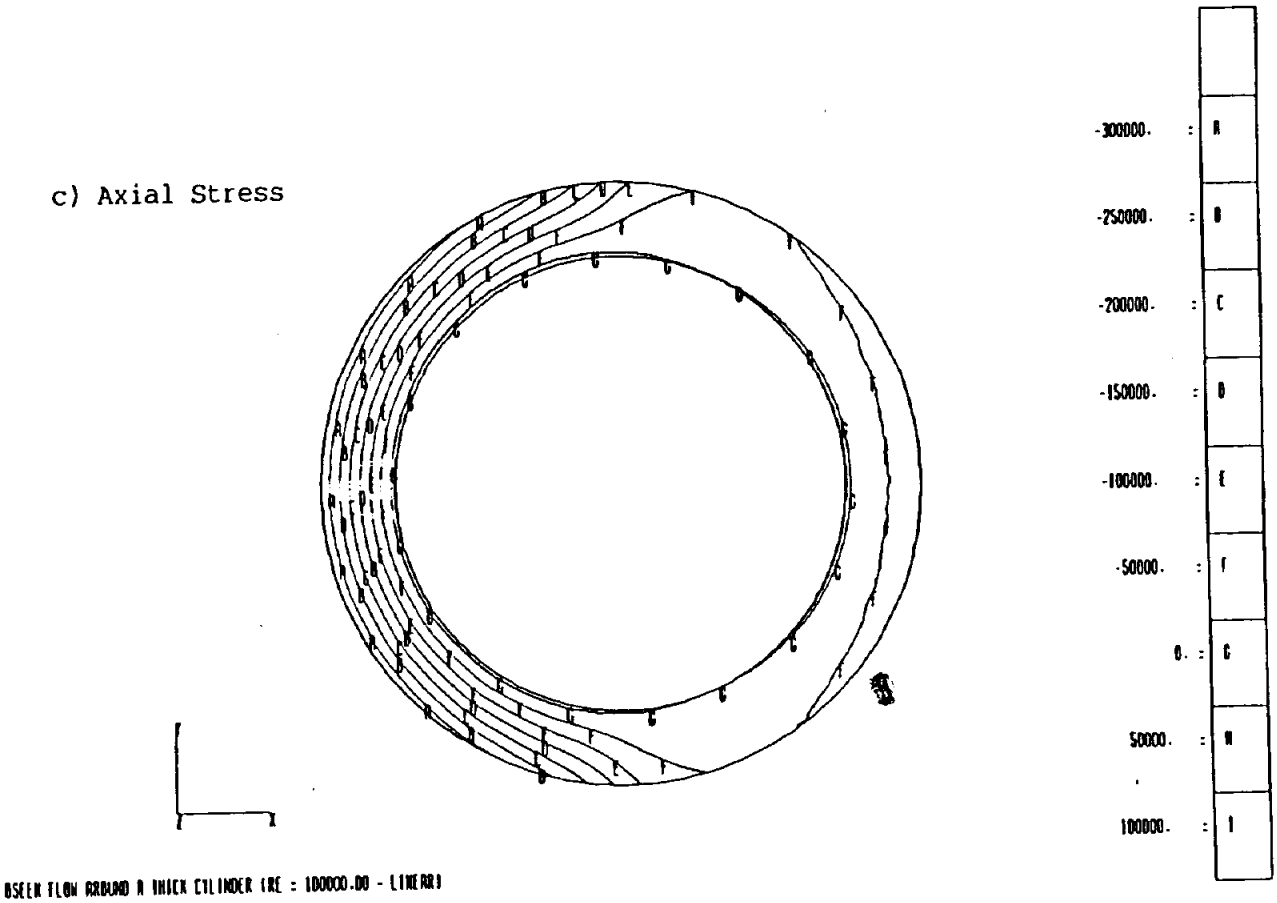

3.7.2 AIRFOIL EXPOSED TO HOT GAS FLOWPATH

In this second example, an NACA0018 airfoil with an internal cooling passage is exposed to the flow of a hot gas. The boundary element model for the airfoil is shown in Figure 3.7.3. Each dash represents an individual quadratic surface element. Throughout this problem, the outer gaseous region is modeled as a linear steady convective domain. Thus, a boundary-only exterior GMR is employed for the fluid. The hot gas at 1000°F flows from left to right, while the inner surface of the airfoil is maintained at 200°F. Material properties from the previous example are once again used to characterize both the solid and fluid.

For the first set of investigations, the behavior of the airfoil is determined under steady-state conditions. Figure 3.7.4a displays the deformed shape at a Reynolds number of 1000 (based upon chord length). The solid line represents the final deformed shape, except that displacements have been scaled by a factor of twenty-five. Meanwhile, Figures 3.7.4b and c present the profiles of temperature and axial stress, respectively, along the upper surface of the airfoil. At this relatively slow speed flow, the airfoil is only effected near its leading edge. More significant response is shown in Figures 3.7.5a-c for $Re = 10,000$ and Figures 3.7.6a-c for $Re = 100,000$. In the latter case, the temperature at the stagnation point is nearly that of the free stream. All three cases considered so far have assumed an angle of attack of 0° with respect to the x-axis. Consequently, the response of the upper and lower surfaces is identical. Next, the angle of attack (α) is modified to 5° and 10°. Results for these cases are shown in Figures 3.7.7 and 3.7.8, respectively. Considerable asymmetry between upper and lower surfaces is now evident, although peak values of temperature and stress are essentially unaffected.

Thermal barrier coatings are often employed to reduce the metal temperatures and stresses in hot section components. The benefit of such coatings can easily be evaluated with the present boundary element formulation. Consider, for example, a coating material with thermal conductivity $k = 0.50$ in.lb./sec.in.°F sprayed to a thickness of .0095in. This is equivalent to an interfacial thermal resistance of .021 sec.in°F/in.lb., which can be specified on the fluid-to-solid GMR interface. Results are displayed in Figure 3.7.9 for $Re = 100,000$ at $\alpha = 10°$. Peak airfoil temperature is reduced from 976°F to 738°F by introducing this particular thermal barrier coating.

Finally, it is of considerable interest to examine the transient response of the airfoil. At time zero, the airfoil is in thermal equilibrium at a temperature of 200°F. Suddenly, it is subjected to the hot gas stream with $Re = 100,000$ and $\alpha = 10°$. The response of the upper surface at 1 msec., 2msec., 5 msec., and 10 msec. is shown in Figures 3.7.10-3.7.13. For this transient case, the peak stress occurs slightly offset from the tip of the airfoil. Additionally, the stress σ_{yy} reaches a maximum at approximately 2 msec., while σ_{zz} and the temperature continue to climb to their steady-state values. This is true of the axial stress only because of the assumption of plane strain. In a full three-dimensional analysis, σ_{zz} would also have a higher peak during transient state.

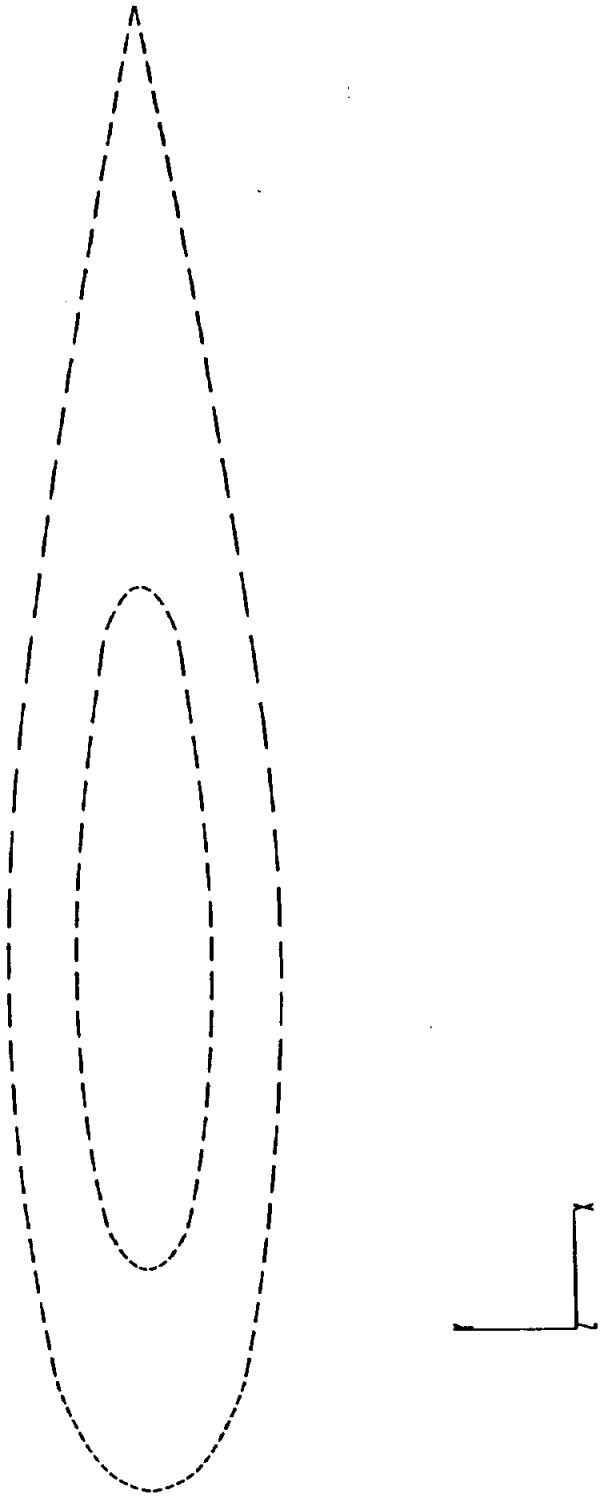

AIRFOIL - BOUNDARY ELEMENT MODEL

Figure 3.7.3

Figure 3.7.4 AIRFOIL (STEADY; Re = 1000; $\alpha = 0^{\circ}$)

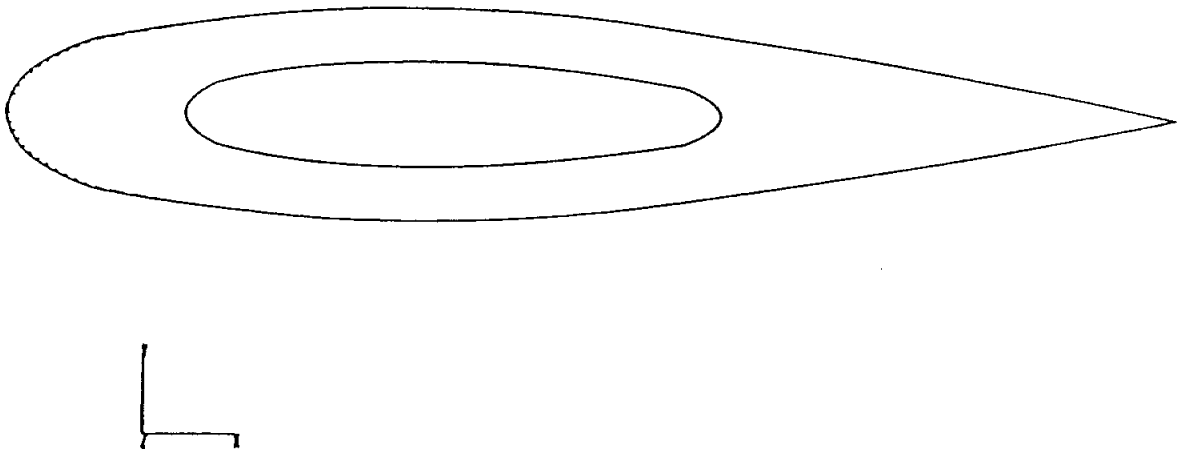

INTERNALLY-COOLED NACA-0018 AIRFOIL (RE : 1000; ANGLE : 0)

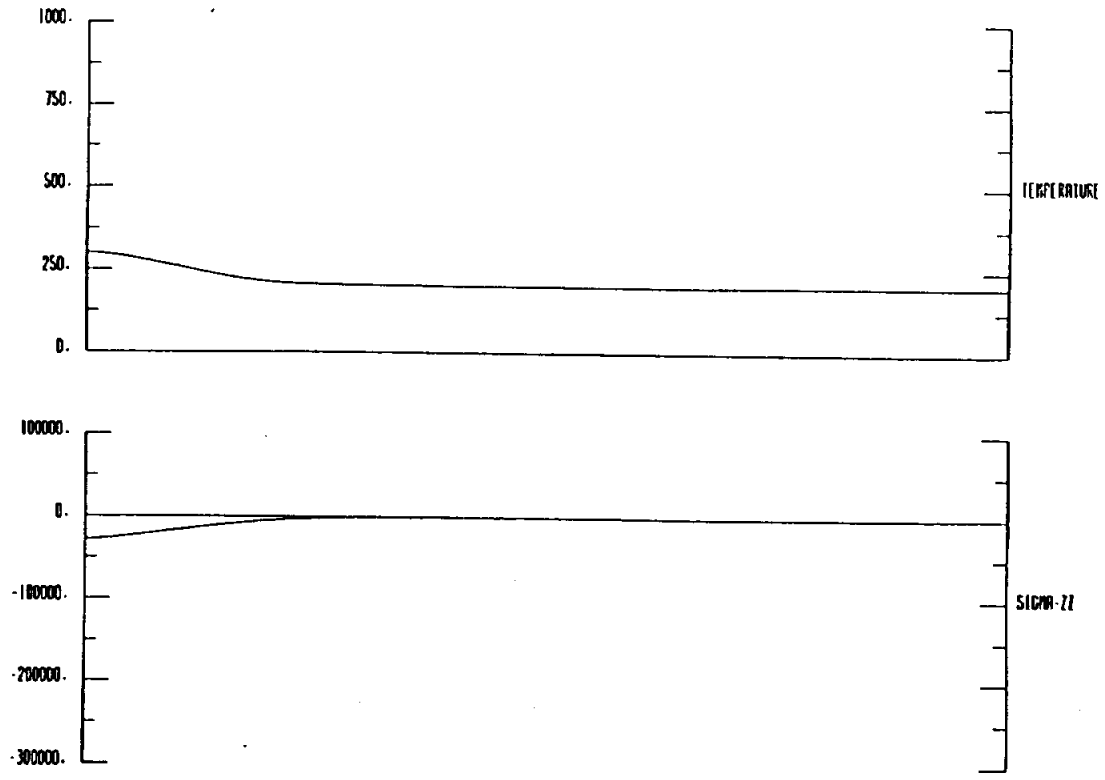

Figure 3.7.5 AIRFOIL (STEADY; Re = 10,000; $\alpha = 0^{O}$)

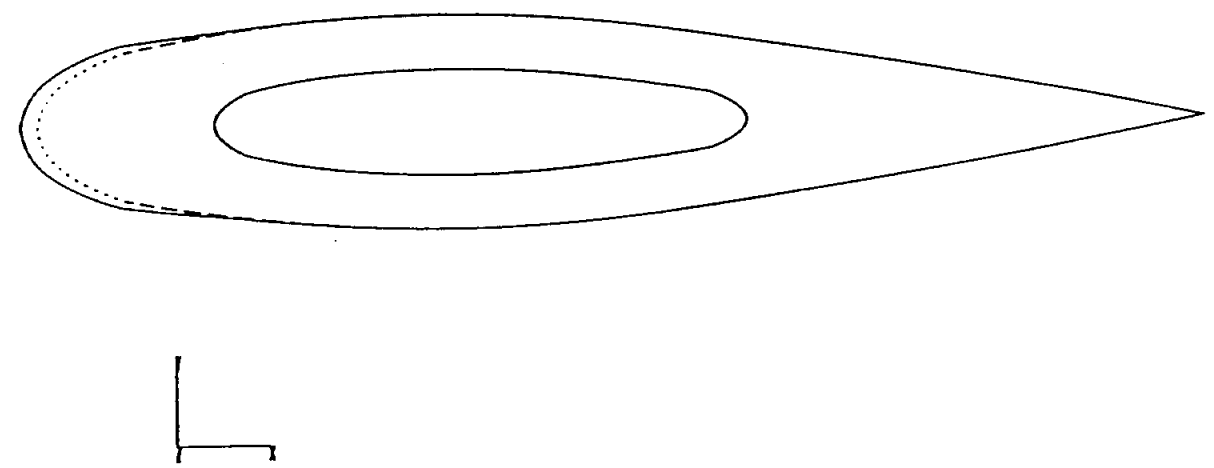

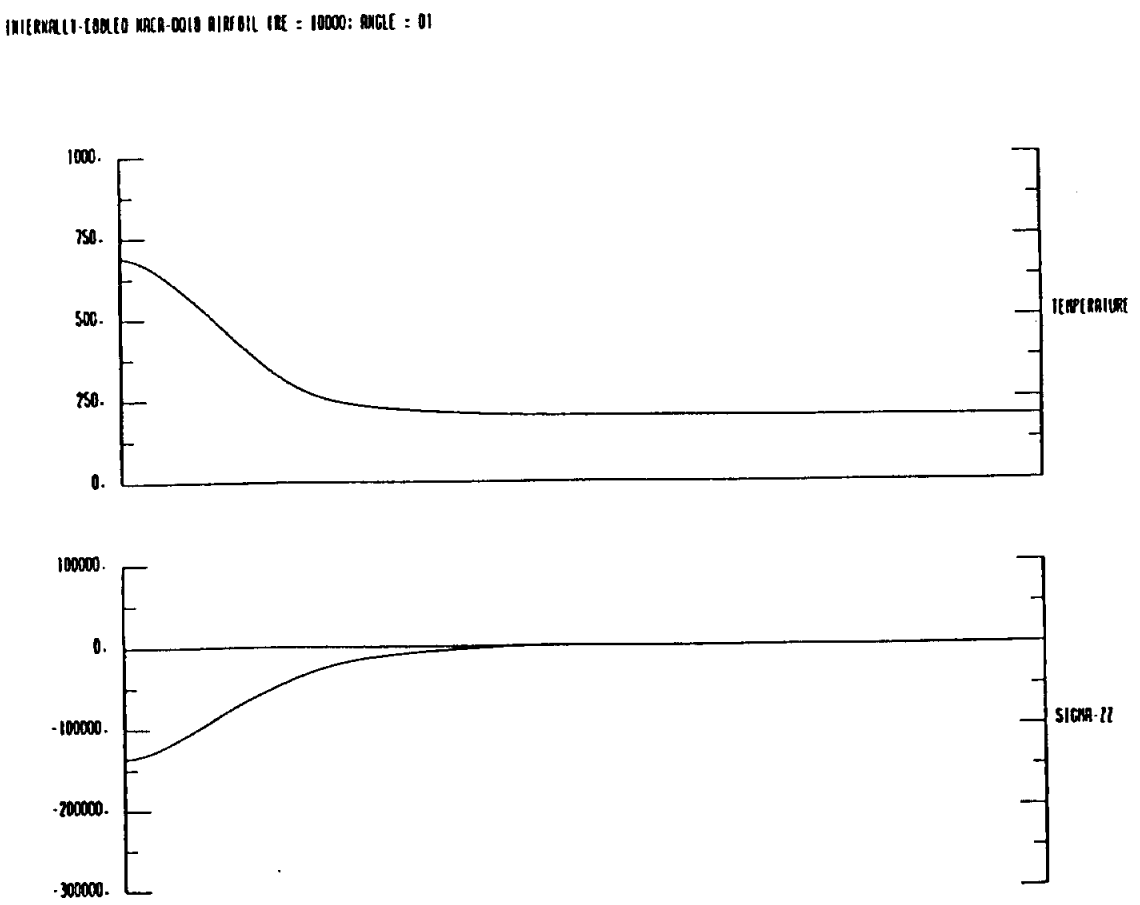

Figure 3.7.6 AIRFOIL (STEADY; Re = 100,000; $\alpha = 0^{\circ}$)

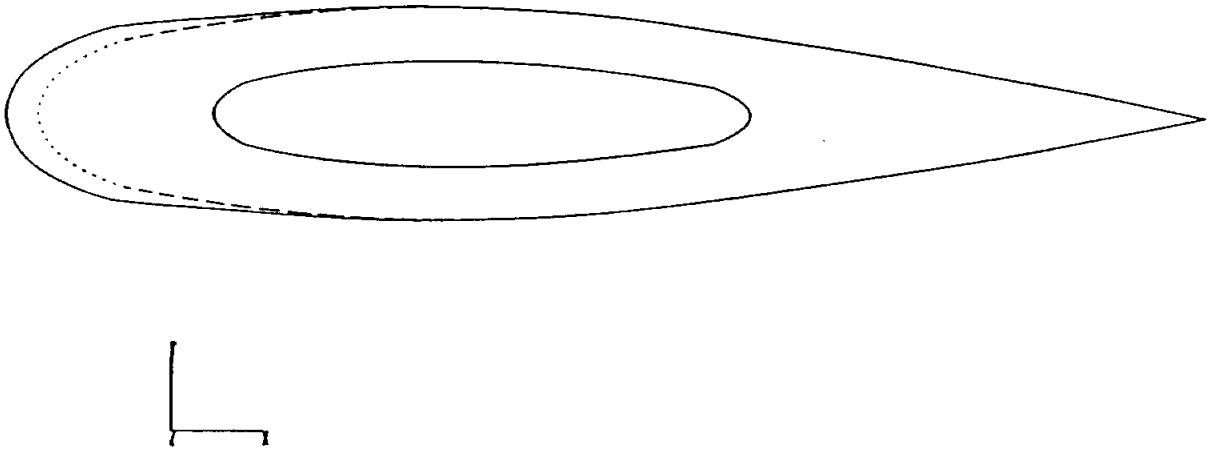

INTERNALLY-COOLED NACA-0018 AIRFOIL RE = 100000; ANGLE = 0

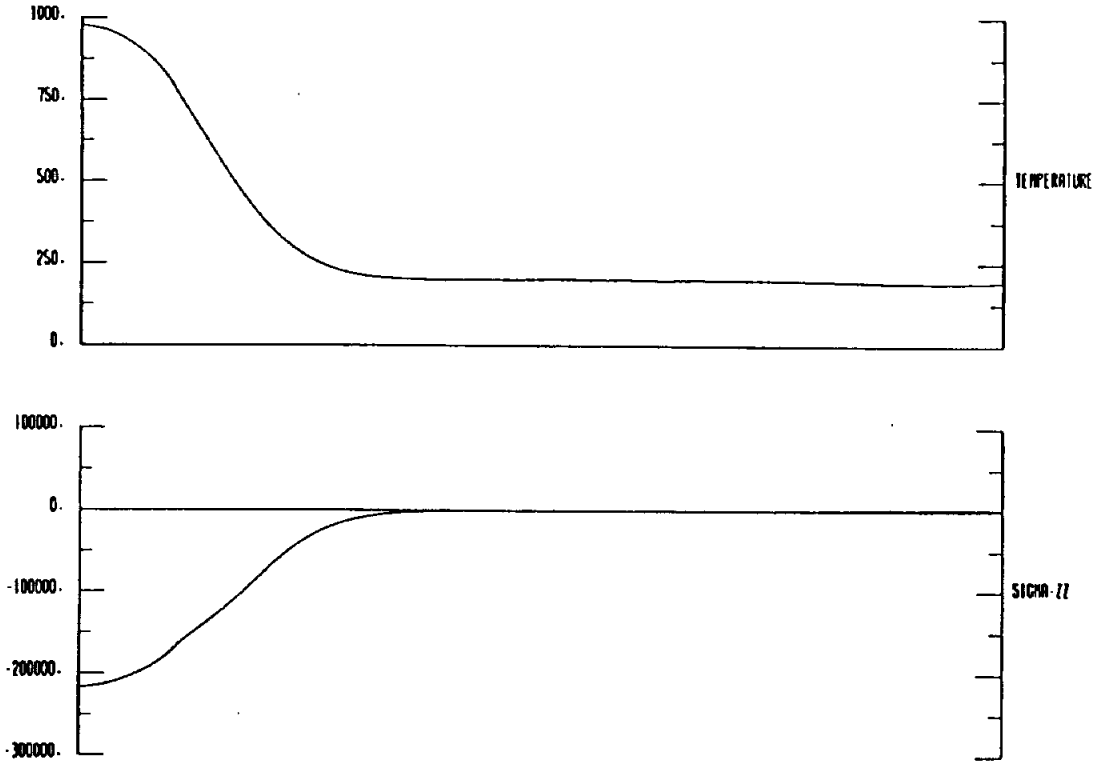

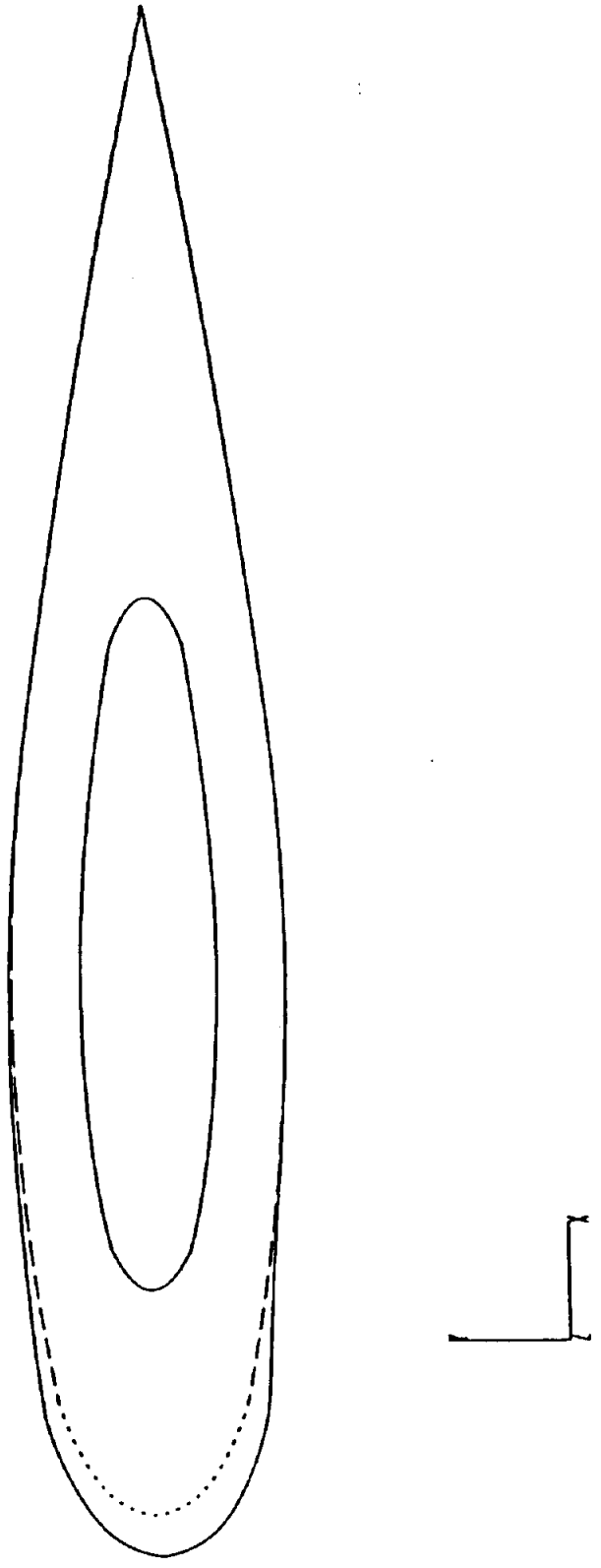

Figure 3.7.7a AIRFOIL (STEADY; Re = 100,000; $\alpha = 5^{o}$)

Figure 3.7.7b-e - AIRFOIL (STEADY; Re= 100,000; $\alpha = 5^{O}$)

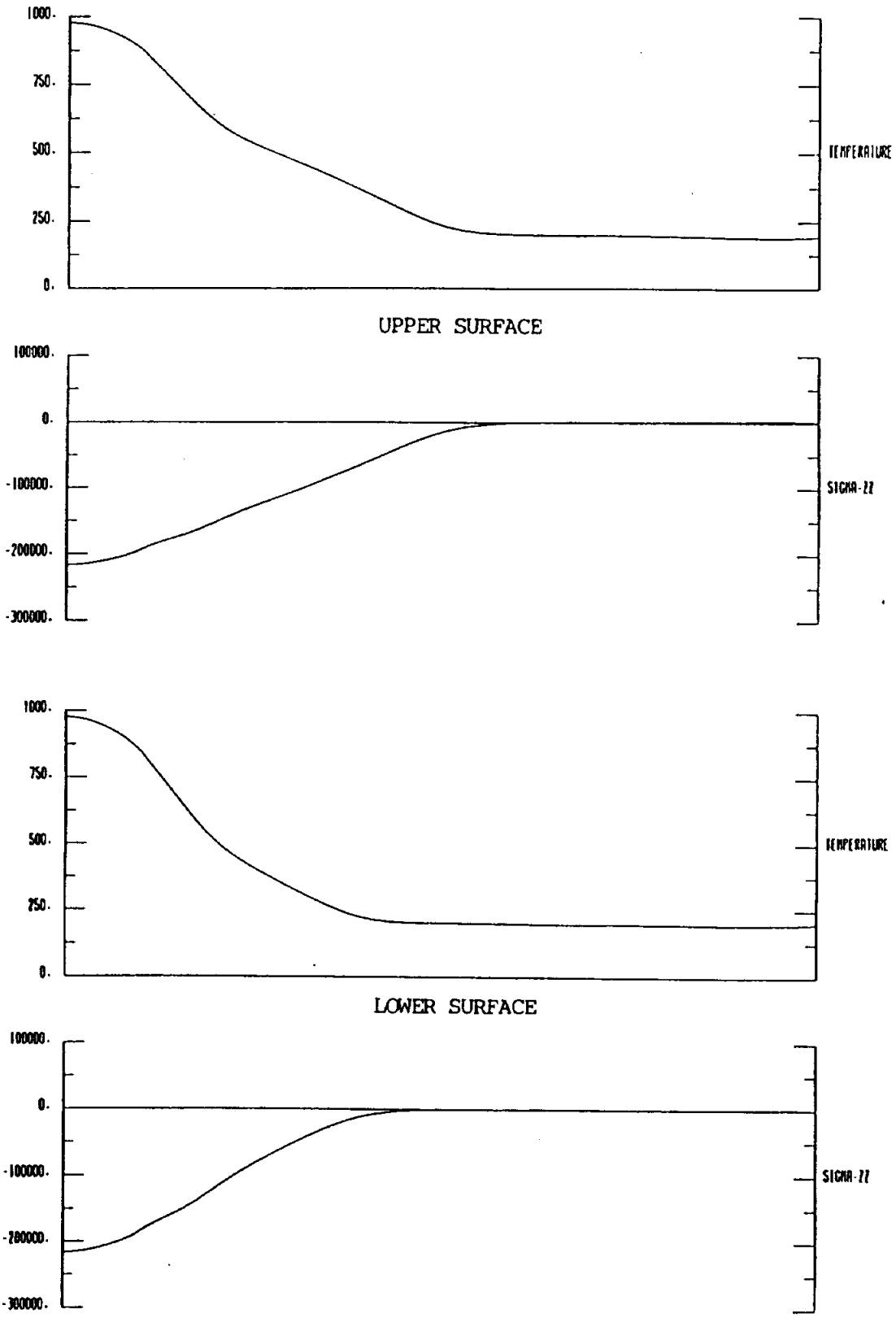

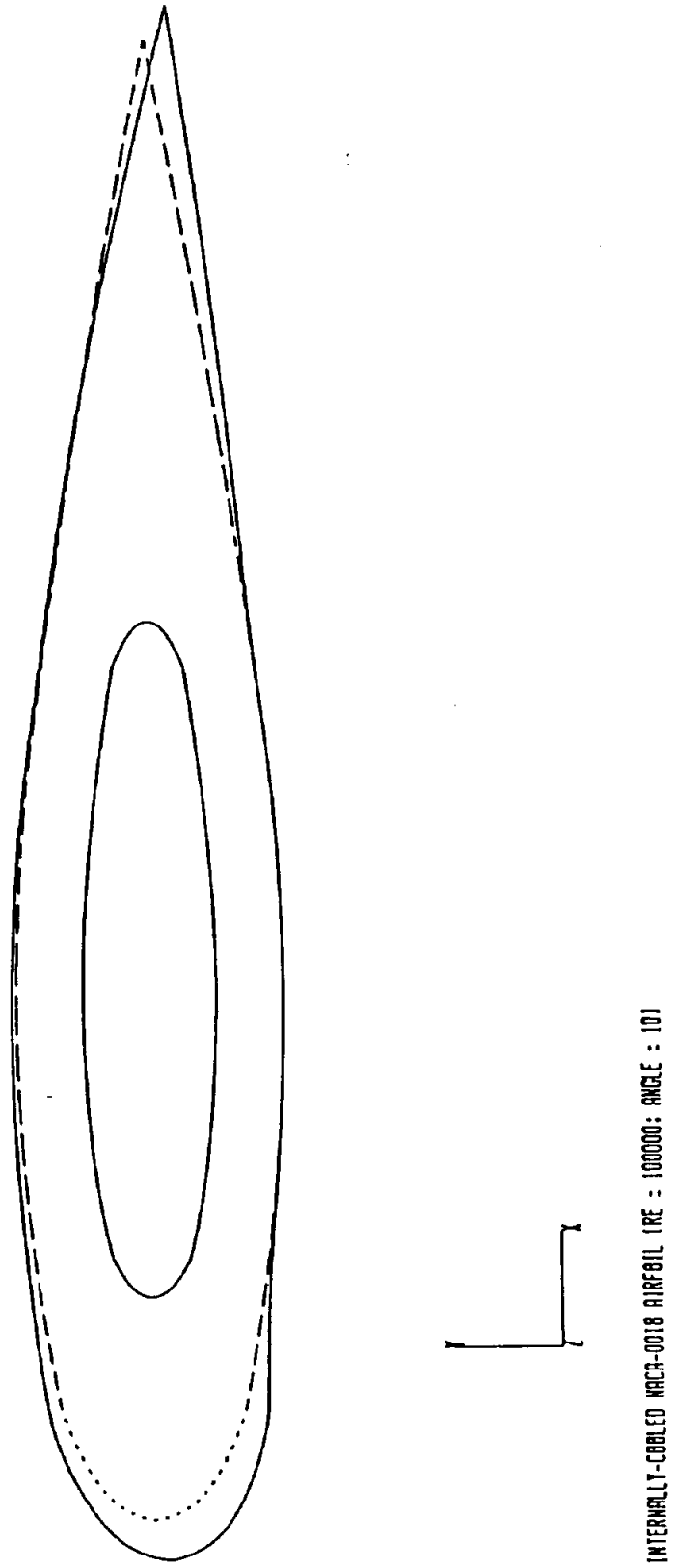

Figure 3.7.8a AIRFOIL (STEADY; Re = 100,000; $\alpha = 10^{o}$)

Figure 3.7.8b-e - AIRFOIL (STEADY: Re = 100,000; $\alpha = 10^{o}$)

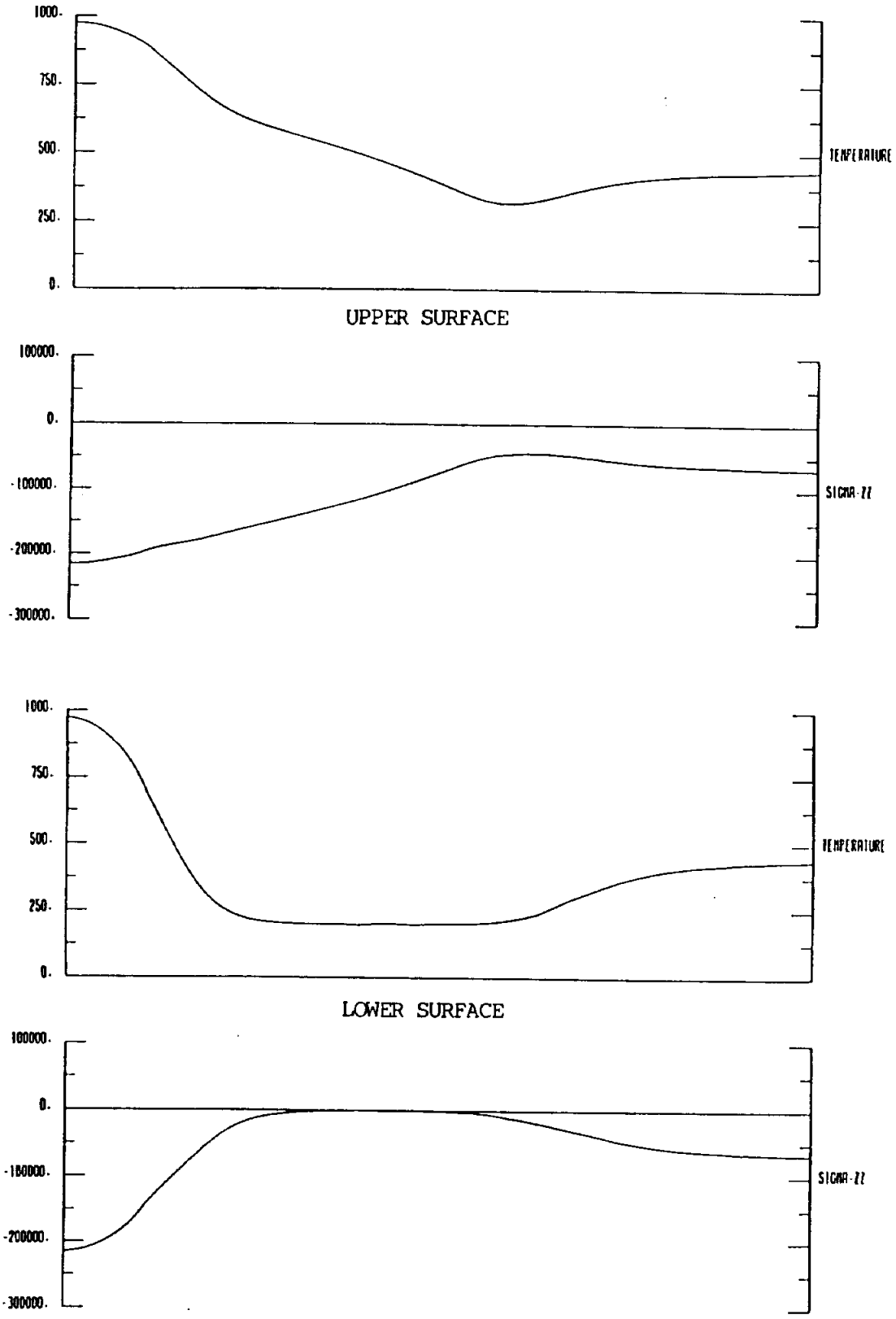

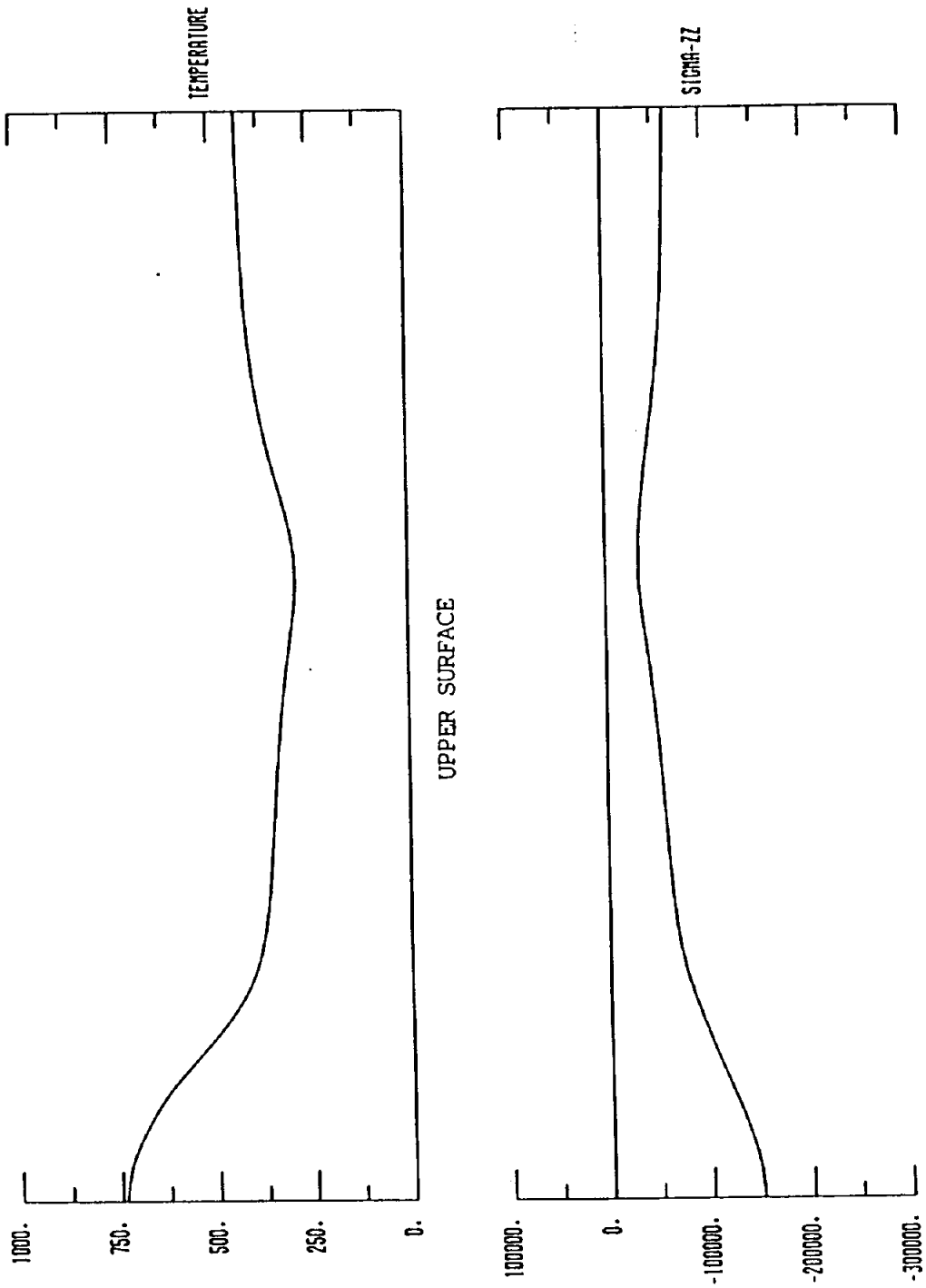

Figure 3.7.9 AIRFOIL WITH COATING (STEADY; Re = 100,000; $\alpha = 10^{o}$)

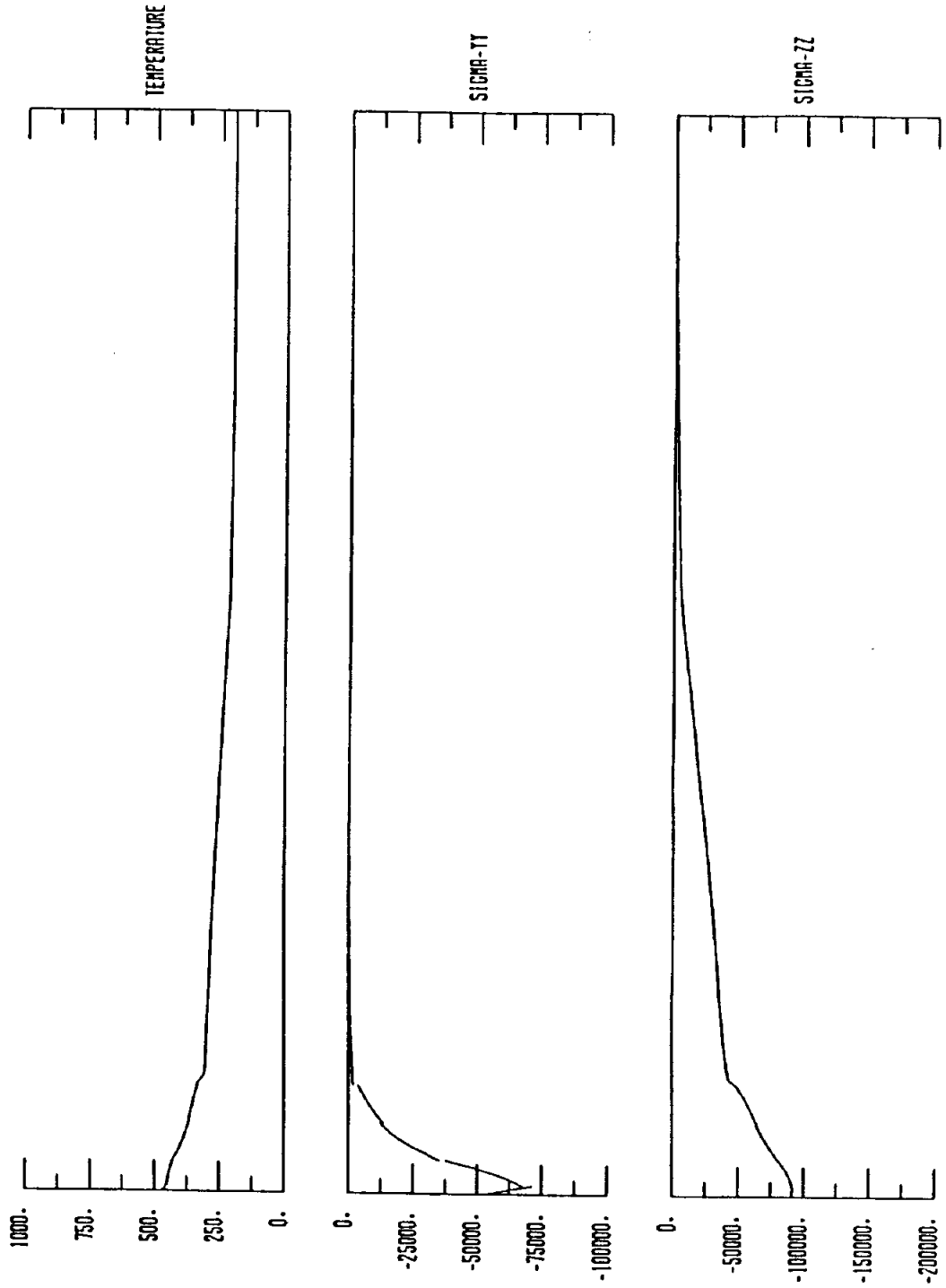

Figure 3.7.10 AIRFOIL (TRANSIENT @ 1 msec; Re = 100,000; $\alpha = 10^{o}$)

Figure 3.7.11 AIRFOIL (TRANSIENT @ 2 msec; Re = 100,000; $\alpha = 10^{o}$)

Figure 3.7.12 AIRFOIL (TRANSIENT @ 5 msec; Re =100,000; α = 10^{o})

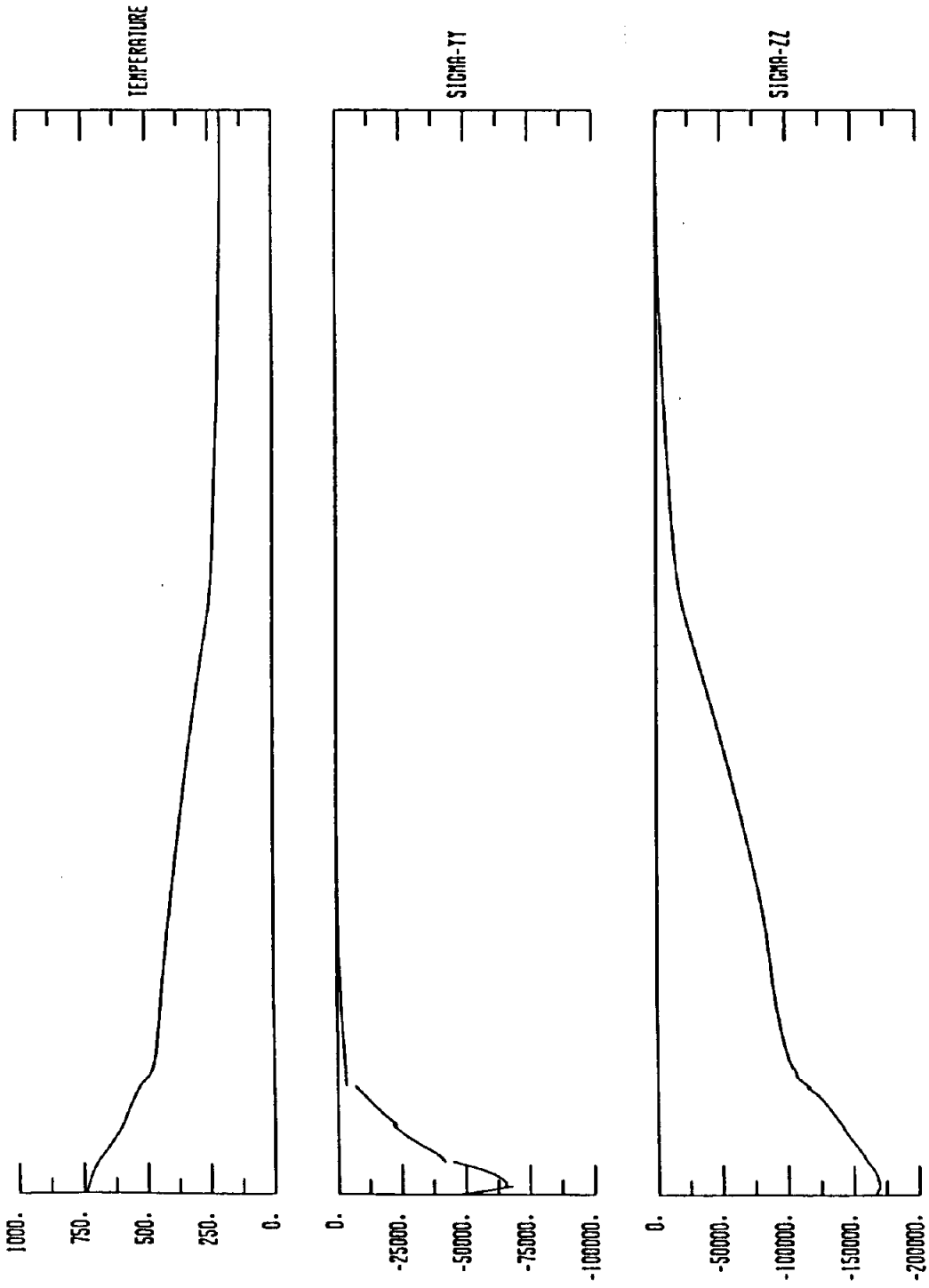

Figure 3.7.13 AIRFOIL (TRANSIENT @ 10msec; Re = 100,000; $\alpha = 10^{o}$)

4.0 GUIDE TO USING BEST-FSI

Since **BEST-FSI** employs the boundary element method rather than the more familiar finite difference or finite element methods, it may appear to be a little difficult for a beginner to get started. This section is therefore written to provide some guidance to such a user. It is hoped to expand this section of the manual fully with wider user participation.

4.1 GETTING STARTED

Generally the first time user is motivated by a specific problem in a given technical area. It is suggested that the new user first read the analysis section of the manual to get some flavor of the BEM in that area. Then the structure and organization of the input data in Section 5 can be examined in conjuction with a sample problem dataset given in Section 6. Additionally Section 3 may contain a brief description of a specific engineering example in the technical area of interest to the user.

It may also be helpful to use a specific test data given in Section 6 and modify it to create a new test problem. In order to do this the user must of course study the relevant parts of Section 5.

4.2 GRAPHICS INTERFACE

BEST-FSI uses **PATRAN**^{TM} as its graphics interface. A graphics interface is essential to generate data for a realistic practical example and the subsequent processing of the results. **PATRAN** is a general purpose graphics input and output system which allows a user to interactively prepare input data for the surface and volume discretizations. It essentially generates the nodal coordinates and connectivities of a given discretization scheme. After the analysis, it allows the user to display the results in a graphics oriented mode. **PATRAN** was developed and is maintained by **PDA**^{TM} Engineering of California.

PATBEST, which is the data preparation interface for **BEST-FSI** takes the output (neutral) file from a **PATRAN** work session and translates the nodal coordinates and connectivities of the model generated by **PATRAN** into a format of nodal coordinates and connectivities consistent with **BEST-FSI** input data.

Post-processing data is generated internally within **BEST-FSI** according to a set of user-defined options. This data is then utilized by **PATRAN** to provide results for visualization.

It is planned to include interfaces to other popular modelling graphics packages, such as SUPERTAB^{TM}/CADES^{TM} and MOVIESTAR.BYU^{TM}, in the near future.

4.3 AVAILABILTY OF BEST-FSI

BEST-FSI is written in FORTRAN 77 and is therefore adaptable to any computer which has such a compiler. An executable version of the code had been developed on IBM^{TM} and CRAY^{TM} mainframes, HP 9000^{TM} (Series 300 and 800), SUN-3^{TM}, SUN-4^{TM}, and SUN Sparcstation^{TM} systems. Depending upon the demand, it is intended to add IBM RISC System/6000^{TM}, Alliant^{TM}, Silicon Graphics IRIS^{TM}, DECstation 3100^{TM}, and all VAX/VMS^{TM} systems to this list.

4.4 FILE SYSTEM IN BEST-FSI

BEST-FSI makes use of unit 5 as its input data file and unit 6 as its output file. In addition to these an extensive set of disk files are used during the execution of the code. For the complete range of analysis used in **BEST-FSI** it is necessary to have 60 simultaneous open files in the system. Not all of these files are necessary for the simpler linear analyses where usually only 1/3 of the total are used. The files are either of sequential or direct access type and are defined as FT** based on IBM terminology.

For the efficient execution of **BEST-FSI**, it is desirable to have at least 8 megabytes of system memory. Additionally, **BEST-FSI** makes extensive use of disk files during execution of the code. While most of these files are of temporary nature, some are required for restart analyses. In any case, it is recommended that workstation-based users have at least 300 MB of disk space free in order to run practical problems.

4.5 SPECIAL FEATURES OF BEST-FSI

4.5.1 DEFINITIONS

The following definitions are used throughout the manual.

Points, Nodes or Nodal Points - are generic names for all points in a data set for which coordinates are defined. These points may be source points and/or geometric points which are used in the boundary and volume discretizations, or they may be used to define a sampling point. All points defined in a data set by the user should have unique node numbering.

Geometric Points - are points used in the geometrical definition of the body of interest. Specifically, geometric points are used in the description of the geometry of a boundary element, or volume cell. Geometric points may or may not be source points.

Source Points - refers to boundary source points, or boundary and volume source points in an analysis. Source points are used in the functional representation of variables across a boundary element, or a volume cell. In a system equation, unknowns are retained at source points.

Functional Nodes - same as source points

Boundary Source Points - are points in a discretization of the boundary surface (or interface) which are used in the functional representation of the field variables across the boundary elements. At every boundary source point (and only at boundary source points) unknowns in the boundary system equation are retained corresponding to the unknown boundary conditions at these points. Likewise, known boundary conditions (implicitly or explicitly defined) are required at these points. Boundary conditions specifications for points other than boundary source points will result in a fatal error. Boundary source points are selected by **BEST-FSI** based on the type of functional variation of the primary variables across the boundary element which is defined in the data set by the user. (see SURF and TYPE cards under **GMR input in Chapter 5)

Volume Source Points - are points in a volume discretization which are used to represent the functional variation of certain variables through the volume of the body via volume cells. These are required only in nonlinear analysis or when the body is subjected to certain types of body forces. In the case of nonlinear analysis, unknowns are retained at volume source points which have to be solved for, along with the unknowns at the boundary source points. This entails writing additional equations at each volume source point. In the case of body forces, the variables are known quantities and additional equations are therefore unnecessary. Volume source points are selected by **BEST-FSI** based on the type of functional variation selected by the user. For the volume cell approach see VOLU and TYPE cards under **GMR input in Chapter 5.

Sampling Points - are (user defined) points in the interior of the body or on the surface of the body for which results are requested. Results at sampling point are calculated after the system equation is solved. Sampling points are input on a separate list (see SAMP card in **GMR input in Chapter 5) and are totally independent of the point list used for boundary and volume discretization. A sampling point may coincide with a boundary discretization point. Sampling points should use unique node numbering.

Volume Cells - Certain analyses require an integration of some variable over all or part of the volume of the body. In this cases the volume is divided into smaller parts called volume cells, where interpolation functions (of some order) are used to represent the variation of the variable to be integrated across the volume cell.

Geometric Modeling Region (GMR) - in a boundary element analysis the body under investigation may be fictitously divided in a number of smaller parts for convienence in mesh modelling and efficiency in computation. Each part is called a geometric modelling region and is modelled as an individual boundary element model. The nodes and elements of each region must match up at common interfaces and are connected by relations defined by the user.

4.5.2 MESH SIZE

Most of the currently available experience of developing mesh for a given problem is based on more than two decades of the finite element or finite difference analyses. It is possible to take only the boundary part of a given finite element mesh system to generate the boundary element mesh system. Unfortunately this often leads to an inefficient BEM analysis because of use of too many elements. In two-dimensional linear problems due to their low computing costs this can easily be tolerated. However, for nonlinear problems where some volume discretization is required care must be exercised to control the number of source point.

5.0 BEST-FSI INPUT

The basic input required by **BEST-FSI** is the definition of **Geometry, Material Properties and Boundary conditions.** While this is the same definition required by a finite element structural analysis program, a somewhat different set of information is required to accomplish the definition for a boundary element program.

The input to **BEST-FSI** is intended to be as simple as possible, consistent with the demands of a general purpose analysis program. Meaningful keywords are used for the identification of data types. Free field input of both keywords and numerical data is permitted, however there are a number of general rules that must be followed.

General Rules for Input Data

1. Upper Case

All alphanumeric input must be provided in upper case.

Proper Usage:

```
**CASE
  TITLE  TRANSIENT FLUID - TEST CASE
  FLUID INCOMPRESSIBLE TRANSIENT
  SYMMETRY QUARTER
```

Improper Usage:

```
  fluid incomp
  SYMMETRY quarter
```

2. Parameter Positioning

Parameters may appear anywhere on an input line, as long as they appear in the proper order and are separated by at least one blank space.

Proper Usage:

```
FLUID INCOMPRESSIBLE STEADY
ELEMENT 1 6 8
```

Improper Usage:

```
FLUIDINCOMPRESSIBLE STEADY
ELEMENT, 1, 6, 8
```

3. Length of Input Line

An input line cannot exceed a maximum of 80 characters including blank spaces.

General Rules for Input Data

4. **Keyword Truncation**

Any keywords that are longer than four letters may be truncated to the first four letters.

Proper Usage:

```
SYMMETRY QUAR
SYMM QUAR
ELEM 1 6 8
```

Improper Usage:

```
SYMMETRY QUA
```

5. **Floating Point Numbers**

Any real parameters may be input in either FORTRAN E or F format, however, the representation used must contain no more than 16 total characters. Additionally, there is a limit of 8 characters to the left of the decimal point.

Proper Usage:

```
EMOD 30.E+7
ALPHA 1.E-06
POINTS
  0.004 1.110 0.0
```

Improper Usage:

```
EMOD 300000000.0
ALPHA 1.-6
POINTS
  4.0-3 1.110 0
```

General Rules for Input Data

6. **Comments**

Comments can be inserted in the data file by placing a dollar sign ($) anywhere on an input line. The remainder of that input line is then ignored by the **BEST-FSI** input processor.

Proper Usage:

```
ELEMENT 1 6 8 $ ELEMENTS ON THE OUTER RIM
$
$ MODIFIED 03/08/88 GFD
  POINTS 25 26 27
```

7. **Blank Lines**

Blank Lines can be inserted anywhere in the data file and are useful for aesthetic purposes.

8. **Units**

A consistent system of units must be used for input of all types (material properties, geometry, boundary conditions, time steps). Output will be in the same consistent system of units. The selection of appropriate units is the user's responsibility.

9. **** Keywords**

Certain keywords are prefixed by the symbol **. These identify the beginning of a block of data of a particular type, and serve to direct the program to the appropriate data processing routine. There should be no blank spaces between the ** symbol and the pertinent keyword. Additionally, the ** data blocks must appear in the following specific order:

**CASE
**MATERIAL
**GMR
**INTERFACE
**BCSET
**BODY

There may be multiple data blocks of each type, except for the **CASE block.

General Recommendations for Input Data

1. **Ordering of Input Items**

   While there is some flexibility in the ordering of lines within a **BEST-FSI** data set, it is strongly recommended that the user follow the order provided in the manual. Examples of proper ordering are provided throughout this chapter.

2. **Documenting Data Sets**

   The $ keyword is provided to permit comments anywhere in the input data set. This should be used generously to fully document the analysis. Blank spaces can also be used to improve readability. The format, displayed in the examples of this chapter and in Section 6.0, is recommended.

General Limits of **BEST-FSI**

It should be noted that there are certain limits which must be observed in the preparation of input for **BEST-FSI** . These limits are of two main types:

1 - Limits on the maximum number of entities of various types within a single analysis.

2 - Limits on the user specified numbering of certain entities.

The present limits are summarized below. It is anticipated that certain of these limits may be relaxed in future versions of **BEST-FSI.**

ENTITY*	LIMIT
GLOBAL PARAMETERS	
total geometric modeling regions	15
total points (including non-source points)	3000
total boundary source points	1200
total volume source points for fluids	1200
total boundary elements	600
enclosing elements	100
cyclic symmetry interfaces	20
REGION (GMR) PARAMETERS	
surfaces in any region	15
points in any region	1000
boundary source points in any region	600
volume source points in any region	600
boundary elements in any region**	300
volume cells in any region	200

ENTITY*	LIMIT
OTHER PARAMETERS	
table points	20
temperature points for material properties	21
USER SPECIFIED NUMBERING	
points	99999
elements	99999

* Definition of the terminology used in this table can be found in Section 4.5.

** Total boundary elements in a region include user specified boundary elements plus elements artificially created in symmetric regions when the symmetry option is invoked.

Individual Data Items

The remainder of this chapter provides detailed information on each of the data items available within **BEST-FSI**. The individual items are grouped in sections, under the associated ** keyword, as follows:

5.1 CASE CONTROL INFORMATION (**CASE)
5.2 MATERIAL PROPERTY DEFINITION (**MATE)
5.3 GEOMETRY DEFINITION (**GMR)
5.4 INTERFACE DEFINITION BETWEEN SUBREGIONS (**INTE)
5.5 BOUNDARY CONDITION DEFINITION (**BCSE)
5.6 BODY FORCE DEFINITION (**BODY)

5.1 CASE CONTROL

This input section provides **BEST-FSI** with information controlling the overall execution. It provides the title and determines which of the major program branches will be executed. It also defines the times at which solutions of the given problem are to be evaluated. This section must be input exactly once for each analysis and must be input before any other data.

A list of keywords recognized in the case control input are given below, and a detailed description follows. It is recommended that the user supply the relevant keywords in the order provided by this list.

SECTION	KEYWORD	PURPOSE
5.1.1	Case Control Input Card	
	**CASE	Start of case control input
5.1.2	Title	
	TITL	Title of job
5.1.3	Times for Output	
	TIME	Times of solution output (static and steady-state analysis)
	TIME STEP	Time step for transient solution algorithms
5.1.4	Dimensionality of the Problem	
	PLAN	Plane strain flag
5.1.5	Type of Analysis	
	FLUI	Fluid dynamic analysis
5.1.6	Analysis Type Modifiers	
	CONV	Convective form of kernel functions
	THER	Thermoviscous fluid dynamics
	BUOY	Include buoyancy in thermoviscous fluid dynamics

SECTION	KEYWORD	PURPOSE
5.1.7	Algorithm Control	
	ITER	Iterative algorithm
	NEWT	Newton-Raphson algorithm
	INCR DENS	Incremental density algorithm for FLUI only
	RECU	Recurring initial condition algorithm for FLUI only
	TOLE	Convergence tolerance
	MAXI	Maximum number of iterations for nonlinear algorithms
5.1.8	Geometric and Loading Symmetry Control	
	SYMM HALF	Symmetry about Y-Z plane
	SYMM QUAR	Symmetry about X-Z and Y-Z planes
5.1.9	Restart Facility	
	REST WRIT	Save integration files for future runs
	REST READ	Use integration files from previous run
	REST VELO	Restart fluid dynamics run from last solution
5.1.10	Output Options	
	ECHO	Produce echo of input data
	PRIN BOUN	Printout displacement and traction results
	PRIN NODA	Print boundary displacement, stress, strain at nodal points
	PRIN LOAD	Print load calculation
	PRIN ALL	Print maximum printed output file
	PRIN LIMI	Print current BEST-FSI limits
	PRIN FEAT	Print current implementation status of BEST-FSI special features
	PATR	Produce PATRAN result files
5.1.11	Miscellaneous Control Options	
	CHEC	Check input data only
	FILE	Specify directory for creation and storage of scratch files

5.1.1 CASE CONTROL INPUT CARD

****CASE**

Status - REQUIRED

Full Keyword - ****CASE** control

Function - Identifies the beginning of the case control input section.

Input Variables - NONE

Additional Information - NONE

Examples of Use -

1. Request a plane stress elastic analysis.

```
**CASE
  TITLE  PLANE STRESS ANALYSIS OF A BAR
  PLANE STRESS
  ELASTIC
```

2. Request a three-dimensional steady-state heat transfer analysis.

```
**CASE
  TITLE  HEAT CONDUCTION IN A MOLD
  HEAT
```

5.1.2 TITLE

TITL CASETITLE

Status - REQUIRED

Full Keyword - TITLE

Function - Defines title for analysis.

Input Variables -

CASETITLE (Alphanumeric) - REQUIRED - 72 chars. max. length

Additional Information - NONE

Examples of Use -

1. Describe the analysis.

```
**CASE
  TITLE  TURBINE BLADE A7311 - THERMOELASTIC ANALYSIS
  ELASTIC
```

5.1.3 TIMES FOR OUTPUT

TIME T1 T2 T3 ... TN

Status - OPTIONAL

Full Keyword - TIMES

Function - Identifies times at which output is required (only for static analysis).

Input Variables -

T1 (Real) - REQUIRED

T2 ... TN (Real) - OPTIONAL

Additional Information -

This input may be continued on more than one card, if required. Each card must begin with the keyword TIME. A maximum of twenty output times may be selected. A minimum of one output time must be chosen.

This card is only functional for static analysis. The 'TIME STEP' card (see next page) is used for transient analysis.

Acoustic Eigenfrequency analysis and Free Vibration analysis do not require a 'TIME' or a 'TIME STEP' card.

Examples of Use -

1. Conduct an elastic analysis at times 1.0, 2.5 and 6.0 and output the results.

```
**CASE
  TITLE  ROTOR - ELASTIC ANALYSIS
  TIMES 1.0 2.5 6.0
  ELASTIC
```

TIME STEP NSTEP DELTA

Status - OPTIONAL (required for transient analysis algorithms)

Full Keyword - TIME STEP

Function - Identifies the number of time steps in a transient solution algorithm and the size of the time steps.

Input Variables -

NSTEP (Integer) - REQUIRED

Sets the number of time steps for which the transient analysis is to be carried out.

DELTA (Real) - REQUIRED

Defines the size of the time step.

Additional Information -

In the present version, only a constant time step size (DELTA) is permitted.

Examples of Use -

1. Conduct a transient elastodynamic analysis of a spherical tank using a linear time variation of field variables.

```
**CASE
  TITLE  SPHERICAL TANK - SUDDEN PRESSURIZATION
  TRANSIENT
  TIME STEP   10  0.01
```

5.1.4 DIMENSIONALITY OF THE PROBLEM (Default is 3-D geometry)

PLAN ETYPE

Status - REQUIRED

Full Keyword - **PLANE**

Function - Identifies a two-dimensional problem.

Input Variables -

ETYPE (Alphanumeric) - OPTIONAL

Allowable values are STRA.

STRAin - specifies a plane strain problem.

Additional Information -

If ETYPE is not specified, STRAIN is assumed.

Examples of Use -

1. Request a plane strain elastic analysis of a dam.

```
**CASE
  TITLE  KOYNA DAM - PLANE STRAIN ELASTIC ANALYSIS OF A DAM
  PLANE STRAIN
  ELASTIC
```

2. Request a two-dimensional steady-state heat conduction analysis of a cylinder.

```
**CASE
  TITLE  CYLINDER - HEAT CONDUCTION
  PLANE
  HEAT
```

5.1.5 TYPE OF ANALYSIS

FLUI ATYPE BTYPE

Status - OPTIONAL

Full Keyword - FLUID

Function - Identifies a fluid dynamics analysis.

Input Variables -

ATYPE (Alphanumeric) - OPTIONAL (Default is INCO)

Allowable values are INCO

INCOMPRESSIBLE - Identifies a viscous, incompressible fluid analysis

BTYPE (Alphanumeric) - OPTIONAL (Default is STEADY)

STEADY - Identifies a steady-state analysis

TRANSIENT - Identifies a transient analysis

Additional Information -

In the present version, only two-dimensional incompressible viscous flow is available.

An incompressible thermoviscous flow may be selected by also including a THERMAL card in case control.

Examples of Use -

1. Conduct a steady viscous fluid analysis for flow around a cylinder. Use ten psuedotime steps with a maximum of five iterations per step.

```
**CASE
  TITLE  STEADY FLOW AROUND A CYLINDER
  PLANE
  FLUID INCOMPRESSIBLE STEADY
  TIME STEP   10  1.0
  NEWTON
  MAXI  5
  INCREMENT DENSITY
  RESTART WRITE
```

2. Perform transient thermoviscous analysis for flow past a turbine blade.

```
**CASE
  TITLE  TRANSIENT FLOW PAST A TURBINE BLADE
  PLANE
  FLUID INCOMP TRANSIENT
  TIME STEP  20  0.0120
  THERMAL
  NEWTON
  MAXI  6
  RECURRING
```

3. Examine steady Stokes flow in a converging channel.

```
**CASE
  TITLE  CONVERGING CHANNEL
  PLANE
  FLUID STEADY INCOMP
  TIME STEP  1  1.0
  ITERATIVE LINEAR
  MAXI 1
  RESTART WRITE
```

5.1.6 ANALYSIS TYPE MODIFIERS

CONV

Status - OPTIONAL

Full Keyword - `CONVECTIVE`

Function - Selects the convective form of the kernel functions for two-dimensional steady-state heat transfer and fluid dynamics.

Input Variables - NONE

Additional Information -

When this option is selected, the uniform free stream velocity must be specified on a VREF card in the **GMR section for each region.

In the current version, this option is only available for PLANE analysis in conjunction with FLUID INCOMP STEADY case control cards.

If the actual velocity field is approximately equal to the free stream velocity, then volume integration may not be required with this option. A boundary-only analysis can be conducted.

Examples of Use -

1. Perform convection heat transfer analysis of the region exterior to an airfoil.

```
**CASE
  TITLE AIRFOIL - CONVECTIVE HEAT TRANSFER
  PLANE
  HEAT STEADY
  CONVECTIVE
  RESTART WRITE
```

THER

Status - OPTIONAL

Full Keyword - THERMAL

Function - In conjunction with the FLUI card, this selects a thermoviscous fluid dynamics analysis.

Input Variables - NONE

Additional Information -

This keyword is only applicable for two-dimensional fluid dynamics analysis.

When this option is selected, a heat conduction analysis is performed along with the viscous flow analysis. As a result, each source point has three degrees of freedom (V_1,V_2,T) for a two-dimensional problem.

Examples of Use -

1. Perform a thermoviscous flow analysis in a channel.

```
**CASE
  TITLE CHANNEL - THERMOVISCOUS FLOW
  PLANE
  FLUID INCOMP TRANSIENT
  TIME STEP  4 0.05
  THERMAL
  NEWTON SKIP 5
  MAXI  10
```

BUOY TYPE

Status - OPTIONAL

Full Keyword - **BUOYANCY**

Function - In conjunction with both the FLUI and THER cards, this permits the inclusion of buoyancy terms based upon the Boussinesq approximation.

Input Variables -

TYPE (Alphanumeric) - OPTIONAL

Allowable value is KERN.

KERN - The linearized buoyancy effect is included in the kernel functions.

Additional Information -

If the keyword KERN is absent, then the entire buoyancy contributionis introduced as a body force through the volume, and volume cells must be included.

In either case, the gravitational acceleration must be specified through an inertial body force (INER) definition.

Buoyancy is only available for steady incompressible thermoviscous flow.

Examples of Use -

1. Examine the buoyancy-driven flow in a lake.

```
**CASE
  TITLE  LAKE ERIE (THERMALLY-INDUCED FLOW)
  FLUID INCOMP STEADY
  THERMAL
  BUOYANCY KERNEL
```

5.1.7 ALGORITHM CONTROL

ITER

Status - OPTIONAL

Full Keyword - ITERATIVE

Function - Selects the iterative algorithm.

Input Variables - NONE

Additional Information -

The iterative algorithm is generally not recommended for problems involving a high degree of nonlinearity.

Examples of Use -

1. Examine unsteady Navier-Stokes flow around an airfoil at low Reynolds number.

```
**CASE
  TITLE  AIRFOIL G-45 (NAVIER-STOKES FLOW)
  FLUID INCOMP
  TIME STEP  15 0.015
  ITERATIVE
  MAXI  10
```

NEWT ITYPE NSKIP

Status - OPTIONAL

Full Keyword - **NEWTON-RAPHSON**

Function - Selects the Newton-Raphson algorithm.

Input Variables -

ITYPE (Alphanumeric) - OPTIONAL

Allowable value is MODI.

MODI - Selects the Modified Newton-Raphson algorithm

A full Newton-Raphson algorithm is assumed if ITYPE = MODI is not input.

NSKIP (Integer) - OPTIONAL (default is NSKIP = 1)

Additional Information -

The Newton-Raphson algorithm is recommended for all nonlinear analysis.

In some cases, the use of the Modified Newton-Raphson algorithm can reduce analysis cost for nonlinear problems, however convergence is slower than for the full Newton-Raphson approach.

Setting NSKIP = 1 is equivalent to a full Newton-Raphson approach.

Examples of Use -

1. Analyze viscous flow in a container, selecting a modified Newton-Raphson algorithm.

```
**CASE
  TITLE  CONTAINER - VISCOUS  FLOW
  FLUID INCOMP STEADY
  TIME STEP  4  1.0
  NEWTON MODI 4
  MAXI  20
  INCREMENT DENSITY
  RESTART WRITE
```

INCR DENS

Status - OPTIONAL

Full Keyword - `INCREMENT DENSITY`

Function - Selects an incremental density algorithm for incompressible viscous fluid dynamics.

Input Variables - NONE

Additional Information -

This option is only applicable for incompressible viscous fluid dynamics, and typically only for steady-state problems. Often the incremental density algorithm provides a convenient method for slowly building toward a desired Reynolds number.

The density values must be defined as a function of time with a convective body force data set. See the **BODY section.

Examples of Use -

1. Analyze the thermoviscous flow of a hot fluid over a gradual step. Increment the fluid density to achieve the desired Reynolds number.

```
**CASE
  TITLE  FLOW OVER A STEP RE=50
  FLUID INCOMP STEADY
  TIME STEP  8  1.0
  NEWTON
  INCREMENT DENSITY
  MAXI  10
  RESTART WRITE
```

RECU

Status - OPTIONAL

Full Keyword - `RECURRING-INITIAL-CONDITION`

Function - Selects a recurring initial condition algorithm for transient viscous fluid dynamics analysis.

Input Variables - NONE

Additional Information -

Two approaches are available for transient fluid dynamics problems. The default is the convolution approach which requires integration at each time step. This is preferred for linear (Stokes flow) analysis. However, if the RECU card is present then the recurring initial condition approach is utilized. In this case, the entire fluid domain must be discretized.

A combined recurring initial condition and convolution approach is also possible. To trigger this option, the user should simply include the RECU keyword. Then, in each region for which the recurring initial condition approach is desired, complete volume discretization is required. The remaining regions, which must be void of volume cells, will employ a convolution approach. This combined approach is particularly attractive when a large portion of the flow field is linear.

Examples of Use -

1. Perform a transient viscous fluid dynamic analysis for flow in a diverging channel.

```
**CASE
  TITLE  CHANNEL - CASE 2 (TRANSIENT ANALYSIS)
  FLUID INCOMP STEADY
  TIME STEP  10  0.25
  NEWTON SKIP 2
  MAXI  10
  RECURRING
  RESTART WRITE
```

TOLE RTOL

Status - OPTIONAL

Full Keyword - TOLERANCE

Function - Sets the convergence tolerance for nonlinear algorithms.

Input Variables -

RTOL (Real) - REQUIRED

Defines the convergence tolerance.

Additional Information -

For fluids, convergence is tested at the end of the i^{th} iteration by computing

$$DNORM = \sum_{n=1}^{N} \frac{|{}_{i}V_n - {}_{i-1}V_n|^2}{|{}_{i-1}V_n|^2}$$

where N is the total number of volume source point.

Convergence is assumed when DNORM $\leq$ RTOL. If the TOLE card is not included in case control, RTOL defaults to 0.005.

Examples of Use -

1. Tighten the convergence tolerance for a problem of thermoviscous flow past an airfoil.

```
**CASE
  TITLE  AIRFOIL - THERMOVISCOUS STEADY FLOW
  FLUID STEADY INCOMP
  TIME STEP  8  1.0
  THERMAL
  NEWTON
  MAXI  8
  TOLERANCE 1.E-4
```

MAXI NITER

Status - OPTIONAL

Full Keyword - **MAXIMUM (ITERATION)**

Function - Define the maximum number of iterations per time step for nonlinear algorithms.

Input Variables -

NITER (Integer) - REQUIRED

Sets the number of maximum iterations per time step.

Additional Information -

The default is a maximum of 20 iterations.

Examples of Use -

1. Fluid dynamic example with a limit of 10 iterations.

```
**CASE
  TITLE  STEADY FLOW AROUND A CYLINDER
  FLUID INCOMPRESSIBLE STEADY
  TIME STEP  10  1.0
  NEWTON
  INCREMENT DENSITY
  TOLERANCE  0.02
  MAXI  10
```

5.1.8 GEOMETRIC AND LOADING SYMMETRY CONTROL

SYMM STYPE

Status - OPTIONAL

Full Keyword - SYMMETRY

Function - Identifies a problem with geometric and loading symmetry.

Input Variables -

STYPE (Alphanumeric) - REQUIRED

Allowable values are HALF, QUAR, and OCTA.

HALF - Half symmetry, about the Y-Z plane (or about the $R-\theta$ plane in axisymmetric analysis).

QUAR - Quarter symmetry, about the X-Z and Y-Z planes.

Additional Information -

To model the problem geometry, in all cases, use the part of the geometry which is on the positive side of the axis (axes) of symmetry.

If the SYMM card is used the plane of symmetry does not have to be modelled, and therefore, boundary elements should not appear on the plane of symmetry (see the figure on the following page).

The use of the SYMM card automatically invokes the condition of zero velocity (and zero flux) on and perpendicular to the plane of symmetry. Therefore velocity (and/or flux) in the perpendicular direction does not have to be set to zero at the plane or at any other point for the purpose of preventing (arbitrary) rigid-body motion (in this direction) as is usually required.

Examples of Use -

1. Perform an elastic analysis on a hollow cylinder utilizing a model of only the first (positive) quadrant.

```
**CASE
  TITLE  HOLLOW CYLINDER WITH INTERNAL PRESSURE
  ELASTIC
  SYMMETRY QUAR
```

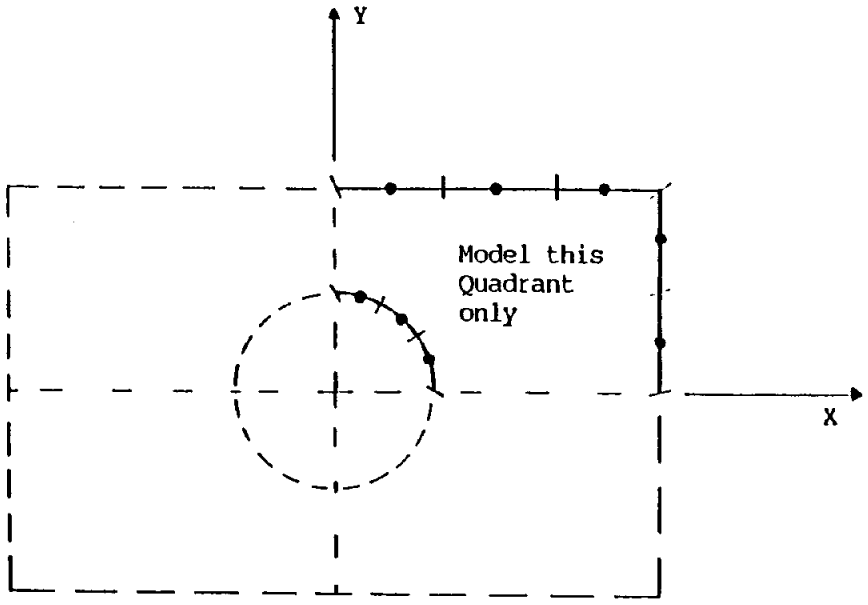

Figure for **CASE: SYMM card
Two-dimensional Quarter symmetry model

5.1.9 RESTART FACILITY

REST RTYPE ISTEP

Status - OPTIONAL

Full Keyword - **RESTART**

Function - Enables the restart facility.

Input Variables -

RTYPE (Alphanumeric) - REQUIRED

Allowable values are WRIT, READ, HOLE, SOLV, GMR, VELO

WRITe - Saves all of the integration files generated during the current run for later reuse.

READ - Bypasses the integration phase for the current run. Instead, the integration files from a previous run are utilized.

VELO - Restart a fluid dynamics from a previously determined solution.

ISTEP (Integer) - REQUIRED only if RESTART VELO is specified.

Defines the time step number of a solution from a previous fluid dynamics run, which will be used as the initial state for the current analysis.

Additional Information -

Integration is generally the most expensive part of any boundary element analysis. Consequently, when the same model is to be run with several sets of boundary conditions, the restart facility should be used.

In the case of linear problems, a complete analysis must first be run with RESTart WRITe specified. The files FT031, FT032, FT033, FT034, FT035, FT036, FT037, FT038 and FT039 are then retained after completion of the run. These files contain all the integration coefficients that were computed. Subsequent runs can then be made, with different sets of boundary conditions, by using RESTart READ. In this case, the integration phase will be skipped. Instead; the integration coefficients will be read from the files FT031, FT032, FT033, FT034, FT035, FT036, FT037, FT038 and FT039. Additional files are retained for nonlinear analysis.

Geometry and material properties must be the same for both the RESTart WRITe and RESTart READ data sets. However, no checking is done by **BEST-FSI**. This is the user's responsibility.

The restart facility is not available for transient analyses.

RESTART VELO is only available for fluid dynamics. It is the user's responsibility to ensure that the requested solution exists in the restart file FT080,

which must have been saved with a RESTART WRITE or READ during a previous analysis.

Generally, RESTART VELO is used in conjunction with either RESTART WRITE or RESTART READ.

Examples of Use -

1. Save the integration files generated during an elastic analysis of an axle.

```
**CASE
  TITLE  AXLE - LOAD CASE 1A
  TIMES  1.0
  ELASTIC
  RESTART WRITE
```

2. Rerun an elastic analysis of the same axle with a different set of boundary conditions by using existing integration files.

```
**CASE
  TITLE  AXLE - LOAD CASE 1B
  TIMES  1.0
  ELASTIC
  RESTART READ
```

3. Restart an incompressible fluid dynamics analysis using the solution obtained during the third time step of the previous run.

```
**CASE
  TITLE  DRIVEN CAVITY - STEADY RE= 1000
  FLUID INCOMP STEADY
  TIME STEP  5  1.0
  NEWTON SKIP 2
  MAXI  10
  RESTART READ
  RESTART VELO 3
  PRINT INTERIOR VELO
```

5.1.10 OUTPUT OPTIONS

ECHO

Status - OPTIONAL

Full Keyword - **ECHO**

Function - Requests a complete echo print of all card images in the input data set.

Input Variables - NONE

Additional Information - Default is no echo print.

Examples of Use -

1. Request a plane strain elastic analysis with an echo of the input data set.

```
**CASE
  TITLE  DAM - PLANE STRAIN ASSUMPTION
  PLANE STRAIN
  ELASTIC
  RESTART WRITE
  ECHO
```

PRIN PTYPE

Status - OPTIONAL

Full Keyword - `PRINTOUT-CONTROL`

Function - Requests specific printed output.

Input Variables -

PTYPE (Alphanumeric) - REQUIRED

Allowable values are BOUN, NODA, LOAD, ALL, LIMI, and FEAT.

BOUN - For printing the displacements and tractions, or corresponding quantities such as velocity, temperature, pressure, and flux at all boundary source points

NODA - For printing the displacements, stresses, and strains at all geometry nodes on the boundary. (available only for linear elasticity, and consolidation. A similar nodal table is also available for fluid dynamics.)

LOAD - For printing the resultant load value on each boundary element and the total load equilibrium of each region, excluding resultant body force.

ALL - For printing BOUN, NODA, and LOAD information with a single request.

LIMI - To printout the current limits of BEST-FSI.

FEAT - To printout a table reporting the current implementation status of BEST-FSI special features in file "BEST-FSI.FEATURES". An integer value may be included after the keyword FEAT (e.g. PRINT FEATURES 80) to indicate the number of lines per page used in the table. The default is 66 which corresponds to the number of lines printed per page by a standard line printer.

Additional Information -

For printing two or more types of output, a separate PRIN request must be included for each type.

If a PRIN, BOUN, NODA or LOAD request does not appear in the case control input then all three types of output (BOUN, NODA, and LOAD) will be printed by default.

Examples of Use -

1. In the elastic analysis of a rotor, print out the resultant boundary element loads.

```
**CASE
  TITLE  ROTOR - ELASTIC ANALYSIS
  TIMES  1.0    2.5    6.0
  ELASTIC
  PRINT LOAD
```

PATR

Status - OPTIONAL

Full Keyword - PATRAN

Function - Requests the generation of PATRAN post-processing result files.

Input Variables - NONE

Additional Information -

A Patran INTERFACE NEUTRAL file is created for MODEL INPUT of BEST-FSI geometry data into Patran. This file is called PATRAN.GEOM.

Upon completion of each time step in an analysis, several files of the form PATRAN.XXX.n are created for PATRAN post-processing. The parameter n is the time step number, and XXX is any of the following:

NOD - Boundary nodal temperatures or pore pressures in the format of a PATRAN Nodal Results Data File

DIS - Boundary nodal displacements or velocities in the format of a PATRAN Displacement Results Data File

ND1 - Interior point displacements/velocities/temperatures/pore pressures in the format of a PATRAN Nodal Results Data File

ND2 - Interior point stresses in the format of a PATRAN Nodal Results Data File

NDS - Boundary nodal displacements, stresses and strains in the format of a PATRAN Nodal Results Data File

ELB - Boundary element velocities, stresses and strain rates in the format of a PATRAN Beam Results Data File

Column assignments within each file are defined in Table 5.1.1 by analysis type.

Examples of Use -

1. Create PATRAN result files for the steady-state thermoelastic response of a turbine blade.

```
**CASE
  TITLE  TURBINE BLADE A7311 - THERMOELASTIC
  CTHERMAL STEADY
  RESTART READ
  ECHO
  PATRAN
```

TABLE 5.1.1

PATRAN Post-processing File Column Definition

GENERAL FILE DEFINITION:

Filename	PATRAN File Type	Contents
PATRAN.NOD.n	NODAL	Boundary Source Points
PATRAN.DIS.n	DISPLACEMENT	Boundary Source Points
PATRAN.ND1.n	NODAL	Volume Source Points and Sampling Points
PATRAN.ND2.n	NODAL	Volume Source Points and Sampling Points
PATRAN.NDS.n	NODAL	Boundary Source Points
PATRAN.ELB.n	BEAM	Boundary Elements

SPECIFIC FILE DEFINITION:

NOMENCLATURE

θ: temperature
p: pore pressure
u_i: displacement
t_i: traction
v_i: velocity
q_i: flux
σ_{ij}: stress
ϵ_{ij}: strain

Analysis Type	Filename	No. of Dimensions	Columns 1 (7 [13	2 8 14	3 9 15	4 10 16	5 11 17	6 12) 18]
FLUID (Viscous)	PATRAN.DIS.n	2	v_1	v_2				
	PATRAN.ND1.n	2	v_1	v_2				
	PATRAN.NDS.n	2	v_1	v_2	$\frac{\partial v_1}{\partial x_1}$	$\frac{\partial v_2}{\partial x_2}$	$\frac{\partial v_1}{\partial x_2}$	$\frac{\partial v_2}{\partial x_1}$
			(ω	σ_{11}	σ_{22}	σ_{12}	p)	
	PATRAN.ELB.n	2	v_1	v_2	t_1	t_2	$\frac{\partial v_1}{\partial x_1}$	$\frac{\partial v_2}{\partial x_2}$
			($\frac{\partial v_1}{\partial x_2}$	$\frac{\partial v_2}{\partial x_1}$	ω	σ_{11}	σ_{22}	σ_{12})
			[p]					
FLUID (Thermoviscous)	PATRAN.NOD.n	2	θ					
	PATRAN.DIS.n	2	v_1	v_2				
	PATRAN.ND1.n	2	v_1	v_2	θ			
	PATRAN.NDS.n	2	v_1	v_2	θ	$\frac{\partial v_1}{\partial x_1}$	$\frac{\partial v_2}{\partial x_2}$	$\frac{\partial v_1}{\partial x_2}$
			($\frac{\partial v_2}{\partial x_1}$	ω	$\frac{\partial \theta}{\partial x_1}$	$\frac{\partial \theta}{\partial x_2}$	σ_{11}	σ_{22})
			[σ_{12}	p]				
	PATRAN ELB.n	2	v_1	v_2	θ	t_1	t_2	q
			($\frac{\partial v_1}{\partial x_1}$	$\frac{\partial v_2}{\partial x_2}$	$\frac{\partial v_1}{\partial x_2}$	$\frac{\partial v_2}{\partial x_1}$	ω	$\frac{\partial \theta}{\partial x_1}$)
			[$\frac{\partial \theta}{\partial x_2}$	σ_{11}	σ_{22}	σ_{12}	p]	

5.1.11 MISCELLANEOUS CONTROL OPTIONS

CHEC

Status - OPTIONAL

Full Keyword - CHECK

Function - Perform only input data checking, and printout an error summary. No analysis is performed.

Input Variables - NONE

Additional Information -

This option is often useful for checking the input data for a new model. In addition to the error summary, all of the relevant material, geometry and boundary condition information is processed and printed in tabular form. Of particular interest is the identification of the boundary and volume source points, since these are determined by the program based upon the element and cell functional variation.

Examples of Use -

1. Check the input data for a thermoelastic turbine blade model.

```
**CASE
  TITLE  TURBINE BLACE A7311 - THERMOELASTIC
  CTHERMAL STEADY
  RESTART WRITE
  CHECK  $  DATA CHECKING ONLY
  STORE SINGLE
```

FILE DNAME

Status - OPTIONAL

Full Keyword - `FILE-CONTROL`

Function - Specifies the directory in which the scratch files (FTNNN) reside during execution of BEST-FSI

Input Variables -

DNAME (Alphanumeric) - REQUIRED

Allowable values are DIRNAMEALL or DIRNAMEFTNNN

DIRNAMEALL - All scratch files (FTNNN) all be created, accessed and stored in directory specified by DIRNAME.

DIRNAMEFTNNN - Scratch file (FTNNN) will be created, accessed and stored in directory specified by DIRNAME.

Additional Information -

Default storage location for scratch files (FTNNN) is the current directory BEST-FSI is being run from

FT file numbers have to be specified in a 3 digit format. For example FT009 is correct while FT9 or FT09 are incorrect.

When specifying an individual FT file, only that file will be created in the specified directory, the rest will be created in the current directory.

FILE directive can be used multiple times, e.g.

```
FILE /home/scr1/ALL
FILE /home/temp/FT035
```

will cause all FT files except FT035 to be created in /home/scr1 directory. But if a combination such as

```
FILE /home/temp/FT035
FILE /home/scr1/ALL
```

is used, this will cause all FT files to be created in /home/scr1 directory.

Examples of Use -

1. Specify the directory /home/scr1 to receive FT037 and /home/scr2 to receive FT038. The rest of the FT files will be created in the current directory (UNIX systems).

```
**CASE
  TITLE  MOLD COMPONENT 6 - STEADY CONDITIONS
  HEAT
  PRECISION LOW
```

```
NEUTRAL RESULTS
FILE  /home/scr1/FT037
FILE  /home/scr2/FT038
```

2. Specify the directory /home/scr1 to receive all FT files except FT037, which will be created in /home/scr2 directory (UNIX systems).

```
**CASE
  TITLE  MOLD COMPONENT 6 - STEADY CONDITIONS
  HEAT
  PRECISION LOW
  NEUTRAL RESULTS
  FILE  /home/scr1/ALL
  FILE  /home/scr2/FT037
```

5.2 MATERIAL PROPERTY DEFINITION

This input section defines the linear and, when required, the nonlinear properties of the various materials used in an analysis. A complete set of material property input must be provided for each material used. At least one set must be input for every analysis. A consistent set of units must be used for all properties.

A list of keywords recognized in the Material input are given below and a detailed description follows.

SECTION	KEYWORD	PURPOSE
5.2.1 Material Property Input Card		
	**MATE	Beginning of a material property input set
5.2.2 Material Identification		
	ID	Identifier of a material type
5.2.3 Mass Parameter		
	DENS	material mass density
5.2.4 Isotropic Elastic Parameters		
	EMOD	Young's modulus
	POIS	Poisson's ratio
5.2.5 Isotropic Thermal Parameters		
	COND	conductivity of material
	SPEC	specific heat
	BETA	buoyancy constant for fluid

SECTION	KEYWORD	PURPOSE
5.2.6 Isotropic Viscous Properties		
	VISC	viscosity for fluid dynamics

Note: Refer to the following table for a list of required material properties corresponding to a particular type of analysis.

A list of material properties required for different types of analysis are defined below:

REQUIRED MATERIAL PROPERTIES

TYPE OF ANALYSIS	MATERIAL PROPERTIES
1. Isotropic Elastic Stress Analysis	EMOD, POIS (TEMP: optional) (ALPH: if thermal body force is present) (DENS: if centrifugal body force is present) (DENS: if inertial body force is present)
2. Concurrent Thermoelastic Analysis	
2a. Steady-state	TEMP, EMOD, POIS, ALPH, COND
2b. Transient (Quasistatic)	TEMP, EMOD, POIS, ALPH, COND, DENS, SPEC
3. Viscous Fluid Dynamic Analysis	
3a. Steady-state	VISC, DENS
3b. Transient	VISC, DENS
4. Thermoviscous Fluid Dynamic Analysis	
4a. Steady-state	VISC, DENS, COND (BETA: if buoyancy force is present)
4b. Transient	VISC, DENS, COND, SPEC

5.2.1 MATERIAL PROPERTY INPUT CARD

****MATE**

Status - REQUIRED

Full Keyword - `MATERIAL PROPERTY`

Function - Signals the beginning of a material property definition.

Input Variables - NONE

Additional Information -

A complete set of material property input must be provided for each material used.

All materials for a problem must be defined before any geometry is specified.

Examples of Use -

1. Define the elastic material properties for a carbon steel.

```
**MATE
  ID STEEL
    EMOD   30.3+6
    POIS   0.30
```

5.2.2 MATERIAL IDENTIFICATION

ID NAME

Status - REQUIRED

Full Keyword - ID

Function - Provides an identifier for a set of material properties related to a given material, thereby allowing later reference to the material property definition.

Input Variables -

NAME (Alphanumeric) - REQUIRED

Additional Information -

The specified name must be unique compared to all other material names included in the problem.

The NAME must be eight or less alphanumeric characters. Blank characters embedded within the NAME are not permitted.

Examples of Use -

1. Define the thermal properties for an aluminum alloy 3003.

```
**MATERIAL
  ID ALUM3003
    COND   25.0
    DENS   0.1
    SPEC   2000.
```

5.2.3 MASS PARAMETERS

DENS DEN1

Status - (see required material property table)

Full Keyword - DENSITY

Function - Defines the material mass density.

Input Variables -

DEN1 (Real) - REQUIRED

Additional Information - NONE

Examples of Use -

1. Define material properties for a free vibration analysis.

```
**MATE
  ID  STEEL
    EMOD   30.E+6      $      PSI
    POIS   0.30
    DENS   7.324E-4
```

5.2.4 ISOTROPIC ELASTIC PARAMETERS

EMOD EM1

Status - (see required material property table)

Full Keyword - EMODULUS

Function - Defines values of Young's modulus

Input Variables -

EM1 (Real) - REQUIRED

Additional Information - NONE

Examples of Use -

1. Specify a elastic material.

```
**MATERIAL
  ID  MAT1
    EMOD      1.E6
    POIS      0.36
    DENS      0.15
```

POIS POI

Status - (see required material property table)

Full Keyword - POISSON

Function - Defines the (temperature independent) value of Poisson's ratio.

Input Variables -

POI (Real) - REQUIRED

Allowable values - $-1.0 < POI \leq 0.5$

Additional Information - NONE

Examples of Use -

1. Specify room temperature elastic properties of carbon steel.

```
**MATE
  ID  STEEL
    EMOD  30.E6
    POIS  0.30
```

5.2.5 ISOTROPIC THERMAL PARAMETERS

COND CD1

Status - REQUIRED (for concurrent thermoelastic, thermoviscous fluid dynamic, or heat conduction analysis)

Full Keyword - CONDUCTIVITY

Function - Defines the isotropic conductivity.

Input Variables -

CD1 (Real) - REQUIRED

Additional Information - NONE

Examples of Use -

1. Specify thermal properties of aluminum for steady-state heat conduction.

```
**MATE
  ID  ALUM
    CONDUCTIVITY  25.0
```

1. Specify thermoelastic properties for a quasistatic analysis.

```
**MATE
  ID  M200
    TEMP  500.0
    EMOD  1.0E+6
    POIS  0.24
    ALPH  1.E-5
    COND  5.86
    DENS  0.05
    SPEC  215.
```

SPEC SP1

Status - REQUIRED (for transient concurrent thermoelasticity, thermoviscous fluid dynamic, or heat conduction)

Full Keyword - SPECIFIC

Function - Defines the specific heat.

Input Variables -

SP1 (Real) - REQUIRED

Additional Information -

The user must be careful in selecting appropriate units for specific heat. The CONDuctivity divided by the product of DENSity times SPECific equals the diffusivity. The diffusivity must have units of (length**2)/time.

Examples of Use -

1. Material model for transient heat conduction.

```
**MATE
  ID  STEEL
    COND   5.8      $      IN.-LB./(SEC.IN.F)
    DENS   0.283    $      LB/(IN3)
    SPEC   1000.    $      IN.-LB./(LB.F)
```

BETA BT1

Status - REQUIRED (for buoyancy effects in thermoviscous fluid dynamics)

Full Keyword - BETA

Function - Defines the coefficient of thermal expansion for the fluid.

Input Variables -

BT1 (Real) - REQUIRED

Additional Information - NONE

Examples of Use -

1. Specify the thermoviscous properties of a liquid.

```
**MATE
  ID   LIQUID1
  VISC   5.3E+3
  DENS   0.0266
  COND   21.4

  SPEC   0.3

  BETA   1.E-3
```

5.2.6 ISOTROPIC VISCOUS PARAMETERS

VISC VSC1

Status - REQUIRED (for fluid dynamic analysis)

Full Keyword - VISCOSITY

Function - Defines the value of the fluid viscosity.

Input Variables -

VSC1 (Real) - REQUIRED

Additional Information - NONE

Examples of Use -

1. Specify an incompressible thermoviscous fluid.

```
**MATERIAL
  ID MAT1
  VISC 5.3E+3
  DENS 0.0266
  COND 21.4
  SPEC 0.3
```

5.3 DEFINITION OF GEOMETRY

In the current version of **BEST-FSI**, surface geometry is defined using and three noded line elements for 2-D problems. These lines can be defined to have either linear, quadratic or quartic variation of the primary field variables. An entire model may be assembled from several geometric modelling regions (GMR). Each generic modelling region is defined in a single block of input introduced with a **GMR card.

The information provided in a single GMR input block consists of five main types:

1 - Region identification
2 - Nodal point definition
3 - Surface connectivity definition
4 - Volume cell connectivity
5 - Sampling point definition (if desired)

A list of keywords recognized in the GMR input are given below and a detailed description follows.

SECTION	KEYWORD	PURPOSE
5.3.1 Geometry Input Card		
	**GMR	start of geometric modelling region input
5.3.2 Region Identification		
	ID	region ID
	MATE	material property(set) for region
	TREF	reference (initial) temperature of region
	TINT	temperature used to determine material properties for integration
	VREF	reference (initial) velocity of region
	VINT	convective velocity used for integration
	EXTE	region is an infinite body
	SOLID	identifies a solid region in a fluid dynamic analysis

SECTION	KEYWORD	PURPOSE
5.3.3 Nodal Point Definition		
	POIN	nodal points for boundary and volume discretization
	(coordinates)	
5.3.4 Surface Element Definition		
	SURF	beginnining of surface discretization
	TYPE LINE	linear surface variation of field quantities
	TYPE QUAD	quadratic surface variation of field quantities
	TYPE QUAR	quartic surface variation of field quantities
	ELEM	element list
	(element connectivity)	
	NORM	defines outer normal of surface
5.3.5 Enclosing Element Definition		
	ENCL	enclosing element list
	(enclosing element connectivity)	
5.3.6 Volume Cell Definition		
	VOLU	beginning of volume discretization
	TYPE LINE	linear variation of cell quantities
	TYPE QUAD	quadratic variation of cell quantities
	TYPE QUAR	quartic variation of cell quantities
	CELL	volume cell definition
	(cell connectivity)	
	FULL	region completely filled with cells
5.3.7 Sampling Points		
	SAMP	start of definition of sampling points
	(coordinates)	

5.3.1 GEOMETRY INPUT CARD

****GMR**

Status - REQUIRED

Full Keyword - **GMREGION**

Function - This card signals the beginning of the definition of a geometric modelling region.

Input Variables - NONE

Additional Information -

At least one GMR must be defined for an analysis. If more than one GMR is defined, then the input for each is initiated with a **GMR card.

GMR definitions must all precede all Interface, Boundary Condition set, and Body Force Definitions. Each GMR must be a closed region of two-dimensional or three-dimensional space. However, under the following two circumstances, the region may be open :

1 - In planar symmetry problems, the body may be sliced into symmetric parts and only one of these parts requires discretization. The interior section exposed by the plane cutting the body does not represent a boundary, and therefore it does not require discretization.

2 - In GMRs with boundaries extending to infinity, a GMR may have open boundaries. However, this must be indicated through the use of the EXTE card or by enclosing the open boundary with Enclosing elements (see the ENCL card). Note : One of the above devices MUST be used in an infinite region.

A GMR may have multiple internal boundaries in addition to a single external boundary.

Examples of Use -

```
**GMR
  ID   REG1
  MATE   STEEL
  TREF   70.0
  TINT   70.0
  POINT
    1   10.0   0.0   2.0
    2   10.0   1.0   2.0
```

5.3.2 REGION IDENTIFICATION

ID NAME

Status - REQUIRED

Full Keyword - ID

Function - This card provides the identifier for the GMR.

Input Variables -

NAME (Alphanumeric) - REQUIRED

Additional Information -

The NAME must be eight or less alphanumeric characters. Blank characters embedded within the NAME are not permitted.

The name provided on this card is used to reference the GMR in other portions of the input as well as in the **BEST-FSI** output file.

The NAME must be unique compared to all the other GMR names defined in the problem.

Examples of Use -

```
**GMR
  ID REG1
  MATE STEEL
```

MATE NAME

Status - REQUIRED

Full Keyword - **MATE**

Function - This card identifies the material property set for the GMR.

Input Variables -

NAME (Alphanumeric) - REQUIRED

Additional Information -

The material name reference must have been previously defined in the material property input (identified as NAME on the ID card in **MATE input).

Examples of Use -

```
**GMR
  ID GMR1
  MATE STEEL
```

TINT TEMP

Status - OPTIONAL

Full Keyword - `TINTEGRATION`

Function - Defines the temperature at which the material properties will be evaluated for use in integration of this GMR.

Input Variables -

TEMP (Real) - REQUIRED

Additional Information -

If temperature dependent material properties were input in **MATE, the material properties used in the integration of the GMR will be calculated based on the temperature specified on this card using linear interpolation.

For problems in which the temperature changes in time and/or space, it is recommended that the reference temperature be chosen as the (time/volume weighted) average temperature over the GMR.

If this card is not input then the reference temperature is used (see TREF card).

Examples of Use -

1. Specify the integration temperature at which the material properties are evaluated.

```
**GMR
  ID REG1
  MATE MAT1
  TINT 70.0
```

TREF TEMP

Status - OPTIONAL (used in temperature dependent problems)

Full Keyword - TREFERENCE

Function - This card defines the reference (or initial) temperature (i.e. the datum temperature of the zero stress-strain state) of the region at the beginning of a temperature dependent problem.

Input Variables -

TEMP (Real) - REQUIRED

Additional Information -

If this card is not input, the initial temperature is assumed as zero.

Examples of Use -

1. Specify the initial temperature of the region REG1.

```
**GMR
  ID REG1
  MATE  MAT1
  TREF  70.0
  TINT 100.0
```

VINT VELX VELY

Status - OPTIONAL

Full Keyword - `VINTEGRATION`

Function - Defines the convective velocity which will be used for kernel evaluation in convective heat transfer and fluid dynamics analysis.

Input Variables -

VELX (Real) - REQUIRED

Reference velocity in the x-direction

VELY (Real) - REQUIRED

Reference velocity in the y-direction

Additional Information -

If this card is not specified in a convective analysis, then the convective velocity for the current region is assumed to be zero.

Examples of Use -

1. Specify a non-zero integration convective velocity for the region named OUTER.

```
**GMR
  ID OUTER
  MAT MAT1
  VINT  1.0   0.0   $ FREE STREAM VELOCITY
  VREF  1.0   0.0
```

VREF VELX VELY

Status - OPTIONAL

Full Keyword - VREFERENCE

Function - Defines the reference velocity or initial velocity of a region in a fluid dynamics problem.

Input Variables -

VELX (Real) - REQUIRED

Reference velocity in the x-direction

VELY (Real) - REQUIRED

Reference velocity in the y-direction

Additional Information -

If this card is not present in a fluid dynamics or convective heat transfer analysis, then the reference velocity is assumed to be zero.

Examples of Use -

1. Specify the components of the reference (initial) velocity of the region called GMR2.

```
**GMR
  ID GMR2
  MAT MAT1
  TINT 460.0
  TREF 0.0
  VREF 0.8  0.0
```

EXTE

Status - OPTIONAL

Full Keyword - `EXTERIOR`

Function - This card identifies that the present GMR is a part of a infinite region.

Input Variables - NONE

Additional Information -

The entire outer boundary of the GMR must extend to infinity.

Infinite elements should not be used in the GMR.

In an analysis of a problem of a body of infinite extent, it is not neccessary to fix the boundary of the body for the sole purpose of preventing rigid body motions. Basically, the mathematics of the problem assumes zero displacement at infinity.

When the entire outer boundary of a GMR is at infinity (e.g cavity in an infinite space) the outer boundary can not and should not be modeled. Instead the EXTE card should be inserted in the GMR input to indicate this fact. The purpose of this card is to account for the contributions of the unmodeled infinite boundary in the calculation of the diagonal terms of the **F** matrix (Rigid body translation technique).

An alternative method to account for infinite boundaries is to model the infinite boundary with enclosing elements (see ENCL card). However, this is not recommended in problems when the entire outer boundary extends to infinity, since the use of enclosing elements would be more expensive then using the EXTE card.

Examples of Use -

1. Specify that the region GMR1 is part of an infinite region.

```
**GMR
  ID  GMR1
  MAT MAT1
  TREF 70.0
  EXTERIOR
  POINTS
        1       0.0       212.00
        2     41.36       207.93
        .         .           .
        .         .           .
        .         .           .
```

SOLI

Status - OPTIONAL

Full Keyword - SOLID

Function - Identifies a solid region within a fluid dynamics analysis.

Input Variables - NONE

Additional Information -

The SOLID keyword permits the analysis of fluid-structure interaction problems. The FLUID keyword must be selected in **CASE. All regions are then assumed to be fluid, unless the SOLID keyword appears.

When this option is selected, a suitable elastic or thermoelastic material model must also be selected with the MATE card.

Examples of Use -

1. Analyze the fluid-structure interaction problem. associated with flow past a turbine blade.

```
**GMR
  ID FLUID
  MATE GAS1
    .
    .
    .
    .
**GMR
  ID BLADE
  MATE HASTX
  SOLID
```

5.3.3 NODAL POINT DEFINITION

POIN

Status - REQUIRED (for defining the GMR)

Full Keyword - POINTS

Function - This card initiates the definition of nodal points for the boundary element and volume cell discretization of the GMR.

Input Variables - NONE

Additional Information -

Sampling Points for which results are requested (at any point on or in the body) is input under the Sampling Point section.

(NONE) NNODE X Y

Status - REQUIRED

Full Keyword - NO KEYWORD REQUIRED

Function - This card defines the node number and the Cartesian coordinates for a single nodal point.

Input Variables -

NNODE (Integer) - REQUIRED

User node number for the node.

X,Y (Real) - REQUIRED

Cartesian coordinates of the node. For 2-D problems only two coordinates x and y need to be input.

Additional Information -

This card is input once for each point.

User node numbering must be unique.

All node numbers must be less than or equal to 99999.

Nodal coordinates for both surface and volume discretization should be input here. If a node is not referenced in the surface or volume discretization, then it is ignored.

Nodal points used for hole and insert elements **CANNOT** be defined here. Instead, the nodal points for holes and inserts must be defined under their respective section.

Sampling Points for which results are requested (at any point on or in the body) is input under the Sampling Point section.

Examples of Use -

1. Define a set of nodal point coordinates in GMR1 for a 2-D analysis.

```
**GMR
  ID  GMR1
  MAT MAT 1
  TREF 70.0
  POINTS
        1      0.0      0.0
        2      0.5      0.0
        3      1.0      0.0
        4      1.0      0.5
        5      1.0      1.0
        6      0.5      1.0
        7      0.0      1.0
        8      0.0      0.5
```

5.3.4 SURFACE ELEMENT DEFINITION

SURF NAME

Status - REQUIRED (minimum of one per GMR)

Full Keyword - SURFACE

Function - This card initiates the definition of a surface of the current GMR.

Input Variables -

NAME (Alphanumeric) - REQUIRED

The name of the surface being defined.

Additional Information -

The NAME must be eight or less alphanumeric characters. Blank characters embedded within the NAME are not permitted.

The names assigned to the various surfaces in the problem must be unique.

Examples of Use -

1. Define a 2-D quadratic surface named SIDE

```
SURFACE  SIDE
TYPE  QUAD
ELEMENT
 1001  1  2  3
 1002  3  4  5
 1003  5  6  7
 1004  7  8  1
NORMAL +
```

TYPE ATYPE

Status - REQUIRED (if REFNAME not input)

Full Keyword - TYPE

Function - This card defines the variation of field quantities over the elements of the current surface.

Input Variables -

ATYPE (Alphanumeric) - REQUIRED

Allowable values are LINE, QUAD and QUAR

LINEar - linear shape function
QUADratic - quadratic shape function
QUARtic - quartic shape function

Additional Information -

See figure on subsequent pages.

A TYPE card must be defined for each surface.

All of the elements of a single surface must have the same type of variation. Different surfaces of the same GMR may have different variation.

A surface may consist of a single element. By contrast a single surface may define the entire boundary of a GMR.

Examples of Use -

1. Specify that the field quantities vary quadratically over the elements of the surface SURF1.

```
SURFACE  SURF1
TYPE  QUAD
ELEMENT
    101   1   2   3
    102   3   4   5
    .     .   .   .
    .     .   .   .
    .     .   .   .
    .     .   .   .
```

2D BOUNDARY ELEMENT FUNCTIONAL VARIATION

LINE

QUAD

QUAR

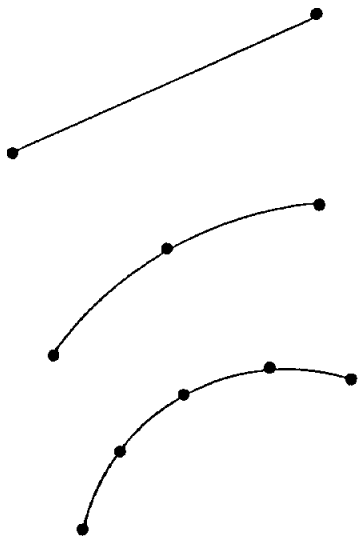

Figure for **GMR: TYPE card

(See element connectivity card for geometrical input)

ELEM

Status - REQUIRED (if REFNAME not input)

Full Keyword - `ELEMENTS`

Function - Signals the beginning of the connectivity definition for surface elements of the current surface.

Input Variables - NONE

Additional Information - NONE

(NONE) NEL NODE1 ... NODEN

Status - REQUIRED (minimum of one card if TYPE is input)

Full Keyword - NO KEYWORD REQUIRED

Function - Each card defines the connectivity for a single surface element.

Input Variables -

NEL (Integer) - REQUIRED

User element number.

NODE1 ... NODEN (Integer) - REQUIRED

User node numbers of the two or three nodes (for 2-D) for defining the geometry of the element. Every surface domain must have two or three nodes, regardless of whether TYPE = LINE, QUAD or QUAR. (The shape functions for geometry is always quadratic)

Additional Information -

This card is input once for each element.

The input card need not specify whether a two or three node element is being defined. For 2-D, the input must be consecutive, starting with an end node, and adjacent elements must be defined in the same direction. The direction is defined with the NORM card.

User element numbers must be unique and less than or equal to 99999.

All of the nodes referenced in the surface element connectivity must have been defined previously in POINts.

Whenever a GMR is of infinite extent either the EXTE card must be used or ENCLosing elements must be defined.

Examples of Use -

1. Specify the connectivity definition for elements of the surface SIDE using four 3-noded quadratic elements.

```
SURFACE  SIDE
TYPE  QUAD
ELEMENT
   101   1   2   3
   102   3   4   5
   103   5   6   7
   104   7   8   1
NORMAL +
```

2-D BOUNDARY ELEMENT FAMILY FOR GEOMETRICAL INPUT

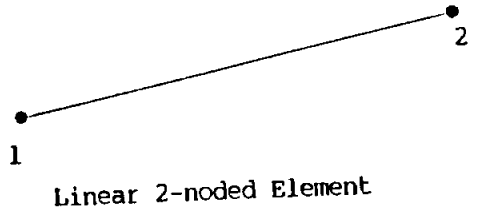

Linear 2-noded Element

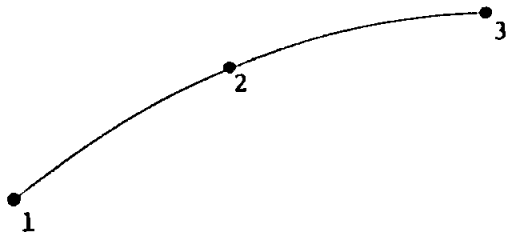

Quadratic 3-noded Element

Figure for **GMR: Element connectivity card
(see TYPE card for functional variation)

NORM SIGN

Status - REQUIRED - (for 2-D)

Full Keyword - **NORMAL**

Function - Defines the outer normal direction in the current GMR.

Input Variables -

SIGN (symbol) - REQUIRED

Allowable symbols are " + " or " – "

+ defines the outward normal as up when numbering an element from right to left while looking down the z axis (see figure).

– defines the outward normal as down when numbering an element from right to left while looking down the z axis (see figure).

Additional Information -

All elements of a GMR must follow the same convention.

Examples of Use -

1. Define the direction of the outward normal to the surface SURF1 as positive.

```
SURFACE  SURF1
TYPE  QUAD
ELEMENTS
    1     1     2     3
    2     3     4     5
    3     5     6     7
    4     7     8     1
NORMAL     +
```

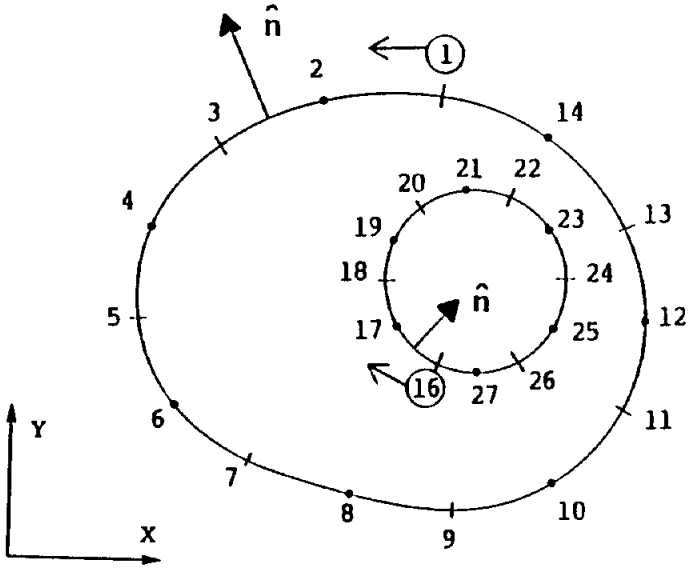

input shown is for
FLAG = +
on NORM card for 2-D

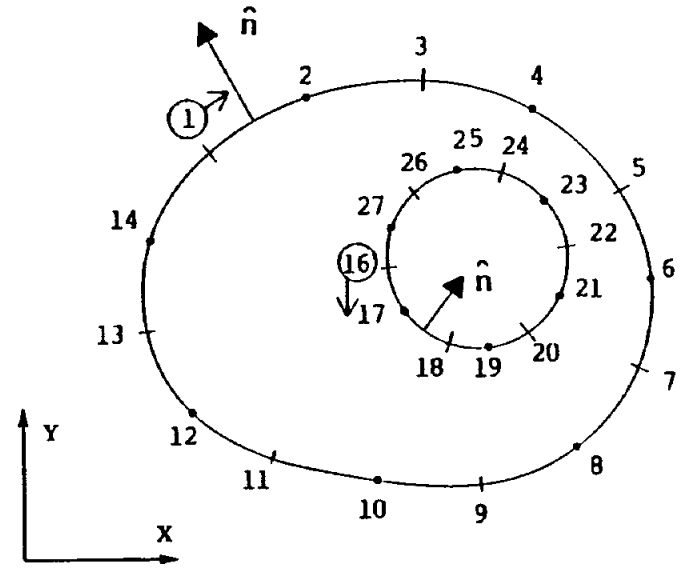

input shown is for
FLAG = -
on NORM card for 2-D

Figure for **GMR: NORM card

Two-dimensional outer normal convention
(In 2-D, all elements in a single GMR must use the same convention)

5.3.5 ENCLOSING ELEMENT DEFINITION

ENCL

Status - OPTIONAL

Full Keyword - **ENCLOSING**

Function - Signals the beginning of the connectivity definition for enclosing elements of the GMR. Enclosing elements are used in GMRs of infinite extent in order to create a fictitious boundary required for correct calculation of the matrix coefficients.

Input Variables - NONE

Additional Information -

In a GMR of infinite extent, it is neccessary to use the EXTE card if enclosing elements are not used.

The nodes in an enclosing element do not become boundary source points (part of the system equation) unless they are also part of a regular boundary. The only purpose of enclosing elements is to define an arbitrary surface for integration so that the contribution of the unmodelled infinite boundary can be taken into account in the calculation of the diagonal terms of the **F** matrix (Rigid Body Translation Technique).

The geometry of the surface defined by the enclosing elements is arbitrary since the contribution (for a particular source point) of any surface enclosing the region is equivalent. Therefore, the discretization of enclosing elements should be crude, utilizing the minimum number of enclosing elements neccessary to enclose the region. It is, however, recommended that the surface defined by the enclosing elements does not pass too close (relative to the size of the enclosing element) to a boundary source point belonging to a regular element contained in that particular region.

In an analysis of a problem of a body of infinite extent, it is not neccessary to fix the boundary of the body for the sole purpose of preventing rigid body translation. Basically, the mathematics of the problem assumes zero displacement at infinity.

Examples of Use -

1. Define enclosing elements for a two-dimensional body.

```
ENCL
  55   95  105  115
  56  115  125  135
```

(NONE) NEL NODE1 .... NODEN

Status - REQUIRED (minimum of one card if ENCL is input)

Full Keyword - NO KEYWORD REQUIRED

Function - Each card defines the connectivity for a single enclosing element.

Input Variables -

NEL (Integer) - REQUIRED

User element number (required for user's purpose only)

NODE1 ... NODEN (Integer) - REQUIRED

User number for the node for defining the geometry of the enclosing element.

N = 3 (for 2-D)

Additional Information -

Only **THREE** noded enclosing elements are allowed in 2-D.

All of the connectivity for enclosing elements must be defined such that their normals are positive.

Examples of Use -

1. Define enclosing elements.

```
ENCLOSING ELEMENTS
 1001   1  2  3
 1002   3  4  5
 etc....
```

5.3.6 VOLUME CELL DEFINITION

VOLU NAME

Status - OPTIONAL

Full Keyword - VOLUME

Function - This card initiates the definition of a volume for the current GMR.

Input Variables -

NAME (Alphanumeric) - OPTIONAL

The name of the volume being defined. (For user's use only)

Additional Information -

In the present version of **BEST-FSI**, only one volume discretization per GMR is allowed. This means only one type (see next card definition) of cells can exist in a single GMR.

Examples of Use -

1. Define three, 8-Noded quadratic volume cells for two-dimensional analysis.

```
VOLUME
TYPE  QUAD
CELL
 1001  1  2  3  103  203  202  201  101
 1002  3  4  5  105  205  204  203  103
 1003  5  6  7  107  207  206  205  105
FULL
$(end of volume cell input)
```

TYPE ATYPE BTYPE

Status - REQUIRED (if VOLU is input)

Full Keyword - TYPE

Function - This card defines the variation of field quantities over the volume cells of the current GMR.

Input Variables -

ATYPE (Alphanumeric) - REQUIRED

Allowable values are LINE, QUAD, or QUAR.

LINEar - Linear shape functions

QUADratic - Quadratic shape functions

QUARtic- Quartic shape functions

BTYPE (Alphanumeric) - OPTIONAL (for fluid dynamics only)

Allowable values are LAGR and SERE. The Default is SERE.

LAGRangian - Lagrangian type shape functions

SEREndipity - Serendipity type shape functions

Additional Information -

Only one TYPE card for cells is allowed per GMR.

QUARtic variation is only available for two-dimensional fluid dynamics. The program automatically generates the extra source points required for a quartic functional variation.

Examples of Use -

1. Specify that the variation of field quantities over the volume cells in GMR1 is quadratic in nature.

```
**GMR
  ID GMR1
  .
  .
  .
  VOLUME
  TYPE QUAD
```

CELL

Status - REQUIRED (if VOLU is input)

Full Keyword - CELLS

Function - Signals the beginning of the definition of volume cell input connectivity.

Input Variables - NONE

Additional Information -

Cell connectivity information is input on data cards following this card.

(NONE) NCELL N1 N2 .... NK

Status - REQUIRED (If VOLU is input)

Full Keyword - NO KEYWORD REQUIRED

Function - Defines a volume cell in terms of previously defined nodal points.

Input Variables -

NCELL (Integer) - REQUIRED

User identification for cell being defined.

N1,N2,...,NK (Integer) - REQUIRED

User nodal point numbers for cell nodes.

K = 3, 4, 6, or 8 for 2-D

Additional Information -

If necessary, this card may be input more than once for each cell. The cell number must be repeated on each card.

2-D: Cell numbering must begin at the corner and be numbered consecutively in either direction.

Nodal points of the surface discretization may also be used in the volume discretization (i.e., a cell face may match up with a boundary element). This is recommended when possible, since it somewhat reduces the computation required. Nodal points of the volume discretization lying on the surface must be nodal points of the surface mesh.

Examples of Use -

1. Define a set of volume cells consisting of a cell number and the connectivity information. There are three 8-noded volume cells with quadratic variation.

```
VOLUME
TYPE QUAD
CELL
   501   1   2   3   103   203   202   201   101
   502   3   4   5   105   205   204   203   103
   503   5   6   7   107   207   206   205   105
```

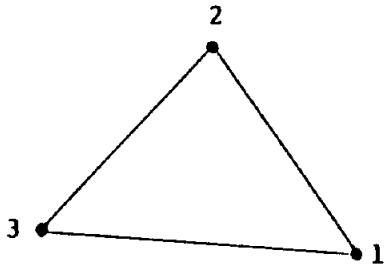

Linear 3-noded Cell

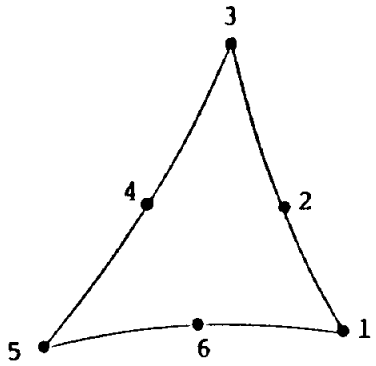

Quadratic 6-noded Cell

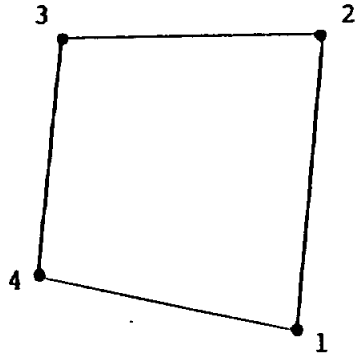

Linear 4-noded Cell

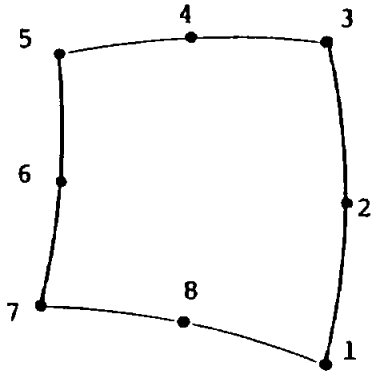

Quadratic 8-noded Cell

Figure for**GMR: Volume Cell Connectivity
Two-dimensional Volume Cells

FULL

Status - OPTIONAL

Full Keyword - `FULL` region of cells

Function - Identifies the GMR is completely filled with cells and that the Indirect Technique should be used to accurately calculate the coefficient corresponding to a singular point in the volume integration.

Input Variables - NONE

Additional Information -

The GMR must be completely filled by cells.

If FULL is not used, all relevant coefficients are calculated by numerical volume integration.

For highly accurate results, it is recommended that a GMR be completely filled with cells and that the FULL card option be exercised.

If the FULL card is included in a GMR for a transient analysis with the RECUrring initial condition option, then convolution is avoided for that GMR. The effect of past events is determined by evaluating an initial condition volume integral at each time step.

Examples of Use -

1. Specify that the GMR (GMR1) is completely filled with volume cells.

```
VOLUME
TYPE QUAD
CELL
  501   1   2   3   103   203   202   201   101
  502   3   4   5   105   205   204   203   103
  503   5   6   7   107   207   206   205   105
FULL
```

5.3.7 SAMPLING POINT DEFINITION

SAMP

Status - OPTIONAL

Full Keyword - `SAMPLING-POINTS`

Function - This card signals the fact that a set of sampling points for which results are requested at any point on or in the body, will be provided for the current GMR.

Input Variables - NONE

ITYP1 (Alphanumeric) - REQUIRED

Additional Information -

This card is used to define points at which velocities, stresses, strains, temperatures, pressures and fluxes are to be calculated. The print flag for sampling points may be set in **CASE input. If, however, nothing is specified in **CASE for sampling points, this flag is set by default depending upon analysis type.

This card is followed by data cards defining the node number and coordinates of the sampling points.

Examples of Use -

1. Request result information at three interior points

```
SAMPLING-POINTS
 1001    0.333   0.25
 1002    0.25    0.1
 1003    0.2     0.5
```

`(NONE)  NNODE X Y`

Status - REQUIRED (if SAMP is input)

Full Keyword - NO KEYWORD REQUIRED

Function - Defines the coordinates of the sampling points for which output will be reported.

Input Variables -

NNODE (Integer) - REQUIRED

User number for the node.

X,Y (Real) - REQUIRED Cartesian coordinates of the nodal point. For 2-D problems only x and y coordinates are needed.

Additional Information -

This card is input once for each point.

User nodal point numbers must be unique, including the surface nodal points and any additional nodal points created for the volume discretization, or discretization.

Point numbers must be less than or equal to 99999.

5.4 DEFINITION OF GMR COMPATIBILITY

When a body is modelled as an assembly of several GMRs suitable conditions must be specified to define the connections among the various regions. In the present version of **BEST-FSI** compatibility is defined between the interface surfaces of each pair of contacting regions. Four types of compatibility are allowed:

1 - Bonded contact : Continuity of all velocity components is imposed across the interface.

2 - Sliding contact : Continuity is required only for the component of velocity normal to the interface. The tractions, in both GMRs, in the tangent plane to the interface are set to zero.

3 - Resistance contact : Thermal resistance is imposed between regions.

4 - Cyclic contact : Symmetric elements within a cyclic symmetric part can have imposed symmetric deformation on these elements.

Continuity of temperature or pressure, when applicable, is imposed across the interface in a similar manner.

A single nodal point location may be part of at most two GMRs. A single nodal point may be referenced in more than one interface definition data set as long as only two GMRs are involved. A single location must have a unique node number in each GMR. Various acceptable and unacceptable arrangements of GMRs are illustrated in the figure following the **INTE card.

The interface compatibility must be specified in such a way that there is one to one correspondence between the source points (field variable nodes) of the two GMR's that are involved. The input required to specify a single interface between two GMRs is described in the following pages, and a list of keywords recognized in the interface input are given below.

SECTION	KEYWORD	PURPOSE
5.4.1 Interface Definition Input Card		
	**INTE	Start of interface compatibility condition
5.4.2 Definition of interface surface 1		
	GMR	name of first GMR
	SURF	surface on first GMR
	ELEM	element of surface

SECTION	KEYWORD	PURPOSE
5.4.3 Definition of interface surface 2		
	GMR	name of second GMR
	SURF	surface on second GMR
	ELEM	element of surface
5.4.4 Type of interface conditions		
	BOND	bonded interface connection
	SLID	sliding interface connection
	RESI	thermal resistence across interface
5.4.5 Cyclic Symmetry interface definition		
	CYCL	cyclic symmetry interface definition
	ANGL	angle for cyclic interface
	DIR	axis of rotation for cyclic interface
5.4.6 Additional Interface Control Options		
	TDIF	reference temperature difference across interface
	VDIF	reference velocity difference across interface

5.4.1 INTERFACE DEFINITION INPUT CARD

****INTE**

Status - OPTIONAL

Full Keyword - `INTERFACE`

Function - Indicates the beginning of an interface definition.

Input Variables - NONE

Additional Information -

A ****INTE** card must begin each interface definition. The complete definition of the connection between two GMRs may require more than one data set, since each data set can refer to only one surface.

The data set initiated with this card may be repeated as many times as required.

The interface surface reference below must be such that the nodes and elements of one GMR can be superimposed on the nodes and elements of the other GMR by translation and/or rotation, without any deformation.

Note that each of the two GMR's involved in the interface definition must contain elements that lie on the interfacial surface.

The interface data sets must follow all GMR definitions, and must precede any boundary condition data sets.

Examples of Use -

1. Defines the interface of two GMR's (default is perfectly bonded connection).

```
**INTERFACE
  GMR   REG1
     SURFACE   TOP
     ELEMENT    3   4   5
  GMR   REG2
     SURFACE   BOTTOM
     ELEMENT   103   104   105
```

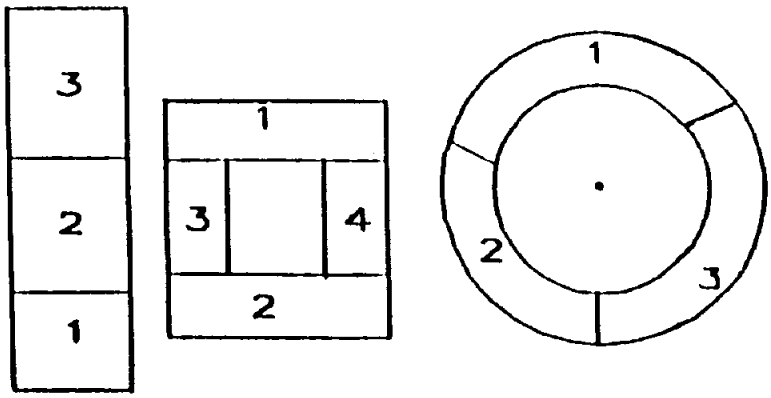

Acceptable Connections

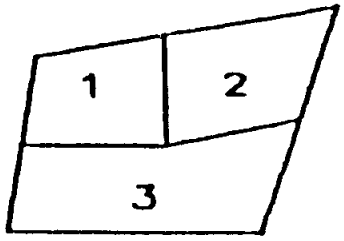

Unacceptable Connection

Figure for **INTE : card Connections among GMRs

5.4.2 DEFINITION OF INTERFACE SURFACE 1

GMR IDGMR

Status - REQUIRED

Full Keyword - **GMR**

Function - Identifies the first GMR for which the interface surface is to be defined.

Input Variables -

IDGMR (Alphanumeric) - REQUIRED

IDGMR is the identifier for the GMR as input during the geometry definition (NAME on ID card in **GMR input).

Additional Information -

A given interface surface must lie entirely on the surface of a single GMR. If an interface compatibility condition is to be applied with more than one GMR, a separate interface compatibility must be defined for each case.

Examples of Use -

1. Identifies the first GMR, say GMR1, of which the interface surface is a part.

```
**INTERFACE
  GMR GMR1
    SURFACE  SURF1
    ELEMENTS 101   102   103   104
```

SURF IDSUR

Status - REQUIRED

Full Keyword - SURFACE

Function - Identifies the surface within the (first) selected GMR which embodies the interface surface (NAME on SURF card in **GMR input).

Input Variables -

IDSUR (Alphanumeric) - REQUIRED

Additional Information -

An interface surface must be contained entirely within a single surface. If the interface compatibility condition is to be applied to more than one surface, then a separate interface compatibility must be defined for each surface involved.

The SURF card may conclude the required input for a interface definition. If the SURF card is not followed by a ELEM card, then BEST-FSI will apply the interface compatibility condition to all of the elements in the surface IDSUR.

Examples of Use -

1. Identifies the interface surface, say SURF1, as part of the first GMR.

```
**INTERFACE
  GMR GMR1
    SURFACE  SURF1
    ELEMENTS 109   110
  GMR GMR2
    SURFACE  SURF2
```

ELEM EL1 EL2 ... ELN

Status - OPTIONAL

Full Keyword - ELEMENTS

Function - Specifies the elements of the surface IDSUR to which an interface compatibility condition is to be applied.

Input Variables -

EL1,EL2,...,ELN (Integer) - REQUIRED

User element numbers of the elements of surface IDSUR which forms the interface surface.

Additional Information -

The effect of this card is to restrict the application of the compatibility condition to a portion of the surface IDSUR.

This input may be continued on more than one card. Each card must begin with the keyword ELEM.

If the ELEM card is specified, BEST-FSI will apply the interface compatibility condition only to the elements specified on this list.

In the present version of **BEST-FSI** , interface compatibility can not be specified at individual nodes.

Examples of Use -

1. Specifies three elements, 120, 121 and 122, for interfacial compatibility on the surface identified by the preceding SURFACE card.

```
**INTERFACE
  GMR  GMR1
    SURFACE  SURF1
    ELEMENTS 120   121   122
  GMR GMR2
```

5.4.3 DEFINITION OF INTERFACE SURFACE 2

GMR IDGMR

Status - REQUIRED

Full Keyword - GMR

Function - Identifies the second GMR for which the interface surface is to be defined.

Input Variables -

IDGMR (Alphanumeric) - REQUIRED

IDGMR is the identifier for the GMR as input during the geometry definition (NAME on ID card in **GMR input).

Additional Information -

A given interface surface must lie entirely on the surface of a single GMR. If an interface compatibility condition is to be applied with more than one GMR, a separate interface compatibility must be defined for each case.

Examples of Use -

1. Identifies the second GMR, say GMR2, of which the GMR surface is a part.

```
**INTERFACE
  GMR GMR1
    SURFACE  SURF1
    ELEMENTS 101   102
  GMR GMR2
    SURFACE  SURF2
    ELEMENTS 201   202
```

SURF IDSUR

Status - REQUIRED

Full Keyword - SURFACE

Function - Identifies the surface within the (second) selected GMR which embodies the interface surface (NAME on SURF card in **GMR input).

Input Variables -

IDSUR (Alphanumeric) - REQUIRED

Additional Information -

An interface surface must be contained entirely within a single surface. If the interface compatibility condition is to be applied to more than one surface, then a separate interface compatibility must be defined for each surface involved.

The SURF card may conclude the required input for a interface definition. If the SURF card is not followed by a ELEM card, then BEST-FSI will apply the interface compatibility condition to all of the elements in the surface IDSUR.

Examples of Use -

1. Identifies the interface, say SURF2, as part of the second GMR.

```
**INTERFACE
  GMR GMR1
    SURFACE  SURF1
    ELEMENTS 101   102
  GMR GMR2
    SURFACE  SURF2
    ELEMENTS 201   202
```

`ELEM  EL1 EL2 ... ELN`

Status - OPTIONAL

Full Keyword - `ELEMENTS`

Function - Specifies the elements of the surface IDSUR to which an interface compatibility condition is to be applied.

Input Variables -

EL1,EL2,...,ELN (Integer) - REQUIRED

User element numbers of the elements of surface IDSUR which forms the interface surface.

Additional Information -

The effect of this card is to restrict the application of the compatibility condition to a portion of the surface IDSUR.

This input may be continued on more than one card. Each card must begin with the keyword ELEM.

If the ELEM card is specified, BEST-FSI will apply the interface compatibility condition only to the elements specified on this list.

In the present version of **BEST-FSI** , interface compatibility can not be specified at individual nodes.

Examples of Use -

1. Specifies three elements, 210, 211 and 212, for interfacial compatibility on the surface identified by the preceding SURFACE card.

```
**INTERFACE
  GMR  GMR1
    SURFACE  SURF1
    ELEMENTS 101   102   103
  GMR  GMR2
    SURFACE SURF2
    ELEMENTS 210   211   212
```

5.4.4 TYPE OF INTERFACE CONDITION

BOND

Status - OPTIONAL

Full Keyword - **BONDED**

Function - Identifies a fully bonded interface.

Input Variables - NONE

Additional Information -

When this card is input continuity of all variables is imposed across the interface.

This is the default condition when the type of interface is not explicitly defined.

Examples of Use -

1. Defines a perfectly bonded interface of three boundary elements.

```
**INTERFACE
  GMR   REG1
    ELEMENT    3    4    5
  GMR   REG2
    ELEMENT  103  104  105
  BOND
```

SLID

Status - OPTIONAL

Full Keyword - `SLIDING`

Function - Identifies a sliding interface.

Input Variables - NONE

Additional Information -

When this card is input only normal velocity compatibility is imposed across the interface. The two GMRs are free to move in the plane tangent to the interface, however, the surfaces remain in contact even under tension. This freedom may require the specification of additional boundary conditions to restrain rigid body motion.

Examples of Use -

1. Defines a sliding interface of five boundary elements.

```
**INTERFACE
  GMR  REG1
    ELEMENT   101   102   103   104   105
  GMR REG2
    ELEMENT   210   212   213   214   215
  SLID
```

RESI R1

Status - OPTIONAL

Full Keyword - `RESISTANCE`

Function - Identifies an interface with thermal resistance between the corresponding surfaces. The flux across this interface is linearly related to the temperature difference between the two surfaces.

Input Variables -

R1 (Real) - REQUIRED

Thermal resistance coefficient (R)

Additional Information -

The RESIstance option utilizes the relationship:

$$q_1 = \frac{1}{R1}(\theta_1 - \theta_2)$$

where

θ_1	local temperature of GMR 1.
θ_2	local temperature of GMR 2.
q_1	local heat flux from GMR 1.

The user is responsible for providing R in the proper units, consistent with the specification of material properties, geometry and boundary conditions.

The resistance R should be a positive real number ($R > 0$). If zero is input, the coefficient will be automatically reset to 1.0E–10.

Examples of Use -

1. Defines thermal resistance at the interface between two regions which were at the same initial temperature (otherwise, a TDIF card should be inserted after the RESI card).

```
**INTERFACE
  GMR GMR1
    SURFACE  SURF1
    ELEMENTS 12
  GMR GMR2
    SURFACE  SURF2
    ELEMENTS 21
  RESI 1.0
```

5.4.5 CYCLIC SYMMETRY PARAMETER DEFINITION

CYCL

Status - OPTIONAL

Full Keyword - CYCLIC

Function - Identifies a cyclic symmetry boundary condition.

Input Variables - NONE

Additional Information -

This type of interface condition establishes a relationship between two boundary surfaces. In order for this condition to be applied the two boundary surfaces involved must be such that one can be exactly superimposed on the other by a rotation about a specified axis passing through the origin of the global coordinate system. Further, the imposed boundary conditions of the problem must be such that the deformed shape of one boundary surface can be exactly superimposed on the other by the same rotation. This option is intended for the analysis of (periodic) structures subjected to periodic loading.

Rigid body translation along the cyclic axis and rigid body rotation about that same axis are **not** automatically prevented by invoking the CYCLIC option. Consequently, these motions must be constrained explicitly by the user.

Since a cyclic interface condition involves all components of displacement and traction, **no other boundary condition may be applied to the elements that are involved.**

Local coordinate systems are established for each node on the second boundary surface. As a result, no other local system may be defined for these nodes. Furthermore, in the current version, it is recommended that displacement (or velocity) boundary conditions **not be applied** to any of the second surface nodes.

In the present version of **BEST-FSI**, a boundary surface to which a cyclic interface is applied may not intersect another interface.

A cyclic interface condition is time independent.

Examples of Use -

1. Activate option for cyclic symmetry boundary condition.

```
**INTERFACE
  GMR GMR1
```

```
SURFACE SURF1
ELEMENT 3
GMR GMR1
SURFACE SURF1
ELEMENT 5
CYCLIC
ANGLE 20
DIRECTION  0.  0.  1.
```

ANGL THETA

Status - REQUIRED (if CYCL is specified)

Full Keyword - **ANGLE**

Function - Specifies the angle of rotation between the two surfaces referenced in the cyclic symmetry condition.

Input Variables -

THETA (Real) - REQUIRED

THETA is the rotation angle (in degrees). A positive rotation is counterclockwise when looking along the positive axis direction.

Additional Information - NONE

Examples of Use -

1. Specifies an angle of 20 degrees between the two surfaces referenced in the cyclic symmetry condition.

```
**INTERFACE
  GMR GMR1
  SURFACE SURF1
  ELEMENT 3
  GMR GMR1
  SURFACE SURF1
  ELEMENT 5
  CYCLIC
  ANGLE 20
  DIRECTION  0.  0.  1.
```

DIRE X Y Z

Status - OPTIONAL

Full Keyword - DIRECTION

Function - Defines the positive direction of the axis of rotation, if CYCL is specified.

Input Variables -

X,Y,Z (Real) - REQUIRED

Components of a vector along the positive direction of the axis of rotation.

Additional Information -

This card may be omitted. In this case the rotation axis defaults to the positive z-axis.

Examples of Use -

1. Defines that the positive direction of the axis of rotation is along the z-axis.

```
**INTERFACE
  GMR GMR1
  SURFACE SURF1
  ELEMENT 3
  GMR GMR1
  SURFACE SURF1
  ELEMENT 5
  CYCLIC
  ANGLE 20
  DIRECTION  0.  0.  1.
```

5.4.6 ADDITIONAL INTERFACE CONTROL OPTIONS

TDIF

Status - OPTIONAL

Full Keyword - TDIFFERENECE

Function - Signals that there is a difference in the reference temperatures of the two regions involved in the current interface.

Input Variables - NONE

Additional Information -

The TDIF card must be included in the interface definition for any temperature-dependent problem for which the reference temperatures of the adjoining regions are different. In such situations, failure to include this card will produce incorrect results.

It is expected that in future releases of **BEST-FSI**, the necessary checks will be done automatically, and the TDIF card will no longer be needed.

Examples of Use -

1. Indicates that a difference in reference temperatures exists between the GMR's, REG1 and REG2, involved in the current interface.

```
**INTERFACE
  GMR REG1
    SURFACE  TOP
    ELEMENTS 101   102
  GMR REG2
    SURFACE  BOTTOM
    ELEMENTS 209   210
  RESI  1.0
  TDIF
```

VDIF

Status - OPTIONAL

Full Keyword - `VDIFFERENECE`

Function - Signals that there is a difference in the reference velocities of the two regions involved in the current interface.

Input Variables - NONE

Additional Information -

This card is applicable only for fluid dynamic analysis.

The VDIF card must be included in the interface definition for any fluid dynamics problem for which the reference velocities of the adjoining regions are different. In such situations, failure to include this card will produce incorrect results.

It is expected that in future releases of **BEST-FSI** , the necessary checks will be done automatically, and the VDIF card will no longer be needed.

Examples of Use -

1. Indicates that a difference in reference velocities exists between the two GMR's, REG1 and REG2, involved in the current interface.

```
**INTERFACE
  GMR REG1
    SURFACE  SURF1
    ELEMENTS 25   26
  GMR REG2
    SURFACE  SURF2
    ELEMENTS 227   228
  VDIF
```

5.5 DEFINITION OF BOUNDARY CONDITIONS

This section describes the boundary condition input set (BCSET) for the input of boundary conditions applied at the surface of the given structure (or body). The input is designed to allow the specification of time dependent boundary conditions in both local and global coordinate systems. In order to allow the generality required, the input system is necessarily somewhat complex. Considerable simplification is possible for problems with less general requirements.

In the boundary element method, the primary load variable is traction (or flux), which acts over a surface area, not point forces (or sources) as in the finite element method. This means that in defining the region of application of a boundary condition in **BEST-FSI** it is necessary to specify both the nodal points and the elements involved.

A variety of options are provided for the definition of boundary conditions on the surface of the part. Each distinct set of boundary condition data defines either numerical values of variables over some portion of the surface of the part (or body), or establishes a relationship among variables. As many sets of boundary condition data may be used, as are required to completely specify the problem. A nodal point or element may be referenced in more than one set of boundary condition data.

A common process to much of the boundary condition input is the specification of the time dependent variables over the surface. To simplify the subsequent discussion of the various boundary condition types, the recurring definition of space/time variation is described only once in section 5.5.6.

SECTION	KEYWORD	PURPOSE
5.5.1 Boundary Condition Set Card		
	**BCSET	start of the B.C. definition
5.5.2 Boundary Condition Identification		
	ID	name of B.C. set
5.5.3 Identification of Boundary Condition Type		
	VALU	for specified B.C. value input
	RELA	for B.C. relation between boundary quantities
	LOCA	for local definition of B.C.

SECTION	KEYWORD	PURPOSE
5.5.4 Definition of Surface for Application of Boundary Conditions		
	GMR	identifies a GMR
	SURF	identifies the surface for this B.C. set
	ELEM	identifies surface elements
	POIN	identifies surface points
	TIME	defines the time for input
5.5.5 Value Boundary Condition for Surface Elements		
	TRAC	traction B.C. input
	VELO	velocity B.C. input
	FLUX	flux B.C. input
	TEMP	temp B.C. input
5.5.6 Definition of Space/Time variation		
	SPLI	source (field variable) point list
	T	nodal value of B.C.
5.5.7 Relation Boundary Condition		
	CONV	convection relation (between temperature and flux)

5.5.1 BOUNDARY CONDITION SET CARD

****BCSE**

Status - REQUIRED

Full Keyword - ****BCSET**

Function - Identifies the beginning of a boundary condition data set.

Input Variables - NONE

Additional Information -

As many boundary condition data sets may be input as are required. Each must begin with this card.

The boundary condition data sets must follow all GMR and INTERFACE definitions, and must precede any BODYFORCE data.

Examples of Use -

1. Fix the normal (local) displacement of all elements for on surface SIDE1 of GMR REG2 for all time (no TIME card required)

```
**BCSET
  ID U1FIX
  VALUE
  LOCAL
  GMR REG2
    SURFACE SIDE1
    DISP 1
    SPLIST ALL
    T 1 0.0
```

5.5.2 BOUNDARY CONDITION IDENTIFICATION

ID NAME

Status - REQUIRED

Full Keyword - ID

Function - Defines the identifier for the current boundary condition data set.

Input Variables -

NAME (Alphanumeric) - REQUIRED

User specified name of for the current data set.

Additional Information -

The NAME must be unique compared to all other boundary condition data set names defined in the problem.

The NAME must be eight or less alphanumeric characters. Blank characters embedded within the NAME are not permitted.

Examples of Use -

1. Define a set of displacement type boundary conditions with the name DISP1.

```
**BCSET
  ID  DISP1
  SURFACE  SURF1
  ELEMENTS  104
  POINT 108
  DISP 1
  SPLIST 108
  T   1   0.0
**BCSET
```

5.5.3 IDENTIFICATION OF BOUNDARY CONDITION TYPE

VALU

Status - OPTIONAL

Full Keyword - **VALUE**

Function - Identifies the boundary condition as one which will define the numerical values of field variables.

Input Variables - NONE

Additional Information -

This card must not be used for relational boundary condition sets.

If VALU, RELA, or VARI do not appear in a boundary condition set, a value-type set is assumed.

Examples of Use -

1. Used here to indicate that the value of a local traction type of boundary condition is specified.

```
**BCSET
  ID  TRAC12
  VALUE
  LOCAL
  GMR GMR1
  SURFACE SURF1
  ELEMENTS 17
    TRAC 1
  SPLIST ALL
    T 1   -100.0
$end of input data
```

RELA

Status - OPTIONAL

Full Keyword - RELATION

Function - Identifies the boundary condition as one which will define a relationship between field variables (e.g. spring or convection boundary conditions).

Input Variables - NONE

Additional Information -

This card is required for all boundary condition sets which define a relationship between field variables. Therefore, this card must be included for SPRING or CONVECTION boundary conditions.

Examples of Use -

1. The RELATION card is used in the following example to indicate specification of convection type of boundary condition.

```
**BCSET
  ID  BCS1
  RELATION
  GMR  GMR1
  SURFACE  SURF1
    ELEMENTS   1   2   3   4
    CONV  1.26   -100.0  $  H = 1.26, TEMP (AMBIENT) = - 100.0
**BCSET
  ID  BCS2
```

LOCA

Status - OPTIONAL

Full Keyword - LOCAL

Function - Indicates that input for the current boundary condition set will be in local coordinates.

Input Variables - NONE

Additional Information -

In the present version of **BEST-FSI** this option is intended for the specification of displacement, traction or spring constants normal to a (not necessarily plane) surface. Specification of conditions other than zero traction or flux in the tangent plane of the surface is unreliable.

In the local coordinate system the outer normal direction is the first coordinate direction.

Once a local boundary condition is specified on a node, the rest of the required boundary conditions on that node must be specified in local coordinates.

Once a local boundary condition is specified on a node of an element, the rest of the required boundary conditions on that element must be specified in local coordinates.

Local boundary conditions are not applicable to scalar problems (i.e. heat conduction; acoustics).

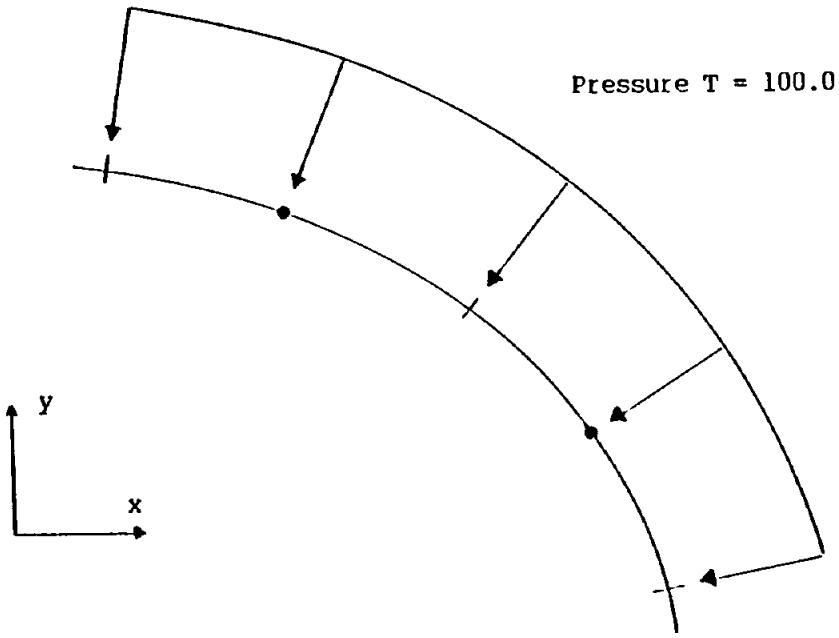


```
**BCSET
  ID BC1
  VALUE
  LOCAL
    GHR GHR1
    SURF SURF1
    ELEMENT  2  3
      TRAC  1
      SPLIST ALL
        T 1  -100.0
```

Figure for **BCSET: LOCAL card
Local traction boundary condition input

5.5.4 DEFINITION OF SURFACE FOR APPLICATION OF BOUNDARY CONDITIONS

In the boundary element method, the primary load variable is traction (or flux), which **acts over a surface area, not nodal forces (or sources)** as in the finite element method. This means that in defining the region of application of a boundary condition in **BEST-FSI** it is necessary to specify both the nodal points and the elements involved.

If no boundary condition is specified (for a particular component) at a node, the primary load variable (of that component) is assumed to be zero.

The input lines involved in defining the element and nodes for a particular boundary condition set are described in this section.

GMR IDGMR

Status - REQUIRED

Full Keyword - GMR

Function - Identifies the GMR of the surface on which the boundary condition is to be defined.

Input Variables -

IDGMR (Alphanumeric) - REQUIRED

IDGMR is the identifier for the GMR as input during the geometry definition (NAME on ID card in **GMR input).

Additional Information -

A given boundary condition set can involve only a single GMR. If a boundary condition is to be applied to more than one GMR, a separate boundary condition set must be defined for each GMR.

Examples of Use -

1. Identifies the GMR name REG1 in connection with the specification of boundary conditions.

```
**BCSET
  ID  TRAC1
  VALUE
  GMR1  REG1
  SURFACE SURF1
  ELEMENTS   101   102
  TRAC  1
  SPLIST  ALL
  T  1  100.0
$ end of input data
```

SURF IDSUR

Status - OPTIONAL

Full Keyword - SURFACE

Function - Identifies the surface within the selected GMR on which the boundary condition is to be defined (NAME on SURF card in **GMR input).

Input Variables -

IDSUR (Alphanumeric) - REQUIRED

Additional Information -

Either this keyword or the HOLE keyword must be input for each boundary condition set.

A boundary condition set can involve only a single surface. If a boundary condition is to be applied to more than one surface, then a separate boundary condition set must be defined for each surface involved.

It is recommended that, whenever possible, surfaces be made to coincide with the regions over which boundary conditions are to be applied. This considerably simplifies the definition of surface for application of boundary condition.

If the SURF card is not followed by an ELEM or POIN card, then BEST-FSI will apply the boundary condition to all of the elements in the surface IDSUR.

Examples of Use -

1. Identifies the surface name SURF1 relevant to the specification of boundary conditions.

```
**BCSET
  ID  TRAC1
  GMR  GMR1
  SURFACE SURF1
  ELEMENTS  101   102   103
  TRAC  1
  SPLIST  ALL
  T  1  100.0
```

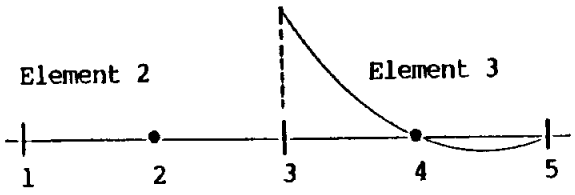

traction at NODE 3 is applied only over element 3

```
**BCSET
  ID BC1
  VALUE
    GHR GHR1
    SURF SURF1
    ELEMENT  3
    POINT  3
      TRAC  2
      SPLIST ALL
        T 1  100.0
```

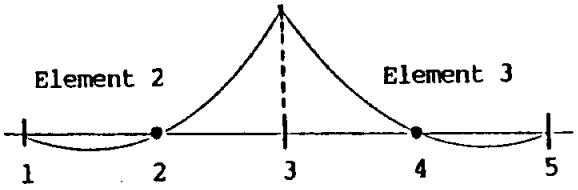

traction at NODE 3 is applied over both elements 2 and 3

```
**BCSET
  ID BC1
  VALUE
    GHR GHR1
    SURF SURF1
    ELEMENT  2  3
    POINT  3
      TRAC  2
      SPLIST ALL
        T 1  100.0
```

Figure for **BCSET: SURF, ELEM, and POIN card
2-D Boundary subset definition

ELEM EL1 EL2 ... ELN

Status - OPTIONAL

Full Keyword - ELEMENTS

Function - Specifies the elements of the surface IDSUR to which a boundary condition is to be applied.

Input Variables -

EL1,EL2,...,ELN (Integer) - REQUIRED

User element numbers of the elements of surface IDSUR which are to be included within the boundary condition set.

Additional Information -

The effect of this card is to restrict the application of the boundary condition to a portion of the surface IDSUR.

This input may be continued on more than one card. Each card must begin with the keyword ELEM.

If the ELEM card is not followed by a POIN card, then BEST-FSI will apply the boundary condition to all of the source points in the specified elements.

Examples of Use -

1. Specifies three elements on the surface SURF1 on which traction boundary conditions are given.

```
**BCSET
  ID  DISP2
  SURFACE  SURF1
  ELEMENTS  101   102   103
  DISP  2
  SPLIST  ALL
  T  1  0.0
**BCSET
```

`POIN  P1 P2 ... PN`

Status - OPTIONAL

Full Keyword - `POINTS`

Function - Restricts the application of a boundary condition to a subset of the source points lying on the surface IDSUR.

Input Variables -

P1,P2,...,PN (Integer) - REQUIRED

Additional Information -

This card restricts the application of the boundary condition to the source points specified.

This card may be repeated as often as required. Each card must begin with the keyword.

If the POIN card is specified, then BEST-FSI will apply the boundary condition to and only to the source points specified in this list.

Examples of Use -

1. Time-dependent input (in the x-direction) for points 5, 6, 7, and 8 over elements 102 and 103.

```
**BCSET
  ID BC1
  VALUE
  GMR REG3
    SURFACE BOTTOM
    ELEMENT 102 103
    POINT 5 6 7 8
    TIME 2.0 5.0 10.0
    TRAC 1
    SPLIST 6     7     5     8
    T 1 100.0 100.0 100.0 100.0
    T 2 200.0 200.0 300.0 300.0
    T 3 500.0 600.0 700.0 200.0
```

`TIME  T1 T2 ... TN`

Status - OPTIONAL

Full Keyword - `TIMES`

Function - Specifies the times at which the variable involved in the boundary condition set will be specified.

Input Variables -

T1 (Real) - REQUIRED

First time point for boundary condition specification.

T2,...,TN (Real) - OPTIONAL

Subsequent time points for boundary condition specification.

Additional Information -

This input may be continued on more than one card if required. Each card must begin with the keyword TIME.

The time values input on this card need not agree with the times at which output was requested in the case control input. Different sets of time points may be used for different boundary conditions in the same analysis.

The time points must be specifed in ascending order.

Boundary condition values at other than input times are calculated by linear interpolation.

If a time card does not appear, the variables involved in the boundary condition are assumed to be time independent. Consequently, only a single time point may be specified for the SPACE/TIME VARIATION (as defined in section 5.5.6).

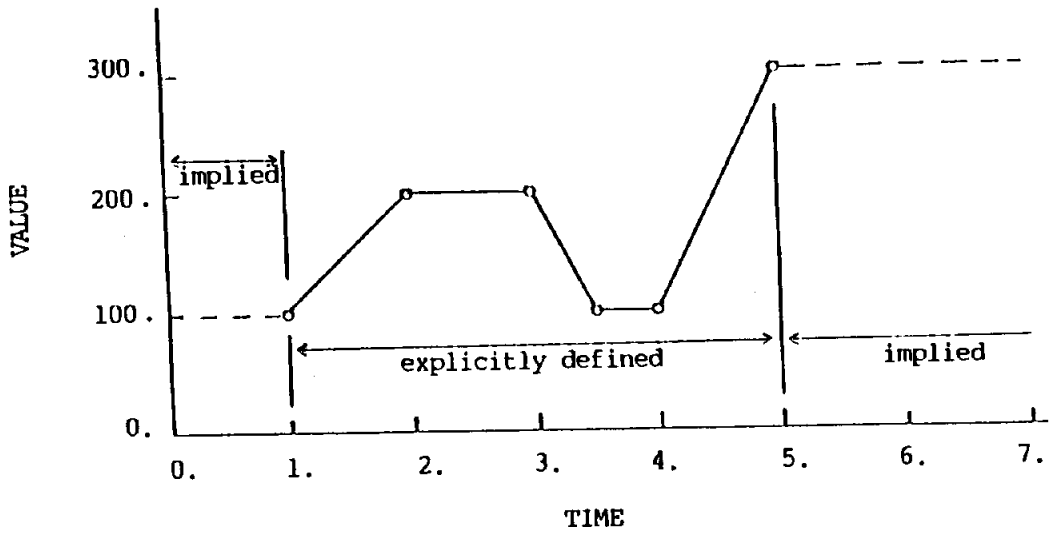

Example:

```
**BCSET
  ID TRAC1
  VALUE
    GNR GNR1
    SURF SURF1
    ELEMENT  3
      TIME  1.0  2.0  3.0  3.5  4.0  5.0
      TRAC  1
      SPLIST ALL
        T 1  100.0
        T 2  200.0
        T 3  200.0
        T 4  100.0
        T 5  100.0
        T 6  300.0
```

Figure for **BCSET: (all specified values)
VALUE vs. TIME for boundary condition input

5.5.5 VALUE BOUNDARY CONDITIONS FOR SURFACE ELEMENTS

TRAC IDIR

Status - OPTIONAL

Full Keyword - `TRACTION`

Function - Indicates that the IDIR component of traction will be specified for all nodes of the current boundary condition set.

Input Variables -

IDIR (Integer) - REQUIRED

Defines the component direction in which traction is specified. For cartesian coordinates:

1 - x direction

2 - y direction

For local coordinates:

1 - outer normal direction

Additional Information -

This card can only be used in a boundary condition data set containing the VALU card.

Up to two sets of traction and/or displacement specifications may be included in the same boundary condition data set. All must refer to the same boundary condition set. Only one condition (displacement or traction) may be applied in a given component direction.

The default condition is always to set traction to zero. After all boundary condition data sets have been processed, any boundary conditions not otherwise specified will be treated as zero traction conditions.

The TRACTION input line must be immediately followed by the space/time variation.

Examples of Use -

1. Defines a traction of magnitude 100.0 units in the positive y direction.

```
**BCSET
  ID TRAC1
  VALUE
  GMR  REG1
  SURFACE  SURF1
  ELEMENTS  105   106
  POINTS    112   113   114
  TRAC 2
  SPLIST    112   113   114
  T   1   100.0   100.0   100.0
```

Examples of Use -

2. Defines a traction of magnitude 100.0 units in the direction of the outward normal.

```
**BCSET
  VALUE
  LOCAL
  GMR  GMR1
  SURFACE SURF1
  ELEMENTS  101  102
  TRAC 1
  SPLIST ALL
  T  1  100.0
$ end of data set
```

VELO IDIR

Status - OPTIONAL

Full Keyword - VELOCITY

Function - Indicates that the IDIR component of velocity will be specified for all nodal points contained in the current boundary condition set.

Input Variables -

IDIR (Integer) - REQUIRED

Defines the component direction in which velocity is specified. For global coordinates:

1 - x direction

2 - y direction

For local coordinates:

1 - outer normal direction

Additional Information -

This card can only be used in a boundary condition data set containing the VALU card.

Up to two sets of traction and/or velocity specifications may be included in the same boundary condition data set. All must refer to the same boundary condition set. Only one condition (velocity or traction) may be applied in a given component direction.

The default condition is always to set traction to zero. After all boundary condition data sets have been processed, any boundary conditions not otherwise specified will be treated as zero traction conditions.

The VELOCITY input line must be immediately followed by the space/time variation.

Examples of Use -

1. Defines a rigid boundary wall on elements 11 and 12 belonging to surface SURF1 which is also part of geometric region GMR1.

```
**BCSET
  ID  BOTTOM
  VALUE
  GMR  GMR1
  SURFACE  SURF1
  ELEMENTS  11   12
```

```
  VELO  1
  SPLIST  ALL
  T  1  0.0
  VELO 2
  SPLIST  ALL
  T  2  0.0
$ provide next set, if any, of boundary conditions
```

FLUX

Status - OPTIONAL

Full Keyword - FLUX

Function - Indicates that the flux will be specified for all nodes of the current boundary condition set.

Input Variables - NONE

Additional Information -

This card can only be used in a boundary condition data set containing the VALU card.

The specification of flux may be included with up to two sets of traction and/or velocity specifications in the same boundary condition data set for thermoviscous analyses. All must refer to the same boundary condition set.

When applicable, the default condition is to set flux to zero.

The FLUX input line must be immediately followed by the space/time variation.

Examples of Use -

1. Defines zero flux conditions across three elements.

```
**BCSET
  ID  ENTER1
  VALUE
  GMR  GMR1
  SURFACE  SURF1
  ELEMENTS  22  23  24
  FLUX
  SPLIST  ALL
  T  1  0.0
```

TEMP

Status - OPTIONAL

Full Keyword - TEMPERATURE

Function - Indicates that the temperature will be specified for all nodes of the current boundary condition set.

Input Variables - NONE

Additional Information -

This card can only be used in a boundary condition data set containing the VALU card.

The specification of temperature may be included with up to two sets of traction and/or velocity specifications in the same boundary condition data set for thermoviscous analyses. All must refer to the same boundary condition set.

When applicable, the default condition is to set flux to zero.

The TEMP input line must be immediately followed by the space/time variation.

Examples of Use -

1. Indicates that a constant temperature is specified on the relevant elements.

```
**BCSET
  ID  TOP
  VALUE
  GMR  GMR2
  SURFACE  SURF2
  ELEMENTS  218  219
  VELO  1
  SPLIST  ALL
  T  1  0.0
  TEMP
  SPLIST ALL
  T  1  0.0
```

5.5.6 DEFINITION SPACE/TIME VARIATION

SPLI N1 N2 ... NN

Status - REQUIRED

Full Keyword - `SPLIST (source point list)`

Function - Defines the order in which nodal values of the variable will be input.

Input Variables -

N1 (Integer or Alphanumeric) - REQUIRED

User nodal point number of first node for which data will be input. Optional values are ALL or SAME, described under Additional Information.

N2,...,NN (Integer) - REQUIRED (if ALL or SAME are not used)

Users nodal point number of all remaining nodes that are defined by the definition of surface for application of Boundary Conditions (section 5.5.4).

Additional Information -

This input may be continued on more than one card if required. Each card must begin with the keyword SPLI.

If N1 = ALL, then **BEST-FSI** assigns the same value of the input variable to all nodes defined by the definition of surface for application of Boundary Condition (section 5.5.4).

If N1 = SAME, then the nodal point ordering is taken to be the same as that defined for the immediately preceding boundary condition specification within the same boundary condition set. N1 = SAME may not be used for the first boundary condition specification within a boundary condition set.

If the node number input is used (i.e. if ALL or SAME are not used) then the **total number of points in SPLI must equal the number of nodes defined by the SURF, ELEM, and POINT cards (section 5.5.4).**

`T  IT V1 V2 ... VN`

Status - REQUIRED

Full Keyword - T

Function - Identifies a data card containing values of a variable specified in a boundary condition at time point IT.

Input Variables -

IT (Integer) - REQUIRED

Time point as specified on the TIME card in the definition of the surface for application of boundary condition (section 5.5.4 and 5.5.6). IT = 1 refers to the first time point, IT = 2 the second, etc.

V1,V2,...,VN (Real) - REQUIRED

Nodal values of the variable in the nodal point order defined on the SPLI card.

Additional Information -

This input may continue for as many cards as required. Each additional card must begin with T and the time point IT. The input for each new time point must begin on a new card.

If N1 = ALL on the SPLI card, then only a single value of the variable is input for each time point.

The results of various uses of the SPLI and T cards are shown in the figure on the following page.

If the card "LOAD COMP" is specified in the case input, i.e. the boundary conditions are complex values, then the real part and imaginary part of nodal values are input in the form V1R V1I V2R V2I ..... VNR VNI.

The results of various uses of the SPLI and T cards are shown in the figure below.

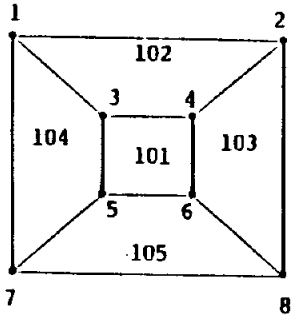

Note differences in traction input of nodes 3 and 4 over elements 101 and 102

Case 1 Input
```
TIME   0.0
TRAC 1
SPLIST ALL
T 1  100.0
```

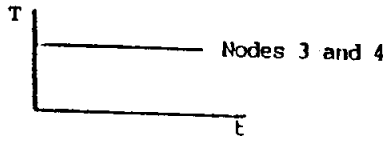

Case 2 Input
```
TIME   0.0
TRAC 1
SPLIST 3  4
T 1  100.0  50.0
```

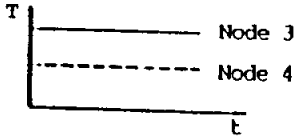

Case 3 Input
```
TIME   0.0  1.0  2.0  4.0
TRAC 1
SPLIST ALL
T 1  50.0
T 2  150.0
T 3  150.0
T 4  50.0
```

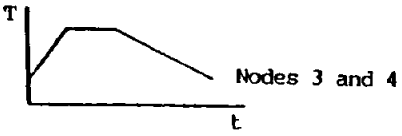

Case 4 Input
```
TIME   0.0  1.0  2.0  4.0
TRAC   1
SPLIST 3  4
T 1  75.0   50.0
T 2  100.0  25.0
T 3  75.0   50.0
T 4  75.0   25.0
```

Figure for BCSET: TIME and SPLIST cards
TIME-SPACE variation

5.5.7 RELATION BOUNDARY CONDITION

CONV FCOEFF TAMBT

Status - OPTIONAL

Full Keyword - CONVECTION

Function - Identifies a boundary condition in which surface temperature minus ambient temperature is linearly related to flux via a film coefficient for all nodal points defined in the current boundary condition.

Input Variables -

FCOEFF (Real) - REQUIRED

Convective film coefficient (h)

TAMBT (Real) - OPTIONAL

Ambient temperature of convective fluid (T_a)

Additional Information -

The CONV card can only be used if the RELA card has been input for the current boundary condition data set.

The CONVection option utilizes the relationship:

$$Q = -H * (T_a - T)$$

The film coefficient must be time independent.

If a TIME card was **not** included in the current boundary condition set, then the ambient temperature is time independent and TAMBT must be specified in the CONV card.

If a TIME card was included in the current BCSET, then T card(s) must follow the CONV card to define the time variation of ambient temperature.

No spatial variation of film coefficient nor ambient temperature is permitted within an individual BCSET.

The film coefficient should be set to a positive value. If zero is input, the coefficient will be automatically reset to 1.0E–10.

Examples of Use -

1. Defines a film coefficient of 1.26 units and a surface to ambient temperature difference of 100 units.

```
**BCSET
  ID  BCS1
  RELATION
  GMR  GMR1
  SURFACE SURF1
    ELEMENTS  1  2  3  4
    CONV      1.26  -100.0
**BCSET
  ID  BCS2
```

2. Define a time dependent convection boundary condition set, with a film coefficient of 10.43 units.

```
**BCSET
  ID  CONV1
   RELATION
   GMR  GMR1
   SURFACE SURF1
     ELEMENTS  1  2  14
     TIME 0.0 4.0 13.0 25.0
     CONV      10.43
     T   1      0.0
     T   2    100.0
     T   3    200.0
     T   4    300.0
```

5.6 BODY FORCE DEFINITION

This section describes the input for body forces.

The following body forces are included in **BEST-FSI**: inertial and convective. The input cards required to define these loads are described below.

SECTION	KEYWORD	PURPOSE
5.6.1 Body Force Input Card		
	**BODY	start of body force input
5.6.2 Inertial body force		
	INER	inertial body force input
	DIRE	direction of acceleration
	TIME	time of input
	ACCE	accleration input
5.6.3 Convective Body Force		
	CONV	convective body force input
	TIME	times for input
	GMR	identifies GMR
	DENS	fluid density input

5.6.1 BODY FORCE INPUT CARD

****BODY**

Status - OPTIONAL

Full Keyword - `BODY FORCE`

Function - Identifies the beginning of body force input.

Input Variables - NONE

Additional Information -

If more than type of body force is present, a separate block starting with **BODY should be defined for each type.

Examples of Use -

1. Request a three-dimensional centrifugal and thermal input.

```
**BODY FORCE
  CENT
  DIRE  0.0   0.0   1.0
  POINT 0.0   0.0   0.0
  TIME  1.   2.   3.   4.
  SPEED  45.   80.   100.   120.

**BODY FORCE
  THER
  TIME  0.   5.
  GMR  REG1
  TEMP
    1    0.0   500.
    2    0.0   500.
    3    0.0   300.
```

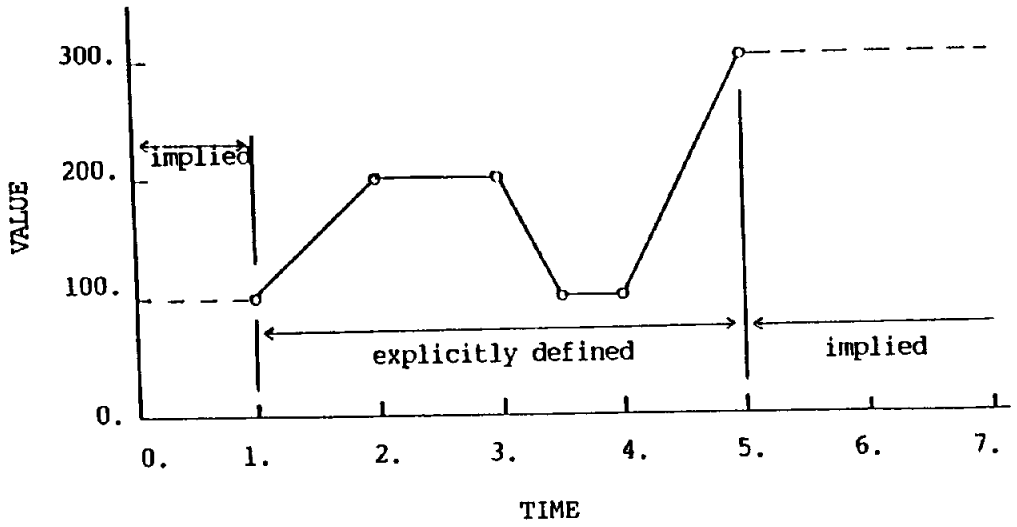

Example:
```
**BODY FORCE
 CENTRIFUGAL
   POINT   0.0   0.0
   TIME    1.0   2.0   3.0   3.5   4.0   5.0
   SPEED 100.0 200.0 200.0 100.0 100.0 300.0
```

Figure for**BODY: (all body force values)
VALUE vs. TIME for body force input

5.6.2 INERTIAL BODY FORCE

INER

Status - OPTIONAL

Full Keyword - INERTIA FORCE

Function - Indicates that an inertia force will be applied.

Input Variables - NONE

Additional Information -

Only one (time dependent) inertia load condition may be defined for an analysis. It is applied to the entire body.

Examples of Use -

1. Request a two-dimensional inertial input

```
**BODY FORCE
  INER
  DIRE    1.0   0.0
  TIME    1.0
  ACCE    300.
```

DIRE X Y

Status - OPTIONAL

Full Keyword - DIRECTION

Function - Defines a vector parallel to the direction of inertia force.

Input Variables -

X,Y (Real) - REQUIRED

Cartesian components of a vector parallel to the inertia force.

Additional Information -

Only one direction can be defined in an analysis.

If this card is omitted, the inertia force is assumed to be parallel to the z-axis of the global system in the negative direction (i.e. gravity loading).

Examples of Use -

1. Defines an inertial force in the positive Y-direction for a two-dimensional analysis.

```
**BODY FORCE
  INER
  DIRE  0.  1.
  TIME  1.0
  ACCE  10.0
```

TIME T1 T2 ... TN

Status - REQUIRED (if INER is input)

Full Keyword - TIMES

Function - Defines the times at which the acceleration of the body will be defined.

Input Variables -

T1,T2,...,TN (Real) - REQUIRED

Times at which acceleration will be defined.

Additional Information -

This card may be input as many times as required. Each card begins with the keyword TIME.

A maximum of 20 time values may be specified.

Examples of Use -

1. Specifies accelerations at three times.

```
**BODY FORCE
  INER
  DIRE  0.    1.
  TIME  1.0   2.0   3.0
  ACCE  10.0  15.0  20.0
```

ACCE ACC1 ACC2 .... ACCN

Status - OPTIONAL

Full Keyword - **ACCELERATION**

Function - Defines the acceleration of the body.

Input Variables -

ACC1,ACC2,...,ACCN (Real) -REQUIRED

Acceleration at times specified on TIME card.

Additional Information -

This card may be input as often as required. Each card begins with the keyword ACCE.

DEFAULT: Gravity loading of 386.4 in/sec/sec.

Examples of Use -

1. Specifies an acceleration of 100.0 units in an inertial body force loading at a single time step.

```
**BODY FORCE
  INER
  DIRE  0.    1.
  TIME  1.
  ACCE  100.
```

5.6.3 CONVECTIVE BODY FORCE

CONV

Status - OPTIONAL

Full Keyword - `CONVECTIVE`

Function - Indicates that convective body force will be applied in a fluid dynamics analysis by using an incremental density algorithm.

Input Variables - NONE

Additional Information -

This type of body force is only applicable to steady-state fluid dynamic analysis. Furthermore, the INCREMENT DENSITY card must be included in case control.

Examples of Use -

1. Indicates that convective body force field is present.

```
**BODY FORCE
  CONVECTIVE
  TIME  0.0    1.0    2.0    3.0
  GMR  GMR1
  DENSITY  0.0    1.0  10.0  100.0
  GMR  GMR2
  DENSITY 0.0    1.0  10.0  100.0
```

TIME T1 T2 .... TN

Status - REQUIRED (if CONV is input)

Full Keyword - TIMES

Function - Defines the times at which the fluid densities will be defined.

Input Variables -

T1,T2,...,TN (Real) - REQUIRED

Times at which fluid densities will be defined.

Additional Information -

If all times do not fit on one card, TIME may be continued on a second card immediately following the first time card, starting with the keyword TIME. Only one time definition is allowed for fluid density input, and therefore densities for each GMR must be defined according to this one definition.

A maximum of 20 time values may be specified.

Examples of Use -

1. Specifies times at which densitites are to be given.

```
**BODY FORCE
  CONVECTIVE
  TIMES   0.0   1.0   2.0
  GMR GMR1
  DENSITY 5.0  10.0  15.0
```

GMR GMRNAME

Status - REQUIRED (if CONV is input)

Full Keyword - **GMR**

Function - Identifies the GMR in which fluid densities will be defined.

Input Variables -

GMRNAME (Alphanumeric) - REQUIRED

Allowable values for GMRNAME are IDGMR or ALL.

IDGMR = the identifier of a specific GMR for which fluid densities are being defined. (NAME on ID card in **GMR input).

ALL = indicates the fluid densities of all GMR's in the problem are identical and will be defined under one definition.

Additional Information -

The fluid density must be defined for every region containing cells.

If ALL is used as the argument of this card, then this GMR card and the DENS card (see next page) are input only once.

If the fluid densities differ in different regions then this GMR card (with IDGMR as the argument) and the DENS card (see next page) must be repeated for every region containing cells.

All GMR's (for which fluid density input is desired) must be contained under a single **BODY FORCE input.

Examples of Use -

The following two examples have identical meaning.

```
**BODY FORCE
  CONV
  TIMES  0.5  1.0
  GMR  REG1
    DENSITY  5.0   15.0
  GMR  REG2
    DENSITY  5.0   15.0
  GMR REG3
    DENSITY  5.0   15.0
  GMR REG4
    DENSITY  5.0   15.0
```

```
**BODY FORCE
  CONV
  TIME  0.5  1.0
  GMR ALL
    DENSITY  5.0   15.0
```

DENS DEN1 DEN2 ... DENN

Status - OPTIONAL

Full Keyword - **DENSITY**

Function - Defines the fluid mass density for the GMR.

Input Variables -

DEN1, DEN2,...,DENN (Real) - REQUIRED

Density at times specified on TIME card.

Additional Information -

This card may be input at often as required. Each card must begin with the keyword DENS.

When convective body forces are defined, the value of density specified in the material section is ignored.

Examples of Use -

Lists densities at the times specified on the TIME card.

```
**BODY FORCE
  CONVECTIVE
  TIMES  0.0  1.0  2.0  3.0
  GMR  GMR1
  DENSITY  0.0  1.0  10.0  100.0
  GMR  GMR2
  DENSITY  0.0  1.0  10.0  100.0
```

6.0 EXAMPLE PROBLEMS

In this section example problems are presented to illustrate data preparation for **BEST-FSI**. An attempt has been made to keep the problem geometry as simple as possible so the user is not burdened with undue complexity. It is hoped that an analyst who is using an analysis procedure for the first time will find these example problems invaluable in the learning process.

Each problem includes the following items:

1) A Brief Problem Description
2) Geometry and Boundary Element Model
3) Input Data for running the problem in **BEST-FSI**
4) Selected Output from **BEST-FSI**

It should be noted that since the boundary element models illustrated utilize coarse meshes, the **BEST-FSI** results may differ somewhat from the theoretical values. However, with a finer mesh, the theoretical values should be obtained. Also, the results may vary somewhat depending on the computer system being used to run **BEST-FSI**.

An estimated RUN TIME is cited for each problem to give the user a feeling for the computer time needed to run the problem. All RUN TIMES are related to problem ELAS605, a simple elastic cube in tension, which will be considered to have a run time of 1 unit using BEST-3D. A different problem which has a RUN TIME of 8 would take approximately eight times longer to run that the ELAS605 problem. However, these times will vary somewhat depending on the computer system being used to run **BEST-3D**and **BEST-FSI**.

EXAMPLE PROBLEM: FLUI601

ANALYSIS TYPE: FLUID DYNAMICS
2-D, STEADY STATE, THERMO-VISCOUS STOKES FLOW, INCOMPRESSIBLE

PROBLEM DESCRIPTION:
FLOW BETWEEN TWO PARALLEL PLATES. THE UPPER PLATE IS MOVING WITH A VELOCITY OF 1. LOWER PLATE IS FIXED.
A UNIFORM PRESSURE OF 100 IS PRESENT EVERYWHERE.
THIS IS OFTEN CALLED "COUETTE FLOW".

BOUNDARY ELEMENT MODEL:
RECTANGULAR REGION, 4 ELEMENTS.

REFERENCE FOR ANALYTICAL SOLUTION:
MORTON DENN, PROCESS FLUID MECHANICS (1980), PG. 176-177.
X-VELOCITY AND TEMPERATURE ARE LINEARLY DISTRIBUTED BETWEEN PLATES.

SOLUTION POINTS TO VERIFY:

(X-VELOCITY AND TEMPERATURE)

NODE	ANALYTICAL	BEST-FSI
4	.500	.500
19	.900	.900

RUN TIME:
0.1 X BASE PROBLEM

MISCELLANEOUS:
TRACTION BOUNDARY CONDITIONS ARE FIXED ON INLET AND OUTLET, FROM THE ANALYTICAL SOLUTION. AMBIGUOUS BOUNDARY CONDITIONS AT THE CORNERS ARE AVOIDED.
THE UNIFORMLY APPLIED PRESSURE DOES NOT AFFECT THE SOLUTION VELOCITIES, BUT IS INCLUDED TO TEST INTEGRATION ACCURACY.

NODES

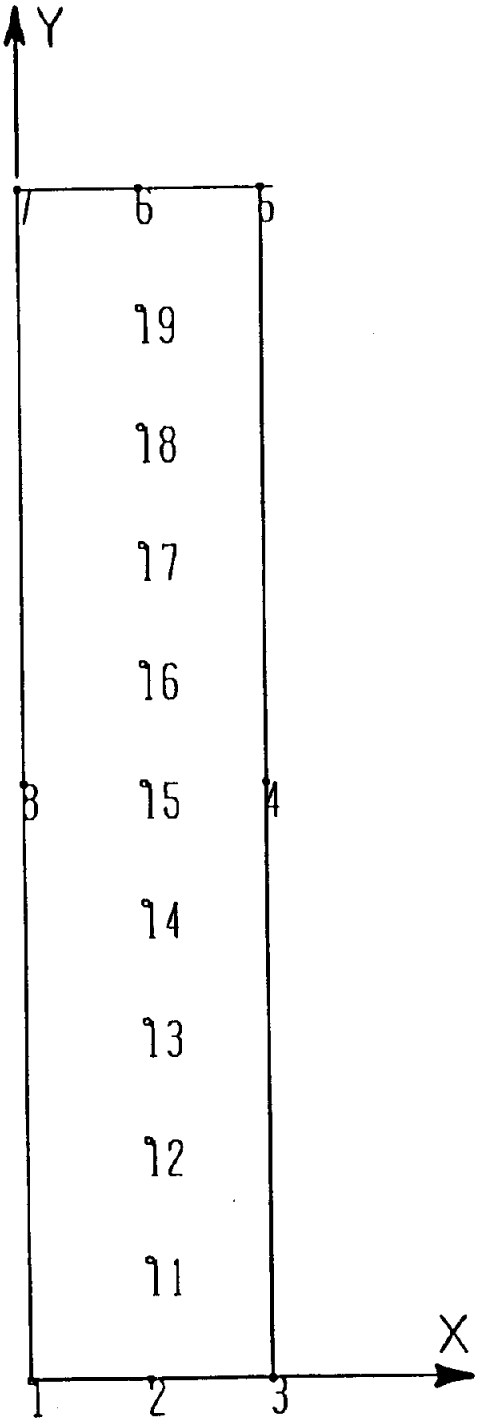

```
**CASE
  TITLE PARALLEL FLOW: STOKES (LINEAR) FLOW
  PLANE
  FLUID INCOMPRESSIBLE STEADY
  TIME STEP  1   1.0
  MAXI  1
  THERMAL                    $ INCLUDE HEAT TRANSFER ANALYSIS ALSO
  ITERATIVE LINEAR           $ ONLY SOLVE STOKES FLOW
  PRECISION MAXIMUM


**MATE
  ID MAT1
  TEMP 460.0
    VISC 1.0
    COND 1.0


**GMR
  ID GMR1
  MAT MAT1
  TINT 460.0
  POINTS
          1          0.0000          0.0000
          2          1.0000          0.0000
          3          2.0000          0.0000
          4          2.0000          5.0000
          5          2.0000         10.0000
          6          1.0000         10.0000
          7          0.0000         10.0000
          8          0.0000          5.0000
  SURFACE SURF1
    TYPE QUAD
    ELEMENTS
          1          1          2          3
          2          3          4          5
          3          5          6          7
          4          7          8          1
  NORMAL  +
  SAMPLING POINTS
         11          1.0000          1.0000
         12          1.0000          2.0000
         13          1.0000          3.0000
         14          1.0000          4.0000
         15          1.0000          5.0000
         16          1.0000          6.0000
         17          1.0000          7.0000
         18          1.0000          8.0000
         19          1.0000          9.0000


**BCSET
  ID BOTTOM
  VALUE
  GMR GMR1
```

```
  SURFACE SURF1
  ELEMENTS       1
  VELO 1
  SPLIST ALL
  T 1        0.0000
  VELO 2
  SPLIST ALL
  T 1        0.0000
  TEMP
  SPLIST ALL
  T 1        0.0000

**BCSET
  ID EXIT
  VALUE
  GMR GMR1
  SURFACE SURF1
  ELEMENTS       2
  TRAC 1
  SPLIST ALL
  T 1        -100.0000
  TRAC 2
  SPLIST ALL
  T 1        0.1000

**BCSET
  ID TOP
  VALUE
  GMR GMR1
  SURFACE SURF1
  ELEMENTS       3
  VELO 1
  SPLIST ALL
  T 1        1.0000
  VELO 2
  SPLIST ALL
  T 1        0.0000
  TEMP
  SPLIST ALL
  T 1        1.0000

**BCSET
  ID ENTRANCE
  VALUE
  GMR GMR1
  SURFACE SURF1
  ELEMENTS       4
  TRAC 1
  SPLIST ALL
  T 1        100.0000
  TRAC 2
  SPLIST ALL
  T 1        -0.1000

$ END OF DATA
```

1 JOB TITLE: PARALLEL FLOW: STOKES (LINEAR) FLOW
BOUNDARY SOLUTION AT TIME = 1.000000 FOR REGION = GMR1

ELEMENT	NODE NO.	X VELOCITY	Y VELOCITY	TEMPERATURE	X TRACTION	Y TRACTION	FLUX
1	1	0.00000E+00	0.00000E+00	0.00000E+00	-0.10000E+00	0.10000E+03	0.10000E+00
1	2	0.00000E+00	0.00000E+00	0.00000E+00	-0.10000E+00	0.10000E+03	0.10000E+00
1	3	0.00000E+00	0.00000E+00	0.00000E+00	-0.10000E+00	0.10000E+03	0.10000E+00
2	3	0.00000E+00	0.00000E+00	0.00000E+00	-0.10000E+03	0.10000E+00	0.00000E+00
2	4	0.50000E+00	0.16170E-08	0.50000E+00	-0.10000E+03	0.10000E+00	0.00000E+00
2	5	0.10000E+01	0.00000E+00	0.10000E+01	-0.10000E+03	0.10000E+00	0.00000E+00
3	5	0.10000E+01	0.00000E+00	0.10000E+01	0.10000E+00	-0.10000E+03	-0.10000E+00
3	6	0.10000E+01	0.00000E+00	0.10000E+01	0.10000E+00	-0.10000E+03	-0.10000E+00
3	7	0.10000E+01	0.00000E+00	0.10000E+01	0.10000E+00	-0.10000E+03	-0.10000E+00
4	7	0.10000E+01	0.00000E+00	0.10000E+01	0.10000E+03	-0.10000E+00	0.00000E+00
4	8	0.50000E+00	-0.16170E-08	0.50000E+00	0.10000E+03	-0.10000E+00	0.00000E+00
4	1	0.00000E+00	0.00000E+00	0.00000E+00	0.10000E+03	-0.10000E+00	0.00000E+00

1 JOB TITLE: PARALLEL FLOW: STOKES (LINEAR) FLOW
INTERIOR VELOCITY AT TIME = 1.000000 FOR REGION = GMR1

NODE	X VELOCITY	Y VELOCITY	TEMPERATURE
1	0.000000E+00	0.000000E+00	0.000000E+00
2	0.000000E+00	0.000000E+00	0.000000E+00
3	0.000000E+00	0.000000E+00	0.000000E+00
4	0.500000E+00	0.161705E-08	0.500000E+00
5	0.100000E+01	0.000000E+00	0.100000E+01
6	0.100000E+01	0.000000E+00	0.100000E+01
7	0.100000E+01	0.000000E+00	0.100000E+01
8	0.500000E+00	-0.161701E-08	0.500000E+00
11	0.100000E+00	-0.198781E-09	0.100000E+00
12	0.200000E+00	-0.879798E-09	0.200000E+00
13	0.300000E+00	-0.220993E-07	0.300000E+00
14	0.400000E+00	0.943855E-08	0.400000E+00
15	0.500000E+00	0.906079E-14	0.500000E+00
16	0.600000E+00	-0.943853E-08	0.600000E+00
17	0.700000E+00	0.220994E-07	0.700000E+00
18	0.800000E+00	0.879830E-09	0.800000E+00
19	0.900000E+00	0.198821E-09	0.900000E+00

EXAMPLE PROBLEM: FLUI602

ANALYSIS TYPE: FLUID DYNAMICS
2-D, STEADY STATE, THERMO-VISCOUS FLOW, INCOMPRESSIBLE,
NEWTON RAPHSON ITERATION ON NONLINEAR TERMS.

PROBLEM DESCRIPTION:
FLOW BETWEEN TWO PARALLEL PLATES. THE UPPER PLATE IS MOVING WITH A VELOCITY OF 1. LOWER PLATE IS FIXED. NO REFERENCE PRESSURE PRESENT. THIS IS OFTEN CALLED "COUETTE FLOW", BUT IS USED HERE TO TEST NONLINEAR ITERATION.

BOUNDARY ELEMENT MODEL:
TWO GMR, TEN CELLS TOTAL.

REFERENCE FOR ANALYTICAL SOLUTION:
MORTON DENN, PROCESS FLUID MECHANICS (1980), PG. 176-177.
X-VELOCITY IS A LINEAR DISTRIBUTION BETWEEN PLATES.

SOLUTION POINTS TO VERIFY:

		(X-VELOCITY AFTER THIRD TIME STEP)	
GMR	NODE	ANALYTICAL	BEST-FSI
1	24	.5000	.4999
1	26	.6000	.5997
2	240	.9000	.9000

RUN TIME:
23 X BASE PROBLEM

MISCELLANEOUS:
TRACTION BOUNDARY CONDITIONS ARE FIXED ON INLET AND OUTLET, FROM THE ANALYTICAL SOLUTION. AMBIGUOUS BOUNDARY CONDITIONS AT THE CORNERS ARE AVOIDED. TIGHT ITERATION TOLERANCES AND MAXIMUM INTEGRATION PRECISION ARE USED TO TEST ACCURACY OF NONLINEAR SOLVER.
THIS ALSO TESTS THE INTERFACE BETWEEN TWO GMR'S, EACH WITH A DIFFERENT FREE-STREAM VELOCITY.

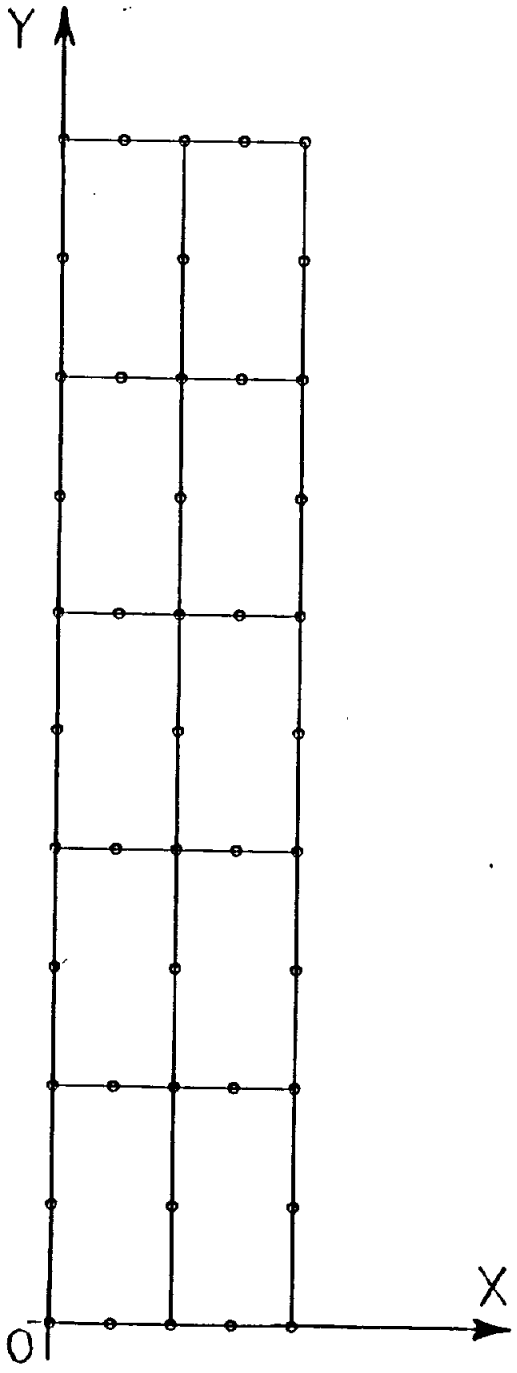

GEOMETRY

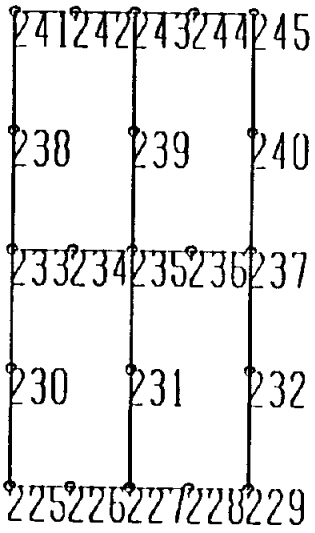

GMR2

NODES

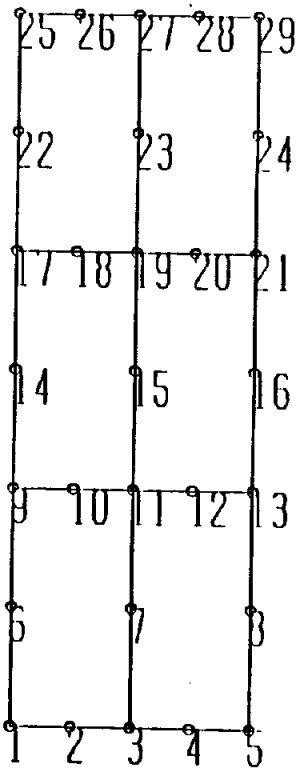

GMR1

NODES

```
**CASE
  TITLE (PARALLEL FLOW) NON-LINEAR NAVIER-STOKES
  PLANE
  FLUID INCOMPRESSIBLE STEADY     $ THIS SPECIFIES 3 TIME STEPS,
  TIME STEP  3   1.0              $ EACH OF 1.0 TIME UNITS LONG.
  MAXI  10                        $ EACH TIME STEP HAS A MAXIMUM
                                  $ OF 10 ITERATIONS.
  THERMAL
  NEWTON
  INCREMENT DENSITY       $  DENSITY IS INCREMENTED TO INCREASE THE
                          $  EFFECT OF THE NONLINEAR CONVECTIVE TERMS.
                          $  THIS REFERENCES THE **BODF CARDS WHICH
                          $  SPECIFY HOW DENSITY IS INCREMENTED.
  TOLERANCE 1.E-9
  PRECISION MAXIMUM


**MATE
  ID MAT1
  TEMP 460.0
    VISC 1.0
    DENS 1.0
    COND 1.0
    SPEC 1.0


**GMR
  ID GMR1
  MAT MAT1
  TINT 460.0
  VREF  0.0  0.0
  POINTS
          1          0.0000          0.0000
          2          0.5000          0.0000
          3          1.0000          0.0000
          4          1.5000          0.0000
          5          2.0000          0.0000
          6          0.0000          1.0000
          7          1.0000          1.0000
          8          2.0000          1.0000
          9          0.0000          2.0000
         10          0.5000          2.0000
         11          1.0000          2.0000
         12          1.5000          2.0000
         13          2.0000          2.0000
         14          0.0000          3.0000
         15          1.0000          3.0000
         16          2.0000          3.0000
         17          0.0000          4.0000
         18          0.5000          4.0000
         19          1.0000          4.0000
         20          1.5000          4.0000
         21          2.0000          4.0000
         22          0.0000          5.0000
```

```
          23          1.0000          5.0000
          24          2.0000          5.0000
          25          0.0000          6.0000
          26          0.5000          6.0000
          27          1.0000          6.0000
          28          1.5000          6.0000
          29          2.0000          6.0000
  SURFACE SURF1
    TYPE QUAD
    ELEMENTS
          11           1               2               3
          12           3               4               5
          13           5               8              13
          14          13              16              21
          15          21              24              29
          25          29              28              27
          26          27              26              25
          22          25              22              17
          23          17              14               9
          24           9               6               1
  NORMAL  +
  VOLUME
   TYPE QUAD
   CELL
          1        1    2    3    7   11   10    9    6
          2        3    4    5    8   13   12   11    7
          3        9   10   11   15   19   18   17   14
          4       11   12   13   16   21   20   19   15
          5       17   18   19   23   27   26   25   22
          6       19   20   21   24   29   28   27   23

**GMR
  ID GMR2
  MAT MAT1
  TINT 460.0
  VREF  0.8  0.0
  POINTS
        225          0.0000          6.0000
        226          0.5000          6.0000
        227          1.0000          6.0000
        228          1.5000          6.0000
        229          2.0000          6.0000
        230          0.0000          7.0000
        231          1.0000          7.0000
        232          2.0000          7.0000
        233          0.0000          8.0000
        234          0.5000          8.0000
        235          1.0000          8.0000
        236          1.5000          8.0000
        237          2.0000          8.0000
        238          0.0000          9.0000
        239          1.0000          9.0000
        240          2.0000          9.0000
        241          0.0000         10.0000
        242          0.5000         10.0000
        243          1.0000         10.0000
        244          1.5000         10.0000
```

```
      245          2.0000          10.0000
  SURFACE SURF2
    TYPE QUAD
    ELEMENTS
      216          229          232          237
      217          237          240          245
      218          245          244          243
      219          243          242          241
      220          241          238          233
      221          233          230          225
      227          225          226          227
      228          227          228          229
  NORMAL  +
  VOLUME
   TYPE QUAD
   CELL
      207       225  226  227  231  235  234  233  230
      208       227  228  229  232  237  236  235  231
      209       233  234  235  239  243  242  241  238
      210       235  236  237  240  245  244  243  239


**INTERFACE
  GMR GMR1
  SURF SURF1
  ELEM      25    26
  GMR GMR2
  SURF SURF2
  ELEM      227    228
  VDIF


$
$ BOUNDARY CONDITIONS ON GMR1:
$
**BCSET
  ID BOTTOM
  VALUE
  GMR GMR1
  SURFACE SURF1
  ELEMENTS      11    12
  VELO 1
  SPLIST ALL
  T 1        0.0000
  VELO 2
  SPLIST ALL
  T 1        0.0000
  TEMP
  SPLIST ALL
  T 1        0.0000

**BCSET
  ID EXIT1
  VALUE
  GMR GMR1
  SURFACE SURF1
  ELEMENTS      13    14    15
  TRAC 1
```

```
   SPLIST ALL
   T 1        0.0000
   TRAC 2
   SPLIST ALL
   T 1        0.1000
   FLUX
   SPLIST ALL
   T 1        0.0000

 **BCSET
   ID ENTER1
   VALUE
   GMR GMR1
   SURFACE SURF1
   ELEMENTS     22    23    24
   TRAC 1
   SPLIST ALL
   T 1        0.0000
   TRAC 2
   SPLIST ALL
   T 1       -0.1000
   FLUX
   SPLIST ALL
   T 1        0.0000


 $
 $ BOUNDARY CONDITIONS ON GMR2:
 $
 **BCSET
   ID EXIT2
   VALUE
   GMR GMR2
   SURFACE SURF2
   ELEMENTS      216    217
   TRAC 1
   SPLIST ALL
   T 1        0.0000
   TRAC 2
   SPLIST ALL
   T 1        0.1000
   FLUX
   SPLIST ALL
   T 1        0.0000

 **BCSET
   ID TOP
   VALUE
   GMR GMR2
   SURFACE SURF2
   ELEMENTS      218    219
   VELO 1
   SPLIST ALL
   T 1        1.0000
   VELO 2
   SPLIST ALL
   T 1        0.0000
   TEMP
```

```
  SPLIST ALL
  T 1        1.0000

**BCSET
  ID ENTER2
  VALUE
  GMR GMR2
  SURFACE SURF2
  ELEMENTS      220    221
  TRAC 1
  SPLIST ALL
  T 1        0.0000
  TRAC 2
  SPLIST ALL
  T 1       -0.1000
  FLUX
  SPLIST ALL
  T 1        0.0000


**BODF
  CONVECTIVE
    TIMES         0.0 1.0 2.0 3.0
    GMR GMR1
      DENSITY     0.0 1.0 10.0 100.0
    GMR GMR2
      DENSITY     0.0 1.0 10.0 100.0
  $  AT TIME T=3.0, THE DENSITY HAS ATTAINED A VALUE OF 100.0

$  END OF DATA
```

1 JOB TITLE: (PARALLEL FLOW) NON-LINEAR NAVIER-STOKES
INTERIOR VELOCITY AT TIME = 3.000000 FOR REGION = GMR1

NODE	X VELOCITY	Y VELOCITY	TEMPERATURE
1	0.000000E+00	0.000000E+00	0.000000E+00
2	0.000000E+00	0.000000E+00	0.000000E+00
3	0.000000E+00	0.000000E+00	0.000000E+00
7	0.999988E-01	0.108385E-06	0.100351E+00
11	0.199997E+00	-0.539313E-06	0.200696E+00
10	0.199996E+00	-0.150204E-06	0.200697E+00
9	0.199996E+00	0.609698E-06	0.200699E+00
6	0.999991E-01	-0.367394E-06	0.100350E+00
4	0.000000E+00	0.000000E+00	0.000000E+00
5	0.000000E+00	0.000000E+00	0.000000E+00
8	0.999991E-01	0.561417E-07	0.100350E+00
13	0.199997E+00	-0.862773E-07	0.200693E+00
12	0.199997E+00	-0.422776E-06	0.200694E+00
15	0.299993E+00	-0.214891E-06	0.301005E+00
19	0.399988E+00	-0.765140E-06	0.401284E+00
18	0.399988E+00	-0.605515E-06	0.401285E+00
17	0.399988E+00	-0.738825E-08	0.401287E+00
14	0.299993E+00	-0.862877E-06	0.301005E+00
16	0.299994E+00	-0.378708E-06	0.301004E+00
21	0.399988E+00	-0.493718E-06	0.401282E+00
20	0.399988E+00	-0.845648E-06	0.401283E+00
23	0.499984E+00	-0.595487E-06	0.501465E+00
27	0.599985E+00	-0.631671E-06	0.601499E+00
26	0.599985E+00	-0.232570E-06	0.601499E+00
25	0.599985E+00	0.351934E-07	0.601500E+00
22	0.499984E+00	-0.103572E-05	0.501469E+00
24	0.499984E+00	-0.578257E-06	0.501463E+00
29	0.599985E+00	-0.988109E-06	0.601495E+00
28	0.599985E+00	-0.717437E-06	0.601497E+00

1 JOB TITLE: (PARALLEL FLOW) NON-LINEAR NAVIER-STOKES
INTERIOR VELOCITY AT TIME = 3.000000 FOR REGION = GMR2

NODE	X VELOCITY	Y VELOCITY	TEMPERATURE
225	0.599985E+00	0.351934E-07	0.601500E+00
226	0.599985E+00	-0.232570E-06	0.601499E+00
227	0.599985E+00	-0.631671E-06	0.601499E+00
231	0.699988E+00	-0.608461E-06	0.701335E+00
235	0.799995E+00	-0.626972E-06	0.800929E+00
234	0.799995E+00	-0.234223E-06	0.800929E+00
233	0.799994E+00	-0.167461E-06	0.800929E+00
230	0.699987E+00	-0.752627E-06	0.701339E+00
228	0.599985E+00	-0.717437E-06	0.601497E+00
229	0.599985E+00	-0.988109E-06	0.601495E+00
232	0.699988E+00	-0.415274E-06	0.701331E+00
237	0.799995E+00	-0.119037E-05	0.800928E+00
236	0.799994E+00	-0.723639E-06	0.800929E+00
239	0.900000E+00	-0.109554E-05	0.900433E+00

243	0.100000E+01	0.000000E+00	0.100000E+01
242	0.100000E+01	0.000000E+00	0.100000E+01
241	0.100000E+01	0.000000E+00	0.100000E+01
238	0.900000E+00	-0.132977E-05	0.900432E+00
240	0.900000E+00	-0.514231E-06	0.900434E+00
245	0.100000E+01	0.000000E+00	0.100000E+01
244	0.100000E+01	0.000000E+00	0.100000E+01

EXAMPLE PROBLEM: FLUI603

ANALYSIS TYPE: FLUID DYNAMICS
2-D, TRANSIENT, THERMO-VISCOUS STOKES FLOW, INCOMPRESSIBLE

PROBLEM DESCRIPTION:
DEVELOPING FLOW BETWEEN TWO PARALLEL PLATES. THE UPPER PLATE IS IS INSTANTLY APPLIED AT TIME T=0. AND IS MOVING WITH A VELOCITY OF 1. LOWER PLATE IS FIXED.
THIS IS OFTEN CALLED "DEVELOPING COUETTE FLOW".

BOUNDARY ELEMENT MODEL:
12 BOUNDARY ELEMENTS, NO INTERIOR CELLS.

REFERENCE FOR ANALYTICAL SOLUTION:
SCHLICHTING, BOUNDARY LAYER THEORY (1979), PG. 91-92, INVOLVING AN INFINITE SERIES.
THE DEVELOPING VISCOUS FLOW IS SIMILAR TO THE DEVELOPING TEMPERATURE PROFILE IN HEAT CONDUCTION.

SOLUTION POINTS TO VERIFY:

		(Y-VELOCITY)	
TIME	NODE	ANALYTICAL	BEST-FSI
2.0	15	.0124	.0166
2.0	22	.3173	.2992
10.0	15	.2627	.2573
10.0	22	.6547	.6486

RUN TIME:
3 X BASE PROBLEM

MISCELLANEOUS:
Y-VELOCITY IS FIXED ON INLET AND OUTLET. AMBIGUOUS BOUNDARY CONDITIONS ARE AVOIDED AT THE CORNERS.

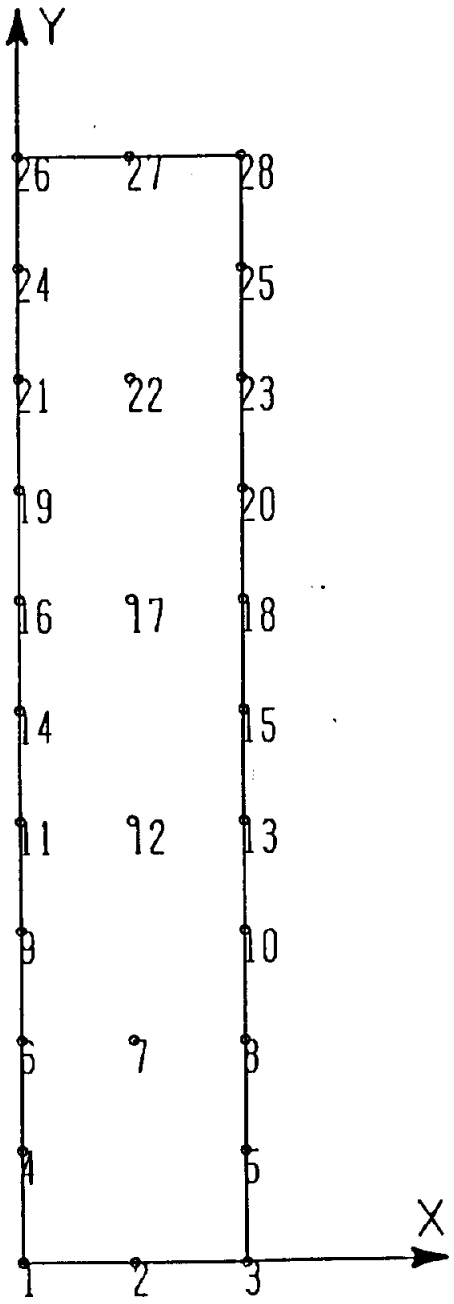

NODES

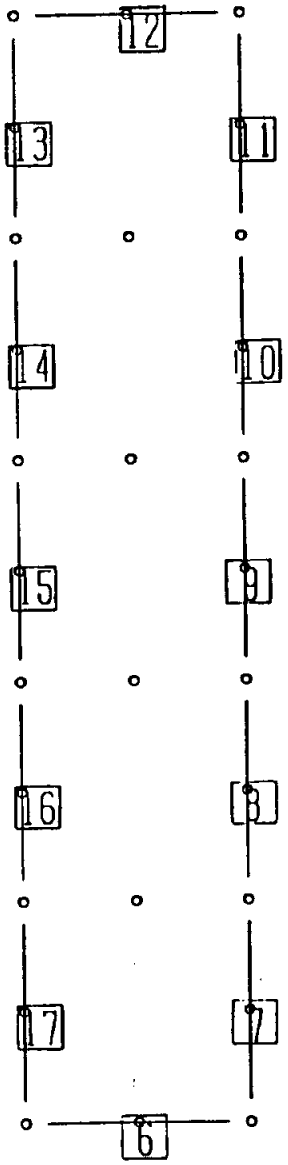

ELEMENTS

```
**CASE
  TITLE TRANSIENT PARALLEL FLOW: STOKES (LINEAR) FLOW
  PLANE
  FLUID INCOMPRESSIBLE TRANSIENT   $ THIS SPECIFIES TEN TIME STEPS,
  TIME STEP  10  1.0    $ EACH ONE TIME UNIT LONG.  SINCE THIS IS
  MAXI  1               $ A LINEAR PROBLEM, ONLY ONE ITERATION PER
                        $ TIME STEP IS REQUIRED.
  THERMAL
  ITERATIVE LINEAR

**MATE
  ID MAT1
  TEMP 460.0
    VISC 1.0
    COND 1.0
    DENS 1.0
    SPEC 1.0

**GMR
  ID GMR1
  MAT MAT1
  TINT 460.0
  POINTS
          1          0.0000          0.0000
          2          1.0000          0.0000
          3          2.0000          0.0000
          4          0.0000          1.0000
          5          2.0000          1.0000
          6          0.0000          2.0000
          8          2.0000          2.0000
          9          0.0000          3.0000
         10          2.0000          3.0000
         11          0.0000          4.0000
         13          2.0000          4.0000
         14          0.0000          5.0000
         15          2.0000          5.0000
         16          0.0000          6.0000
         18          2.0000          6.0000
         19          0.0000          7.0000
         20          2.0000          7.0000
         21          0.0000          8.0000
         23          2.0000          8.0000
         24          0.0000          9.0000
         25          2.0000          9.0000
         26          0.0000         10.0000
         27          1.0000         10.0000
         28          2.0000         10.0000
 SURFACE SURF1
   TYPE QUAD
   ELEMENTS
          6          1          2          3
          7          3          5          8
```

```
          8          8         10         13
          9         13         15         18
         10         18         20         23
         11         23         25         28
         12         28         27         26
         13         26         24         21
         14         21         19         16
         15         16         14         11
         16         11          9          6
         17          6          4          1
  NORMAL  +
  SAMPLING POINTS
          7          1.0000          2.0000
         12          1.0000          4.0000
         17          1.0000          6.0000
         22          1.0000          8.0000


**BCSET
  ID BOTTOM
  VALUE
  GMR GMR1
  SURFACE SURF1
  ELEMENTS       6
  VELO 1
  SPLIST ALL
  T 1        0.0000
  TRAC 2
  SPLIST ALL
  T 1        0.0000
  TEMP
  SPLIST ALL
  T 1        0.0000


**BCSET
  ID EXIT
  VALUE
  GMR GMR1
  SURFACE SURF1
  ELEMENTS       7    8    9   10   11
  TRAC 1
  SPLIST ALL
  T 1        0.0000
  VELO 2
  SPLIST ALL
  T 1        0.0000
  FLUX
  SPLIST ALL
  T 1        0.0000


**BCSET
  ID TOP
  VALUE
  GMR GMR1
  SURFACE SURF1
  ELEMENTS      12
```

```
  VELO 1
  SPLIST ALL
  T 1       1.0000
  TRAC 2
  SPLIST ALL
  T 1       0.0000
  TEMP
  SPLIST ALL
  T 1       1.0000


**BCSET
  ID ENTRANCE
  VALUE
  GMR GMR1
  SURFACE SURF1
  ELEMENTS      13    14    15    16    17
  TRAC 1
  SPLIST ALL
  T 1       0.0000
  VELO 2
  SPLIST ALL
  T 1       0.0000
  FLUX
  SPLIST ALL
  T 1       0.0000

$ END OF DATA
```

1 JOB TITLE: TRANSIENT PARALLEL FLOW: STOKES (LINEAR) FLOW

BOUNDARY SOLUTION AT TIME = 2.000000 FOR REGION = GMR1

ELEMENT	NODE NO.	X VELOCITY	Y VELOCITY	TEMPERATURE	X TRACTION	Y TRACTION	FLUX
6	1	0.00000E+00	0.00000E+00	0.00000E+00	-0.44523E-02	0.00000E+00	-0.51950E-05
6	2	0.00000E+00	0.10840E-13	0.00000E+00	-0.25984E-02	0.00000E+00	0.38557E-04
6	3	0.00000E+00	0.00000E+00	0.00000E+00	-0.44523E-02	0.00000E+00	-0.51950E-05
7	3	0.00000E+00	0.00000E+00	0.00000E+00	0.00000E+00	0.73689E-03	0.00000E+00
7	5	0.23464E-02	0.00000E+00	0.44977E-04	0.00000E+00	0.20111E-02	0.00000E+00
7	8	0.40676E-02	0.00000E+00	0.23187E-03	0.00000E+00	0.16017E-02	0.00000E+00
8	8	0.40676E-02	0.00000E+00	0.23187E-03	0.00000E+00	0.16017E-02	0.00000E+00
8	10	0.54336E-02	0.00000E+00	0.10192E-02	0.00000E+00	0.22512E-02	0.00000E+00
8	13	0.78373E-02	0.00000E+00	0.41377E-02	0.00000E+00	0.69760E-02	0.00000E+00
9	13	0.78373E-02	0.00000E+00	0.41377E-02	0.00000E+00	0.69760E-02	0.00000E+00
9	15	0.16623E-01	0.00000E+00	0.15159E-01	0.00000E+00	0.21987E-01	0.00000E+00
9	18	0.46134E-01	0.00000E+00	0.48516E-01	0.00000E+00	0.57779E-01	0.00000E+00
10	18	0.46134E-01	0.00000E+00	0.48516E-01	0.00000E+00	0.57779E-01	0.00000E+00
10	20	0.12630E+00	0.00000E+00	0.13279E+00	0.00000E+00	0.13105E+00	0.00000E+00
10	23	0.29802E+00	0.00000E+00	0.30638E+00	0.00000E+00	0.22857E+00	0.00000E+00
11	23	0.29802E+00	0.00000E+00	0.30638E+00	0.00000E+00	0.22857E+00	0.00000E+00
11	25	0.59051E+00	0.00000E+00	0.59578E+00	0.00000E+00	0.35270E+00	0.00000E+00
11	28	0.10000E+01	0.00000E+00	0.10000E+01	0.00000E+00	0.36991E+00	0.00000E+00
12	28	0.10000E+01	0.00000E+00	0.10000E+01	0.54071E+00	0.00000E+00	-0.56559E+00
12	27	0.10000E+01	-0.11061E-12	0.10000E+01	0.47462E+00	0.00000E+00	-0.44176E+00
12	26	0.10000E+01	0.00000E+00	0.10000E+01	0.54071E+00	0.00000E+00	-0.56559E+00
13	26	0.10000E+01	0.00000E+00	0.10000E+01	0.00000E+00	-0.36991E+00	0.00000E+00
13	24	0.59051E+00	0.00000E+00	0.59578E+00	0.00000E+00	-0.35270E+00	0.00000E+00
13	21	0.29802E+00	0.00000E+00	0.30638E+00	0.00000E+00	-0.22857E+00	0.00000E+00
14	21	0.29802E+00	0.00000E+00	0.30638E+00	0.00000E+00	-0.22857E+00	0.00000E+00
14	19	0.12630E+00	0.00000E+00	0.13279E+00	0.00000E+00	-0.13105E+00	0.00000E+00
14	16	0.46134E-01	0.00000E+00	0.48516E-01	0.00000E+00	-0.57779E-01	0.00000E+00
15	16	0.46134E-01	0.00000E+00	0.48516E-01	0.00000E+00	-0.57779E-01	0.00000E+00
15	14	0.16623E-01	0.00000E+00	0.15159E-01	0.00000E+00	-0.21987E-01	0.00000E+00
15	11	0.78373E-02	0.00000E+00	0.41377E-02	0.00000E+00	-0.69760E-02	0.00000E+00

1 JOB TITLE: TRANSIENT PARALLEL FLOW: STOKES (LINEAR) FLOW
BOUNDARY SOLUTION AT TIME = 2.000000 FOR REGION = GMR1

ELEMENT	NODE NO.	X VELOCITY	Y VELOCITY	TEMPERATURE	X TRACTION	Y TRACTION	FLUX
16	11	0.78373E-02	0.00000E+00	0.41377E-02	0.00000E+00	-0.69760E-02	0.00000E+00
16	9	0.54336E-02	0.00000E+00	0.10192E-02	0.00000E+00	-0.22512E-02	0.00000E+00
16	6	0.40676E-02	0.00000E+00	0.23187E-03	0.00000E+00	-0.16017E-02	0.00000E+00
17	6	0.40676E-02	0.00000E+00	0.23187E-03	0.00000E+00	-0.16017E-02	0.00000E+00
17	4	0.23464E-02	0.00000E+00	0.44977E-04	0.00000E+00	-0.20111E-02	0.00000E+00
17	1	0.00000E+00	0.00000E+00	0.00000E+00	0.00000E+00	-0.73689E-03	0.00000E+00

1 JOB TITLE: TRANSIENT PARALLEL FLOW: STOKES (LINEAR) FLOW
INTERIOR VELOCITY AT TIME = 2.000000 FOR REGION = GMR1

NODE	X VELOCITY	Y VELOCITY	TEMPERATURE
1	0.000000E+00	0.000000E+00	0.000000E+00
2	0.000000E+00	0.108400E-13	0.000000E+00
3	0.000000E+00	0.000000E+00	0.000000E+00
4	0.234635E-02	0.000000E+00	0.449766E-04
5	0.234635E-02	0.000000E+00	0.449766E-04
6	0.406761E-02	0.000000E+00	0.231874E-03
8	0.406761E-02	0.000000E+00	0.231874E-03
9	0.543361E-02	0.000000E+00	0.101922E-02
10	0.543361E-02	0.000000E+00	0.101922E-02
11	0.783732E-02	0.000000E+00	0.413767E-02
13	0.783732E-02	0.000000E+00	0.413767E-02
14	0.166229E-01	0.000000E+00	0.151592E-01
15	0.166229E-01	0.000000E+00	0.151592E-01
16	0.461342E-01	0.000000E+00	0.485159E-01
18	0.461342E-01	0.000000E+00	0.485159E-01
19	0.126305E+00	0.000000E+00	0.132787E+00
20	0.126305E+00	0.000000E+00	0.132787E+00
21	0.298025E+00	0.000000E+00	0.306377E+00
23	0.298025E+00	0.000000E+00	0.306377E+00
24	0.590507E+00	0.000000E+00	0.595779E+00
25	0.590507E+00	0.000000E+00	0.595779E+00
26	0.100000E+01	0.000000E+00	0.100000E+01
27	0.100000E+01	-0.110610E-12	0.100000E+01
28	0.100000E+01	0.000000E+00	0.100000E+01
7	0.402738E-02	0.553125E-14	0.346183E-03
12	0.752621E-02	0.460987E-14	0.550220E-02
17	0.457630E-01	-0.753553E-13	0.566311E-01
22	0.299224E+00	0.126423E-12	0.324723E+00

EXAMPLE PROBLEM: FLUI604

ANALYSIS TYPE: FLUID DYNAMICS
2-D, STEADY STATE, VISCOUS STOKES FLOW, INCOMPRESSIBLE

PROBLEM DESCRIPTION:
CONVERGING FLOW BETWEEN TWO NON-PARALLEL PLATES.
A REFERENCE PRESSURE OF 192 PSI IS APPLIED.
THIS IS OFTEN CALLED "HAMMEL FLOW", "JEFFERY FLOW", OR "CONVERGING CHANNEL FLOW".

BOUNDARY ELEMENT MODEL:
20 QUADRATIC ELEMENTS AROUND BOUNDARY, 5 ON EACH SIDE.
GLOBAL BOUNDARY CONDITIONS SPECIFIED EVERYWHERE.

REFERENCE FOR ANALYTICAL SOLUTION:
MORTON DENN, PROCESS FLUID MECHANICS (1980), PG. 217-218.
ALSO: GARTLING, ET. AL., IJNME, VOL. 11 (1977), PG. 1155-1174.
THE ANALYTICAL SOLUTION INVOLVES RADIAL FLOW ONLY, WITH THE MAXIMUM FLUID VELOCITY ALONG THE CENTERLINE.
THIS PROBLEM HAS ATTRACTED A GREAT DEAL OF ATTENTION BECAUSE THE CORRESPONDING NONLINEAR PROBLEM POSESSES AN ANALYTICAL SOLUTION. HOWEVER, ONLY THE LINEAR (STOKES) SOLUTION IS DETERMINED HERE.

SOLUTION POINTS TO VERIFY:

	(Y-VELOCITY)	
NODE	ANALYTICAL	BEST-FSI
1	-24.00	-23.35
86	-1.50	-1.51

RUN TIME:
0.3 X BASE PROBLEM

MISCELLANEOUS:
TRACTION BOUNDARY CONDITIONS ARE FIXED ON INLET AND OUTLET, FROM THE ANALYTICAL SOLUTION. THESE ESTABLISH THE FLOW RATE. AMBIGUOUS BOUNDARY CONDITIONS AT THE CORNERS ARE AVOIDED.

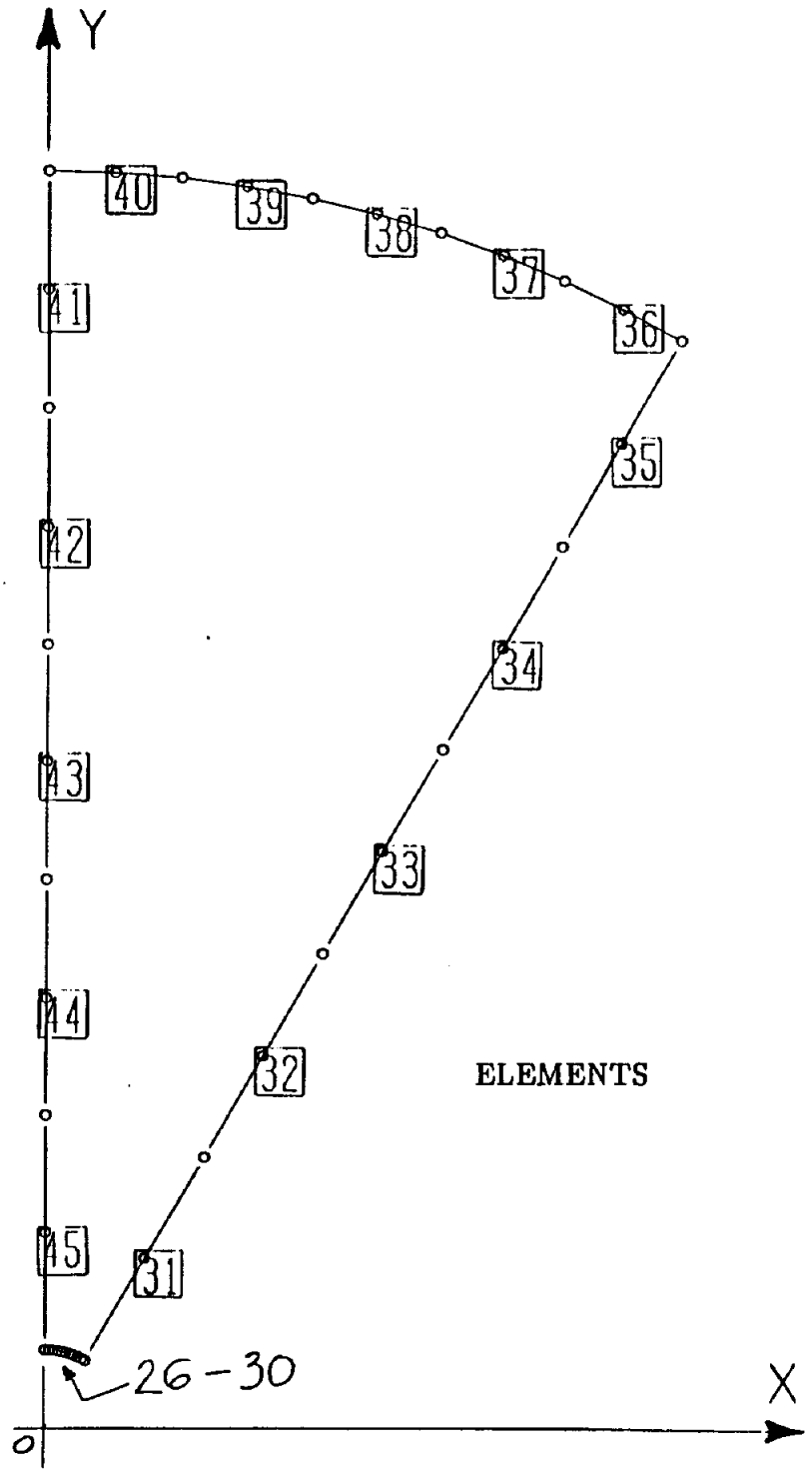
Y
40
39
38
37
36
41
35
42
34
43
33
44
32
ELEMENTS
45
31
26-30
X
0

```
**CASE
  TITLE (CHAN   ) NAVIER-STOKES
  PLANE
  FLUID INCOMPRESSIBLE STEADY
  TIME STEP  1    1.0
  MAXI  1
  ITERATIVE LINEAR


**MATE
  ID MAT1
  TEMP 460.0
    VISC 1.0
    COND 1.0


**GMR
  ID GMR1
  MAT MAT1
  TINT 460.0
  POINTS
          1          0.0000          0.2500
          2          0.0131          0.2497
          3          0.0261          0.2486
          4          0.0391          0.2469
          5          0.0520          0.2445
          6          0.0647          0.2415
          7          0.0773          0.2378
          8          0.0896          0.2334
          9          0.1017          0.2284
         10          0.1135          0.2228
         11          0.1250          0.2165
         12          0.0000          0.6250
         17          0.3125          0.5413
         18          0.0000          1.0000
         28          0.5000          0.8660
         29          0.0000          1.3750
         34          0.6875          1.1908
         35          0.0000          1.7500
         45          0.8750          1.5155
         46          0.0000          2.1250
         51          1.0625          1.8403
         52          0.0000          2.5000
         62          1.2500          2.1651
         63          0.0000          2.8750
         68          1.4375          2.4898
         69          0.0000          3.2500
         79          1.6250          2.8146
         80          0.0000          3.6250
         85          1.8125          3.1393
         86          0.0000          4.0000
         87          0.2093          3.9945
         88          0.4181          3.9781
         89          0.6257          3.9508
```

```
          90              0.8316              3.9126
          91              1.0353              3.8637
          92              1.2361              3.8042
          93              1.4335              3.7343
          94              1.6269              3.6542
          95              1.8160              3.5640
          96              2.0000              3.4641
    SURFACE SURF1
      TYPE QUAD
      ELEMENTS
          26          1           2           3
          27          3           4           5
          28          5           6           7
          29          7           8           9
          30          9          10          11
          31         11          17          28
          32         28          34          45
          33         45          51          62
          34         62          68          79
          35         79          85          96
          36         96          95          94
          37         94          93          92
          38         92          91          90
          39         90          89          88
          40         88          87          86
          41         86          80          69
          42         69          63          52
          43         52          46          35
          44         35          29          18
          45         18          12           1
    NORMAL  +

  **BCSET
    ID EXIT
    VALUE
    GMR GMR1
    SURFACE SURF1
    ELEMENTS      26   27   28   29   30
    POINTS         1    2    3    4    5    6    7    8    9   10
    POINTS        11
    TRAC 1
    SPLIST         1    2    3    4    5    6    7    8    9   10
    SPLIST        11
    T 1       0.0000   -39.8638   -77.6465  -111.3215  -138.9692
    T 1    -158.8274  -169.3377  -169.1868  -157.3417  -133.0780
    T 1     -96.0005
    TRAC 2
    SPLIST         1    2    3    4    5    6    7    8    9   10
    SPLIST        11
    T 1       0.0000        6.3021       25.0361       55.6887       97.4192
    T 1     149.0797      209.2443      276.2438      348.2084      423.1136
    T 1     498.8307

  **BCSET                    $ NO-SLIP BOUNDARY CONDITION AT THE WALL
    ID WALL
    VALUE
    GMR GMR1
```

```
    SURFACE SURF1
    ELEMENTS      31    32    33    34    35
    VELO 1
    SPLIST ALL
    T 1             0.0000
    VELO 2
    SPLIST ALL
    T 1             0.0000

  **BCSET
    ID INLET
    VALUE
    GMR GMR1
    SURFACE SURF1
    ELEMENTS      36    37    38    39    40
    POINTS        96    95    94    93    92    91    90    89    88    87
    POINTS        86
    TRAC 1
    SPLIST        96    95    94    93    92    91    90    89    88    87
    SPLIST        86
    T 1           -286.5001       -259.9573       -232.7506       -204.9528       -
176.6371
    T 1           -147.8771       -118.7465        -89.3195        -59.6699        -
29.8720
    T 1             0.0000
    TRAC 2
    SPLIST        96    95    94    93    92    91    90    89    88    87
    SPLIST        86
    T 1  -498.8312       -512.8684       -525.5074       -536.7214       -546.4866
    T 1  -554.7829       -561.5933       -566.9043       -570.7053       -572.9889
    T 1  -573.7505

  **BCSET                    $ SYMMETRY BOUNDARY CONDITION ALONG CENTERLINE
    ID CENTERLINE
    VALUE
    GMR GMR1
    SURFACE SURF1
    ELEMENTS      41    42    43    44    45
    VELO 1
    SPLIST ALL
    T 1             0.0000
    TRAC 2
    SPLIST ALL
    T 1             0.0000

  $  END OF DATA
```

1 JOB TITLE: (CHAN) NAVIER-STOKES
BOUNDARY SOLUTION AT TIME = 1.000000 FOR REGION = GMR1

ELEMENT	NODE NO.	X VELOCITY	Y VELOCITY	X TRACTION	Y TRACTION
41	86	0.00000E+00	-0.15434E+01	0.57444E+03	0.00000E+00
41	80	0.00000E+00	-0.16946E+01	0.57500E+03	0.00000E+00
41	69	0.00000E+00	-0.18794E+01	0.57477E+03	0.00000E+00
42	69	0.00000E+00	-0.18794E+01	0.57477E+03	0.00000E+00
42	63	0.00000E+00	-0.21190E+01	0.57455E+03	0.00000E+00
42	52	0.00000E+00	-0.24339E+01	0.57406E+03	0.00000E+00
43	52	0.00000E+00	-0.24339E+01	0.57406E+03	0.00000E+00
43	46	0.00000E+00	-0.28614E+01	0.57339E+03	0.00000E+00
43	35	0.00000E+00	-0.34754E+01	0.57171E+03	0.00000E+00
44	35	0.00000E+00	-0.34754E+01	0.57171E+03	0.00000E+00
44	29	0.00000E+00	-0.44301E+01	0.56985E+03	0.00000E+00
44	18	0.00000E+00	-0.60816E+01	0.55862E+03	0.00000E+00
45	18	0.00000E+00	-0.60816E+01	0.55862E+03	0.00000E+00
45	12	0.00000E+00	-0.99308E+01	0.54571E+03	0.00000E+00
45	1	0.00000E+00	-0.23311E+02	0.39956E+03	0.00000E+00

7.0 PATBEST INTERFACE

PATRAN is a general purpose, Mechanical Computer Aided Engineering (MCAE) software system that uses interactive graphics to create engineering design data and to evaluate analysis results. It utilizes an open-ended "gateway" architecture that facilitates access to most design, analysis and manufacturing software programs. PATRAN is developed, supported, and maintained by PDA Engineering of California.

PATBEST is the pre-processing interface for BEST-FSI. It was developed by the Computational Mechanics division of the Department of Civil Engineering, State University of New York at Buffalo. It is named PATBEST indicating the direction of the translation; PATRAN to BEST-FSI. This translator converts a PATRAN generated model into a BEST-FSI data set containing nodal coordinates, elements, GMR's and boundary conditions.

7.1 PROGRAM DESCRIPTION

PATBEST is written in standard Fortran 77, therefore will run on all systems that support Fortran 77. Great care has been taken to maintain portability. All variables within the program are declared explicitly and the code is compiled with range checking.

The code is divided into two sections. The first section reads the PATRAN neutral file and stores into a database. The second section then queries the database to write out the BEST-FSI data set.

7.2 GETTING STARTED

To start up a PATBEST session, enter the appropriate RUN PATBEST command for your installation, i.e. for UNIX based computers it would be "patbest". The PATBEST translator will then prompt you for a PATRAN neutral file, you can enter a name or hit "return". By hitting "return", the program will accept the default, which is the latest PATRAN.OUT file in your directory. After the correct PATRAN neutral file is selected, you will be asked to select the BEST-FSI data file, which after completion of PATBEST will contain the results of the translation.

7.3 PATRAN INPUT REQUIREMENTS

This section defines the PATRAN directives used to build a BEST-FSI data set. The geometry for the data set is built within PATRAN and the boundary conditions can be applied from within PATRAN . The interface compatibility between regions for a perfectly bonded interface is automatically generated by PATBEST. The user can further alter the interface conditions to satisfy his/her own needs. The case control, the material sets and the body force input must be input by the user directly in the BEST-FSI data set.

7.3.1 GEOMETRY INPUT

Table 7.1 lists the PATRAN directives to build BEST-FSI elements and volume cells for two dimensional problems.

Multiple GMR models are created by using the PATRAN named component directive. Nodes or elements on the GMR interface should not have a common I.D.

The permissible element types and cell types that are supported for BEST-FSI are shown in the following figures.

TABLE 7.1

PATBEST/PATRAN Element Library (Two-dimensional)

PATRAN CFEG CODE	BEST-FSI Element Name
BAR /2	Linear 2 noded surface element
BAR /3	Quadratic 3 noded surface element
TRI /3	Linear 3 noded volume cell
QUAD /4	Linear 4 noded volume cell
TRI /6	Quadratic 6 noded volume cell
QUAD /8	Quadratic 8 noded volume cell

PATBEST/PATRAN Element Types

Linear 2-noded Element

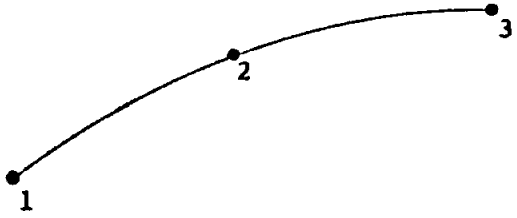

Quadratic 3-noded Element

Two-dimensional (surface) boundary elements

PATBEST/PATRAN Element Types

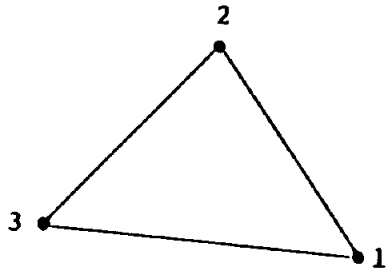

Linear 3-noded Cell

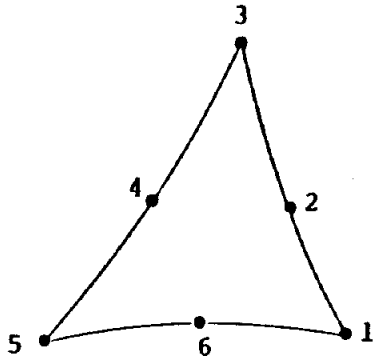

Quadratic 6-noded Cell

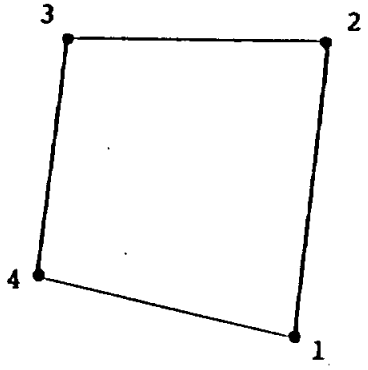

Linear 4-noded Cell

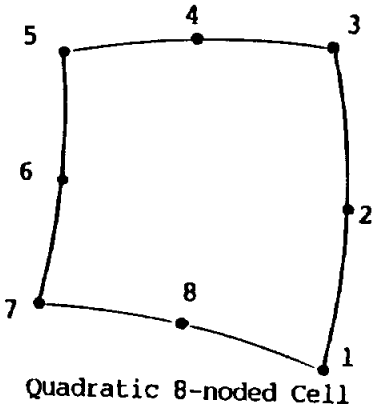

Quadratic 8-noded Cell

Two-dimensional Volume Cells

7.3.2 BOUNDARY CONDITION INPUT

Table 7.2 lists the PATRAN directives to create BEST-FSI boundary conditions. Unlike finite element programs, all boundary conditions in BEST-FSI are applied to elements instead of nodes. Unfortunately, PATRAN is limited in the types of boundary conditions that can be applied to elements. In order to get around this problem, a set-id is associated with pressure boundary conditions within PATRAN . PATBEST will convert these to the appropriate BEST-FSI boundary condition sets.

BEST-FSI assumes a default value of zero for the traction and/or flux for any component not specified, on any element (or points on an element) therefore, any traction or flux component of zero value does not have to be explicitly specified.

TABLE 7.2

PATBEST/PATRAN Boundary Conditions Library

PATRAN DFEG CODE	BEST-FSI Boundary Condition
PRES/E with set-id 1	Traction (non-zero) boundary condition
PRES/E with set-id 3	Velocity (non-zero) boundary condition
PRES/E with set-id 31	Velocity boundary condition with zero X component
PRES/E with set-id 32	Velocity boundary condition with zero Y component
PRES/E with set-id 34	Velocity boundary condition with zero X & Y components
PRES/E with set-id 6	Spring (non-zero) boundary condition
TEMP/E	Temperature boundary condition
HEAT/E	Flux boundary condition
CONV/E	Convection boundary condition

IMPORTANT: PATRAN DFEG command with PRES/E option will not work with zero data values. When specifying a zero value boundary condition (set-id 31-36) you must input a non-zero value, however, this value will have no consequence on the resulting boundary condition set.

7.4 PATBEST FILES

PATBEST requires as input a PATRAN neutral file. It generates three output files; a BEST-FSI input file, which contains the nodes and connectivity information, a log file containing a running log of all PATBEST processing information, and a result file from interactive data generation session. The default names are :

PATRAN neutral file	prompted file name or latest patran.out.*
BEST-FSI raw data file	prompted file name or best.dat
PATBEST log file	patbes.log

8.0 REFERENCES

Ahmad, S. and Banerjee, P.K. (1988), 'Transient Elastodynamic Analysis of Three Dimensional Problems by BEM,' Int. Jour. Numerical Methods in Engineering, Vol. 26, No. 8, pp. 1560-1580.

Banerjee, P.K., Ahmad, S. and Manolis, G.D. (1986), 'Transient Elastodynamic Analysis of Three-dimensional Problems by Boundary Element Method,' Earthquake Engineering and Structural Dynamics, Vol. 14, pp. 933-949.

Banerjee, P.K. and Butterfield, R. (1981), 'Boundary Element Methods in Engineering Science,' McGraw-Hill, London.

Banerjee, P.K. and Morino, L. (1990), Boundary Element Methods in Nonlinear Fluid Dynamics, Developments in Boundary Element Methods-6, Elsevier Applied Science, England.

Banerjee, P.K. and Raveendra, S.T. (1987), 'A New Boundary Element Formulation for Two-dimensional Elastoplastic Analysis,' Jour. of Engrg. Mech., ASCE, V113, No. 2, pp. 252-265.

Banerjee, P.K., Wilson, R.B. and Miller, N (1985), 'Development of a Large BEM System for Three-dimensional Inelastic Analysis,' in Advanced Topics in Boundary Element Analysis, ed. T.A. Cruse, A.B. Pifko and H. Armen, AMD-V72, ASME, New York.

Banerjee, P.K., Wilson, R.B. and Miller, N. (1988), 'Advanced Elastic and Inelastic Three-dimensional Analysis of Gas Turbine Engine Structures by BEM,' Int. J. Num. Meth. Engrg., V26, pp. 393-411.

Banerjee, P.K., Wilson, R.B. and Raveendra, S.T. (1987), 'Advanced Applications of BEM to Three-dimensional Problems of Monotonic and Cyclic Plasticity,' Int. Jour. Mech. Sciences, V29, No. 9, pp. 637-653.

Batchelor, G.K. (1967), An Introduction to Fluid Dynamics, Cambridge University Press, Cambridge, U.K.

Boley, B.A. and Weiner, J.H. (1960), 'Theory of Thermal Stresses,' John Wiley and Sons, New York.

Brueckner, F.P. and Heinrich, J. (1991), 'Petrov-Galerkin Finite Element Method for Compressible Flows,' Int. J. Num. Meth. Eng., V32, pp. 255-274.

Burggraf, O.R. (1966), 'Analytical and Numerical Studies of the Structure of Steady Separated Flows,' J. Fluid Mech., V24, Part 1, pp. 113-151.

Carslaw, H.S. and Jaeger, J.C. (1959), Conduction of Heat in Solids, Clarendon Press, Oxford.

Chaudouet, A. (1987), 'Three-dimensional Transient Thermoelastic Analysis by the BIE Method,' Int. J. Num. Meth. Engrg., V24, pp. 25-45.

Cruse, T.A. (1974), 'An Improved Boundary Integral Equation Method for Three Dimensional Elastic Stress Analysis,' Comp. and Struct., V4, pp. 741-754.

Cruse, T.A. and VanBuren, W. (1971), 'Three-dimensional Elastic Stress Analysis of a Fracture Specimen with an Edge Crack,' Int. J. Fract. Mech., V7, pp. 1-16.

Cruse, T.A., Snow, D.W. and Wilson, R.B. (1977), 'Numerical Solutions in Axisymmetric Elasticity,' Comp. and Struct., V7, pp. 445-451.

Dargush, G.F. (1987), BEM for the Analogous Problems of Thermoelasticity and Soil Consolidation, Ph.D. Dissertation, State University of New York at Buffalo.

Dargush, G.F. and Banerjee, P.K. (1988), 'Development of an Integrated BEM for Hot Fluid-Structure Interaction,' Advanced Earth-to-Orbit Propulsion Technology Conference, NASA CP-3012, Huntsville, May 1988.

Dargush, G.F. and Banerjee, P.K. (1989a), 'Development of an Integrated BEM for Hot Fluid-Structure Interaction,' International Gas Turbine and Aeroengine Congress and Exposition, ASME, Paper 89-GT-128, Toronto; also in J. Eng. Gas Turbines and Power, V112, pp. 243-250.

Dargush, G.F. and Banerjee, P.K. (1989b), 'Development of a Boundary Element Method for Time-dependent Planar Thermoelasticity,' Int. J. Solids Struct., V25, pp. 999-1021.

Dargush, G.F. and Banerjee, P.K. (1989c), Development of an Integrated BEM Approach for Hot Fluid Structure Interaction, NASA Annual Report, Grant NAG3-712.

Dargush, G.F. and Banerjee, P.K. (1990a), 'Boundary Element Methods in Three Dimensional Thermoelasticity,' Int. J. Solids Struct., V26, pp. 199-216.

Dargush, G.F. and Banerjee, P.K. (1990b), 'Advanced Boundary Element Methods for Steady Incompressible Thermoviscous Flow,' in Developments in BEM-6, ed. P.K. Banerjee and L. Morino, Elsevier Applied Science Publishers.

Dargush, G.F. and Banerjee, P.K. (1990c), 'A Time-dependent Incompressible Viscous BEM for Moderate Reynolds Number,' in Developments in BEM-6, ed. P.K. Banerjee and L. Morino, Elsevier Applied Science Publishers.

Dargush, G.F. and Banerjee, P.K. (1991a), 'A Boundary Element Method for Steady Incompressible Thermoviscous Flow,' Int. J. Num. Meth. Eng., V31, pp. 1605-1626.

Dargush, G.F. and Banerjee, P.K. (1991b), 'A Time Dependent Incompressible Viscous BEM for Moderate Reynolds Numbers,' Int. J. Num. Meth. Eng., V31, pp. 1627-1648.

Dargush, G.F. and Banerjee, P.K. (1992), 'Time Dependent Axisymmetric Thermoelastic Boundary Element Analysis,' Int. J. Num. Meth. Eng., V33, pp. 695-717.

Dargush, G.F., Banerjee, P.K. and Dunn, M.G. (1987), Development of an Integrated BEM Approach for Hot Fluid Structure Interaction, NASA Annual Report, Grant NAG3-712.

Dargush, G.F., Banerjee, P.K. and Honkala, K.A. (1988), Development of an Integrated BEM Approach for Hot Fluid Structure Interaction, NASA Annual Report, Grant NAG3-712.

Dargush, G.F., Banerjee, P.K. and Shi, Y. (1991), Development of an Integrated BEM Approach for Hot Fluid Structure Interaction, NASA Contractor Report 187236.

Deb, A. and Banerjee, P.K. (1989), 'A Comparison Between Isoparametric Lagrangian Elements in 2D BEM,' Int. J. Num. Meth. Eng., V28, pp. 1539-1555.

Dongarra, J.J. et al (1979), Linpak User's Guide, SIAM, Philadelphia.

Gartling, D.K., Nickell, R.E., Tanner, R.E. (1977), 'A Finite Element Convergence Study for Accelerating Flow Problems,' Int. J. Num. Methods Eng., V11, pp. 1155-1174.

Ghia, U., Ghia, K.N. and Shin, C.T. (1982), 'High-Re Solutions for Incompressible Flow Using the Navier-Stokes Equations and a Multigrid Method,' J. Comp. Physics, V48, pp. 387-411.

Gladden, H.J. (1989), 'Aerothermal Loads on Actively Cooled Components: Analyses and Experiment,' HITEMP Review, NASA Conference Publication 10039, Cleveland, Ohio, Oct. 31-Nov. 2, pp. 68.1-68.12.

Goldstein, M.E. (1976), Aeroacoustics, McGraw-Hill, New York.

Gunn, M.J. and Britto, A.M. (1984), CRISP User's and Programmer's Guide, Engineering Department, Cambridge University.

Henry, D.P. and Banerjee, P.K. (1988), 'A Variable Stiffness Type Boundary Element Formulation for Axisymmetric Elastoplastic Media,' Int. Jour. for Num. Methods in Engrg., V25, pp. 1005-1027.

Honkala, K.A. (1992), Boundary Element Methods for Two Dimensional Coupled Thermoviscous Flow, Ph.D. Dissertation, State University of New York at Buffalo.

Latchat, J.C. and Watson, J.O. (1976), 'Effective Numerical Treatment of Boundary Integral Equations: A Formulation for Three-dimensional Elastostatics,' Int. J. Num. Meth. Engrg., V10, pp. 991-1005.

Lighthill, M.J. (1952), 'On Sound Generated Aerodynamically I. General Theory,' Proc. Roy. Soc. A, V211, pp. 564-587.

Millsaps, K. and Pohlhausen, K. (1953), 'Thermal Distributions in Jeffery-Hamel Flows Between Nonparallel Plane Walls,' Journal of the Aeronautical Sciences, March, pp. 187-196.

Morse, P.M. and Feshbach, H. (1953), Methods of Theoretical Physics, McGraw-Hill, New York.

Mustoe, G.G.W. (1984), 'Advanced Integration Schemes Over Boundary Elements and Volume Cells for Two- and Three-dimensional Nonlinear Analysis,' in Developments in Boundary Element Methods - III, ed. P.K. Banerjee and S. Mukherjee, Applied Science Publishers, England.

Oseen, C.W. (1911), Über die Stokes'sche Formel und über eine verwandte Aufgabe in der Hydrodynamik II, Ark. f. mat., astr. och fysik, V7.

Oseen, C.W. (1927), Neuere Methoden und Ergebnisse in der Hydrodynamik, Akad. Verlagsgellschaft, Leipzig.

Panton, R.L. (1984), Incompressible Flow, John Wiley and Sons, New York.

Piva, R. and Morino, L. (1987), 'Vector Green's Function Method for Unsteady Navier-Stokes Equations,' Meccanica, Vol. 22, pp. 76-85.

Piva, R. Graziani, G. and Morino, L. (1987) 'Boundary Integral Equation Method for Unsteady Viscous and Inviscid Flows,' IUTAM Symposium on Advanced Boundary Element Method, San Antonio, Texas.

Prandtl, L. (1904), Verhandlunger IIIrd, International Mathematiker Kongresser, Heidelberg, pp. 484-491 (trans. as NACA Tech. Mem. 452).

Rizzo, F.J. and Shippy, D.J. (1977), 'An Advanced Boundary Integral Equation Method for Three-dimensional Thermoelasticity,' Int. J. Num. Meth. Eng. V11, pp. 1753-1768.

Schlicting, H. (1955), Boundary Layer Theory, McGraw-Hill, New York.

Sharp, S. and Crouch, S.L. (1986), 'Boundary Integral Methods for Thermoelasticity Problems,' J. Appl. Mech., V53, pp. 298-302.

Shi, Y. (1991), Fundamental Solutions and Boundary Element Formulations for Convective Fluid Flow, Ph.D. Dissertation, State University of New York at Buffalo.

Stroud, A.H. and Secrest, D. (1966), Gaussian Quadrature Formulas, Prentice Hall, New York.

Telles, J.C.F. (1987), 'A Self-Adaptive Co-ordinate Transformation for Efficient Numerical Evaluation of General Boundary Element Integrals,' Int. J. Num. Meth. Engrg., V24, pp. 959-973.

Timoshenko, S.P. and Goodier, J.N. (1970), Theory of Elasticity, McGraw-Hill, New York.

Tosaka, N. and Kakuda, K. (1986), 'Numerical Solutions of Steady Incompressible Viscous Flow Problems by Integral Equation Method,' pp. 211-222 in R.P. Shaw et al, eds. Proc. 4th Intl. Symp. Innov. Num. Methods Engrg., Springer, Berlin.

Tosaka, N. and Kakuda, K. (1987), 'Numerical Simulations of Laminar and Turbulent Flows by Using an Integral Equation,' Boundary Element IX, eds. Brebbia, Wendland and Kuhn, pp. 489-502.

Tosaka, N. and Onishi, K. (1986), 'Boundary Integral Equation Formulations for Unsteady Incompressible Viscous Fluid Flow by Time-differencing,' Engineering Analysis, V3, No. 2, pp. 101-104.

Zienkiewicz, O.C. and Taylor, R.L. (1991), The Finite Element Method, Volume 2, 4th edition, McGraw-Hill, London.

REPORT DOCUMENTATION PAGE

Form Approved
OMB No. 0704-0188

1. AGENCY USE ONLY (*Leave blank*)	2. REPORT DATE	3. REPORT TYPE AND DATES COVERED
	March 1992	Final Contractor Report

4. TITLE AND SUBTITLE
Development of an Integrated BEM Approach for Hot Fluid Structure Interaction
BEST-FSI: Boundary Element Solution Technique for Fluid Structure Interaction

5. FUNDING NUMBERS
WU-590-91-11
NAG3-712

6. AUTHOR(S)
G.F. Dargush, P.K. Banerjee, and Y. Shi

7. PERFORMING ORGANIZATION NAME(S) AND ADDRESS(ES)
State University of New York at Buffalo
Buffalo, New York 14214

8. PERFORMING ORGANIZATION REPORT NUMBER
None

9. SPONSORING/MONITORING AGENCY NAMES(S) AND ADDRESS(ES)
National Aeronautics and Space Administration
Lewis Research Center
Cleveland, Ohio 44135-3191

10. SPONSORING/MONITORING AGENCY REPORT NUMBER
NASA CR-189202

11. SUPPLEMENTARY NOTES
Project Manager, C.C. Chamis, Structures Division, NASA Lewis Research Center, (216) 433-3252.

12a. DISTRIBUTION/AVAILABILITY STATEMENT
Unclassified - Unlimited
Subject Category 39

12b. DISTRIBUTION CODE

13. ABSTRACT (*Maximum 200 words*)

This report is intended to serve multiple purposes. First, it serves as a report summarizing the work developed under the grant. Section 2 provides all of the relevant theoretical background, while numerous applications are discussed in Section 3. It should be noted that all of those examples were run on Sun SPARC workstations. The remainder of the report focuses on the documentation of the computer code BEST-FSI. Section 4 presents a brief introduction for a first-time boundary element user. Complete details of the input data required to execute BEST-FSI are contained in Section 5. Each data item is described individually and examples of use are provided. Then, in Section 6, several sample problems are examined.

14. SUBJECT TERMS	15. NUMBER OF PAGES
Boundary elements; Flows; Structures; Computer program	388
	16. PRICE CODE: A17

17. SECURITY CLASSIFICATION OF REPORT	18. SECURITY CLASSIFICATION OF THIS PAGE	19. SECURITY CLASSIFICATION OF ABSTRACT	20. LIMITATION OF ABSTRACT
Unclassified	Unclassified	Unclassified	

NSN 7540-01-280-5500

U.S. GOVERNMENT PRINTING OFFICE: 1992 - 750-034/60304

Standard Form 298 (Rev. 2-89)
Prescribed by ANSI Std. Z39-18
298-102